Resilient Operation of Active Distribution Networks via Self-learning Smart Devices

BY

MOHSEN HOSSEINZADEHTAHER
M.S., Amirkabir University of Technology, 2014

THESIS

Submitted as partial fulfillment of the requirements
for the degree of Doctor of Philosophy in Electrical and Computer Engineering
in the Graduate College of the
University of Illinois Chicago, 2022
Chicago, Illinois

Defense Committee:

Mohammad Shadmand, Chair and Advisor
Danilo Erricolo
Line He
Sabri Cetin, Department of Mechanical and Industrial Engineering
Frede Blaabjerg, Aalborg University

Dedicated to my Mother and Father

ACKNOWLEDGEMENTS

First and foremost, I would like to express my special and deepest gratitude to my Ph.D. Advisor Professor Mohammad Shadmand for all his unconditional technical support, guidance, and help over these years. I would like to thank you for instructing me how to do research and allowing me to grow as a researcher. Your advice on both my research and career has been invaluable.

I would also like to thank my Ph.D. committee members, Professor Frede Blaabjerg, Professor Sabri Cetin, Professor Danilo Erricolo, and Professor Lina He, for all their guidance through this process; your discussion, guidance, and feedback have been absolutely invaluable.

Special thanks to Professor Haitham Abu-Rub, Professor Sertac Bayhan, Professor Shady Khalil, and all my friends at Texas A&M University at Qatar and Smart Grid Center. I highly appreciate all your unique advice and support over the years.

I would especially like to thank all my research fellows in Intelligent Power Electronics at Grid Edge (IPEG) Research Laboratory at University of Illinois Chicago (UIC), who wonderfully supported me during these years. I am very grateful to all of you.

Finally, I need to express my deepest thanks to my father, mother, sister, brother, and his esteemed wife. I have gotten support, encouragement, and love from all of you all the time. I believe without your amazing support during these years, I could not achieve this accomplishment.

MH

PREFACE

This dissertation is an original intellectual product of the author, Mohsen Hosseinzadehtaher. All the work presented here was conducted in the Intelligent Power Electronics at Grid Edge (IPEG) Research Laboratory at University of Illinois Chicago.

The results of our research have been previously published as journal, conference, workshop articles in:

- IEEE Transaction on Energy Conversion, 2020
- IEEE Energy Conversion Congress and Exposition (ECCE, 2021)
- IEEE Industrial Electronics Magazine, 2020
- IEEE Power Electronics Magazine, 2021
- IEEE 12th International Symposium on Power Electronics for Distributed Generation Systems (PEDG, 2021)
- IEEE International Conference on Smart Grid and Renewable Energy (SGRE 2019)
- IEEE International Conference on Smart Grid and Renewable Energy (SGRE 2022)
- IEEE CyberPELS, 2020
- IEEE Kansas Power and Energy Conference (KPEC, 2020)

The results of our research are currently in review:

- IEEE Transactions on Industrial Electronics, 2022

The copyright permissions for reusing the published materials are given in the Appendix.

Mohsen Hosseinzadehtaher

October 19, 2022

CONTRIBUTION OF AUTHORS

Major parts of the results and discussions in this dissertation are taken from my published or submitted papers with permission from the journals that allow re-publication in thesis. Below, the contributions of all the co-authors are listed:

Authors' contributions in IEEE Transaction on Energy Conversion 2020: M. Hosseinzadehtaher and M. Shadmand conceived the main idea. M. Hosseinzadehtaher led the investigations and conducted the analytical analysis, technical results, and write-up. A. Khan and M. Easley contributed to some part of write-up and drawing some figures. P. Fajri contributed to review the write-up of the manuscript.

Authors' contributions in EEE Transactions on Industrial Electronics 2022: M. Hosseinzadehtaher and M. Shadmand conceived the main idea. M. Hosseinzadehtaher led the investigations and conducted the analytical analysis, technical results, experimental results, and write-up. A. Zare, M. Farooq Umar, and S. D'silva contributed to experimental results. A. Khan contributed to review the write-up of the manuscript.

Authors' contributions in IEEE Energy Conversion Congress and Exposition (ECCE 2021): M. Hosseinzadehtaher and M. Shadmand conceived the main idea and M. Hosseinzadehtaher led the investigations and conducted the analytical analysis, technical results, and write-up. A. Fard contributed to some part of write-up of manuscript and drawing some figures.

Authors' contributions in IEEE Industrial Electronics Magazine 2020: A. Khan, M. Hosseinzadehtaher and M. Shadmand conceived the main idea. A. Khan and M. Hosseinzadehtaher led the investigations and conducted the analytical analysis, technical

CONTRIBUTION OF AUTHORS (Continued)

results. M. Hosseinzadehtaher contributed to the write-up of manuscript and drawing some figures. S. Bayhand and H. Abu-Rub contributed to concept of the write-up of the manuscript.

Authors' contributions in IEEE 12th International Symposium on Power Electronics for Distributed Generation Systems (PEDG 2021): M. Hosseinzadehtaher and M. Shadmand conceived the main idea and M. Hosseinzadehtaher led the investigations and conducted the analytical analysis, technical results, and write-up. A. Fard contributed to some part of write-up of manuscript and drawing some figures. P. Fajri contributed to review the write-up of the manuscript.

Authors' contributions in IEEE International Conference on Smart Grid and Renewable Energy (SGRE 2019): M. Hosseinzadehtaher and M. Shadmand conceived the main idea. M. Hosseinzadehtaher led the investigations and conducted the analytical analysis, technical results, and write-up. A. Khan and M. Baker contributed to some part of write-up of manuscript and drawing some figures.

Authors' contributions in IEEE International Conference on Smart Grid and Renewable Energy (SGRE 2022): M. Hosseinzadehtaher and M. Shadmand conceived the main idea. M. Hosseinzadehtaher led the investigations and conducted the analytical analysis, technical results, and write-up. M. Greidanus, H. Althuwaini, K. Sullivan contributed to the analytical analysis, technical results, write-up and drawing some figures. S. K. Mazumder contributed to review the write-up of the manuscript.

CONTRIBUTION OF AUTHORS (Continued)

Authors' contributions in IEEE CyberPELS 2020: M. Hosseinzadehtaher and M. Shadmand conceived the main idea. M. Hosseinzadehtaher led the investigations and conducted the analytical analysis, technical results, and write-up. A. Khan and H. Abu-Rub contributed to review the write-up of the manuscript.

Authors' contributions in IEEE Kansas Power and Energy Conference 2020: G. Amariucai and M. Shadmand conceived the main idea. S. Harshbarger led the investigations and conducted the analytical analysis, technical results, and write-up. M. Hosseinzadehtaher contributed to some analytical analysis, technical results, write-up and drawing some figures. B. Natarajan and E. Vasserman contributed to review the write-up of the manuscript.

Authors' contributions in IEEE Power Electronics Magazine 2021: O. Abu-Rub and M. Shadmand conceived the main idea. O. Abu-Rub, A. Fard and M. Farooq umar led the investigations and conducted the analytical analysis, technical results, and write-up. M. Hosseinzadehtaher contributed to some part of analytical analysis, technical results, drawing some figures and write-up of the manuscript.

TABLE OF CONTENTS

CHAPTER PAGE

TABLE OF CONTENTS (Continued)

CHAPTER PAGE

LIST OF TABLES

TABLE PAGE

LIST OF FIGURES

LIST OF FIGURES (Continued)

FIGURE PAGE

LIST OF FIGURES (Continued)

FIGURE PAGE

LIST OF FIGURES (Continued)

FIGURE PAGE

LIST OF FIGURES (Continued)

FIGURE PAGE

LIST OF FIGURES (Continued)

FIGURE PAGE

LIST OF FIGURES (Continued)

FIGURE PAGE

LIST OF FIGURES (Continued)

FIGURE PAGE

LIST OF ABBREVIATIONS

AI	Artificial Intelligence
AI-PRC	Artificial Intelligence-Based Power Reference Correction
AMI	Advance Metering Infrastructure
ANN	Artificial Neural Network
AVR	Automatic Voltage Regulator
BESS	Battery Energy Storage System
BRA	Bayesian Regularization Algorithm
CDMSC	Cohesive Data-Extracted Methodology Built-In Shadow Control
CMV	Condition Monitoring Vector
DAB	Dual Active Bridge
DER	Distributed Energy Resource
DoS	Denial Of Service
FDI	False Data Injection
FTL	Fast Transient Load
GFLI	Grid Following Inverter
GFMI	Grid Forming Inverter
HIL	Hardware-In-The-Loop
IDMPC	Integrated Data-Driven and Model-Based Predictive Control
IDS	Intrusion Detection System
IPS	Integrated Power System

LIST OF ABBREVIATIONS (Continued)

LFC	Load Frequency Control
LIPS	Low Inertia Power System
LQG	Linear Quadratic Gaussian
MPC	Model Predictive Control
MPSC	Model Predictive Self-Healing Control
NERC	North American Reliability Corporation
PEDG	Power Electronic Dominated Grids
PLL	Phase-Locked Loop
POI	Point Of Interconnection
PPL	Pulsed Power Load
PSO	Particle Swarm Optimization
ROCOF	Rate of Change of Frequency
SCR	Short Circuit Ratio
SG	Synchronous Generator
USTDF	Ultra-Short-Term Demand Forecasting
VSG	Virtual Synchronous Generator

SUMMARY

This dissertation focuses on developing Artificial Intelligence (AI)-based and self-healing control techniques to enhance the resiliency of active distribution networks for upcoming power grid challenges. In the first stage of this work, a high bandwidth primary control layer is developed to achieve an ultra-fast predictive controlled dual active bridge converter interfaced grid-following inverter for voltage and frequency support. The primary control layer is developed by a novel model predictive self-healing control (MPSC) scheme. This control technique heals intrinsic drawbacks in commonly used control approaches by decreasing the potential errors in the control processes. However, the frequency restoration process needs more advanced techniques due to the high nonlinearity of the active distribution networks such as power electronic dominated grids (PEDG). Therefore, an artificial intelligence-based power reference correction (AI-PRC) mechanism is developed to address the shortcomings of frequency restoration of the state-of-the-art virtual synchronous generator (VSG)-based or droop-based grid following inverters (GFLIs) and grid forming inverters (GFMIs) via re-defining GFLI role at grid-edge. A detailed analytical validation is provided that shows control rules in PEDG intrinsically follow the underlying dynamic of the swing-based machines to extend its stability boundary. Considering this fact, comprehensive transient and steady state-based mathematical models are used for constructing the learning database of the proposed AI-PRC mechanism. Subsequently, a neural network is trained by Bayesian Regularization Algorithm (BRA) to realize the proposed AI-PRC for GFLIs. The proposed training approach can deal with all grid characteristics alterations and uncertainties. Thus, this approach incorporates all PEDG's effective variables that shape its dynamic response during transient disturbances. Several simulations and experimental case studies were provided that evaluate the functionality of the proposed AI-PRC for GFLIs towards enhancing transient response and resiliency of PEDG. The provided evaluations demonstrate significant improvement in frequency restoration in response to transient disturbances.

Moreover, the proposed control technique is exploited as a shadow controller in the case that the attacker aims to threaten the entire grid stability via stealthy attacks. Some stealthy attack scenarios are investigated on the 14-bus PEDG, and the results have proven the effectiveness of the proposed approach in fast supporting of the grid in the event of stealthy attacks, thus the grid resiliency is enhanced in this case as well.

Due to the high importance of power grid resiliency, in the final stage of this work, an intrusion detection system (IDS) is developed to provide another layer of security that monitors grid dynamics and vital variables in other time scales. The groundwork of this technique is based on a load forecasting procedure that benefits from an artificial intelligence approach. In more details, an anomaly detection technique based on a condition monitoring vector and ultra-short demand forecasting is designed and developed for achieving the above-mentioned goals. The designed IDS is more robust against attack scenarios that could bypass other primary control layers. Thus, the proposed approach enables grid operators to take proper and prompt actions for providing a secure operation of the grid.

Chapter 1

1. Introduction

Part of this chapter, including figures and text are based on my following papers:

- A. Khan, M. Hosseinzadehtaher, M. B. Shadmand, S. Bayhan and H. Abu-Rub, "On the Stability of the Power Electronics-Dominated Grid: A New Energy Paradigm," in IEEE Industrial Electronics Magazine, vol. 14, no. 4, pp. 65-78, Dec. 2020.

1.1. Toward Resilient Power Electronic Dominated Grid

Nowadays, the existing energy network is being modernized by an ever-increasing penetration of renewable energy resources and energy storage systems (i.e., the energy-paradigm) [1-3] . For instance, the wind energy installation is expected to reach 903 GW by 2023 [4]. Similarly, solar photovoltaic (PV) energy installation will reach 1296 GW in 2023 [5]. As well as, the global deployment of energy storage systems will reach 2500 MW by 2023 [6]. In other words, the new energy paradigm is transforming the current energy network from being reliant on synchronous generators to power electronics-based power generation [7-9]. This high renewable energy generation-based power grid is termed as the power-electronics-dominated-grid (PEDG).

A generic example of a PEDG is depicted in Figure 1. 1. This PEDG contains high number of power electronic converters. The power electronic converters are employed in PV systems, wind farms, battery banks, high voltage DC (HVDC), multi-terminal DC (MTDC), micro-grids, etc. Furthermore, PEDG can be interconnected to a larger power network through point of common coupling. PEDG also requires three level of controls: (i) primary control, (ii) secondary control, and (iii) tertiary control [10].The primary control is associated with each individual power electronic interface. The secondary control level of PEDG is responsible of managing the different energy generation assets by assuring optimal and reliable operation. Furthermore, the secondary control communication level is observing and controlling the meters, relays, and breakers in PEDG. In fact, this is the reason that the secondary control is often termed in the literature as the central control or the supervisory control. Additionally, the role of tertiary control is similar to the secondary control role but on a larger scale. In more details, the tertiary control ensures operational optimality and reliability from the perspective of the upper power network requirements. Based on the grid aggregation architecture, the secondary and tertiary control layers may have communication interactions.

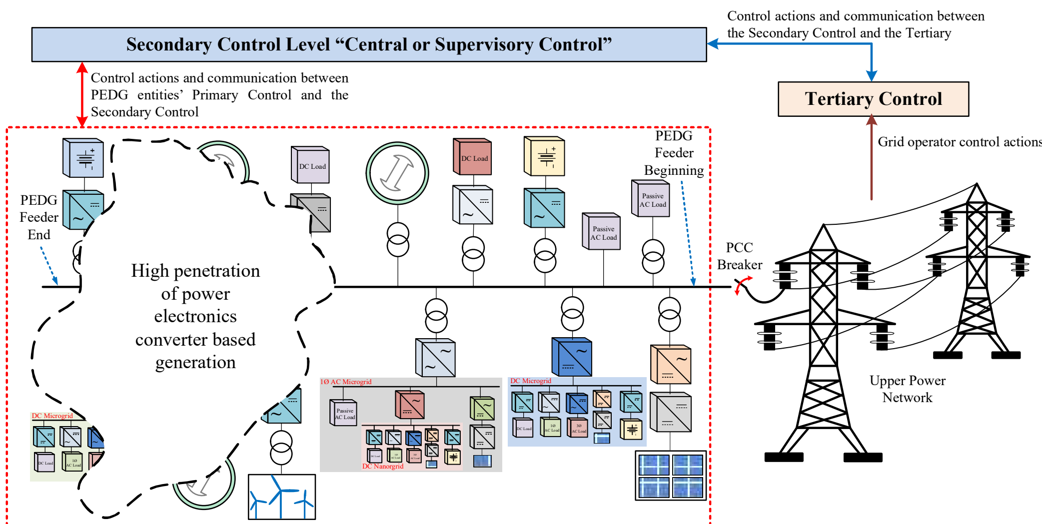

Figure 1. 1. Generic example of PEDG

Essentially, the main functionalities of these three-level controls collectively are: sustaining the frequency and voltage in their acceptable levels, achieving balanced demand and power supply, seamless transition between the grid-connected and islanded operation modes, accomplishing economic dispatch, and providing proper demand side management. Nevertheless, the stability topic is majorly linked to control level that possess fastest dynamics. In such hierarchy, the primary level of the PEDG is the fastest control. The primary control is responsible of voltage control, frequency control, islanding detection, and active and reactive power allocation and balance [11]. However, the stability study in conditions where the PEDG is tied with a larger power grid is so far limited to the stability of a single or multiple power generation assets, motors, or loads. Example of such instabilities are termed as harmonic instabilities or harmonic resonance [12, 13]. Moreover, voltage and frequency stability in grid connected PEDG is governed by the stability of the upper power network. Thus, the operation of the PEDG in such mode is limited to active power injection and ancillary services. In other words, major instabilities in non-islanded mode of operation are power quality related from the perspective of the upper power network. Moreover, with the recent leveraging by grid codes for encouraging the islanded operation [14, 15]; islanded PEDGs are anticipated to rule the future of the current energy network. In the islanded operation of PEDGs, the frequency and voltage are no longer supported by the upper power network. Thereby, the individual energy resources in the PEDG are required to sustain the voltage and frequency in their satisfactory ranges. Though, the PEDG's primary control in standalone mode highly variates depending on the control approach adopted for the energy assets. For instance, the behavior of grid-forming synchronous machines is different compared to the droop-controlled inverters [16]. Precisely, for synchronous machines, the frequency and voltage are controlled through the governor and the field current control loop, respectively [17]. In contrast, in islanded PEDG the network's inverters rely on rapid control loops for voltage, current, and PLL. In other words, PEDG has low mechanical inertia and rapid and multi-time scale dynamics [18], not forgetting the dominant stochastic generation nature of PEDG's energy assets.

The key feature that distinguishes the PEDG paradigm compared to the conventional interconnected power system is mainly the loads and generation assets proximity. This means that PEDG has shorter feeders, making medium voltage level operation optimal for such network. Also, because of feeder's short length, PEDG has lesser reactance to resistance ratio (X/R) in comparison to the interconnected traditional bulk power system [22]. Consequently, the mathematical representation of PEDG's voltage, frequency, bus angles, active power flow, and reactive power flow dynamics are significantly different compared to bulk power systems. Additionally, the proximity between loads and generation units in PEDG makes the stochastic nature of renewable energy resources or any existing uncertainties to have a higher impact on PEDG's elements. In other words, the proximity feature of PEDG results in high correlated behavior among the components of the PEDG. Furthermore, balancing the demand and supply in PEDG is challenging due to the dominant intermittence nature of the PEDG energy resources [23]. Combining that challenge with the bidirectional power flow feature of PEDG requires complex control and protection coordination among network's prosumers.

With the expectation that the number of synchronous machines will be lesser in PEDG compared to static power electronics-based generators, this will have a substantial impact on system's overall inertia. Specifically, PEDG inertia is significantly lower compared to the bulk interconnected power system. The low inertia problem of PEDG is severe with low short circuit capacity of the network. Precisely, slight deviations in the PEDG architecture due to any intentional load or generator disconnection would have a drastic effect on the voltage and frequency. In fact, the mixture of synchronous machines with inverter-based generations results in a combination of large time constants with small time constants. This might force inverters-based generation units to unintentionally shut down during perturbation in system parameters due to network architecture's alteration. Thus, the crucial distinction between traditional bulk power grid and PEDG considering system stability are generations and loads proximity, high penetration of stochastic nature energy generation assets, low feeders' *X/R* ratio, low short circuit capacity, low inertia, high correlation between the generation units, and unbalanced phase voltage and loading. Considering these distinctive characteristics of PEDG, the concept of resiliency is reassessed in the next section.

1.2. The concept of Resiliency in PEDG

As several challenges regarding the PEDG's features and stability issues were contained in previous section, it is essential to provide another feature for PEDG which is provoked but not limited by consequences of traditional power system modernization. PEDG suffers mainly from lack of minimum required inertia which results in some other challenges which were reviewed previously. Thus, this issue decreases PEDG tolerance when confronted with different types of disturbance. Moreover, deploying smart devices in this new energy paradigm necessitates PEDG to come up with more communication links which makes PEDG to be more vulnerable to different sorts of Cyberattack. Therefore, in general, the ability of the PEDG to tolerate and rapidly recover severe impact disturbances is known as resiliency. In fact, resiliency add a new aspect to system management and reliability. Most incidents that threaten PEDG resiliency can be categorized as low-frequency occurrences while they can have severe impact on the system. Resiliency is a kind of ability that can be added to the power system to restrict the severity and duration of negative and destructive damages following by extreme disruptions. The main factors that have high influence on PEDG resiliency can be categorized as weather-related incidents and infrastructure damages, cyberattacks, and energy source limitations. Severe weather incidents can damage transmission lines and accordingly PEDG's infrastructure. To have better insight about the severe weather effects, Figure 1. 2 illustrates the event trends and related imposed costs for flooding, freeze, severe storm, tropical cyclone, winter storms, etc., from 1980-2022 in USA. For instance, according to power outages. US, as an aggregator of utility blackout data, customers have experienced 1.33 billion outage hours in 2020, up 73% from roughly 770 million in 2019. Extensive generation loss is the main consequence of severe weather incidents that effortlessly can result in a wide area blackout if the PEDG is not resilient enough.

As a matter of fact, in PEDG, the number of remote-control capabilities that utilizes information communication technologies is high compared to the bulk power system. Initially, the thought of using more intelligent devices in the PEDG paradigm might appear attractive [19]. This large integration of intelligent devices in the PEDG paradigm created a dangerous trade-off regarding security [20]. Meaning that, the PEDG network is highly susceptible to malicious cyber intrusions. The seriousness of these cyber-attacks is ranging from simple thefts and consumer loads damage to high impacts that leads to shut down, cascaded failures and large blackouts that impact the energy market operation [21]. Intelligent cyber-attacks on the PEDG network are targeting the physical layer to violate the network stability limits by appearing as normal network uncertainties. Given the PEDG paradigm multi-time scale nature, this dictates the detection of cyber-attacks in a very short to avoid serious consequences on the PEDG operation. Otherwise, these intelligent cyber-attacks go in penetrating the system till it become a stealthy attack that is undetected. Cyber-

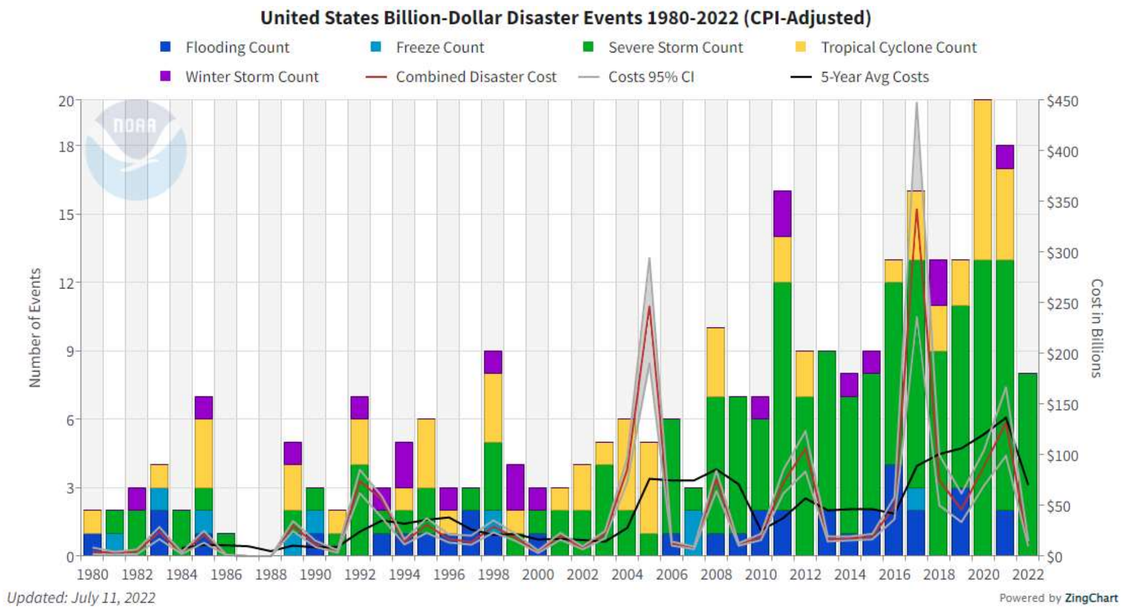

Figure 1. 2. US billion-dollar disaster events 1980-2022 (CPI-Adjusted) [22]

attacks can also downgrade the responsivity of physical system that are providing services in PEDG as well.

Moreover, PEDG with distinct characteristics compared to the traditional system might encounter with power source limitations, particularly in transient durations when a severe disturbance occurs. As the inertia is low, it is crucial to have plenty amount of power reserves or battery energy storage systems to contribute to voltage and frequency restoration procedure during severe impact incidents [23, 24]. Considering all limitations regarding the energy storage systems such as their control dynamic, environmental restrictions, and cost issues, if PEDG cannot be supported properly and promptly with the existing sources, the system would experience unstable conditions. Thus, the resiliency of PEDG can be affected by the power source limitations of the grid as well. In PEDG, several grid-following inverters (GFLI) are supporting the local loads or suppling a share of demand in grid-connected mode.

It seems the maximum capabilities of the GFLI in PEDG are not utilized in critical conditions of grid if just limited to have a contribution to the base load of the grid. Therefore, if GFLIs contribute to frequency and restoration procedures in transient periods effectively, the resiliency of the PEDG can be enhanced considerably based on the provided definitions. Regarding the grid forming inverters (GFMI), if the grid benefits from their maximum contributions to voltage and frequency restoration, some other challenges will be evolved such as power sharing problems and oscillatory behaviors. Thus, utilizing the current source assets in transient periods by considering all technical limitations can be an attractive solution for rapid restoration of the PEDG.

Considering all above-mentioned issues, PEDG resiliency can be described as a function of three major features such as damage restraint, recovery, survivability, and rapid system restoration abilities. As an example, damage restraint can include physical and cyber security of supply centers, transmission lines, and dispatching centers against different types of damages. For instance, strengthening the physical infrastructures of energy sources against weather-related issues can enhance the resiliency of the PEDG. System recovery is associated with procedures that can speed up service restoration appropriately. Evaluating the occurred damage to the system, managing power outages, and availability of recovery power equipment such as power transformers can be classified in this category. Survivability has a substantial role in enhancing resiliency. Survivability can be linked but not limited to some actions that enable PEDG to sustain some level of electricity either at a basic level or survive some of its clusters during severe disturbances. Besides, survivability can be enhanced by deploying innovative technologies to provide a basic level of functionality for the customers. System restoration ability is one of the most significant features that can improve system resiliency. This will include some complicated decisions that are made by PEDG operators as well as applying novel control techniques to reinstate the PEDG's ability to sustain its electricity continuity and return the system to operating in normal condition. It should be remarked that by equipping PEDG with smart control or self-healing approaches, the ground level of resiliency can be enhanced. However, a sort of tradeoff is required and should be considered when these approaches are applied to the vulnerable PEDG. In this dissertation, it is aimed to focus on rapid system restoration aspect of resiliency. Extensive disturbances can jeopardize system stability boundary and based on the definitions that provided for resiliency, having more stable system results in more resilience system. Thus, the concept of stability is presented in the next sections.

1.2.1. Concept of Stability in PEDG

Take an example of a PEDG that is operating in equilibrium point. This means all network state variables are sustaining their operational constrains. Specifically, voltages and the frequency are in their appropriate values in steady state. This network is stable if its state variables - after the network is being subjected to disturbance - reach to new steady-state levels that are also sustaining the operational constrains and without unintentional load shedding. Moreover, in a network paradigm that loads are participating as controllable assets [25, 26], intentional load shedding that makes the network satisfy the abovementioned operational constrains is stable. Also, in situation where loads are intentionally tripped to clear faults and not perform load shedding for solely supporting voltage and frequency issues and given that the network satisfies the previously mentioned operational conditions, the network is also considered to be stable.

In the traditional interconnected bulk power network, no individual load operation and energy availability is more crucial than the network whole stability. This is because of the conventional interconnected network vast scale that makes load shedding process an acceptable action to assure the network operation continuity. However, with PEDG paradigm the operator has the liberty to prioritize certain load feeders over the rest of the network loads. For instance, feeders that are delivering power to critical loads such as hospitals, airports, and data centers must have the highest priority in PEDG. Therefore, unlike bulk power system, the intentional load shedding of the critical loads to maintain the PEDG operation render the network to be unstable.

The disturbance in the operation of PEDG is categorized into small or large which in fact can be defined as an external input that is resultant from loads variations, elements failures, or intentional and nonintentional operation mode or operation set-point adjustments. Fortunately, small disturbances can be captured by the linearized state space models and hence such disturbances are classified as small-signal perturbations. On the other hand, the large disturbances cannot be captured by the linearized state space models. Example of such large disturbances are generations loss, short-circuit faults, nonintentional transition from non-islanded to islanded mode of operation. Additionally, both large and small disturbances are further subcategorized into short and long term. For instance, small variations of loads in a heavy loaded network might trigger undamped power oscillations in the long term. In contrary, unbalanced power sharing among power generation assets excites power resonance phenomena that builds up rapidly in short term.

1.2.2. Stability Categorization and Vulnerabilities

Given the distinctive characteristics of PEDG, instabilities associated with voltage or transient operation which are dominant in the bulk power system are not expected to occur in the islanded PEDG. The high portion of stability issues in the PEDG paradigm are related to frequency due to the intrinsic low inertia nature of the system. This indicates the need for a light shedding on vulnerabilities for PEDG stability. Furthermore, stability of a power network in the literatures are classified based on: (i) magnitude of the disturbance causing instability, (ii) duration of the instability, (iii) physical root-cause of the instability, (iv) components caused or involved in the instability, (v) instability analysis approach, and (vi) instability trajectory and prediction approach. Categorizing stability in the PEDG paradigm according to the established stability concept is not simple, as PEDG variables dynamics are strongly coupled. In more details, any instability phenomena in a PEDG will result in oscillations in all the variables. In other words, it would be hard to distinguish voltage instability from frequency instability in a PEDG. Hence, the most logical categorization for instability in the PEDG is based on the origin of the instability. In the next section, considering the scope of this work, normal disturbance, and severe disturbance stability as well as supply demand stability are discussed.

1.2.3. Normal Disturbance and Severe Disturbance Stability

The origin of normal disturbance instabilities is majorly linked to the low damping availability for critical eigenvalues of the network. normal disturbance instabilities can be captured by the linearized state-space model of the network. However, the duration of the small-perturbation instabilities is due to the root cause of the instabilities, disturbance magnitude, inherent nature of the network. For instance, undamped power oscillations are witnessed when poor power sharing among multiple distributed generation occurs; this power oscillations grows quickly violating the operation constrains of the network in short term. On the contrary, small demand and supply change in a heavy loaded network rises undamped power oscillations that take long time to violate the operational constraints.

Instabilities that cannot be captured by the linearized state-space model of the network are considered as severe disturbance instabilities. This type of instabilities originates from amount and location of short-circuit faults, unintentional transition from non-islanded to islanded mode of operation, and generation units' loss. Regarding severe disturbance instability time frame, instability is always a short-term phenomenon. For instance, unplanned islanding makes the system rapidly unstable due to drastic large variations in the frequency and the voltage.

1.2.4. Demand and Supply Stability

Demand and supply balance stability is concerned about attaining the power generation and the required power demand equilibrium with assuring the optimal power sharing among the network energy resources assets, not forgetting, satisfying the network parameters operation constrains. Poor power sharing among multiple energy generation assets, loss of energy generation resources, and unintentional load loss are examples that might originate a demand and supply instability issue.

The stochastic generation nature, small number of conventional generation units, and the low inertia nature of a PEDG make frequency regulation a crucial challenge. For instance, a disturbance, such as loss of a generation unit in the PEDG paradigm, puts the system in risk of high rate of change of frequency occurrence. In fact, even with an adequate power reserve existence, such frequency instability issues in low inertia systems cannot be recovered. Furthermore, in the PEDG paradigm the P-f droop relation does not express the dynamics of the system accurately, since PEDG feeders' short length and low X/R ratio make a strong coupling between frequency dynamics with active power flow as well as voltage dynamics. Any voltage variations at the generation busses reflects instantaneously on the network loads, which indirectly affect the system demand and supply (i.e., system frequency) due to voltage sensitive loads tripping. Furthermore, frequency instabilities originate from various reasons, such as an unexpected huge demand increase without enough generation reserve availability. In such case, with PEDG low inertia, the frequency will decrease abruptly resulting in a blackout that is triggered by the protection relays [27]. Another root-cause of frequency instability in the PEDG paradigm that does not happen in bulk power systems, is poor power sharing among the network energy assets. This poor power sharing results in small perturbation instability for durations ranging from seconds to minutes [28]. The duration of the frequency instability (i.e., short, or long term) is linked to the time that the frequency protection relay is activated. Also, frequency instabilities in PEDG are extended to steady-state operation. For example, for a network operating at its maximum capacity, small variations in the demand might trigger frequency protection relays, which is considered as a long-term frequency instability. On contrary, this long-term frequency instability problem is tackled by controlling the governor valves of the interconnected power system synchronous generators. However, such mechanism is irrelevant to the PEDG paradigm.

PEDG definitions, its characteristics and consequences challenges were discussed in previous sections with details. As the objective of this work is to enhance the PEDG resiliency, a concept of resiliency which mostly covers all PEDG features is provided. Moreover, stability concept in PEDG is reviewed as it is believed that having greater stability boundary can enhance the PEDG resiliency. Categorization and vulnerability of stability challenges were analyzed. Finally, demand supply stability considering normal and sever disturbances were investigated. Thus, as PEDG comprise numerous GFMIs and GFLIs as the main power sources, in the next section, different control modes of these two types of inverters are reviewed and a general description for GFMI and GFLI interaction are studied.

1.3. Interaction of Grid Following and Grid Forming Inverters in PEDG

Moving toward PEDG, it is required to comply with grid's supply-demand balance constraints mostly by power electronic-based renewable resources. Traditional power system is known as a mature system that can offer acceptable stability boundary to cope with most of external disturbances. In fact, power system takes advantages from mechanical features that are involved in control loops for maintaining the stability margin. Although, they are vulnerable to some severe disruptions but commonly they can provide a kind of reliable operation. However, due to the practical evolution that are being occurred from traditional power system to PEDG, most of system's mechanical characteristics are noticeably lessened.

Thus, in low-inertia PEDG, it is crucial to compensate these missed and essential attributes for sustaining the system stability. Basically, by substituting synchronous generators with more power electronic based resources, total kinetic energy of the system is demoted. This momentary and available reserved energy, which is due to the rotation of SG shaft, could be used to support system during short but severe transients' periods as the control loops needs this short period to take up their output to meet new operation point of the system. Based on the contemporary improvements in control schemes of power electronic based resources, it is attainable to emulate similar features of traditional power system to extend new energy paradigm's stability boundary particularly during grid severe disturbances. However, new, and several control and stability challenges come up here, when numerous control loops are interacting with each other in PEDG. As PEDG comprise several grid following inverters (GFLI) and grid forming inverters (GFMI), in this section, some thoughts regarding different aspects of these two inverters are provided. Primarily, GFLIs act as current sources that follow the grid's voltage and GFMIs act as voltage source that shape the grid's voltage and frequency. GFLIs effectively can contribute to support and control the grid's demands while follow the voltage of the grid. However, GFMIs can mimic a synchronous machine dynamic that actively interacts with grid's loads based on the power balance fundamentals. For example, the *p-f* droop in GFMIs approximately emulates swing equation in power electronic based systems. Moreover, this emulation can be more accurate if GFMI control loops directly are shaped based on the swing equations of SGs which in this case are called as virtual synchronous generator (VSG). Figure 1. 3 and Figure 1. 4 depict a generic illustration of GFMI and GFLI respectively. As shown, GFLIs mainly control the injected active and

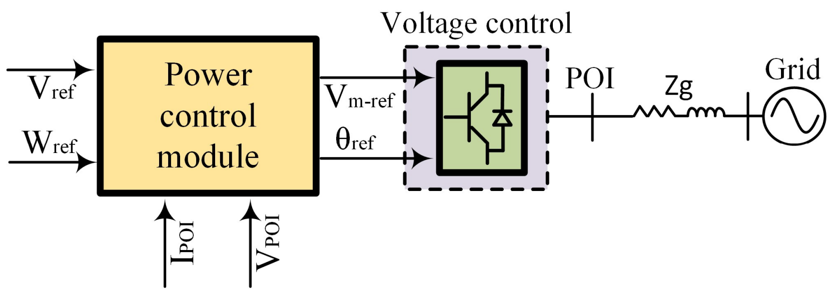

Figure 1. 3. Generic example of a basic grid forming inverter.

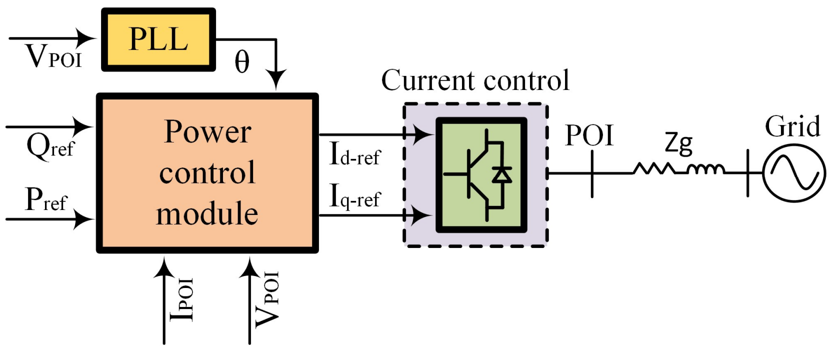

Figure 1. 4. Generic example of a basic grid following inverter

reactive powers to the grid while follow the grid's voltage angle but the GFMIs shape the grid voltage and frequency by following the required grid's demand. As shown, having a phase-locked loop (PLL) in the control schemes of GFLIs are requisite. Nevertheless, if the grid has a large impedance which is known as weak grid, PLLs can jeopardize system stability boundary [29, 30]. Certainly, increasing the number of GFLIs in PEDG can resonate this drawback. Plausibly, the experts have decided to increase GFMI's contributions in the new energy paradigm as they independently can form a grid based on frequency and voltage magnitude reference values. However, this fact will bring up some other technical challenges such oscillatory dynamic and power circulation among GFMIs. Based on the fundamental of electrical circuits, GFLIs can be modeled as a current source with shunt

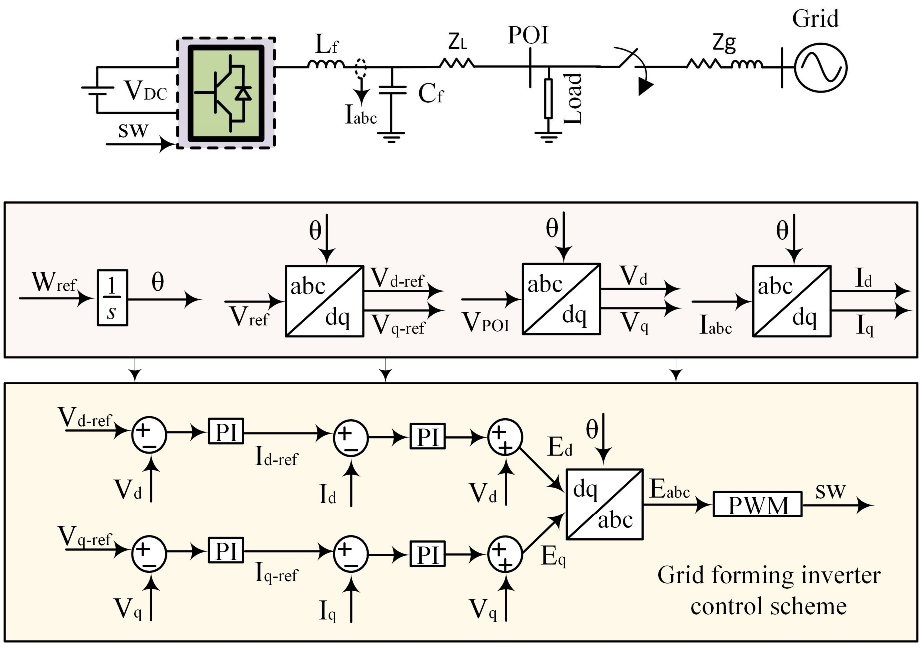

Figure 1. 5. Fundamental control scheme of a grid forming inverter

impedance at the point of interconnection (POI) with the grid. However, using the Thevenin rule, a current source can be demonstrated with a voltage source that is in series with an impedance. In Figure 1. 5 and Figure 1. 6, the fundamental control loops of these two inverters are illustrated. A mentioned before, GFMIs follow the grid's demand while form the voltage and frequency of the grid based on the predefined reference values. To emphasize the notion that a GFLI needs to have the grids' voltage angle to inject the predefined active and reactive power, Figure 1. 6 provides a basic methodology for generating the voltage angle that should be followed by GFLI. As shown, the q-component of the voltage is passed through a PI controller and the grid frequency is added as feed forward to this loop. By integrating the result, the angle is captured. By comparing this stage in GFMI, it is realized that by integrating the reference frequency, the angle is captured forthrightly. Moreover, the manner that control loops are presented can intuitively reveal a kind of similarity in the rest

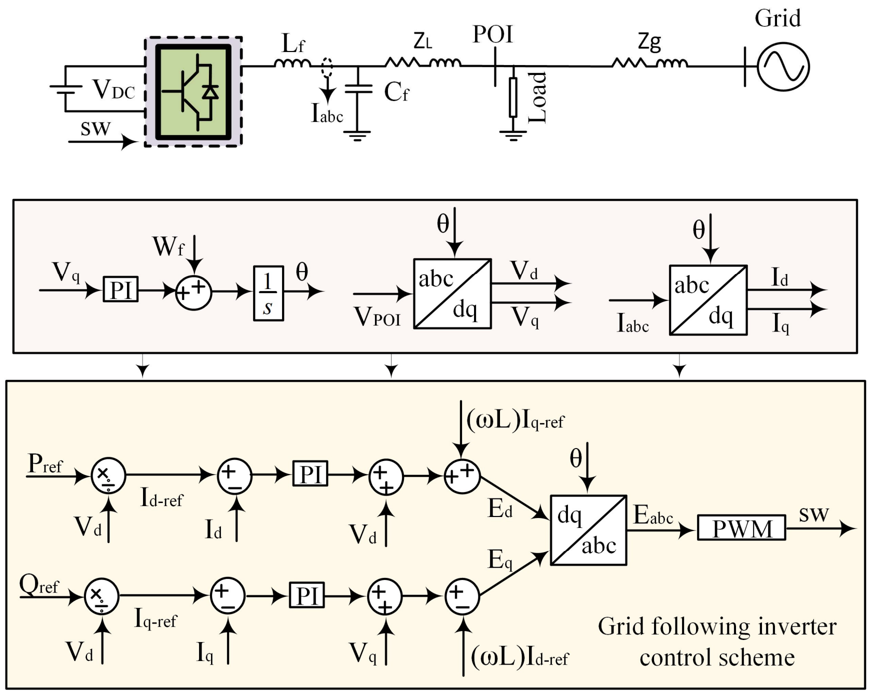

Figure 1. 6. Fundamental control scheme of a grid following inverter

of control loops. This concept is valid even if the details of these control loops are studied such as comprising output power measurement and processing modules, different droop-based curves and swing based equations. Figure 1. 7and Figure 1. 8 show a detailed and more comprehensive control loops of these two inverters. Should be noted that, Figure 1. 8 illustrates a VSG based control for GFMIs which mimics the power balance and field voltage control loops in SG. Analyzing these two controls schemes, reveals high similarities between these two inverters as well. Interestingly, deploying any other varieties of controls will reach to the same conclusion. Thus, as an initial guess, these two distinct varieties of inverters can be converted to each other while some researchers believe they are completely of different type. There are some studies that have focused on discovering some sort of resemblances in behavior of these two-inverter structure while interacting with each other. What is imperative

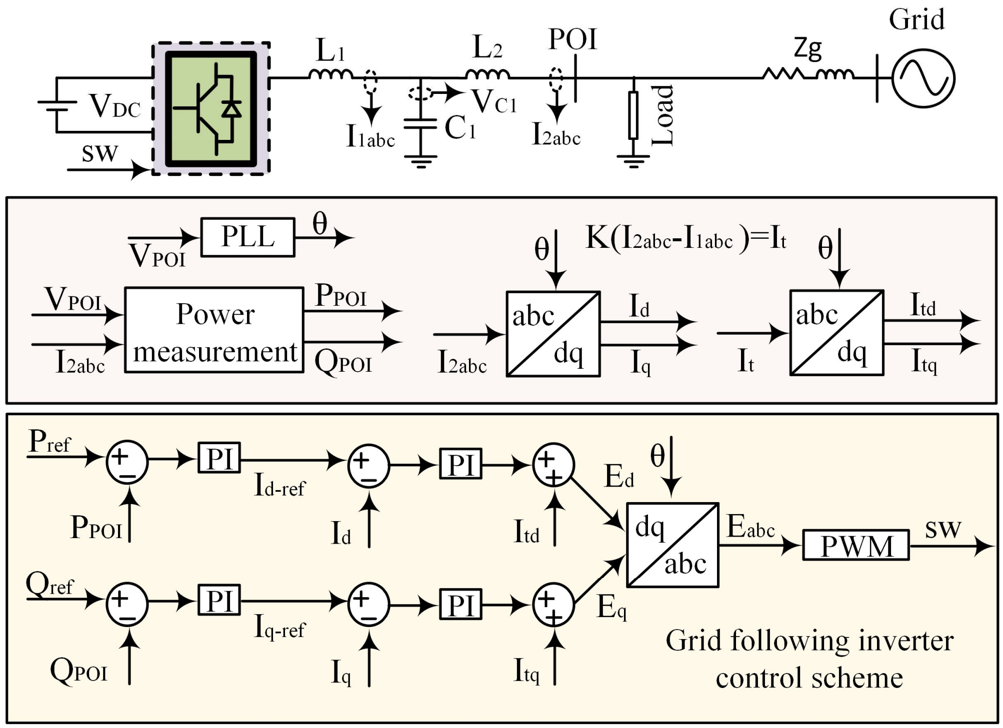

Figure 1. 7. Comprehensive control loop of a grid following inverter

here is to find their basic dynamic response similarities and interactions. If this is proved, some new prospects will come up that can be useful specifically in operation methodologies of the PEDG during transient periods. Thus, if a GFMI could effectively support the grid during severe disruptions why GFLIs have not been considered in this critical stability issues. Moreover, if a GFMI can operate in islanded mode, why this ability is not scrutinized in GFLIs. Undoubtedly, by accepting the conventional belief that declares that these two inverters are basically different, their applications will be restricted in term of grid supporting and resiliency enhancement of the PEDG. For instance, GFLIs can be regulated easily due to their relatively simple control schemes. However, with conventional idea, they are not able to shape grid's frequency and voltage. Moreover, they have some drawbacks to be operated in standalone mode or if the grid has large impedance. On the other hand, GFMIs

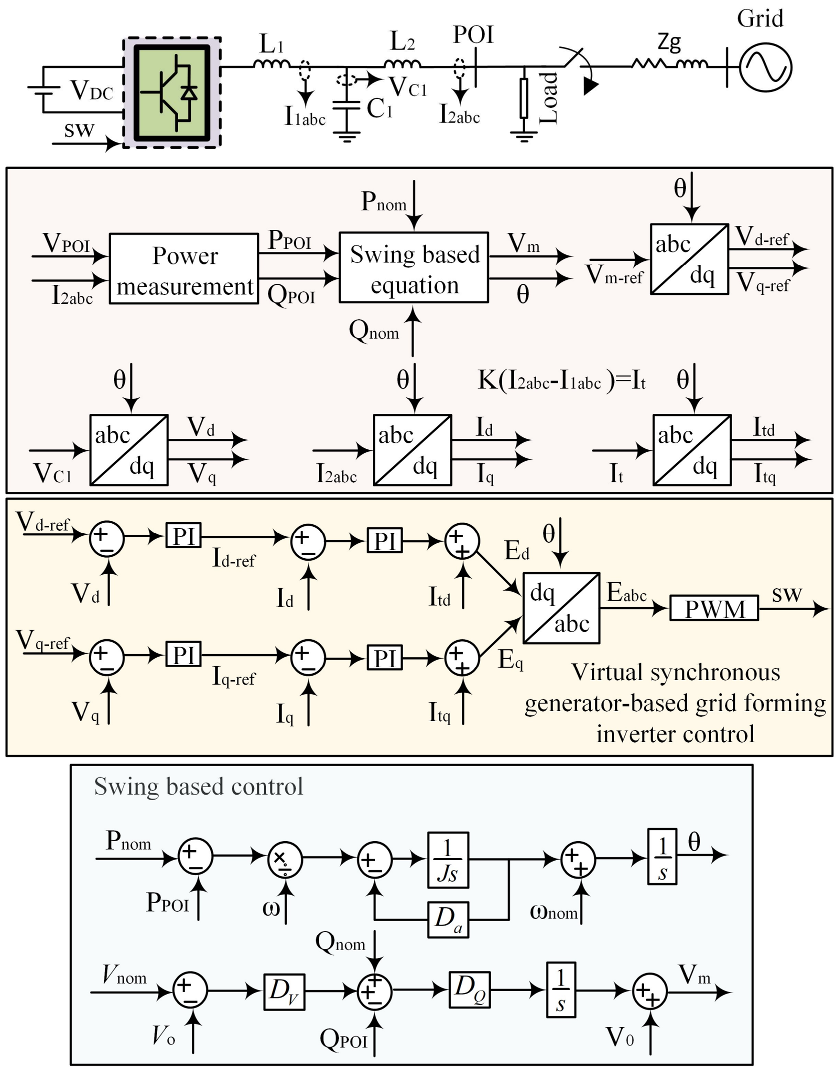

Figure 1. 8. Comprehensive control loop of a virtual synchronous generator-based grid forming inverter

will encounter with some stability issues if they are tied with a stiff grid while they can have acceptable functionality if they are supporting an islanded cluster of a grid. Also, as mentioned before, GFMI will have some challenges regarding power sharing among themselves or if they experience a sever disturbance, their functionality would be downgraded considerably[31]. However, by benefitting from each advantage of GFMIs and GFLIs and considering the improvements in control and measuring devices, they can shift their responsibilities in grid supporting if their similarities are discovered accurately. In chapter 3 of this dissertation, the dynamic response similarities between these two inverters for some commonly used control schemes are discovered mathematically. Later, by deriving this observation and integrating a novel artificial intelligence-based technique, GFLIs are exploited as available grid supporter resources during severe transient periods while the GFMIs drawbacks are sidestepped. The next section details the problem statements and the proposed approaches in this dissertation.

1.4. Problem statement and the proposed approaches in this dissertation

This dissertation focuses on developing Artificial Intelligence (AI)-based and self-healing control techniques to enhance the resiliency of active distribution networks, particularly during normal and severe grid disturbances. Developed smart control methodologies enhance control layers' functionalities with different time scales that are being exploited in the modernized power grid. In power electronic dominated grids (PEDG), the total system inertia is lessened significantly, and thus frequency and voltage stability boundaries can be jeopardized during grid disturbances. Hence, in the first stage of this work, it is intended to facilitate battery energy storage systems (BESS) with high bandwidth control techniques to effectively contribute to grid resiliency enhancement. BESS locally supports different grid points and extends the stable boundary of the entire power system. This effort will be more beneficial if the grid is confronted with some sort of severe disturbances. In this dissertation, the designed primary control layer improves the functionality of battery energy storage systems by employing a novel model predictive self-healing control (MPSC) scheme. This control technique heals intrinsic drawbacks in common control approaches utilized for BESS by decreasing the potential errors in the control processes. In other words, the proposed control scheme improves the dynamic behavior of the charging and discharging process during any potential grid disturbances. However, the frequency restoration process needs more advanced techniques due to the high nonlinearity low- inertia of the PEDG. Therefore, it is necessary to develop an artificial inspired technique to realize a self-learning control scheme with ultra-fast frequency restoration via maximizing the existing grid's source capabilities.

PEDG comprises several grid-forming (GFM) and grid-following (GFL) inverters to achieve the most important grid's stability constraint, i.e., supply-demand balance in all operation time. Thus, the next step in this dissertation focuses on maximizing the grid following inverter capabilities to enhance grid resiliency. In fact, involving more GFLIs in frequency and voltage restoration, decrease the existing challenges of GFMIs during sever disturbances. An artificial intelligence-based power reference correction (AI-PRC) mechanism is designed and developed for GFLIs to autonomously adjust their predefined power setpoints during potential disturbances. A detailed mathematical proof is presented to demonstrate that the GFM and GFL inverters' control rules and their interactions fundamentally follow the underlying dynamic of the swing-based machines to extend the stability boundary of low inertia PEDGs. Considering this fact, comprehensive transient and steady state-based mathematical models that can deal with all grid's characteristic alterations are used in this dissertation. The concept of this dynamic model is exploited to construct a thorough learning database that includes all grid physical features such as feasible alterations in PEDG configurations, demand and supply side disturbances, a wide range of inertia constants, grid's natural and damping frequency as well as the optimal injecting/absorbing power to/from the grid. The proposed approach incorporates all PEDG's effective variables for shaping the dynamic response during potential disturbances. Subsequently, a neural network is trained by deploying a Bayesian regularization algorithm (BRA). BRA improves the learning process when there are some limitations in the training data such as data size, noise levels, and the uncertainties of the trained network's inputs. In the training process, the constructed mathematically based learning data is employed, and the entire AI-PRC module is implemented in the control loop of GFLIs to adjust their pre-defined power references in real time based on the grid's disturbances. The AI-PRC receives frequency, and rate of change of frequency (ROCOF) as input measurements and provide a power adjustment for GFLI set points in a way to maximize their contribution to the frequency restoration process in transient and steady state periods. The proposed method was evaluated by MATLAB simulation on the 14-bus PEDG; the results attested to the promising functionality of the proposed technique. To assess the proposed technique's functionality in a more realistic condition, a hardware setup was developed. In this setup, two three-phase inverters have been used. Inverters' control cores are based on the model predictive control approach. To mimic the real dynamic of a PEDG, one of the inverters is operated as the grid forming, and the other one acts as a grid following source. Hardware test results have shown that, by activating the AI-PRC mechanism in the GFLI control loops, frequency is restored fast and smoothly during any potential disturbances. Also, the proposed approach was compared with other frequency restoration techniques. In all comparisons, the priority of the proposed approach was attested. Taking into consideration that in a relatively big network such as our system, it is crucial to evaluate results in a real-time simulator and observe the real dynamic of the system parameters. Hence, the understudy 14-bus PEDG was modeled in an OPAL-RT simulator. Attained results proved the promising functionality of the AI-PRC mechanism, particularly during the grid's disturbances.

In the new energy paradigm, cyber-attacks are recognized as a dangerous phenomenon that can undoubtedly jeopardize the grid's stability constraints[32]. Therefore, the proposed control technique is exploited as a shadow controller for the case that the attacker aims to threaten the entire grid stability via stealthy attacks. Stealthy attacks diverge the state variables before their consequences are propagated into the grid's global and measured variables. Therefore, they can endanger the system's demand-supply balance if not detected and controlled in a short time. In this work, a detail of stealthy attacks and the attacker approaches to generate these kinds of attacks are provided and discussed. Later, some stealthy attack scenarios are investigated on the 14-bus PEDG. The results have proven the effectiveness of the proposed approach in fast reacting in the event of a stealthy attack, thus the grid resiliency is enhanced in this case as well.

Based on the importance of power grid stability, it is crucial to have another layer of control that monitors the grid dynamic and vital variables in other time scales. For any reason, if any control approaches fail due to any type of cyber-attacks, the designed ultra-fast load forecasting methodology will take proactive action to maintain system stability. The groundwork of this control layer is based on the load forecasting procedure which take advantage from artificial intelligence approaches. In this work, an anomaly detection technique based on a condition monitoring vector and ultra-short demand forecasting is designed and developed for achieving the mentioned goal. Temperature data and historical loads are the input of this technique. According to the high level of safety in historical load and temperature data and the employed AI-based in the core of this technique, it is claimed that the designed intrusion detection system (IDS) is more robust against attack scenarios. The supervisory layer can forecast the load in a short duration several times across the network and compare it with real-time data. The designed condition monitor vector acts based on a defined upper and lowers bound. These bounds are defined based on the acceptable and inherent tolerances in forecasting processes and measurements and will be able to make the final decision to isolate an area, flag an area or confirm the safety level of grid operation.

Chapter 2

2. Battery Energy Storage System- Primary Control Layer

Parts of this chapter, including figures and text, are based on my following papers:

- M. Hosseinzadehtaher, A. Khan, M. Easley, M. B. Shadmand and P. Fajri, "Self-Healing Predictive Control of Battery System in Naval Power System with Pulsed Power Loads," in IEEE Transactions on Energy Conversion, vol. 36, no. 2, pp. 1056-1069, June 2021.
- M. Hosseinzadehtaher, A. Khan, M. W. Baker, and M. B. Shadmand, "Model Predictive Self-Healing Control Scheme for Dual Active Bridge Converter," 2019 2nd International Conference on Smart Grid and Renewable Energy (SGRE), 2019, pp. 1-6.

2.1. Self-healing Predictive Control of Battery Energy Storage Systems

In this section, a primary control layer is proposed which enable a low-inertia power system (LIPS) to provide fast response regarding grid's disturbances. Thus, a model predictive self-healing control (MPSC) scheme is designed for battery system interfaced dual active bridge (DAB) converter in a LIPS that experience sever disturbances. The voltage and frequency of the understudy LIPS are vulnerable to load energization. A properly controlled battery system with fast dynamic response can mitigate this vulnerability. Model predictive control (MPC) is a potential solution for the battery system interfaced DAB converter to achieve fast dynamic response and mitigate disturbances imposed to the grid. However, conventional MPC framework suffers from current prediction error due to the pulsating AC-link inductor's voltage profile in DAB converter. This work proposes a self-healing control loop that utilizes the feasible range of power transfer in conjunction with the AC-link inductor's voltage profile. The proposed method can validate and autonomously correct the predicted current and phase shift in DAB converter interfaced a battery system. The devised control scheme on DAB converter prevents voltage and frequency collapse in a hybrid AC/DC LIPS particularly during sever load disturbances occurs periodically which can be a threatening phenomenon for a hybrid AC/DC LIPS. The system stability is studied based on Lyapunov stability analysis. The theoretical concepts are validated by several case studies implemented on a hardware-in-the-loop (HIL) testbed of a small scaled-microgrid. The case studies demonstrate voltage and frequency regulation of the understudy system with fast dynamic response during sever disturbances. The proposed MPSC performance is compared with proportional-integral (PI) based control to highlight the priority of the proposed control approach.

2.2. Literature Review

Hybrid AC/DC LIPS commonly consists of loads with different behaviors. Some of LIPS' loads do not have significant fluctuating patterns, which are considered steady-state loads. However, others require large amount of energy in a very short duration that can behave as a sort of pulsed power loads (PPLs) such as electromagnetic guns, electromagnetic aircraft launch systems, free electron lasers, radar, and sonar [33]. Thus, due to existence of PPLs, the transient stability of LIPS should be considered when designing their control schemes [34-36]. Due to the inherent slow dynamic response of synchronous generator in LIPS, considerable voltage and frequency deviations occur due to PPLs energization. If not properly addressed, the undesired voltage and frequency deviations can cause collapse of the voltage sensitive loads or even the whole LIPS.

Energy storage systems (ESS) such as battery banks and super-capacitors are typically used in LIPS for mitigating the voltage and frequency fluctuations due to PPLs [37-39]. Dual active bridge (DAB) converter is known as a proper power electronics interface for ESS in response to fast transient loads (FTLs) [40, 41]. Due to periodic sudden changes of FTLs which requires frequent charging and discharging of ESSs, a high efficiency power conversion unit, such as DAB converter, is recommended [42]. Although the DAB converter features can be leveraged for ESS to realize fast restoration of voltage and frequency in LIPS, but the drawback of this converter is its control complexity [43]. Several control schemes have been proposed in literature for DAB converter. A voltage control with power balancing

Table 1. Existing DAB Converter Control Approaches

Control Objective	Features	Drawbacks
Voltage and Power Balance Control for a Converter-Based Solid-State Transformer.	• Regulating the DC-Bus voltage and determining the proper phase shift. • Balancing the rectifier capacitor voltages and the real power through parallel DAB modules.	• Slow dynamic response • Vulnerable to fail in response to fast transient loads • large changing in the operation point cause malfunction for the control scheme
Modeling and Control of a Resonant Dual Active Bridge with a Tuned CLLC Network.	• Regulating the phase shift and resonant tank currents in this system for transferring the power. • Fast simulation • Using dq framework to convert all AC state variables to DC states • Improving the soft switching range of the converter.	• All challenges related to PI-controller tuning • Changing the operation point will make problem for tuning
Optimized Phase-Shift Modulation for Fast Transient Response in a Dual-Active-Bridge Converter.	• Proposing a modified asymmetric double-side modulation for the aim of improving the dynamic response. • Minimizing the settling time of the inductor current	• Converter gain should be available • It has not been tested for close loop system with large load variation
Fast Transient Boundary Control of the Dual Active Bridge Converter Using the Natural Switching Surface.	• Improving dynamic response to sudden load changes • Curved switching surface has been presented for control of DAB converter • Fixed-frequency operation • Optimizing the design of the high-frequency transformer	• The step change is small (less than 4 amperes) • Fast transient response is for startup not for large loads • No guarantee to work with large load pulsation
Enhanced Load Step Response for a Bidirectional DC–DC Converter.	• Minimizing the DC-Bus capacitance • Utilizing harmonic modeling strategy	• linearized model will have challenges facing with large disturbance • Tuning effort of PI-based controller can be challenging • The controller gain will not be remained valid for different operation points.

mechanism is proposed in [44] for solid state transformer (SST) based on parallel DAB modules. The proposed PI based control scheme regulates DC-Bus voltage and determines the proper phase shift. In [45], power transfer in resonant DAB converter is enabled by regulating the phase shift and resonant tank currents in this system. To make the control process easier, the authors have used a *dq* framework to convert all AC state variables to DC states with slow dynamics. Hence, for controlling phase shift and tank currents, three PI controllers are used. It is worth mentioning that the DAB converter highly-nonlinear plant for a PI controller results in slow dynamic response which may fail in response to fast transient loads such as PPLs [46]. The transient response of a single-side modulation and symmetric double-side modulation of a DAB converter are studied in [47]; a modified asymmetric double-side modulation is then proposed for improving the dynamic response. In [48], a curved switching surface has been presented for control of DAB converter for improving dynamic response to sudden load changes. Furthermore, the authors of [49], have provided a method for enhancing the transient response of DAB converters to sudden load disturbances by utilizing harmonic modeling strategy. However, the downside of these PI-based control methods are tuning effort and the assumptions that the controller gain will remain valid for different operation points as the equilibrium point changes. These available controllers along with their features and drawbacks are summarized in Table 1

Model Predictive control (MPC) is one of the attractive control approaches in power electronics applications that has been widely used in industry and academia [50, 51]. This is due to MPC fast dynamical response and ability in solving multi-objective constraints optimization problems with substantially less effort in gain tuning or re-tuning process compared to linear controllers [52-56]. Moreover, for the DAB converter, very few MPC frameworks have been reported in the literature due to challenges associated with design of MPC for DAB converter. In fact, unlike MPC of other power electronics application, conventional MPC framework is not applicable for DAB converter and requires modification in the algorithm. For instance, [57] introduces a predictive control approach that eliminates transient dc offset currents that have been superimposed on the high frequency transformer currents in one switching cycle. This protects the high frequency transformer from reaching saturation. However, this approach is based on increasing the control bandwidth which is a challenging requirement for application of MPC on DAB converter for PPLs. Authors in [58] have introduced a moving discretized-control-set MPC approach for DAB converters. The purpose of this control approach is to regulate load voltage of the DC microgrid and minimize the DAB converter high frequency transformer peak current. However, the MPC model is based on simplified DAB averaged model that is subjected to inaccuracies given DAB converter's high nonlinearity. Therefore, up to the best knowledge of the authors, the limited existing MPC frameworks are not best fit for the DAB converter in applications such as PPLs and this is due to DAB topology and its non-linear behavior specially when an accurate prediction of AC link inductor current is required. Thus, the main contribution of this work is to address the challenges associated with design of MPC framework for DAB in LIPS in response to voltage and frequency deviations due to FTLs energization.

This work proposes a novel model predictive self-healing control (MPSC) for DAB converter in LIPS with FTLs [59]. The proposed controller takes advantage of the full model of the DAB converter as opposed to using the average model to regulate the DC-bus voltage and frequency of the LIPS. The proposed control scheme predicts the AC-link inductor current for one-step ahead in horizon of time. There are periodic pulsations in high frequency AC-link inductor's voltage which extremely decrease current prediction accuracy; therefore, two validation modules are developed in this control scheme for correcting the AC-link inductor current. The inductor voltage is monitored by the first validation module and the power transfer is checked to be in the feasible range by the second validation module. The proposed control framework is developed based on root-finding algorithm. The proposed MPSC for DAB converter does not require significant tuning effort compared to conventional PI-based control. The self-healing feature of the MPSC enhances the dynamic performance of controller particularly for extreme FTLs. The fast-dynamic feature of the proposed MPSC ensures the LIPs voltage and frequency stability and maximizes its resiliency in response to extreme FTLs.

2.3. Hybrid AC/DC Low Inertia Power System: An Overview

A proper and practical representation of a hybrid AC/DC low inertia power system can be found in ship power systems. These power systems basically are shaped based on radial architecture and the loads are supplied by separate generators. As an example of a well-known LIPS which has this power system architecture is SS Canberra. The propulsion systems are supplied by generators with around 32MW capacity while for services loads, the scale of generator can reach to around 1MW [60-62]. Also, some ships use integrated power system (IPS) architecture for their propulsion and services loads; as an example, Queen Elizabeth II has IPS architecture in its power system. The distribution part is operated at 10kV. However, for supplying some services loads, this voltage level is decreased by a step-down transformer. Some cruise ships, ferries and vessels follow the IPS architecture with different voltage level in distribution part for increasing the efficiency [60-67]. AC zonal electric distribution is another architecture that has been proposed for improving the reliability and efficiency of this type of power system and is known as modern power system for ships [68-70]. Also, a DC zonal electric distribution has been considered by Electric Ship Research and Development Consortium (ESRDC) [64, 70]. These two recent types of power system separate the whole system to different zone with independent power supplies. In this

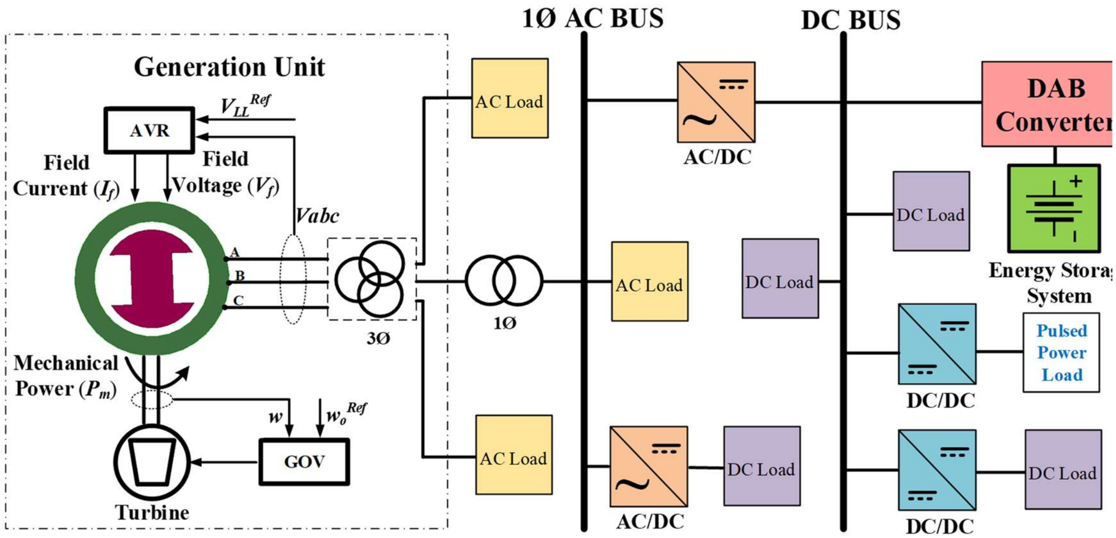

Figure 2.1. The considered low inertia power system.

work, we have followed this approach to form an AC and DC-Buses representing a hybrid zone of a common navy ship power system. Figure 2.1 shows the considered hybrid AC/DC LIPS in this work. The major elements include synchronous generator unit, ESS interfaced DAB converter, AC loads, DC loads, PPLs, single and three-phase transformers, etc. A synchronous generator supplies the system loads in steady state. Thus, due to slow dynamic response of the main generation unit, any significant change in the system loads such as FTLs energizing, causes a frequency and voltage deviation and consequently lead to instability in the system. The synchronous generator is controlled by two controllers: automatic voltage regulator (AVR) and load frequency control (LFC). A three-phase transformer steps up voltage for supporting medium-voltage loads in LIPS; these loads are energized independently in the system as shown in Figure 2.1. A single-phase transformer energizes the AC-Bus to supply single-phase loads and DC-Bus through a DC/AC converter forming

Table 2. Synchronous Generator Specifications.

Parameter	Value
Output Voltages	460V
Nominal Power	10.2 kVA
Frequency	60 Hz
Inertia coefficient	0.0923 $kg.m^2$
Inertia constant	13117.8 $kg.m^2/sec$
Pole pairs	2
Friction Factor	0.0125 N.m.s
Nominal Rotor Speed	1800 RPM

a hybrid LIPS. The ESS interfaced DAB converter is connected to the DC-Bus of the LIPS supplying the FTLs.

2.3.1. Root Cause of Voltage and Frequency Deviation

The considered synchronous generator specifications are provided in Table 2. The three-phase synchronous generator has been modelled in the *dq* rotor reference frame and stator windings are connected in wye to an internal neutral point [71]. The two control loops of the synchronous generators regulate the output terminal voltage and the frequency. Based on the synchronous generator fundamentals, if for any reasons, the output-power changes suddenly, the whole system frequency will be affected. The root-cause of this issue can be observed by the swing equation. The rotor motion equation is given by,

$$\theta_m = \omega_s t + \delta_m \tag{2.1}$$

where θ_m is defined as the angular position of the rotor with respect to a stationary axis, ω_s is the synchronous speed and δ_m is the angular position with respect to the synchronously rotating reference frame. Thus, the swing equation is given by,

$$P_m - P_e = \omega_m J \frac{d}{dt}\left(\frac{d}{dt}(\omega_s t + \delta_m)\right) \tag{2.2}$$

where P_m, P_e and ω_m are the mechanical power, electrical power, and angular velocity of the rotor, respectively. It should be noted that $\omega_m J$ is defined as the inertia constant of machine at synchronous speed of ω_s. The angular momentum of the rotor at synchronous speed is calculated as Jw_s^2. Where J is the inertia coefficient and w_s is the synchronous speed. The inertia constant in this work is 13117.88 kg.m^2/sec which indicates that the synchronous machines have considerable inertia. Based on (2.2), the system frequency is vulnerable to sudden changes in power demand due FTLs. The rate of frequency change highly depends on inertia constant of the machine. In this work, a three-phase PLL is used to obtain the instantaneous frequency; and this value is compared with a desired value and regulated via a PI controller. Furthermore, the generator output voltage is sensitive to load disturbances. By triggering the PPLs, the frequency of the system decreases. In fact, the frequency of the system is related to rotor speed. When the rotor speed decreases, the internal voltage of synchronous generator changes. The induced internal voltage of the generator in a given stator is defined as $k\o 2\pi f$, where k is a constant related to the structure of the machine, ø is the flux, and f is the frequency. For increasing the internal voltage, the AVR should increase the flux by increasing the field current. However, after a certain value of the field current, the relation of the flux and the field current will not be linear. Therefore, if the load changes suddenly and the frequency drops considerably, the output voltage of synchronous machine will be affected by this event. Thus, commonly the generator field voltage is controlled via AVR.

2.3.2. Proposed Control Scheme Principle for ESS based DAB

This section provides a brief overview of the proposed MPSC, the detail control formulation is provided in Section 2.4. The block diagram of the proposed MPSC scheme for DAB converter is depicted in Figure 2.2. A DAB converter consists of two H-bridges

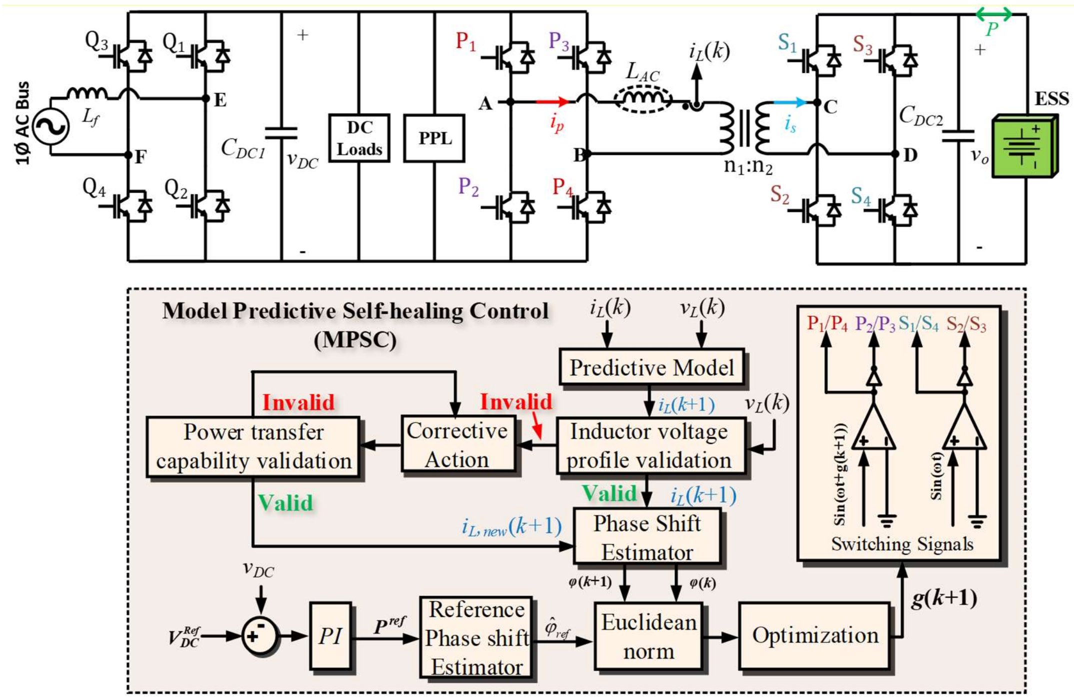

Figure 2.2. Structure of the proposed control scheme for dual active bridge converter.

connected through a high-frequency transformer. The main control goal for DAB converter is to impose a phase shift between the high frequency transformer terminal voltages to permit bidirectional power flow.

The MPSC process is initiated by the AC-link inductor current prediction, and it ends by an accurate estimation of desired phase shift to obtain the optimum switching signal. The initial estimation of the phase shift is carried out by a PI controller when required power by ESS is calculated for regulating DC-Bus voltage. The distinctive features of the proposed controller are the two validation modules to heal prediction errors and maximize the accuracy of the phase shift estimation. The first validation module evaluates the inductor current prediction by monitoring the AC-link inductor voltage for potential prediction errors. If the

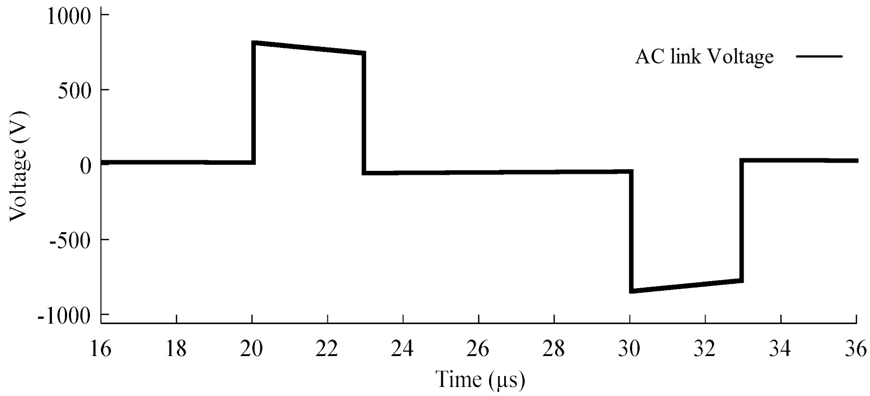

Figure 2.3. Typical voltage waveform of dual active bridge converter's AC-link inductor.

first validation module detects that the current prediction is not valid, then a corrective action and consequently second validation module are triggered.

The second validation module notion is built on the synergy between the power transfer capability of DAB and the value of the phase shift. The corrective action to heal the predicted current occurs between first and second validation modules, once the healing is processed, the resultant predicted current will be sent to second validation module. This process is repeated in an iterative manner to compensate the current prediction and consequently estimate an accurate phase shift.

The validated predicted AC-link inductor current is used to estimate the phase shift for one step ahead in horizon of time $\varphi(k+1)$. The phase shift optimum value is obtained by comparing $\varphi(k)$ and $\varphi(k+1)$ with respect to $\hat{\varphi}_{ref}$ value which is determined by minimization of the Euclidean norm. This optimal phase shift is used to realize the switching signals. The detailed theoretical analysis and mathematical formulation of this self-healing process for the proposed control scheme is provided in the next section.

2.4. Model Predictive Self-Healing Control

2.4.1. Self-Healing Mechanism

As mentioned in the previous section, the self-healing mechanism consists of two validation modules. In the first module, inductor voltage is monitored for detecting the potential error in the predicted AC-link inductor current. Figure 2.3 depicts the AC-link voltage in one period with an arbitrary phase shift. The output of this module is defined as binary valid and not-valid sections based on the AC-link inductor voltage profile. Considering the relation between AC-link inductor voltage and current and using Euler approximation method, the current of the AC-link inductor for one-step ahead is given by,

$$i_L(k+1) = \frac{v_L(k)}{f_s L_{AC}} + i_L(k) \tag{2.3}$$

where f_s is sampling frequency, $v_L(k)$ and $i_L(k)$ are the AC-link inductor voltage and current respectively. To detect valid and not-valid sections, the AC-link inductor L_{AC} minimum and maximum voltages are given by,

$$\begin{aligned} v_{L_{\max}} &= v_{AB} + \frac{n_1}{n_2} v_{CD} \\ v_{L_{\min}} &= -v_{AB} - \frac{n_1}{n_2} v_{CD} \end{aligned} \tag{2.4}$$

If none of the voltages in (2.4) are detected, it means there is no prediction error and this validation block sends a binary digit “1”; hence, the controller goes ahead to select the optimum switching. However, if one of the voltages in (2.4) is detected, it means that there is an error in prediction process and the output of this block will be a binary digit “0” and the second validation module triggers the corrective action mechanism for mitigating the prediction error. The corrective action is based on an incremental adjustment and is given by,

$$i_{L,new}(k+1) = \frac{v_L(k)}{L_{AC} f_s} + \beta \times i_{L,old}(k+1) + i_L(k) \tag{2.5}$$

where β is decreased in each iteration incrementally. This process is repeated until the power transfer capability module verifies the predicted current.

The DAB converter's power transfer ability is the basis of the second validation module. A brief overview of power transfer fundamental of DAB is provided to clarify the necessity of this validation module. The power transfer fundamental of DAB is similar to power transfer in power system given by,

$$p_r = \frac{v_s v_r}{x} \sin(\delta) \tag{2.6}$$

where v_s and v_r are sending and receiving-end voltages, and δ is the difference of the angle of Bus voltages. This equation shows that current direction and magnitude are controlled by adjusting the voltage angle (δ). The concept is used to develop power transfer in DAB converter; though, there are some differences between power transfer in power system and DAB converter. The DAB converter operates at high frequency while the power system operates at a relatively low frequency, i.e., line frequency.

Another difference is the square shape voltage of the primary and secondary side of the transformer in DAB converter. Furthermore, the AC-link inductor of the DAB converter can be regarded as the line inductance of (6).

Using (6) in per-unit system and applying aforementioned differences on DAB converter power transferring principle, the DAB converter's AC-link inductor current is as (7),

$$i_L = \frac{v_{CD}}{x}\varphi\left(1-\frac{\varphi}{\pi}\right) \tag{2.7}$$

Thus, the power transfer in DAB converter is given by,

$$p_o = \begin{cases} \left(\frac{n_1 v_{AB} v_{CD}}{n_2 x}\right)\left(\varphi - \frac{\varphi^2}{\pi}\right) & \forall \varphi \in \left[0, \frac{\pi}{2}\right] \\ \left(\frac{n_1 v_{AB} v_{CD}}{n_2 x}\right)\left(\varphi + \frac{\varphi^2}{\pi}\right) & \forall \varphi \in \left[-\frac{\pi}{2}, 0\right] \end{cases} \tag{2.8}$$

where (v_{AB}) and (v_{CD}) are DAB terminal voltages and φ is the phase shift between these voltages. One unique aspect of the proposed control scheme is the validation module which is independent to the DAB converter voltage magnitude and the AC-link inductors value – resulting in a dynamic power transfer capability for the MPSC realization. This is tackled by defining a new variable ξ which normalizes the power transfer equation in (8) by,

$$\xi = \frac{n_2 p_o x}{n_1 v_{AB} v_{CD}} \tag{2.9}$$

thus, the normalized power transfer is given by,

$$\xi = \begin{cases} \left(\varphi - \frac{\varphi^2}{\pi}\right) & \forall \varphi \in \left[0, \frac{\pi}{2}\right] \\ \left(\varphi + \frac{\varphi^2}{\pi}\right) & \forall \varphi \in \left[-\frac{\pi}{2}, 0\right] \end{cases} \tag{2.10}$$

Equation (10) shows that there are two regions of operation for power transferring in DAB converter. When $0 \le \varphi \le \pi/2$, the power is transferred from DC-Bus to ESS; otherwise, the power direction is reversed and flows from ESS to DC-Bus. Equation (10) is the mathematical explanation of power transfer capability module which is used in self-healing loop and is depicted in Figure 2.4.

The output of corrective action process is validated via the determined feasible operation range of DAB converter – power transfer capability. The phase shift between the high frequency transformer terminal voltages of DAB converter is determined by,

$$\varphi(k) = \frac{\pi}{2}\left(1 - \sqrt{y(k)}\right) \tag{2.11}$$

where,

$$y(k) = \left(1 - \frac{8\,p(k) n_2\, L_{AC}\, f_{sw}}{n_1\, v_{AB}\, v_{CD}}\right) \tag{2.12}$$

where n_1 and n_2 are the transformer turns ratio. Hence, the criterion for power transfer capability module is formulated using (2.8), (2.11), and (2.12). The criteria function is given by,

$$f_t(k) = \left(\frac{8\,p(k)\, n_2\, L_{AC}\, f_{sw}}{n_1\, v_{AB}\, v_{CD}}\right) \tag{2.13}$$

The satisfactory range of $f_t(k)$ can be determined by solving (2.11) for its feasible range of $-\pi/2 \le \varphi \le \pi/2$. This results in the valid range for $f_t(k)$,

$$-3 \le f_t(k) \le 1 \tag{2.14}$$

The power transfer validation module uses (2.14) as a criterion to validate the corrective action process output for charging process.

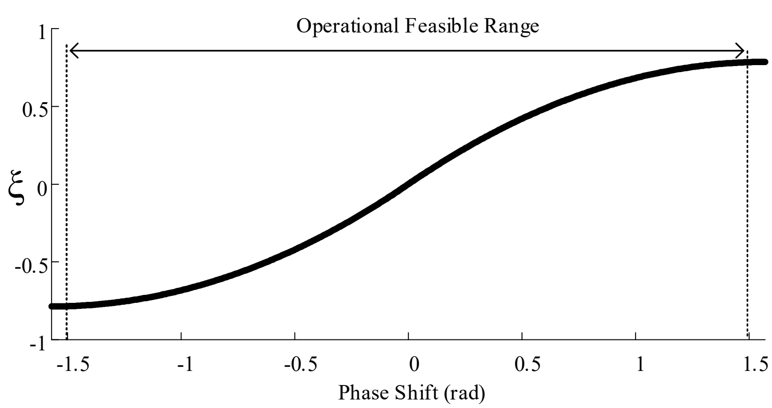

Figure 2.4. Dual active bridge converter power transfer capability

To have better understanding, a detail analysis for necessity of a self-healing mechanism for conventional MPC for DAB converter is provided here. The imposed voltage on AC-link inductor is given by,

$$v_L(k) = v_{AB} - \frac{n_1}{n_2}(v_{CD}) \tag{2.15}$$

Based on the phase shift applied to the transformer terminal voltages, two short time slots in every switching cycle are formed when v_{AB} has positive value and v_{CD} has negative value, the imposed voltage on AC-link inductor is given by,

$$v_{L_{\max}} = v_{AB} + \frac{n_1}{n_2} v_{CD} \tag{2.16}$$

when v_{AB} has negative value and v_{CD} has positive value; the imposed voltage on the inductor is calculated by,

$$v_{L_{\min}} = -v_{AB} - \frac{n_1}{n_2} v_{CD} \tag{2.17}$$

While the imposed voltage on the AC-link inductor is zero approximately rest of the time. When a pulsation in current occurs, the predicted phase shift can have invalid value. For clarifying this issue, it is proved that why these pulsations cause the phase shift to be invalid. The phase shift for charging process is given by,

$$\varphi(k) = \frac{\pi}{2}\left(1 - \sqrt{\left(1 - \frac{8\,p(k) n_2\, L_{AC}\, f_{sw}}{n_1\, v_{AB}\, v_{CD}}\right)}\right) \tag{2.18}$$

To have a valid value for phase shift, the basic constraint for this equation is given by,

$$1 - \frac{8\,p(k) n_2\, L_{AC}\, f_{sw}}{n_1\, v_{AB}\, v_{CD}} \geq 0 \tag{2.19}$$

Considering the primary winding of high frequency transformer as high voltage side, the following equation is valid always. This is given by,

$$v_{AB} + \frac{n_1}{n_2} v_{CD} \geq v_{AB} + v_{CD} \tag{2.20}$$

Satisfying the equality constraint, the next step of maximum predicted AC-link inductor current is given by,

$$i_{L_{\max}}(k+1) = \frac{v_{AB} + v_{CD}}{f_s L_{AC}} + i_L(k) \tag{2.21}$$

Hence, the amount of power that is transferred through DAB converter is calculated by,

$$p(k+1)=\frac{{v_{AB}}^2+v_{AB}v_{CD}}{f_s L_{AC}}+v_{AB}i_L(k) \tag{2.22}$$

Checking this equation by the constraint in (2.19) results in,

$$\frac{{v_{AB}}^2+v_{AB}v_{CD}}{f_s L_{AC}}+v_{AB}i_L(k)\le\frac{n_1\, v_{AB}\, v_{CD}}{8n_2\, L_{AC}\, f_{sw}} \tag{2.23}$$

After simplifying the inequality and considering $k^{\dagger}={f_s}/{8\, f_{sw}}$, equation (2.23) is rewritten by,

$$v_{AB}+v_{CD}(1-k^{\dagger})+f_s L_{AC} i_L(k)\le 0 \tag{2.24}$$

As mentioned, there are instants that results in positive values for all terms in (2.24) and violates the inequality. Hence, it is proved that the phase shift will not have a valid value and the conventional MPC algorithm fails to proceed. Considering the inequality in (2.20), the condition for satisfying (2.19) become worse and this is due to the increase in the inductor current.

Equation (2.25) represents the restrictions in the phase shift values for determining the power transfer in DAB converter,

$$p_o=\begin{cases}\left(\dfrac{n_1 v_{AB}v_{CD}}{n_2 x}\right)\left(\varphi-\dfrac{\varphi^2}{\pi}\right) & \forall\varphi\in\left[0,\dfrac{\pi}{2}\right]\\[2ex] \left(\dfrac{n_1 v_{AB}v_{CD}}{n_2 x}\right)\left(\varphi+\dfrac{\varphi^2}{\pi}\right) & \forall\varphi\in\left[-\dfrac{\pi}{2},0\right]\end{cases} \tag{2.25}$$

Now, by determining φ in term of power transfer,

$$\varphi=\frac{\pi\pm\sqrt{\pi^2-4\pi\dfrac{p_o n_2\, x}{n_1\, v_{AB}\, v_{CD}}}}{2} \tag{2.26}$$

valid range of phase shift in charging process is analyzed. It means that whenever ξ as the normalized power is zero, the phase shift should be zero too; also, when the normalize power is $\frac{\pi}{4}$, the phase shift should reach to $\frac{\pi}{2}$ which is the maximum accepted phase shift. For discharging interval, the same process is repeated. However, to find a unique criterion for this problem and decreasing computational process in the core of self-healing module, the feature of an odd function has been used; it is stated that the function f(x) is odd if,

$$f(x) + f(-x) = 0 \tag{2.27}$$

this equation is valid if the domain of the function is symmetrical. Also, f (0) = 0, if and only if x=0 is in the domain of this function. Checking the power transferring function, it is realized that,

$$\varphi = \begin{cases} \dfrac{\pi - \sqrt{\pi^2 - 4\pi \dfrac{p_o n_2 x}{n_1 v_{AB} v_{CD}}}}{2} & \forall \xi \in \left[0, \dfrac{\pi}{4}\right] \\ \dfrac{-\pi + \sqrt{\pi^2 + 4\pi \dfrac{p_o n_2 x}{n_1 v_{AB} v_{CD}}}}{2} & \forall \xi \in \left[-\dfrac{\pi}{4}, 0\right] \end{cases} \tag{2.28}$$

By rearranging this function, it is explained as,

$$\varphi = \begin{cases} \dfrac{\pi}{2} - \sqrt{\dfrac{\pi^2}{4}\left(1 - \dfrac{\dfrac{8 p_o n_2 L_{AC} \pi f_{sw}}{n_1 v_{AB} v_{CD}}}{\pi}\right)} & \forall \xi \in \left[0, \dfrac{\pi}{4}\right] \\ \dfrac{-\pi}{2} + \sqrt{\dfrac{\pi^2}{4}\left(1 + \dfrac{\dfrac{8 p_o n_2 L_{AC} \pi f_{sw}}{n_1 v_{AB} v_{CD}}}{\pi}\right)} & \forall \xi \in \left[-\dfrac{\pi}{4}, 0\right] \end{cases} \tag{2.29}$$

In a simplified form, this equation is given by,

$$\varphi = \begin{cases} \dfrac{\pi}{2}\left(1 - \sqrt{1 - \dfrac{8 p_o n_2 L_{AC} f_{sw}}{n_1 v_{AB} v_{CD}}}\right) & \forall \xi \in \left[0, \dfrac{\pi}{4}\right] \\ \dfrac{-\pi}{2}\left(1 - \sqrt{1 + \dfrac{8 p_o n_2 L_{AC} f_{sw}}{n_1 v_{AB} v_{CD}}}\right) & \forall \xi \in \left[-\dfrac{\pi}{4}, 0\right] \end{cases} \tag{2.30}$$

Considering $f_t(k) = \dfrac{8 p_o n_2 L_{AC} f_{sw}}{n_1 v_{AB} v_{CD}}$ and the fact that $-\pi/2 \le \varphi \le \pi/2$, the optimal range for $f_t(k)$ in both charging and discharging process are given by,

$$\begin{aligned}
&\frac{-\pi}{2} \leq \frac{\pi}{2}\left(1-\sqrt{1-\frac{8\, p_o\, n_2\, L_{AC}\, f_{sw}}{n_1\, v_{AB}\, v_{CD}}}\right) \leq \frac{\pi}{2} \\
&\frac{-\pi}{2} \leq \frac{-\pi}{2}\left(1-\sqrt{1+\frac{8\, p_o\, n_2\, L_{AC}\, f_{sw}}{n_1\, v_{AB}\, v_{CD}}}\right) \leq \frac{\pi}{2}
\end{aligned} \tag{2.31}$$

By rearranging the first inequality, $-3 \leq f_i(k) \leq 1$; and for the second one, rearranging the inequality results in $-1 \leq f_i(k) \leq 3$; In the self-healing process, the algorithm checks the constraints based on the power transferring direction, features of the odd function, and the overlapped region of two inequalities.

2.4.2. Optimal Switching Selection Mechanism

The formulation of the MPSC cost function and optimization procedure is provided in this section. The absolute value of instantaneous AC-link inductor current can be accurately estimated by its RMS value, which is given by,

$$I_{RMS} = 2\sqrt{i_0\, i_m\,(2D-1) + \frac{(i_0+i_m)^2}{3}(1-D) + \frac{(i_m-i_0)^2}{3}D} \tag{2.32}$$

where i_0, i_m are the initial and maximum values of the inductor current, respectively. By considering D = 0.5 for DAB converter, equation (2.32) is simplified as,

$$I_{RMS} = \sqrt{\frac{4}{6}\left[(i_0^2+2i_0 i_m+i_m^2)+(i_m^2-2i_0 i_m+i_0^2)\right]} \tag{2.33}$$

Equation (2.33) can be further simplified given the fact that i_0 is negligible compared to i_m,

$$I_{RMS} \cong 1.15\left|i_m\right| \tag{2.34}$$

By observing the instantaneous AC-link inductor current, the current is almost constant with negligible slope, where the change in current ΔI_{LAC} is given by,

$$\left|\Delta I_{LAC}\right| = \left|\frac{1-D}{2 f_s\, L_{AC}}\left(v_{AB}-\left(\frac{n_1}{n_2}\right)v_{CD}\right)\right| \tag{2.35}$$

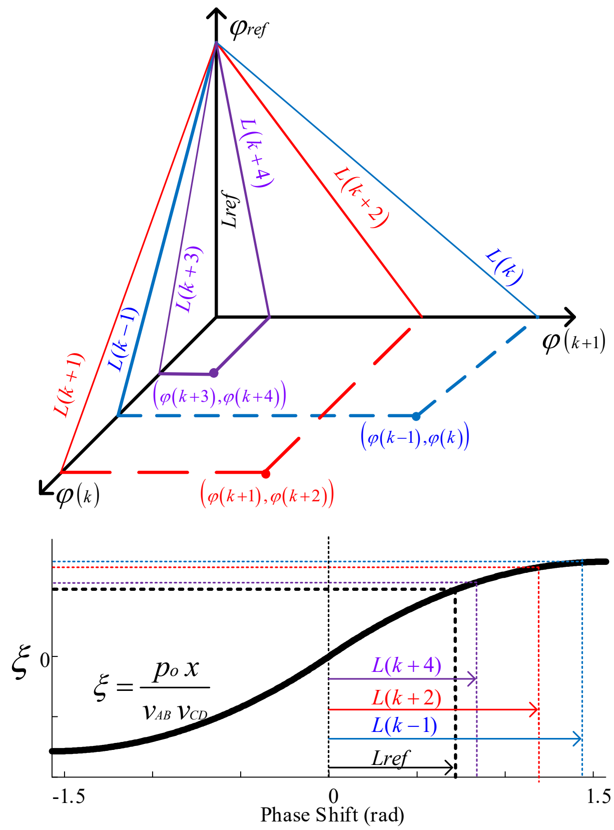

Figure 2.5. Graphical representation of the proposed MPSC cost function (g) optimization via Euclidean norm approach.

Thus, the RMS value of AC-link inductor current can be accurately estimated by instantaneous current. In other words, during one switching cycle, most of the time, $|i_m|$ is very close to the absolute value of the instantaneous AC-link inductor current. The phase shift can be estimated based on its relation with RMS value of the AC-link inductor current,

$$|\varphi|^3 + \frac{\pi^3}{4}|\varphi|^2 + \left(\frac{6\pi^3 I_{L\ RMS}^{2} f_s^2 L_{AC}^2}{v_{AB} v_{CD}} - \frac{\pi^3}{8}\left(\frac{v_{CD} + v_{AB}}{v_{AB}} \right) \right) = 0 \tag{2.36}$$

Furthermore, as it is shown in (2.32) -(2.35), I_{RMS} can be substituted by AC-link inductor current instantaneous value in (2.36). The first potential phase shift $\varphi(k)$ can be determined by solving (2.36) using the instantaneous AC-link inductor current. The second potential phase shift $\varphi(k+1)$ can be determined by solving (2.36) using the predicted AC-link inductor current given by (2.3) or (2.5). The validation modules in the previous section verify the feasibility of the resultant phase shift $\varphi(k+1)$. The estimated reference phase shift $\hat{\varphi}_{ref}$ is determined by regulating the DC-Bus voltage via a PI controller as shown in Figure 2.2. The instantaneous phase shift $\varphi(k)$, the predicted phase shift $\varphi(k+1)$, and the estimated reference phase shift $\hat{\varphi}_{ref}$ are used in the Euclidean norm calculation framework for optimization process and determination of the switching signals. This process is depicted in Figure 2.5. The optimal switching states that minimize the feasible phase shift $\varphi(k)$ and $\varphi(k+1)$ Euclidean norms with the estimated phase shift reference $\hat{\varphi}_{ref}$ are determined by the proposed cost function. The phase shift vectors based on the defined unity vectors in each sampling time (k) are given by,

$$\hat{i} = \frac{\varphi(k)}{|\varphi(k)|}, \hat{j} = \frac{\varphi(k+1)}{|\varphi(k+1)|}, \hat{k} = \frac{\hat{\varphi}_{ref}}{|\hat{\varphi}_{ref}|} \tag{2.37}$$

$$\vec{\varphi}_k = \varphi(k)\vec{i} + \varphi(k+1)\vec{j}, \vec{\hat{\varphi}}_{ref} = \hat{\varphi}_{ref}\vec{k}$$

$$\theta(k) = \tan^{-1}\left(\frac{\varphi(k+1)}{\varphi(k)}\right) \tag{2.38}$$

$\vec{m}_k$ is representing a new vector which is used in the final cost function (g) and it is given by,

$$|\vec{m}_k| = \min\{|\vec{\varphi}_k||\sin(\theta(k)|, |\vec{\varphi}_k|\cos(\theta(k))\} \tag{2.39}$$

The direction of $\vec{m}_k$ will be aligned with $\hat{j}$ if the first component of (2.39) has the minimum value; otherwise, $\vec{m}_k$ direction is aligned with $\acute{i}$. Thus, the proposed MPSC cost function (g) for optimization can be formulated as,

$$|g(k+1)| = \sqrt{|\vec{m}_k|^2 + |\vec{\hat{\varphi}}_{ref}|^2} \tag{2.40}$$

where (2.40) obtains the next sampling time (k+1) optimum phase shift value. The resultant optimal phase shift by (2.40) is used to generate the switching signals. The switching signals are generated by the two functions given in (2.41),

$$\begin{aligned} Y_1 &= \sin(2\pi f_{sw} k) \\ Y_2 &= \sin(2\pi f_{sw} k + |g(k+1)|) \end{aligned} \tag{2.41}$$

In more details, the gate signals with the appropriated optimal phase shift are generated by comparing the two function Y_1 and Y_2 with zero. A unique feature of the proposed MPSC is the autonomous determination of the optimal phase shift and accurate estimation of the initial phase shift to be tracked using a root-finding mechanism, this feature enhances the dynamic response of the controller and mitigates the steady state tracking error.

2.4.3. Stability Analysis

The Stability of the system is investigated by means of the Lyapunov stability analysis. The next-state converter output phase shift $\varphi(k+1)$ for optimal tracking is represented by,

$$\varphi(k+1) = \varphi_{opt}(k+1) + e(k+1) \tag{2.42}$$

where, $\varphi(k+1)$ is the phase shift which is applied on the transformer terminal voltages and $\varphi_{opt}(k+1)$ is the phase shift that will produce zero error in DC-Bus voltage in the following time step. $e(k+1)$ is defined as the phase shift quantization error. In this case, the magnitude of $e(k+1)$ is less than or equal to l, where $l \in \mathbb{R}+$. It is guaranteed that l is certain to exist, and hysteresis bounds with length $\varphi(k+1)$ is bounded. $\varphi(k+1)$ remains bounded and this is due to the self-healing mechanism that has been proposed in this work.

$$\|e(k+1)\| \le l \ , \ l \in R^{+} \tag{2.43}$$

The error in DC-Bus voltage is given by,

$$\begin{gathered}V_{DC-error}=V_{DC}(k+1)-V_{DC-ref}(k+1)\\ V_{DC-error}(k+1)=x_L\left[\frac{v_L(k)}{f_sL_{AC}}+i_L(k)\right]+\frac{n_1}{n_2}v_{cd}-V_{DC-ref}(k+1)\end{gathered}\tag{2.44}$$

The objective of the control is to reduce tracking error asymptotically to zero or to a small error tolerance. The Lyapunov function $L(k)$ is defined as:

$$L(V_{DC-error})=\frac{1}{2}\left[V_{DC-error}\right]^2\tag{2.45}$$

Based on Lyapunov theorem for system stability, the time derivative of the Lyapunov function $\Delta L(V_{DC-error})$ should be negative for the convergence of $V_{DC-error}$ to zero. The time derivative of the Lyapunov function is defined as:

$$\Delta L(V_{DC-error})=L(V_{DC-error}(k+1))-L(V_{DC-error}(k))\tag{2.46}$$

For finding the relation between the next step of AC-link inductor current and the phase shift, AC-link inductor voltage is calculated in term of phase shift based on the DAB converter fundamental and is given by,

$$v_L(k)=\frac{n_1\,v_{CD}}{2n_2\pi}\left(\varphi(k)-\frac{\varphi^2(k)}{\pi}\right)-\frac{L_{AC}\,2\pi f_s\,i_L(k)}{2\pi}\tag{2.47}$$

Therefore, the next step of AC-link inductor current is calculated by,

$$\frac{v_L(k)}{f_sL_{AC}}+i_L(k)=\frac{n_1\,v_{CD}}{n_2\,L_{AC}\,2\pi f_s}\left(\varphi(k)-\frac{\varphi^2(k)}{\pi}\right)\tag{2.48}$$

Using (2.44-2.48), the time derivative of the Lyapunov function is given by:

$$\Delta L(V_{DC-error})=\frac{1}{2}\begin{bmatrix}x_L\left[\dfrac{v_L(k)}{f_sL_{AC}}+i_L(k)\right]+\\ \dfrac{n_1}{n_2}v_{CD}(k+1)-V_{DC-ref}(k+1)\end{bmatrix}^2-\frac{1}{2}\left[V_{DC-error}(k)\right]^2\tag{2.49}$$

considering $\frac{n_1}{n_2}v_{CD}=\alpha$, equation (2.49) is simplified by,

$$\Delta L(V_{DC-error}) = \frac{1}{2}\begin{bmatrix} \alpha\,\varphi(k+1) - \dfrac{\alpha\,\varphi^2(k+1)}{\pi} - \dfrac{n_1}{n_2} v_{cd} \\ -V_{DC-ref}(k+1) \end{bmatrix}^2 - \frac{1}{2}\left[V_{DC-error}(k)\right]^2 \tag{2.50}$$

For converging $V_{DC-error}$ to zero, it is necessary to find a proper phase shift which satisfy $\Delta L(V_{DC-error}) \le 0$. Rearranging this inequality results in,

$$\alpha\,\varphi(k+1) - \frac{\alpha\,\varphi^2(k+1)}{\pi} - \frac{n_1}{n_2} v_{CD} - V_{DC-ref}(k+1) \le V_{DC-error}(k) \tag{2.51}$$

Using (2.44), this equation is simplified by,

$$\varphi^2(k+1) - \pi\,\varphi(k+1) + \frac{\pi\,(\alpha + V_{DC}(k+1))}{\alpha} \ge 0 \tag{2.52}$$

By solving this inequality and considering the DAB phase shift limitation and (25), the phase shift which ensures a negative time derivative of $\Delta L(V_{DC-error})$ is defined as $\varphi(k+1)$ and is given by,

$$\begin{aligned} \varphi_{opt}(k+1) + l &= \frac{\pi \pm \sqrt{\pi^2 - \dfrac{4\pi}{\alpha}(\alpha + V_{DC}(k+1))}}{2} \\ \varphi_{opt}(k+1) &\ge \frac{\pi}{2} - \sqrt{\frac{\pi^2}{4} - \frac{\pi}{\alpha}(\alpha + V_{DC}(k+1))} - l \\ \varphi(k+1) &= \frac{\pi}{2} - \sqrt{\frac{\pi^2}{4} - \frac{\pi}{\alpha}(\alpha + V_{DC}(k+1))} \end{aligned} \tag{2.53}$$

The system should meet the following Lyapunov criteria:

$$\begin{aligned} & L(V_{DC-error}(k)) \ge c_1 \left|V_{DC-error}(k)\right|^{\vartheta} \quad \forall V_{DC-error}(k) \in \Upsilon \\ & L(V_{DC-error}(k)) \ge c_2 \left|V_{DC-error}(k)\right|^{\vartheta} \quad \forall V_{DC-error}(k) \in \Gamma \\ & L(V_{DC-error}(k+1)) - L(V_{DC-error}(k)) \le -c_3 \left|V_{DC-error}(k)\right|^{\vartheta} + c_4 \\ & c_1, c_2, c_3, c_4 \in R^+ \;,\; \vartheta \ge 1 \;,\; \Upsilon \in R \;,\; \Gamma \subset \Upsilon \end{aligned} \tag{2.54}$$

Substituting calculated $\varphi(k+1)$ into (2.50) and assuming $\varphi(k+1)=\varphi$,

$$\Delta L(V_{DC-error}) = \frac{1}{2}\begin{bmatrix} \alpha(\varphi_{opt}(k+1)+l) - \dfrac{\alpha(\varphi_{opt}(k+1)+l)^2}{\pi} \\ -\dfrac{n_1}{n_2}v_{CD} - V_{DC-ref}(k+1) \end{bmatrix}^2 - \frac{1}{2}\left[V_{DC-error}(k)\right]^2$$
$$\Delta L(V_{DC-error}) = \frac{1}{2}\begin{bmatrix} \alpha\varphi - \dfrac{\alpha}{\pi}\varphi^2 - \alpha - V_{DC-ref}(k+1) \\ +\alpha l - \dfrac{\alpha}{\pi}(2\varphi l) - \dfrac{\alpha}{\pi}l^2 \end{bmatrix}^2 - \frac{1}{2}\left[V_{DC-error}(k)\right]^2 \tag{2.55}$$

Based on (2.53), (2.55), the bounded form of $\Delta L(V_{DC-error})$ is given by,

$$\Delta L(k) \le \frac{1}{2}\left[\alpha - \frac{\alpha}{\pi}l - \frac{2\varphi\alpha}{\pi}\right]^2 l^2 - \frac{1}{2}\left[V_{DC-error}(k)\right]^2 \tag{2.56}$$

Furthermore, the DC-Bus voltage converges to a condensed equation which is given by,

$$\Omega = \left\{ \left\| V_{DC-error}(k) \right\|^2 \le (\alpha - \frac{\alpha}{\pi}l - \frac{2\varphi\alpha}{\pi})\, l \right\} \tag{2.57}$$

Finally, from (2.54),

$$c_1 = c_2 = 1; c_3 = 0.5, c_4 = 0.5\left(\frac{\pi}{\alpha l(\pi - l - 2\varphi)}\right)^2 l^2 \tag{2.58}$$

Thus, controlled parameter is within a bounded region, and therefore satisfy Lyapunov's stability criterion.

2.5. Case Studies and Discussion

Several case studies are carried out in OPAL-RT HIL environment for the LIPS of Figure 2.1; the HIL setup is shown in Figure 2.6. System specifications for DAB converter has been provided in Table 3. The conducted case studies validate the controller performance to the PPLs energization in the LIPS. The overall goal is to maximize the LIPS resiliency by regulating voltage and frequency of the system via the MPSC of DAB converter interfaced ESS. A comparison with conventional PI controller is also provided demonstrating the superiority of the proposed MPSC scheme.

Table 3. DAB Converter Specifications

Parameter	Value
Input Voltage	400V
Output Voltage	200V
DC Capacitors	1.2mF
Switching Frequency	50 kHz
High Frequency Transformer Turn Ratio	2:1
Secondary Side Leakage Inductor	10 µH
AC Link Inductor	5 µH

Figure 2.6. OPAL-RT platform HIL setup of LIPS.

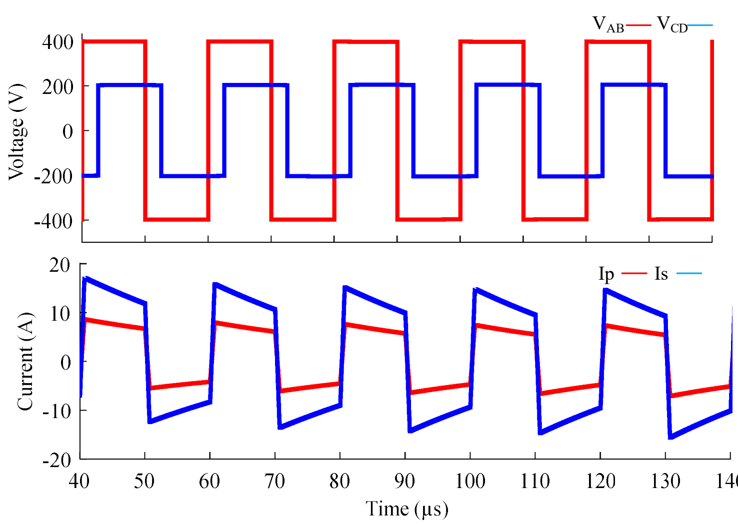

Figure 2.7. AC-link transformer’s high frequency current and voltage waveforms using MPSC.

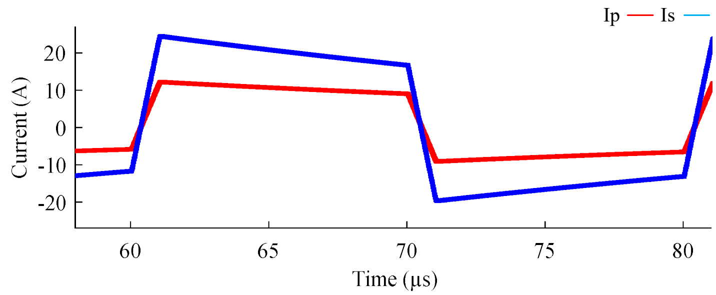

Figure 2.8. One cycle ac-link transformer's primary and secondary side current using MPSC.

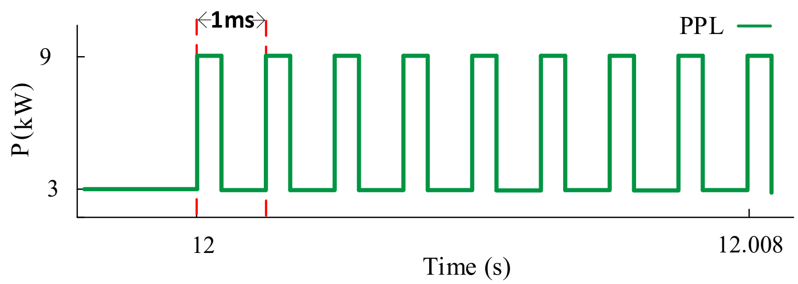

Figure 2.9. Pulsed power load pattern, triggered at instant 12s.

Figure 2.7 depicts the DAB converter high frequency transformer's voltage and current waveforms in steady state. Precisely, the high frequency transformer terminal voltages are 50 kHz square wave. Furthermore, a phase shift is observable between the high frequency transformer terminal voltages (see Figure 2.7). This phase shift enables the bidirectional power flow capability of the DAB converter. Moreover, Figure 2.8 shows the DAB converter high frequency transformer currents in one switching period. PPL has a periodic pattern of a square wave with amplitude of 6 kW, 1 kHz frequency and duty cycle of 40%. It is worthy to mention that when the PPL is triggered, the amplitude of the instantaneous demand is 6 kW (i.e. 0.59 pu) and the average PPL is 2.4 kW (i.e. 0.23 pu). Note that, the PPL is triggered at instant 12s and adds 6 kW to the base load (3 kW) of the system. The base for pu calculations is the nominal apparent power of the synchronous generator. Considering just a

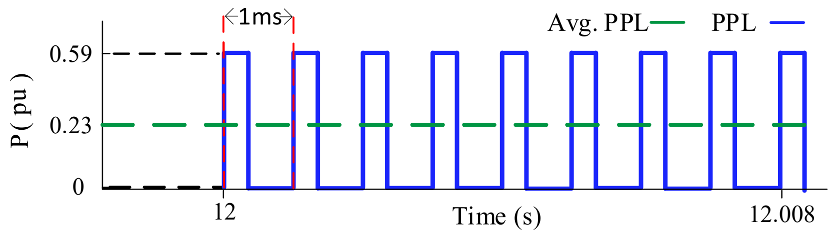

Figure 2.10. Pulsed power load pattern in per unit considering synchronous generator apparent power as base power, triggered at instant 12s.

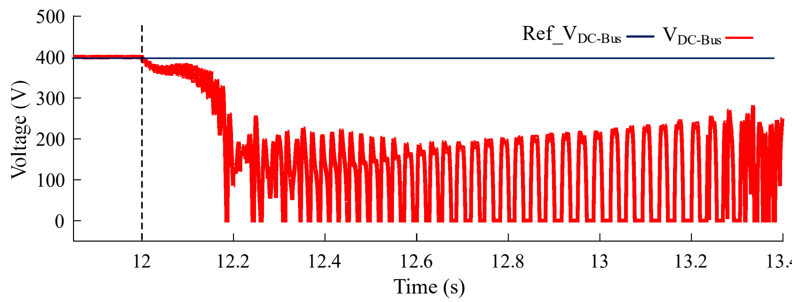

Figure 2.11. DC- Bus voltage dynamic using PI controller: the bus voltage collapses after energization of PPL.

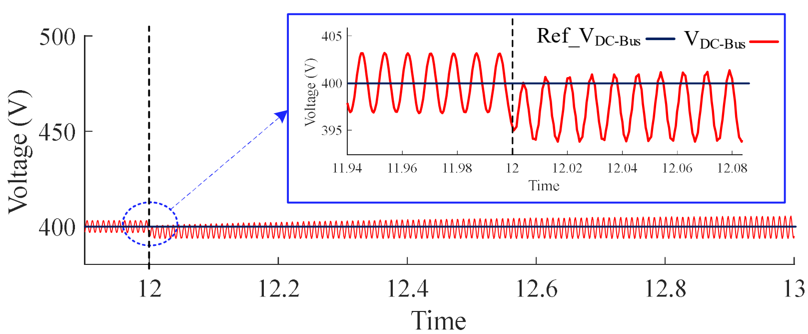

Figure 2.12. DC- Bus voltage dynamic using MPSC: the bus voltage restored after energization of PPL.

single phase of the entire system, the base load has the value of 0.88 pu and the average PPL load which is imposed on the system is about 0.7 pu; thus, when PPLs are triggered, the system faces with serious frequency and voltage challenges; this scenario accurately

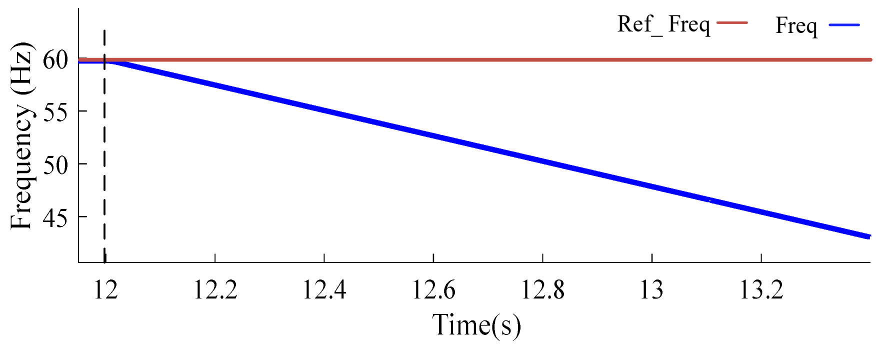

Figure 2.13. AC- Bus frequency dynamic using PI controller: the bus frequency collapses after energization of PPL.

replicates the model of a critical condition for a system in real-time which is handled by the proposed MPSC scheme. The considered PPL profile is illustrated in Figure 2.9 and Figure 2.10. Figure 2.11 shows the LIPS DC-Bus voltage when a conventional PI controller is used to control the DAB converters in response to the PPL energization. As it is seen, the DC-Bus voltage is collapsed within 0.2s after energization of the PPL. Figure 2.12 shows that DC-bus voltage is restored after energization while using MPSC. Figure 2.13 shows that the system frequency deviates and then collapses by about 15 Hz when the PPL is triggered. This case study demonstrates that due to slow dynamic response of the DAB based PI-controller, the voltage and frequency of the system collapses and causes loss of loads etc. Although, DAB based PI-controller may have relatively acceptable dynamic response for arbitrary load patterns without pulsating behavior, but its dynamic response is not fast enough to regulate the voltage and frequency of the system in response to PPL energization. This eventually results in voltage and frequency collapse after couple of PPL cycles as it is shown in Figure 2.11 and Figure 2.13.

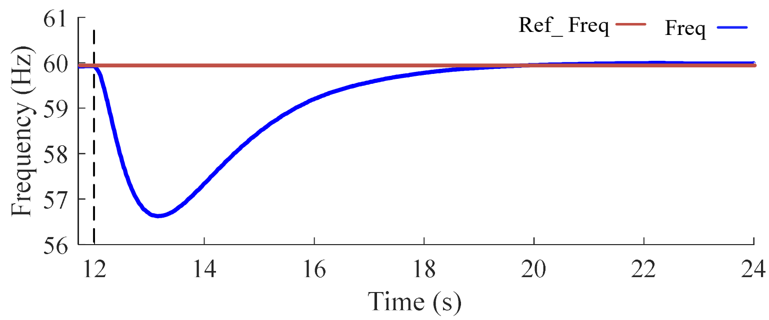

Figure 2.14. AC- Bus frequency dynamic using MPSC: the bus frequency restored after energization of PPL.

The proposed controller performance in response to PPL energization is analyzed in Figure 2.12 and Figure 2.14. The AC-Bus frequency dynamic when using the proposed MPSC is shown in Figure 2.14. As it is demonstrated, once the PPL is triggered for energization, there is a deviation in frequency at instant 12s, but the DAB based MPSC restores the system frequency with around 3.5 seconds. Ship classification societies have put restrictions on the frequency deviations from the nominal value in both steady-state and transient conditions [65]. These rules allow a ±5% deviations from the nominal frequency at steady state. For transient conditions the standard allows ± 10% deviations for a duration of 5 sec and less. Table 4 provides standard requirements and metrics for LIPS frequency and voltage regulation. The results are quantified, compared, and listed in Table 5.

Table 4. Standards allowable frequency and voltage deviations [30]

Variable	Deviation	Duration
Frequency	±5%	Permanent
	±10%	5 sec
Voltage	-10% ~ 6%	Permanente
	±20%	1.5 sec

Results show that the proposed MPSC scheme restores the frequency deviation of around 4 Hz, due to the activation of the PPL, in less than 3.5 seconds which is satisfactory according to the specification defined by the standard for ships. On the other hand, the conventional PI-based controller fails to restore the frequency and voltage to their nominal steady state values. It worth mentioning that the PPL of 6 kW is a considerable sudden load added to the LIPS buses.

Table 5. PI and proposed MPSC frequency and voltage deviation comparison

Variable	PI		MPSC	
	Deviation	**Duration**	**Deviation**	**Duration**
Frequency	Collapses	Permanent	±4.75%	3.5 sec
	Deviation	**Duration**	**Deviation**	**Duration**
Voltage	Collapses	Permanent	Negligible	-

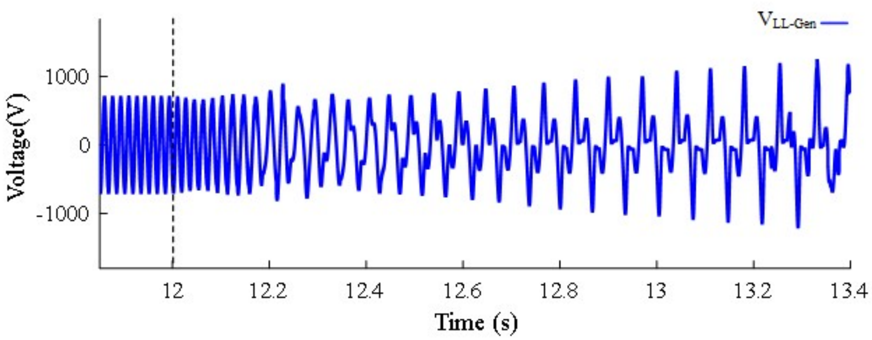

Figure 2.15. Generator output voltage dynamic using PI: the generator voltage and consequently AC-Bus voltage collapses after energization of PPL.

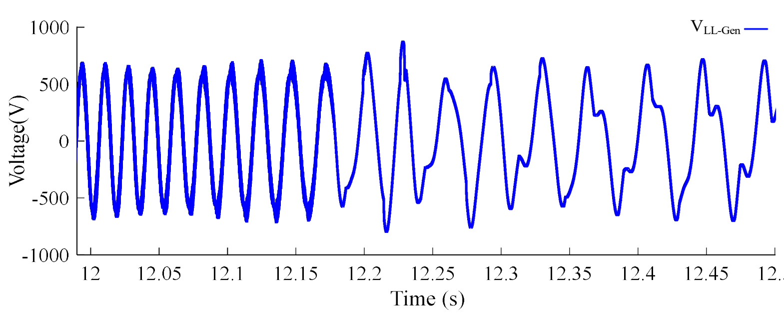

Figure 2.16. Zoomed-in Generator output voltage dynamic using PI: the generator voltage and consequently AC-Bus voltage collapses after energization of PPL.

The impact of PPL energization on the system AC-Bus voltage, derived by synchronous generator, is studied. Figure 2.15 demonstrates the generator output voltage dynamic response where the DAB based PI controller is implemented in LIPS. As it is shown,

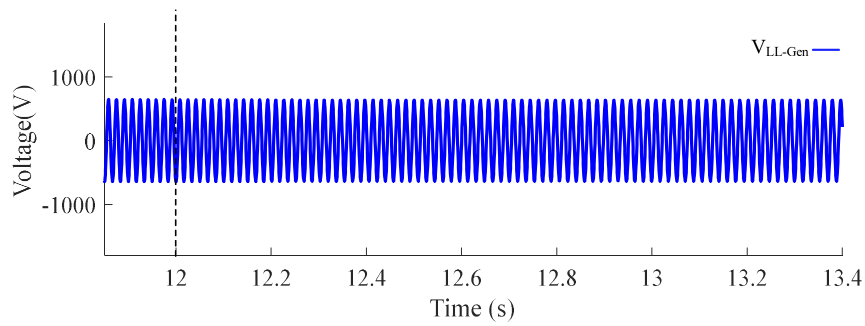

Figure 2.17. Generator output voltage dynamic using MPSC: the generator voltage and consequently AC-Bus voltage are regulated and stable after energization of PPL.

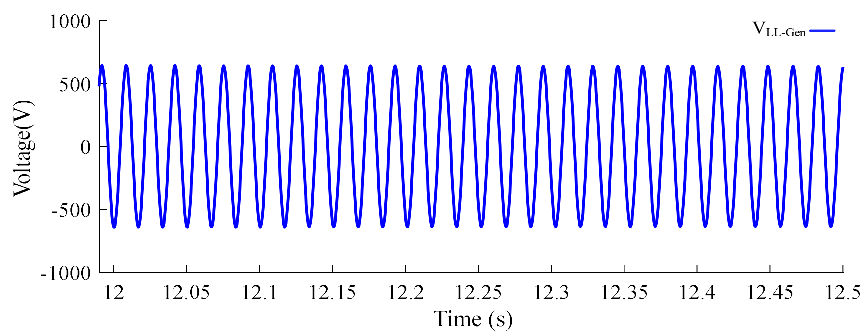

Figure 2.18. Zoomed-in Generator output voltage dynamic using MPSC: the generator voltage and consequently AC-Bus voltage are regulated and stable after energization of PPL.

generator and ESS cannot restore the AC-Bus voltage due to PPL pattern in LIPS. In fact, the AVR tries to regulate the generator output voltage; however, due to considerable unbalance between demand and supply and frequency collapse, the generator output voltage cannot follow the desired voltage and the AC-bus is collapsed; thus, the voltage is not sinusoidal anymore which cause triggering of protection relays and eventually results in system shutdown. Figure 2.16 is the zoomed-in format of Figure 2.15. As it is seen voltage collapse after the PPL is activated. In comparison, the generator output voltage when DAB based MPSC is implemented is shown in Figure 2.17. In this case, the generator voltage and

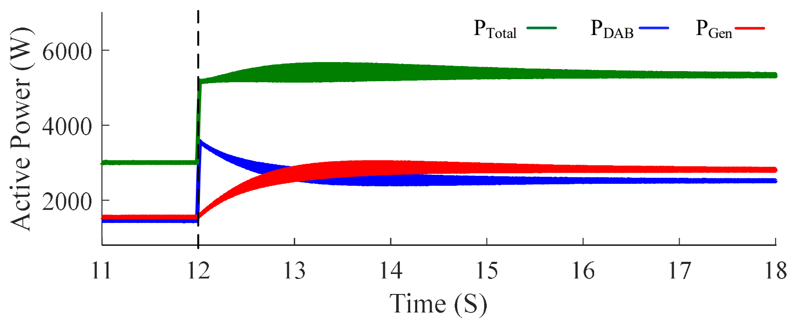

Figure 2.19. Active power dynamic of synchronous generator, DAB based MPSC and the total generation.

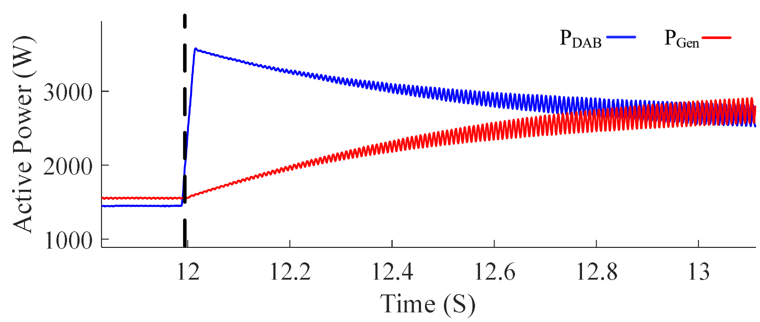

Figure 2.20. Active power dynamic of synchronous generator, DAB based MPSC zoomed-in around instant 12s.

consequently the AC-Bus voltage is well-regulated and stable even after energizing PPLs. It is worthy to mention that because DAB based MPSC scheme supports system frequency by compensating the sudden demand in the system, LFC is able to restore the sudden drop in system frequency; therefore, generator output power can increase based on its inherent dynamic response.

Also, the AVR adjusts the exciter voltage for supporting any voltage transient during PPLs energization. Figure 2.18 is the zoomed-in version of Figure 2.17, as it is shown voltage remains stable and sinusoidal after the PPL is activated. The demand-supply balancing mechanism by the proposed controller is studied next. Figure 2.19 shows the dynamic behavior of the total power supplied by generator and ESS as well as their individual power generation when using DAB based MPSC. As it is shown, the overall system resiliency is enhanced by the fast-dynamic response of the DAB based MPSC. The LIPS base load is 3 kW, and the PPL is 6 kW with duty cycle of 0.4. Therefore, before PPL energization, the ESS and synchronous generator should supply the 3kW demand. By energizing the PPL, the average PPL increases to around 5.4 kW considering PPL duty cycle in steady state. Moreover, Figure 2.20 shows the dynamic responses of the proposed controller and synchronous generator in response to sudden load change. As it is shown, the synchronous generator needs about 2s to regulate its output power to compensate increased demand, while the gap between demand and supply is compensated in less than 0.1s by fast dynamic response of ESS interfaced with DAB based MPSC.

2.6. Conclusion

This section addresses the challenges associated with design of MPC framework for DAB in LIPS in response to voltage and frequency deviations due to FTLs energization. A model predictive self-healing control scheme is proposed for a DAB converter that is interfacing ESS to the DC-Bus in a hybrid AC/DC LIPS with FTLs. The proposed controller can keep the LIPS voltage and frequency regulated and stable particularly when a considerable PPL is energized – enhancing the system resiliency to PPL energization. The proposed MPSC tackles the challenges and drawbacks associated with MPC framework for DAB converters while leveraging its inherent fast dynamic response to address the voltage and frequency deviation in LIPS with PPL. The proposed controller main characteristics are the two validation modules to mitigate the possible error in the predicted AC-link inductor current of DAB converter. This unique aspect of the proposed approach enables robust implementation of predictive control for DAB converter with inherent pulsating AC-link inductor voltage at high frequency. A cost function is developed to determine the possible switching states that minimizes the Euclidean norm of the possible phase shift with respect to the estimated phase shift reference. It is proved that the implemented estimating block in the proposed controller have high accuracy. Several case studies are conducted in HIL environment to evaluate the functionality of the proposed DAB based MPSC in LIPS and validate its ability to enhance the system resiliency by restoration of voltage and frequency when PPL is energized. The provided case studies demonstrate the superiority of the proposed MPSC compared to PI based controller for ESS interfaced DAB converter in LIPS.

Chapter 3

3. Artificial Intelligence Inspired Model Predictive Control for Frequency Restoration

Parts of this chapter, including figures and text, are based on my following papers:

- M. Hosseinzadehtaher, A. Zare, A. Khan, M. F. Umar, S. Dsilva, and M. B. Shadmand, "AI-based Technique to Enhance Transient Response and Resiliency of Power Electronic Dominated Grids via Grid-Following Inverters," IEEE Transactions on Industrial Electronics, submitted for review Oct. 2022.

3.1. AI-based Technique to Enhance Transient Response and Resiliency of Power Electronic Dominated Grids via Grid-Following Inverters

This section presents a frequency restoration method to enhance power electronic-dominated grid (PEDG) resiliency by maximum utilization of grid following inverters' (GFLIs) capability. An artificial intelligence-based power reference correction (AI-PRC) module is designed and developed for GFLIs to autonomously heal their predefined power setpoints during potential disturbances. A detailed mathematical proof is presented to demonstrate that the grid forming (GFM) and GFL inverters' control rules intrinsically follow the underlying dynamic of the swing-based machines to extend the stability boundary of low inertia PEDGs. Considering this fact, comprehensive transient and steady state-based mathematical models that can deal with all grid's characteristic alterations are used in this work. The concept of this dynamic model is exploited to construct a thorough learning database that includes all grid physical features such as feasible alterations in PEDG configurations, demand and supply side disturbances, wide range of inertia constants, grid's natural and damping frequency as well as the optimal injecting/absorbing power to/from the grid. The proposed approach incorporates all PEDG's effective variables for shaping the dynamic response during potential disturbances. Subsequently, a neural network is trained by deploying Bayesian regularization algorithm (BRA). In the training process, the constructed mathematically based learning data is employed, and the entire AI-PRC module is implemented in the control loop of GFLIs to adjust their pre-defined power references in real-time based on the grid's disturbances. Several use cases are simulated and analyzed in a realistic 14 bus PEDG by MATLAB/Simulink and OPAL-RT simulator to evaluate the functionality of the proposed approach for enhancing the grid resiliency. Moreover, several experimental assessments are conducted to support the simulation outcomes and provide practical validation of the proposed frequency restoration mechanism.

3.2. Literature Review

The augmented contribution of renewable-based energy resources for upholding sustainable and clean energy utilization in the modernized power system is affecting the grid conventional operation methodologies. Power electronic-dominated grids (PEDGs) suffer from the lack of minimum obligatory inertia required for sustaining the grid stability[7, 9]. Specifically, frequency and voltage stability are vulnerable in networks with low inertia[72]. Total system inertia and short circuit ratio (SCR) are the parameters that have more influence on the resiliency boundary of the PEDGs[73]. Thus, system frequency, rate of change of frequency (ROCOF) and voltage stability are jeopardized effortlessly by grid potential disruptions during any manner of operation. Likewise, due to the intermittent nature of renewable energy-based supplies, restoring the frequency excursion to the nominal and stable value is another substantial hurdle to providing proper operation for PEDG in real-time.

Typically, GFMIs have the mainstream contributions for sustaining grid resiliency when a disturbance takes place in the system, and this is due to their characteristic obligations[74]. Moreover, in the steady state condition, they can share the total system load among other suppliers in the operation period[75]. However, they have some restriction when large disturbances occurs either in demand side or supply side. Considering the restriction in their power rating, if they are coerced to contribute to a specific amount of a load more than their nominal rating, the inverter cannot provide a proper dynamic response which could results in significant stability issues. Even though GFMIs can be interfaced with energy storage systems to support the grid stability in a timely manner, they do not consider the minimum mandatory system inertia which is essential to have a secure and stable operation[76]. Therefore, the transient stability boundary of the PEDG is limited particularly when a large disturbance occurs. Also, having numerous GFMIs operating in parallel can be problematic due to the possibility of power circulating amongst them[77, 78]. However, by implementing a sort of synthetic droop control which is predominantly adopted from the primary frequency control loop of a synchronous generator (SG), the total load can be shared among the inverters while the grid's voltage and frequency are regulated autonomously.

Thanks to GFLIs that can be employed to strengthen the upstream grid voltage and frequency if their control is equipped with droop fundamentals[78, 79]. To benefit from the GFLIs to enhance system resiliency during disturbances, it is vital to add up another higher level of voltage and frequency adjustment loop. The active power is tweaked based on a thorough *f-p* control gain and the reactive power is regulated by using another gain that relates the voltage magnitude to the required reactive power of the converter. A PLL is requisite to understand the grid voltage phasor at the point of interconnection (POI). It is essential to realize accurate gains which are contingent on quite a few other parameters such as the grid's physical features and the intensity of disturbances. For instance, the *p-f* gain has a direct impact on the ROCOF dynamic and the final regulated value of the system frequency. Therefore, need to employ a kind of tradeoff among these parameters during the disturbances. Moreover, the cut-off frequency of the employed low-pass filters plays a significant role to certify the stability of the control and the whole system stability. Irrespective of grid forming or grid following inverters, if the *p-f* droop coefficient is slightly lessened, consequently the ROCOF is heightened. However, the frequency is regulated much better. Considering the same constraint for droop coefficient in GFMI and GFLI, varying the cut-off frequency has an explicit influence on the ROCOF and frequency as well. Reducing the cutoff frequency in the grid following control results in a decrease in the ROCOF and a higher cut-off frequency in grid following enables the control loop to restore the frequency excursion much faster while this has inverse effect on the grid forming inverters. Thus, frequency and voltage restoration can seriously be challenging in a PEDG with several GFLIs and GFMIs while in their control loop, different droop gains and cut-off frequencies have been deployed. Should be noted that different inverters manufactured by different vendors effortlessly resonant drawbacks of these issues.

Contemplating the low level of PEDG inertia and existing mentioned operational challenges, a variety of basic to advanced frequency restoration control approaches are described in the literature. The notion of virtual synchronous generator (VSG) can be implemented in grid forming and grid following inverters to relatively damp system oscillatory transients due to the external disturbances with lower uncertainty regarding the stability violation[80]. In [81], a nonlinear control technique is introduced to expand the transient stability boundary which is extremely influenced by the frequency dynamics of the system. The authors proposed that in VSG-based control schemes, the inertial value cannot be assumed as a constant and a correlation should be established between the frequency excursion and inertia constant. Additionally, it is declared that to have a more precise comparison between VSG dynamic performance with SG, the same power rating must be considered, and the SG must be considered as with a high number of poles machine. However, in their proposed mathematical representation, which is a sort of binary algorithm, the drawback is related to the ROCOF. In fact, this approach cannot follow the industry standards such as IEEE 1547 regarding the ROCOF constraints. Consequently, it is crucial to have a faster frequency detection. Note that, even by enhancing the sensitivity of the proposed approach to frequency alterations, the challenge still exists when the ROCOF fluctuates slightly while it could be a resultant of some ignorable system noises. A droop-based control in combination with ROCOF control for providing the active power set point in the event of frequency excursion is presented in [82] and is aimed to adopt the frequency control concepts from the SG control. Here, both mechanical and electrical models of SG are assessed and represented on the inverter control loop to control frequency excursions in the system. it is worthy to mention that the conventional droop and VSG based controls are not able to pick up the load for distinct dynamic characteristics either in grid-tied or standalone mode of operation at the same time.

A comparison has been conducted on the VSG dynamic response and droop-based control scheme in inverter-based distributed generators in [16, 83]. Both control approaches are built by the fundamental thought of a droop concept. It should be noticed that a droop-based control characteristically does not engender any inertia for the system. Nevertheless, by employing a kind of lag in their control loops, the system can come up with virtual inertia. Even so, an inertial droop control method is proposed in this work to provide a comprehensive assessment of the control loop functionalities. As mentioned in [84], VSG and inertia droop-based controls can take the advantage of the droop features and simultaneously could add up virtual inertia to the operating grid. However, the response of the VSG is more oscillatory compared to the droop-based techniques during system transients [16]; in addition, the droop-based control does not need a PLL. Thus, lessening some stability concerns that could ensue due to the PLL and its interaction with the power control loop. Still, the droop controls have their well-known innate downsides when the system confronting with large disturbances. In [85], a VSG-based GFMI is used in combination of a super capacitor-based energy storage system to enhance the dynamic response of a microgrid during load disturbances. Here, the base load at steady state is supported by GFLIs all over the grid and the GFMIs support the grid frequency in transient periods. In fact, the GFMI is just employed as power reserve in the critical time of the grid operation. As well, a low-bandwidth communication line is used to send correction signals from GFMIs to GFLIs all over the grid. Although the system robustness is enhanced but having communication links raise the vulnerability of the system to the possible cyber-attacks. Moreover, all drawbacks regarding the VSG-based controls exist while the maximum benefit of GFLIs are not realized. In [86]a generalized droop control is presented for supporting the grid. The power loop in this approach is constructed flexibly to different conditions and enables the control system to provide virtual inertia and damping factor in standalone conditions. Moreover, in grid-connected mode, the fluctuations in the output power are diminished better. Nevertheless, the impediments of tuning and designing optimal controller gains and droop coefficient could limit control functionalities especially if the network configuration is altered, or a large disturbance occurs.

Due to the high level of nonlinearity in PEDG and prevailing mentioned shortcomings in the operational methodologies, artificial intelligence (AI)-based techniques have attained more attraction. AI techniques can cope up with multi-objective optimization problems such as frequency and voltage restoration. In fact, AI techniques are believed as a suitable potential to accommodate complicated dynamic modification of the system. Since, most frequency control loops in power system include proportional-integral (PI) controllers, an intelligent approach is presented in [87] to tune the PI parameters autonomously using a hybrid technique of fuzzy logic and particle swarm optimization (PSO) approaches. This adaptive technique comprises a conventional PI controller in conjugate with a fuzzy system for enhancing the PI controller coefficients. Due to the inherent limitation of fuzzy logic regarding fuzzification and defuzzification approach, a PSO algorithm is deployed to enhance the parameters that are used in membership function. Although some improvement in frequency regulation is prominent but generalizing the functionality of the proposed technique to a larger network has not been evaluated yet. Furthermore, there is no guarantee that the PSO can overwhelm premature convergence when the network is not operated as standalone. A frequency control AI technique approach is presented in [88] which focuses on an isolated hydro power plant; this methodology is valid for isolated plants which the required data are available for training. Therefore, the training process does not cover all the system incidents. Besides, any modification in the network configuration will have negative impacts on the outcome of the offline trained network. Also, in [89-91], a multi-agent reinforcement learning methods is explored to remove the centralized control approaches by estimating the frequency at primary and secondary levels. Still, the practical implementation of the proposed approaches is limited by the required communication infrastructure. Moreover, selecting a proper AI technique, as well as training and implementing methodologies for the targeted system are undeniable challenges.

To the best knowledge of the author, there is no study that aims to maximize the utilization of GFLIs toward enhancing the resiliency while fulfilling most deficiencies in the literature. Thereby, this work proposes a novel AI-based power set points correction for GFLIs to autonomously heal their power set-points during disturbances in real-time. To achieve the problem objective, two main modules are developed: *i*) data mining module, and *ii*) real-time AI prediction module. The data mining module benefits from a comprehensive transient and steady state-based mathematical model to construct a thorough database. All PEDG physical features such as practical alterations in configurations, demand and supply side disturbances, different inertia constants, network natural and damping frequency related to the power angle, and the optimal power injection/absorption are considered in this study. A swing equation is solved statistically while consider all variables that shapes the system dynamic effectively. All feasible variables are valued based on their practical ranges in a realistic PEDG. In this process, different parameters are considered such as inertia constant, alterations in configuration (i.e., the *X/R* ratio), demand and supply disturbances, system damping coefficient, natural frequency, and damped natural frequency. Thereafter, the required injecting/ absorbing power is calculated forthrightly. After that, a two-layer feedforward neural network with optimal number of sigmoid hidden neurons and linear output neuron is learned by using the mathematical-driven database. It should be noted, a Bayesian regularization algorithm (BRA) is employed in the training stage of this work to compensate the dataset size limitations, mitigate the noisy dataset impact, and cover other potential uncertainties. The second module accurately predicts frequency trajectory of the system when a disturbance occurs in the system. Thus, the proposed methodology scrutinizes frequency eccentricities during wide range of disturbances. The proposed methodology is employed in the control loop of GFLIs to ensure resilient operation of PEDG under disturbances.

3.3. Understudy PEDG Configuration Description

The understudy PEDG, see Figure 3. 1, is an IEEE 14 Bus test case that represents approximately a portion of the American Electric Power System as of February 1962. In the initial edition, there are five SGs as the main grid supplier and 11 Loads. However, to make it more consonant with low inertia PEDG, 4 SGs are removed and substituted with power electronic-based resources as well as some minor modifications in the line and load parameters. Seven GFLIs and one relatively small SG are contributing to support system loading. The total amount of load in this study is 500 kW. SG output power in steady state is limited to 150kVA while its power rating is 800kVA.

As planned, 350 kW of system demand is supplied by renewable resources which is equivalent to 70% of the total loads. This assures the entire system inertia is low. Moreover, the total inertia of the SG is in the minimum available that compatible to its power rating. The grid is enabled to be operated in islanded mode with two different voltage level or operated as tied with upstream network at 69kV via a circuit breaker (CB) installed at substation location of bus #10. Considering the islanded mode of operation, medium voltage (MV) cluster supplies the loads at 13.8 kV and the low voltage (LV) cluster maintain the loads at

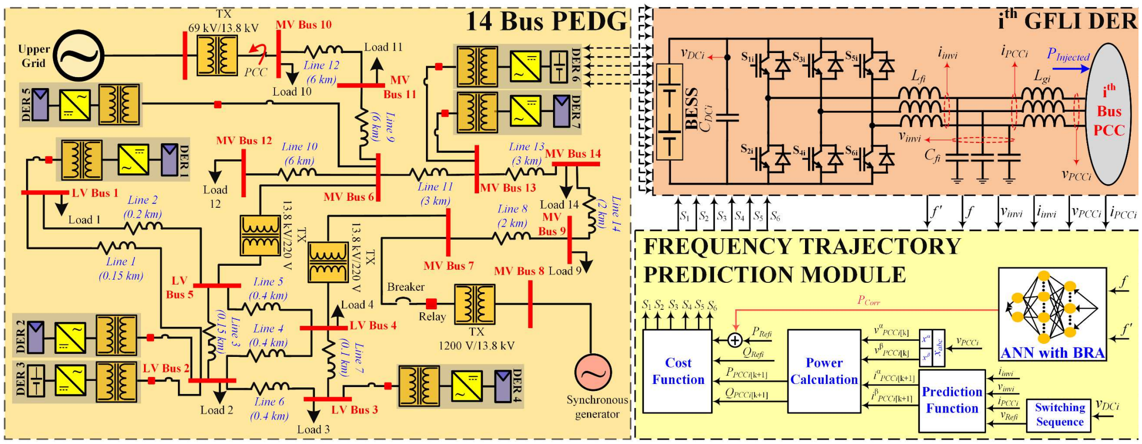

Figure 3. 1. The understudy 14-Bus PEDG.

380 V. Two different level and self-sufficient clusters are interconnected via two 13.8 kV/380 V transformers. Ensuring the minimum prerequisites of the protection aspects of PEDG, all distributed energy resources (DERs) are equipped with coordinated protection relays and CBs to act in the event of any violation of IEEE-1547 standard or short circuit faults.

3.4. PEDG Prevailing Fundamentals

In this section, the main control concepts of SG, VSG-based GFMIs and any droop-based control approaches that contribute to frequency and voltage restoration are presented. Mathematical representations of the necessary control concepts are demonstrated to prove that there is high similarity between a PEDG dynamic response and existing power system. This study should be carried out to authorize us to take the advantage of comprehensive mathematical model for constructing the learning dataset. Should be remarked that, although the inertia level of PEDG can be much lower than a traditional power grid, but the frequency dynamic follows the fundamental role of swing equation. As clear, in bulky power system with different rotational inertia, power balance equation defines the frequency trajectory of the system based on the equivalent inertia of the entire system, and this is based on the fundamental of swing equation that is valid for all SG-based power systems. As discussed in previous section, PEDG demands are supplied by different types of distributed energy resources (DERs) such as: SGs, GFMIs and GFLIs. Emulating a minimum value of virtual inertia is crucial to provide a stable condition for PEDG during the disturbances. Thus, we start by introducing the control fundamentals of SG and later convert it into virtual manner for VSGs. Considering that at least one GFMI of PEDG is controlled as a VSG, (1) show the virtual torque balance equation that is applied in the VSG-based control loops and is given by,

$$T_m - (T_e + D_a \Delta w_v) = 2H \frac{dw_v}{dt} \tag{3.1}$$

Where H is the inertia constant, T_m is the mechanical torque of the prime-mover and T_e is defined as the torque that applied in reverse rotation due to the demand alterations. D_a is the damping factor and ω_v represents the VSG frequency. As shown, with any load disturbances and the consequent variation in frequency, the equivalent system electrical load is compromised indirectly, and this is due to the influence of damping factor in this equation. The primary effect of H is on the ROCOF while D_a has influence on the steady-state value of the frequency. To declare the legitimacy of this idea in mathematical form, one can simplify (3.1) by transferring torque equation in term of power balance at nominal frequency during load increase and ignoring the damping factor just at the disturbance instance. Two independent equations for ROCOF and accelerating power are given by,

$$\Delta p = 2H \frac{df}{dt}, \;\; \Delta p = -\sqrt{-4H\Delta f \frac{dp_{gov}}{dt}} \tag{3.2}$$

Where $\dot{p}_{gov}$ represent the governor dynamic. As droop-based approaches are typically used in control schemes of GFLIs or GFMIs for the sake of voltage and frequency restoration, it is necessary to provide a methodical evaluation regarding the influence of this control on the PEDG dynamic and observe the similarity of this control dynamic with the one which is used in SGs or VSGs. It is worth mentioning that the focus of this part is on the power control loop because the rest of the control are the same in both approaches. In all droop-based control, there is a basic relation between the frequency and the output active power, this is given by,

$$f = \frac{D_p}{2\pi}\left(\frac{\omega_{cut}}{\omega_{cut}+s}\right)(p_0 - p) + f_0 \tag{3.3}$$

Where f shows the output voltage frequency and f_0 is the nominal system frequency. P represents the output power which is provided by the inverter and p_0 is the nominal value of the active power. D_p is known as droop coefficient and ω_{cut} is the cut-off frequency in the low-pass filter. As mentioned before, the latter parameters are influential elements in shaping the frequency dynamics of a PEDG governed via these types of control. Due to the inherent alliance of inertia momentum with the inertia constant, the (3.1) can be represented in the term of power balance as,

$$p_m - (p_e + D_a(w_v - w_0)) = Jw_0 \frac{d(w_v - w_0)}{dt} \tag{3.4}$$

Here, P_m can be represented as reference active power of inverter which in SGs known as prime mover power, P_e is the inverter output power and ω_v is the output voltage angular frequency. D_a and ω_0 are the damping factor and nominal system angular frequency respectively. Basically, a typical representation of the governor can be found as,

$$p_m - p_{nom} = k_G(\omega_0 - \omega) \tag{3.5}$$

Where k_G is known as governor gain. Substituting (3.5) into (3.4) subjected to $\omega_v = \omega$ and applying Laplace transform,

$$p_{nom} - k_G(w - w_0) - p_e - D_a(w - w_0) = (sw - sw_0)(Jw_0) \tag{3.6}$$

Involving the impact of a low-pass filter in the conventional droop while including a proportional controller corresponding to damping factor D_a value in the traditional droop-based control can modify (3.6) as,

$$p_{nom} - p_e + G_{sec}\left(\omega_{sec} - \omega\right) - \frac{1}{D_{cut}}\left(\omega - \omega_0\right) = \frac{s}{D_{cut}}\left(\frac{\omega - \omega_0}{\omega_{cut}}\right) \tag{3.7}$$

where G_{sec} is the proportional control representation with a reference frequency of ω_{sec} which is equal to ω_0. Comparing each term of (3.7) with (3.6) will result in,

$$J\omega_0 = \frac{1}{D_{cut}\omega_{cut}}, \; k_G = \frac{1}{D_{cut}} \tag{3.8}$$

Which proves the power control in droop-based control can be translated as VSG-based control which follow the fundamental of swing equation. Thus, it is proved that the dynamic of a PEDG with different control schemes for GFMIs and GFLIs is like the conventional power system encountering the disturbances. Moreover, no limitation if the PEDG is operating in grid connected or islanded mode.

3.5. PEDG Data Mining Methodology: Constructing Comprehensive Learning Dataset Based on Transient and Steady State Dynamic of The PEDG Fundamentals

3.5.1. PEDG frequency dynamic in steady state duration

To provide a comprehensive dataset regarding any impending variations in the grid such as PEDG's physical feature or different disruption types, transient and steady-state intervals should be investigated accurately. Transient durations are imperative that if not supported promptly, the steady state resiliency investigations would be worthless. Nevertheless, if transient circumstances' constraints are satisfied, the next step would be to satisfy the grid code constraints for post-transient time. As demonstrated in the previous section, the dominant dynamic response rule of a PEDG follows the swing equation. Thus, a transient-based mathematical model in term of the swing equation is investigated to shape the data-mining module during sever disturbances. Moreover, the steady state dynamic of the PEDG is analyzed as well to provide a thorough data base to cover primary and secondary frequency responses. Subsequently, an innovative methodology is proposed to encompass all PEDG disturbances and alterations. These procedures assure that all events would be monitored and captured mathematically in a database that is exploited for learning a neural network. The final objective is to predict the PEDG frequency trajectory and provide an optimal power reference correction for GFLIs in real time. This real-time power correction is corresponding to the adjustment of accelerating power in conventional power systems by SGs contributions all over the grid. The intrinsic dynamic of PEDG during normal disturbances is evaluated by exploring the fundamental of power balance equation, which is given by,

$$\begin{aligned} &f.(P_m - P_e) = \frac{H}{\pi}\left(\frac{d}{dt}\left(\frac{d\delta}{dt}\right)\right), \\ &d\delta = \Delta w dt, P_e = P_M \sin(\delta) \end{aligned} \tag{3.9}$$

where P_m is the per unit value of the inverters' input powers that are adjusted based on (5) and P_e represents the output electrical power respectively. H is the virtual inertia constant, and δ is the electrical power angle. Any deviation in $\Delta\omega$ results in different frequency dynamic and ROCOF based on the PEDG inertia constant. For evaluating the inherent dynamic of this equation, a general perturbation such as $\delta = \Delta\delta + \delta_0$ is applied on the power angle, which is corresponded to a normal disturbance, (3.9) is approximated in term of angle perturbation by,

$$\left(\frac{d}{dt}\left(\frac{d\Delta\delta}{dt}\right)\right) = -\frac{\pi f}{H} P_M \cos(\delta_0)\Delta\delta \tag{3.10}$$

As cited earlier, the effect of damping factor in inverter-based control loop can be demonstrated as kind of variable power $P_{dam}= D_a\, \Delta\omega$ that manipulates the electrical demand and thus the entire frequency dynamic during any potential disturbances are affected. Implementing this impact on (3.10), gives,

$$\left(\frac{d}{dt}\left(\frac{d\Delta\delta}{dt}\right)\right) = -\frac{D\pi f}{H}\frac{d\Delta\delta}{dt} - \frac{\pi f}{H} P_M \cos(\delta_0)\Delta\delta \tag{3.11}$$

By solving the characteristic equation, the power angle with respect to initial point of electrical power angle is given by,

$$\begin{aligned}
&\frac{\delta}{\delta_0} = 1 + \frac{\Delta\delta}{\delta_0\sqrt{1-(\frac{D^2\pi f}{4H\,P_M\cos(\delta_0)})}} e^{-\frac{D\sqrt{\pi f}}{\sqrt{4H\,P_M\cos(\delta_0)}}\sqrt{\frac{\pi f}{H}P_M\cos(\delta_0)}\;t} \\
&\sin\left(\sqrt{\frac{\pi f}{H} P_M \cos\left(\delta_0\right)\left(1-\left(\frac{D^2\pi f}{4H\,P_M\cos(\delta_0)}\right)\right)}\;t+\theta\right) \\
&\theta = \tan^{-1}\left(\frac{\sqrt{1-\left(\frac{D^2\pi f}{4H\,P_M\cos(\delta_0)}\right)}}{\frac{D\sqrt{\pi f}}{\sqrt{4H\,P_M\cos(\delta_0)}}}\right)
\end{aligned} \tag{3.12}$$

Based on the second order differential equations, natural frequency, damped frequency, and damping ratio can be found in term pf PEDG feature such as,

$$
\begin{aligned}
\omega_d &= \sqrt{\frac{\pi f}{H} P_M \cos\left(\delta_0\right)\left(1-\left(\frac{D^2 \pi f}{4H\, P_M \cos(\delta_0)}\right)\right)} \\
\omega_n &= \sqrt{\frac{\pi f}{H} P_M \cos\left(\delta_0\right)}\ ,\ \xi = \frac{D\sqrt{\pi f}}{\sqrt{4H\, P_M \cos\left(\delta_0\right)}}
\end{aligned}
\tag{3.13}
$$

Therefore, PEDG as a nonlinear system has natural frequency which has influence on the nodal voltages, global frequency, and the amount of power contribution from each DER. Furthermore, natural frequency is affected reversely by *H* while the damping ratio has a direct relation with damping factor. As expected, by increasing the inertia constant, damping ratio of the PEDG is decreased. Certainly, the generalized power angle equation can provide a comprehensive database for frequency and ROCOF dynamic if the input variables are valued in a feasible and practical range. These variables are different power angle deviation, different inertia constant, PEDG damping ratio, PEDG natural and damped frequency and demand-supply disturbances.

3.5.2. PEDG momentary frequency dynamic during severe disturbances

As discussed in previous section, PEDG dynamic was evaluated by considering its physical features when a normal disturbance happens. This type of disturbances is studied in the steady state stability category. However, by contemplating potential sever disturbances and degree of nonlinearities in a PEDG dynamic, the former explanation would not be pertinent to assess the PEDG dynamic. In other word, when the disturbance is extensive, common, and straightforward solutions are not reasonable for a highly coupled nonlinear differential equation. Therefore, this problem should be classified as transient stability studies. In this section, the PEDG dynamic facing with a sever disturbance is achieved by using Euler arithmetical methodology. In this approach, some adjustments which are based on prediction and correction techniques are applied. Basically, (3.9) can be divided in two first order differential equation as,

$$\frac{\Delta p\,\pi f}{H} = \frac{d\Delta w}{dt},\; d\delta = \Delta w\,dt \qquad (3.14)$$
$$\Delta p = P_m - P_e$$

Here, predicted solutions are found for each equation and denoted by subscript N. Also, a corrective action is carried out on the predicted values and shown by subscript c. At the state of $k+1$, the predicted values for power angel are given by,

$$\left.\frac{d\delta}{dt}\right|_{(\Delta w_{k+1}^{N})} = \Delta w_{k+1}^{N}$$
$$\Delta w_{k+1}^{N} - \Delta w_k = \left.\frac{dw}{dt}\right|_{(\delta_k)} .(t_{k+1} - t_k) \qquad (3.15)$$

With the same logic, the angular frequency deviation is given by,

$$\left.\frac{d\Delta w}{dt}\right|_{(\delta_{k+1}^{N})} = \frac{\pi f}{H}((P_m - P_e)\Big|_{\delta_{k+1}^{N}})$$
$$\delta_{k+1}^{N} - \delta_k = \left.\frac{d\delta}{dt}\right|_{(\Delta w_k)} .(t_{k+1} - t_k)\,, \qquad (3.16)$$

The corrected values are calculated by averaging the values of two found derivatives and is given by,

$$(\delta_{k+1}^{c} - \delta_k) = \frac{\left.\frac{d\delta}{dt}\right|_{(\Delta w_k)} .(t_{k+1} - t_k) + \left.\frac{d\delta}{dt}\right|_{(\Delta w_{k+1}^{N})} .(t_{k+1} - t_k)}{2}\,,$$
$$(\Delta w_{k+1}^{c} - \Delta w_k) = \frac{\left.\frac{dw}{dt}\right|_{(\delta_k)} .(t_{k+1} - t_k) + \left.\frac{dw}{dt}\right|_{\delta_{k+1}^{N}} .(t_{k+1} - t_k)}{2} \qquad (3.17)$$

For the next step, corrected values are substituted in associated equations and the process is repeated to find the last approximated solution for the objective states as,

$$\delta_{k+1}^{c} - \delta_{k+1} \cong 0,\; \Delta\omega_{k+1}^{c} - \Delta\omega_{k+1} \cong 0 \qquad (3.18)$$

with the same logic, by finding the angle dynamic, frequency and ROCOF are found considering different grid features such as inertia constant, damping factor and the supply-demand disturbances.

3.6. Training Mechanism Based on Bayesian Regularization Algorithm Rules

Once a comprehensive dataset is formed, an artificial neural network (ANN) is needed to be trained for predicting the required corrective accelerating power to support the grid under different disturbances. In other word, the trained network, predict PEDG inertia based on the frequency trajectory and ROCOF and find an optimal power to restore frequency excursion in a timely manner. Typically, AI- based approaches suffers from lack of required database size, non-optimal regularization parameters, heterogenous dataset, overfitting problems and potential uncertain inputs. Using Bayesian regularization in the learning algorithm of ANN, enhances the training performance by finding the optimal parameters during training process. In Bayesian regularization algorithm (BRA), defining a cost function is required to adaptively decide on terminating the training process based on different problem objectives and regularization parameters. A typical problematic issue in feed forward neural networks is regarded to overfitting challenges that have direct influence on the network weights. This results in poor NNs generalization when they get new input data. The best method to resolve this issue is to regularize the estimation process. This is carried out by inflicting a penalty factor on the network cost function. Based on the problem objective in this work, the inputs are system frequency and ROCOF while target dataset include the required corrective active power to stabilize the PEDG under applied disturbances. Training data set are presented as,

$$T_d = \{((f_1, f_1'), \Delta p_1), ((f_2, f_2'), \Delta p_2), ..., ((f_N, f_N'), \Delta p_N)\} \tag{3.19}$$

Where f, f' are frequency and ROCOF and ΔP is the required corrective active power. A nonlinear mapping mechanism can be found to represent the input-output relation if a proper interpolating function is shaped. The mapping function is given by,

$$MP_i = \sum_{r=1}^{l} w_r \Psi_r(X_i) + G_i \ , \ X_i = (f_i, f_i'), MP_i = \Delta p_i \tag{3.20}$$

where $\psi(X_i)$ is defined as interpolating function with the weigh factor w_r. Should be remarked that G_i is a Gaussian random variable with average of zero. The probability density function of this variable can be shaped in a general format to be involved in optimization problem. In the proposed trajectory prediction process, it is aimed to minimize the prediction error, which is given by,

$$E_{T_d} = \frac{1}{N} \sum_{i=1}^{N} \left(MP_i - \widehat{MP}_i \right) \tag{3.21}$$

Where $\widehat{MP}_i$ is the predicted value which is the output of the trained NN. A Hessian matrix is estimated by Levenberg-Marquardt algorithm for a given function g: $\mathbb{R}^n \to \mathbb{R}$ as,

$$H_g = \begin{bmatrix} \frac{\partial^2 g}{\partial x^2_1} & \frac{\partial^2 g}{\partial x_1 \partial x_2} & \cdots & \frac{\partial^2 g}{\partial x_1 \partial x_n} \\ \frac{\partial^2 g}{\partial x_2 \partial x_1} & \frac{\partial^2 g}{\partial x^2_1} & \cdots & \frac{\partial^2 g}{\partial x_2 \partial x_n} \\ \vdots & & & \\ \frac{\partial^2 g}{\partial x_n \partial x_1} & \frac{\partial^2 g}{\partial x_n \partial x_2} & \cdots & \frac{\partial^2 g}{\partial x^2_n} \end{bmatrix}_{n \times n} \tag{3.22}$$

a second order of partial derivatives for all pairs of variables in domain of g shape all elements of this matrix. It should be noted that this matrix is used in machine learning algorithms for finding the saddle points and extremum of the given function. An objective cost function is defined by,

$$E_{r_d} = \eta \sum_{h=1}^{l} \sum_{p,q=1}^{m} (w_{pq}^{h})^2 + \frac{(1-\eta)}{N} \sum_{i=1}^{N} \left(MP_i - \widehat{MP_i} \right) \tag{3.23}$$

As mentioned, this cost function is used to maintain the generalization performance of the NN and η is defined as the weight factor of regularization with the value of $0 < \eta < 1$. In this stage, two different parameters are defined for the later objective function and (3.23) is reformed by,

$$\begin{gathered} F_{reg_d} = \rho E_{reg_d} + \mu E_{T_d} \\ E_{reg_d} = \sum_{h=1}^{l} \sum_{p,q=1}^{m} (w_{pq}^{h})^2, E_{T_d} = \frac{1}{N} \sum_{i=1}^{N} \left(MP_i - \widehat{MP_i} \right) \end{gathered} \tag{3.24}$$

Based on the BRA fundamental, the NN weight factors are selected in a random manner. Thus, probability function of NN's weights is given by,

$$f(w|T_d, \rho, \mu, N_n) = \frac{f(T_d|w, \mu, N_n) f(w|\rho, N_n)}{f(T_d|\rho, \mu, N_n)} \tag{3.25}$$

In this equation, network model is involved and represented by N_n. Also, the initial information regarding the weight factors is identified as a prior density function of $f(w|\rho, N_n)$. Considering given weight factors, the probability of receiving the data T_d is shown by $f(T_d|w, \mu, N_n)$. Also, based on the probability fundamentals, a normalization term as $f(T_d|\rho, \mu, N_n)$is used to ensure the total probability of 1 in (3.25).

$f(T_d|w, \mu, N_n)$ by considering the Gaussian random variable with variance σ^2 in the mapping function can be found by,

$$f(T_d|w, \mu, N_n) = \frac{e^{-\frac{\mu}{N} \sum_{i=1}^{N} \left(MP_i - \widehat{MP_i} \right)}}{\sqrt{(2\pi\sigma^2)^N}} \tag{3.26}$$

With the same approach,

$$f(w|\rho,N_n)=\frac{e^{-\rho\sum_{h=1}^{l}\sum_{p,q=1}^{m}(w_{pq}^h)^2}}{\int e^{-\rho\sum_{h=1}^{l}\sum_{p,q=1}^{m}(w_{pq}^h)^2}dw} \tag{3.27}$$

Considering (3.26) and (3.27), (3.25) can be represented as,

$$f(w|T_d,\rho,\mu,N_n)=\frac{e^{-(\frac{\mu}{N}\sum_{i=1}^{N}\left(MP_i-\widehat{MP_i}\right)+\rho\sum_{h=1}^{l}\sum_{p,q=1}^{m}(w_{pq}^h)^2)}}{\int e^{-\rho\sum_{h=1}^{l}\sum_{p,q=1}^{m}(w_{pq}^h)^2}dw\,\sqrt{(2\pi\sigma^2)^N}} \tag{3.28}$$

By rearranging (3.25), the normalization term is given by,

$$f(T_d\mid\rho,\mu,N_n)=\frac{e^{-(\frac{\mu}{N}\sum_{i=1}^{N}\left(MP_i-\widehat{MP_i}\right)+\rho\sum_{h=1}^{l}\sum_{p,q=1}^{m}(w_{pq}^h)^2)}}{\left(\int e^{-\rho\sum_{h=1}^{l}\sum_{p,q=1}^{m}(w_{pq}^h)^2}dw\right)^2(2\pi\sigma^2)^N} \tag{3.29}$$

The nominator of (3.29) is estimated around the minimum point of w_m. Thus, to find the optimum point, derivative of (3.29) with respect to ρ,μ should be equal to zero. By applying Hessian matrix in optimization process, the optimum parameters are given by,

$$\begin{aligned}\rho_{op}&=\eta(2\sum_{h=1}^{l}\sum_{p,q=1}^{m}(w_{pq}^h)^2\left|w_m\right)^{-1}\\ \mu_{op}&=(N-\eta)(\frac{2}{N}\sum_{i=1}^{N}\left(MP_i-\widehat{MP_i}\right)\left|w_m\right)^{-1}\end{aligned} \tag{3.30}$$

Getting the optimum parameters based on the training dataset structure, ensures high prediction accuracy of the trained network while enable the network to deal with noisy and small dataset with uncertain dynamic of inputs.

3.7. Simulation Results and Discussion

In this section, the functionality of the proposed approach is verified on the understudy 14-bus PEDG under several circumstances and MATLAB/Simulink is employed for simulation purposes. In the next step, the underlying concept of the proposed methodology is validated in the research Lab by a hardware setup in small scale. The setup can emulate the main dynamic of the 14-bus PEDG under different case studies. Briefly, two three phases GFMI and GFLI are feeding their local loads while are tied to each other by a resistive line. To emulate the disturbance scenario, a load step occurs in the grid buses. Three major categories of use cases are simulated and assessed in this section which comprise: *i)* extensive power generation loss in the grid due to any external grid's disturbances *ii)* generation loss in a reconfigured grid topology and *iii)* Load decrease in the reconfigured grid. For all categories, thorough comparisons are carried out with and without the proposed approach.

3.7.1. Power generation loss

In this scenario, the 14 bus PEDG's DERs are driving the total load in a steady state manner. Therefore, there is a stable power flow in the grid due to the steadied voltage and current conditions in all grid buses. GFLIs are feeding the loads based on their predefined power set points. For evaluating the efficacy of the proposed frequency restoration methodology, one of the GFLIs is equipped with the AI-based power reference correction module (AI-PRC). In the first scenario, a 200kW generation loss occurs while none of the DERs are equipped with the AI-PRC. As expected, a considerable frequency drop should be detected at the time of disturbance. Generation loss transpired at instant of t=8s. Figure 3. 2 illustrates the grid's frequency before and after this disturbance. As shown, a frequency drop of 3 Hz is observed. In this scenario, SG is the main contributor to governing the voltage and frequency particularly in the black start and during grid potential disturbances. Here, frequency is restored to the nominal value after about 4s. Figure 3. 3 shows the restoration

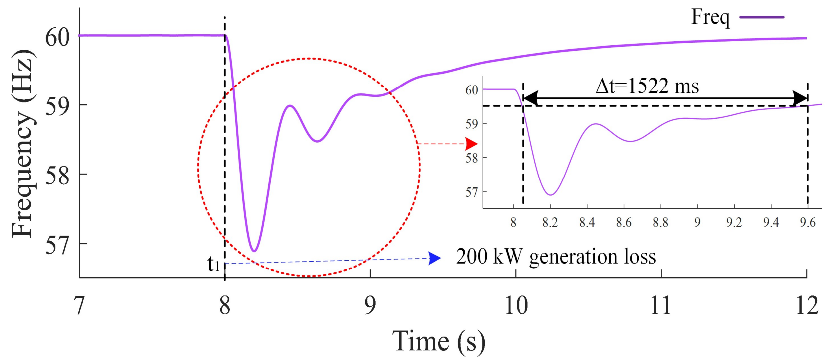

Figure 3. 2. Frequency dynamic when AI-PRC is disabled: 200 kW generation loss occurs and frequency drops to 57 Hz, the system is restored with 1522 ms.

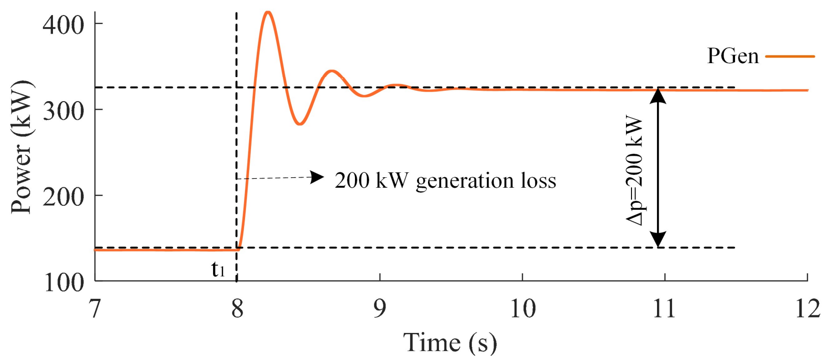

Fig. 3

Figure 3. 3. SG power dynamic without contribution of GFLIs in frequency restoration.

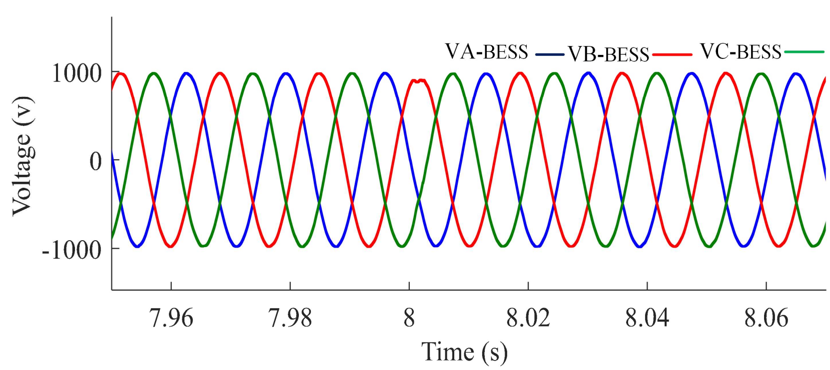

Figure 3. 4. GFLI voltage located at bus 13: generation loss occurs, and the voltage is stable at point of interconnection before transformer.

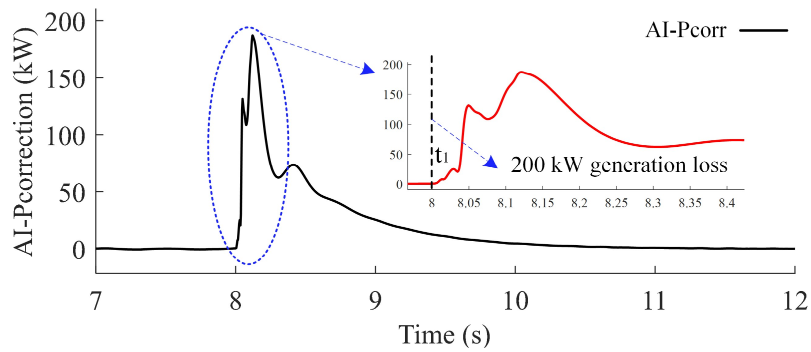

Figure 3. 5. AI-PRC output before and after 200 kW generation loss: power reference correction dynamic is added to GFLI power setpoint to contribute to frequency restoration.

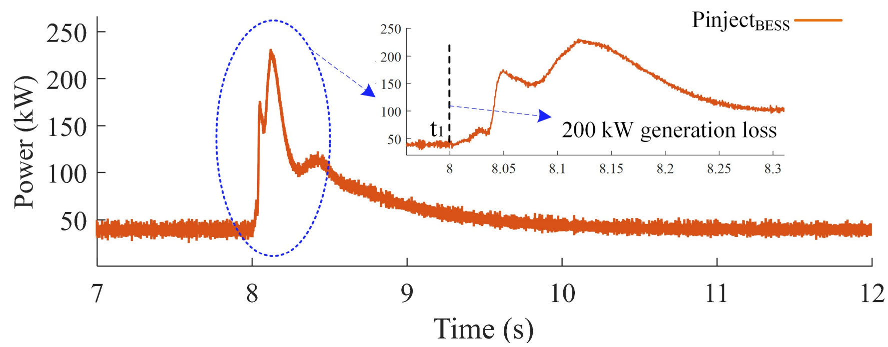

Figure 3. 6. Power injection by GFLI#6: 200 kW generation loss occurs and the grid following contribute to frequency restoration till SG increases its output power.

procedure carried out by the SG. This figure demonstrates the SG power dynamic during supporting the grid which relatively is slow.

The same as the frequency dynamic, the entire system needs around 4 s to establish a supply-demand balance. Should be remarked that the nadir frequency passes 57 Hz which most probably triggers the protection relay. Happening this condition certainly will result in a wide blackout which is not acceptable. Figure 3. 4 illustrates the GFLI#6 voltage before and after the scenario. The voltage waveform does not show considerable sag here due to the active and reactive support from SG. In the next use case, it is aimed to evaluate the

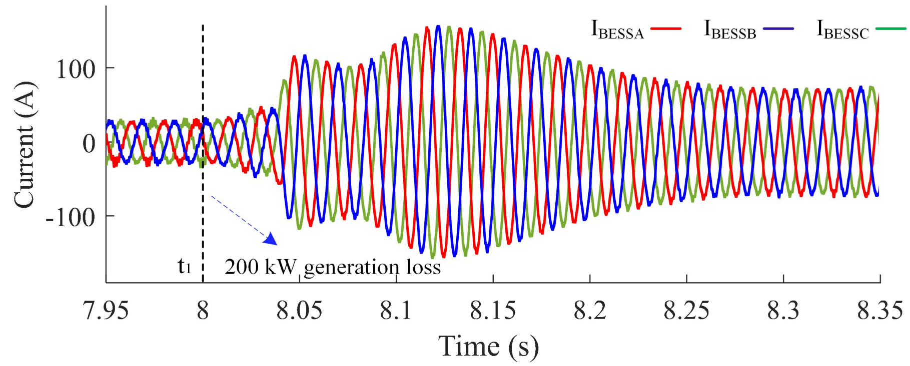

Figure 3. 7. Current dynamic of GFLI#6: 200Kw generation loss occurs and the power-supply balance is established in transient period by contribution of GFLI.

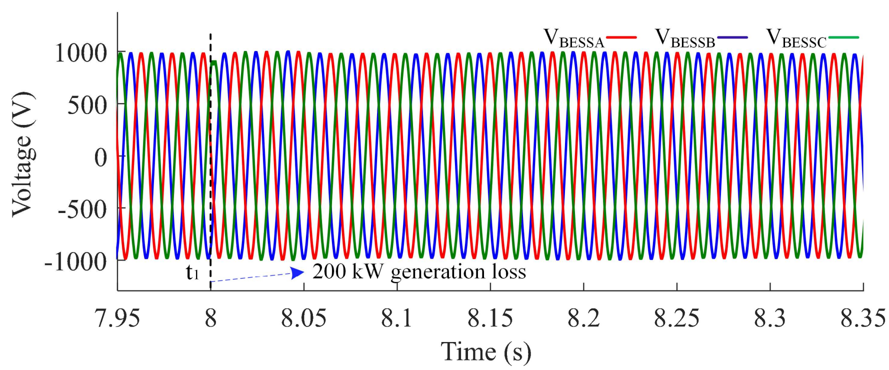

Figure 3. 8. Output voltage of GFLI at the point of interconnection: after generation loss, the voltage keeps stable by fast frequency restoration.

functionality of the proposed approach during the same disturbance and GFLI#6 is equipped with the AI-PRC. Figure 3. 5 shows the correction value that should be added to the power set point of GFLI. As shown, when the generation is lost, the entire grid experience lack of power, due to this fact the frequency is dropped with high steep. Considering the logic of training, the power correction value is increased and touches 200 kW with high accuracy. At the same time, SG is increasing the output power. As SG power increases, smartly, the AI module decreases the corrected power which results in decreasing the GFLI power reference

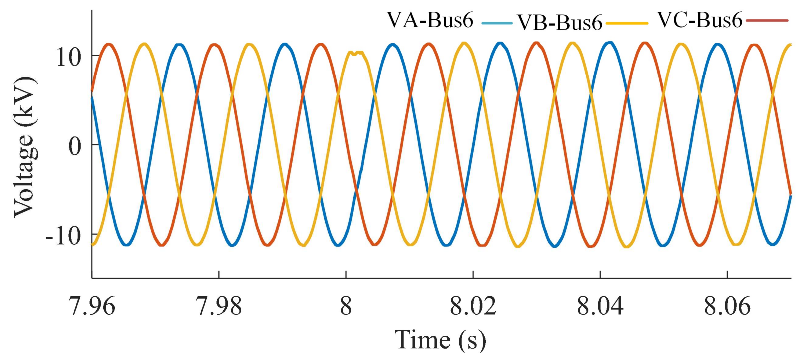

Figure 3. 9. Bus#6 voltage profile: generation loss occurs, and Bus 6 voltage is evaluated, Bus voltage at MV level is stable during the transient period.

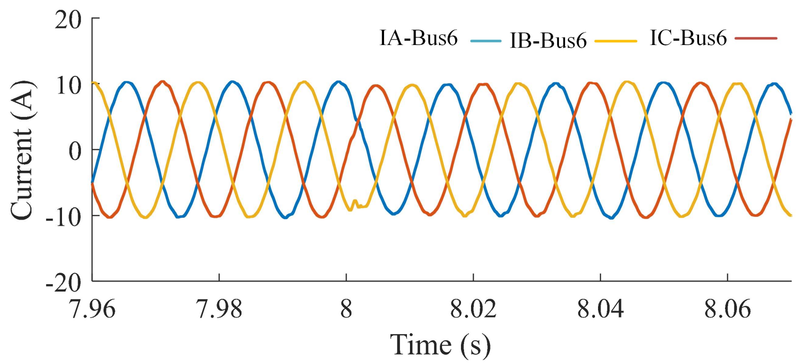

Figure 3. 10. Bus#6 current profile: generation loss occurs, and Bus 6 current is evaluated, current at MV level is stable during the transient period.

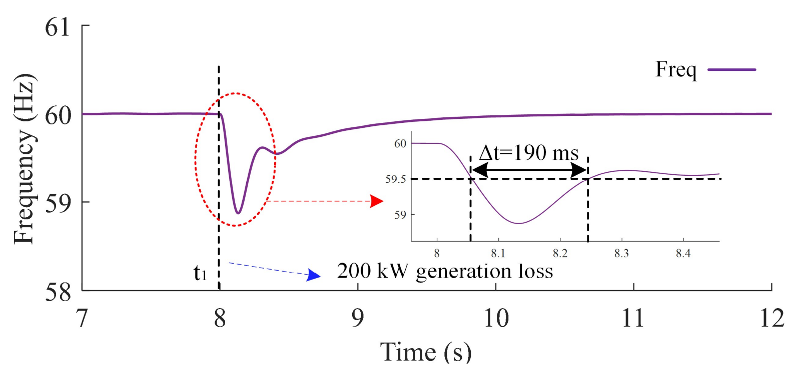

Figure 3. 11. Frequency dynamic by employing AI-PRC at control loop of GFLI#6: generation loss occurs, and frequency nadir reach to 59 Hz. Frequency is restored beyond 59.5 Hz by 190 ms.

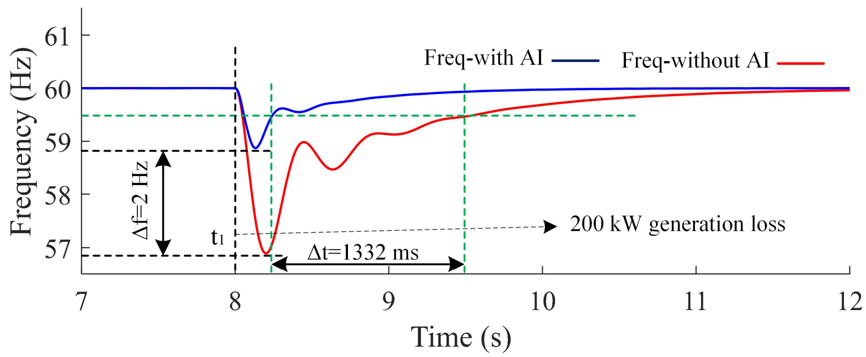

Figure 3. 12. Frequency dynamic comparison with and without deploying AI-PRC in GFLI#6 control loop: nadir frequency decreases 2 Hz when AI-PRC is enabled, and the restoration time decreases about 1332 ms.

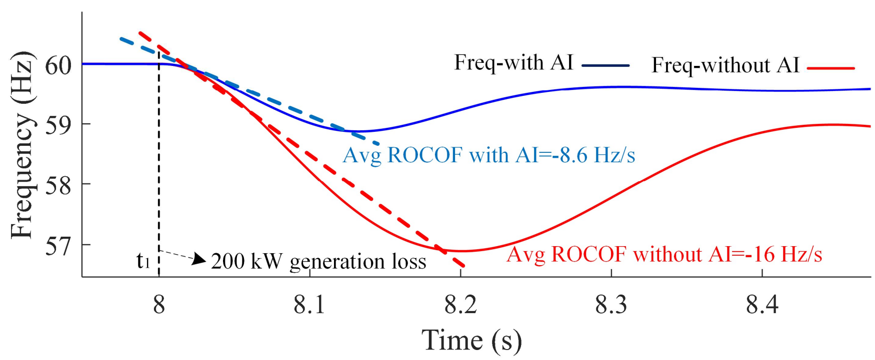

Figure 3. 13. Frequency dynamic and average ROCOF: generation loss occurs, average ROCOF decreases about 8 Hz/s when the GFLI contributes to frequency restoration process by deploying AI-PRC module in the control loop.

to its default value after about 4 s. Figure 3. 6 shows the active power injection dynamic of GFLI#6 which accurately follows its reference. Figure 3. 7 illustrates the current dynamic during the occurred disturbance. As shown, in the same manner of the corrected power reference, the current increases in three stage and converge to its nominal value after the disturbance is damped. GFLI voltage at its local POI is shown in Figure 3. 8. For evaluating the other buses of the grid, the voltage and current of Bus 6 are shown in Figure 3. 9 and Figure 3. 10 respectively. The frequency dynamic is shown in Figure 3. 11. This figure

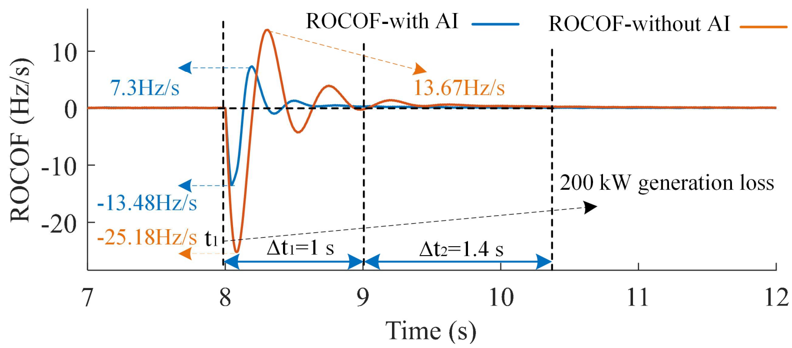

Figure 3. 14. Instantaneous ROCOF: generation loss occurs, peak to peak values in ROCOF domain decreases by 18.07 Hz/s when AI-PRC is enabled for GFLI. ROCOF reached to zero 400 ms faster.

illustrates that the frequency drop is around 1 Hz and is restored immediately. To have an evaluation metrical of the fast frequency restoration when the proposed approach is deployed, Figure 3. 11 shows the time duration that needs to stabilize the frequency beyond the 59.5 Hz is 190 ms. To have a better comparison of when the GFLI contributes to grid support, Figure 3. 12 and Figure 3. 13 provide details of the frequency excursion dynamic. Figure 3. 12 shows that the nadir frequency has improved by 2 Hz and the restoration process duration is decreased by about 1332 ms when the GFLI supports the grid in transient time. Figure 3. 13 demonstrates that the average ROCOF improves approximately twice the time the AI-PRC approach is not employed in the GFLI's control loops. Figure 3. 14 provides exhaustive information regarding instantaneous ROCOF for both use cases. As indicated, the maximum ROCOF is 13.48 Hz/s when the AI-PRC is deployed in the control loop of GFLI. This value reaches 25.18 Hz/s when GFLI does not contribute to frequency restoration.

3.7.2. Generation loss and grid structure reconfiguration

To generalize the functionality of the proposed approach in grid support during sever disturbances, it is crucial to contemplate some considerations that have meaningful influence

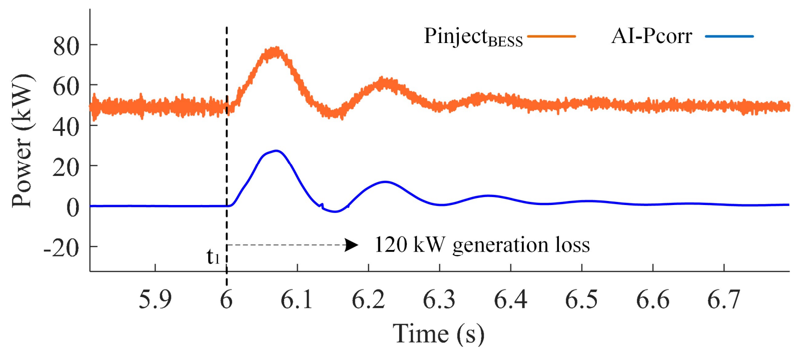

Figure 3. 15. Power reference corrective value generated by AI-PRC module when 120 kW generation loss occurs, GFLI output power follows the real time power reference correction value. GFLI Power rating limitation is 80 kW.

on the dynamic response of the grid. In this section, the grid structure is reconfigured and the limitation of the GFLI power rating is considered during their frequency restoration contribution. This physical variation would have explicit impact on the X/R ratio of the grid and the amount of short circuit ratio (SCR). Both can affect the dynamic response of the grid during severe disturbances. Should be commented that the provided use cases in this section can be great indication that the trained neural network is well generalized and can predict the frequency trajectory when the physically modified understudy grid is confronted with severe disturbances. Thus, the reconfigured grid is supposed to experience a severe disturbance and the effectiveness of the proposed approach in involving the GFLIs in frequency and voltage restoration is assessed. Two different transmission lines located in critical points of two different voltage level clusters committed to be disconnected. The employed modification

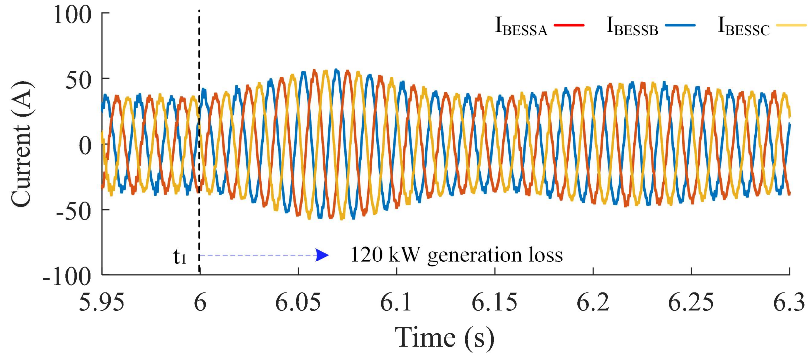

Figure 3. 16. Current dynamic of GFLI#6: 120 Kw generation loss occurs, and the power-supply balance is established in transient period by contribution of GFLI.

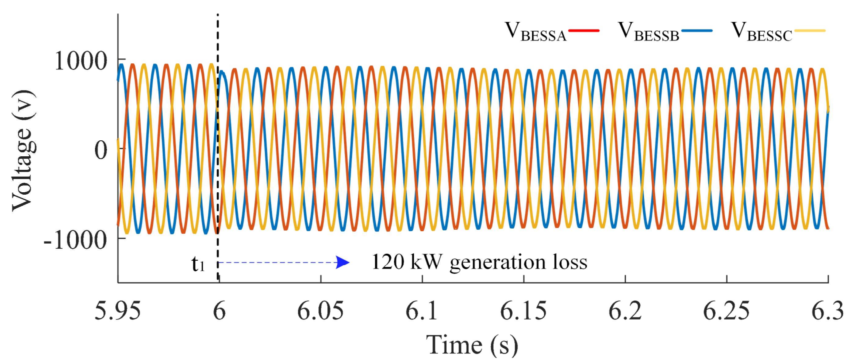

Figure 3. 17. Output voltage of GFLI at the point of interconnection: after generation loss, the voltage keeps stable by fast frequency restoration.

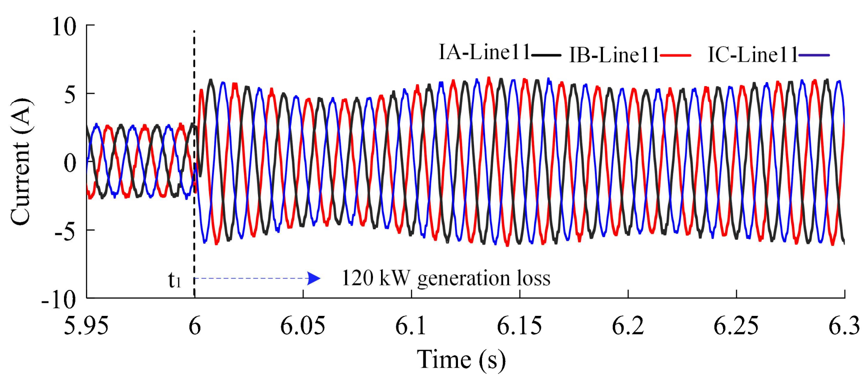

Figure 3. 18. Current profile during disturbance in Line 11 located at MV cluster: Power flow increases after contribution of GFLI in frequency restoration.

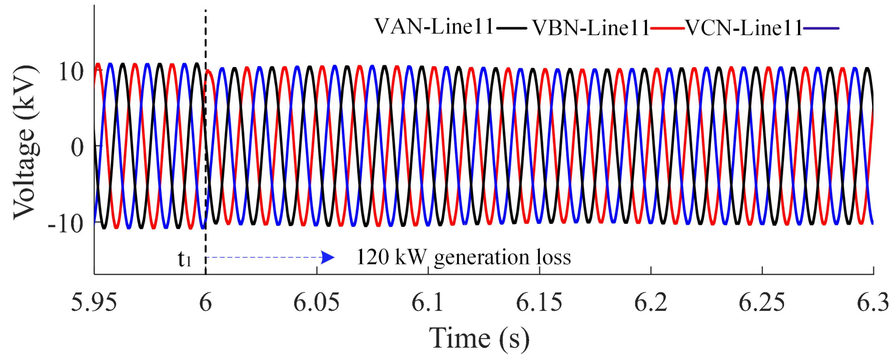

Figure 3. 19. Line to neutral voltage profile during disturbance in Line 11 located at MV cluster: Voltage profile is stable before and after generation loss.

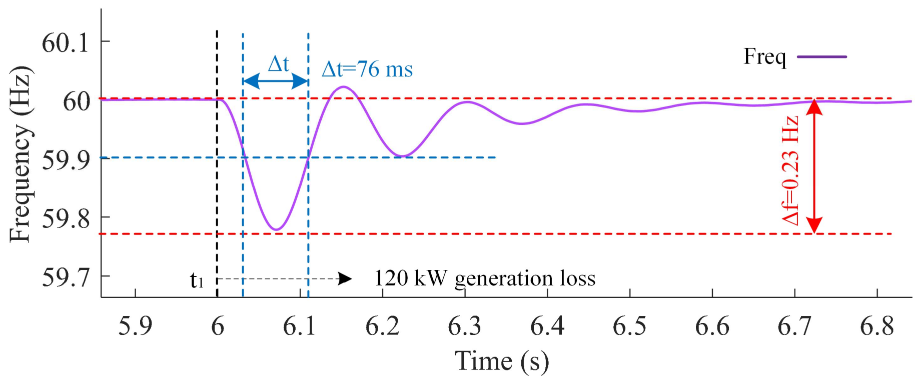

Figure 3. 20. Frequency dynamic by employing AI-PRC at control loop of GFLI#6: generation loss occurs, and frequency nadir reach to 59.8 Hz. Frequency is restored beyond 59.9 Hz by 76 ms.

alters the basic power flow paths remarkably. Assuming the hotline power rating is not jeopardized in this scenario after reconfiguration, a 120-kW power generation loss occurs in the understudy 14 bus PEDG. Here, the GFLI at bus 13 will support the grid in transient. This inverter has a power rating of 80 kW. Based on the local load of 50 kW of this inverter, the maximum power contribution of this inverter is confined to 30 kW. Line 14 was being operated at MV voltage level and line 4 was at LV level. As a result, it is anticipated that the power flow of line 11 increase during the power contribution of GFLI#6. Figure 3. 15 shows the power contribution of the GFLI during the transient following the power correction

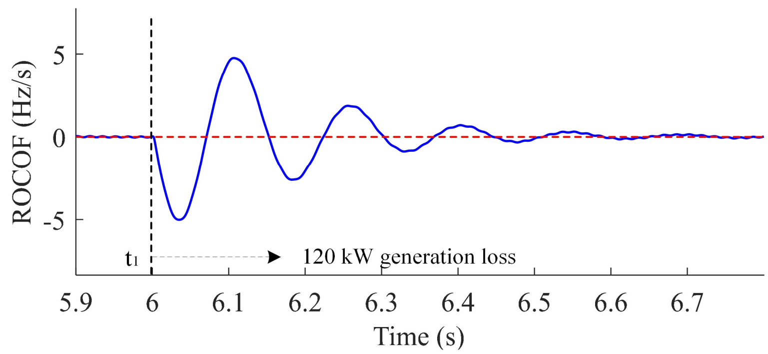

Figure 3. 21. Instantaneous ROCOF: generation loss occurs, ROCOF peak is controlled in the band of 5 Hz/s when AI-PRC is enabled for GFLI. ROCOF reached to zero with 160 ms.

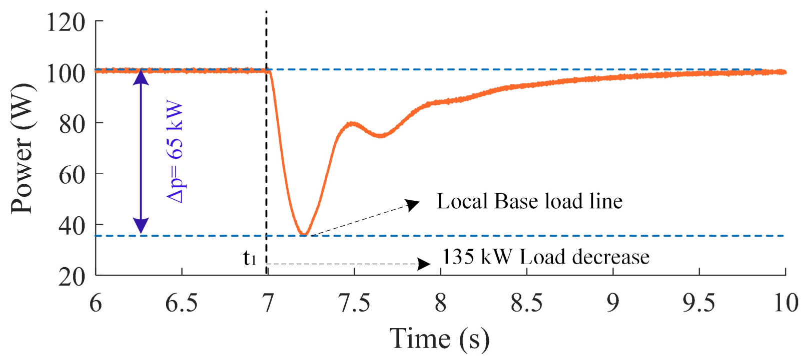

Figure 3. 22. Power injection by GFLI#6: generation loss occurs and the grid following contribute to frequency restoration by decreasing the output power till SG decreases its output power.

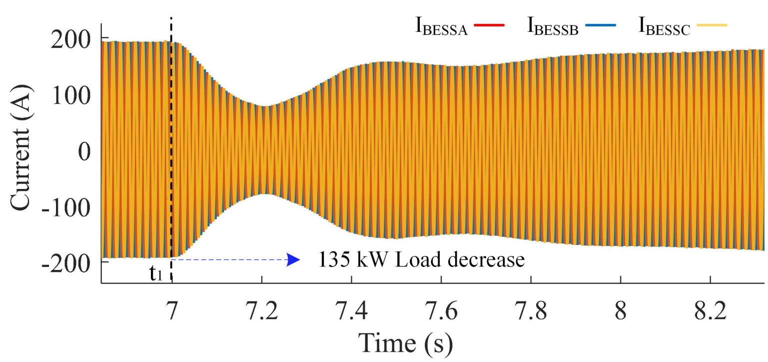

Figure 3. 23. Current dynamic of GFLI#6: generation loss occurs, and the power-supply balance is established in transient period by contribution of GFLI.

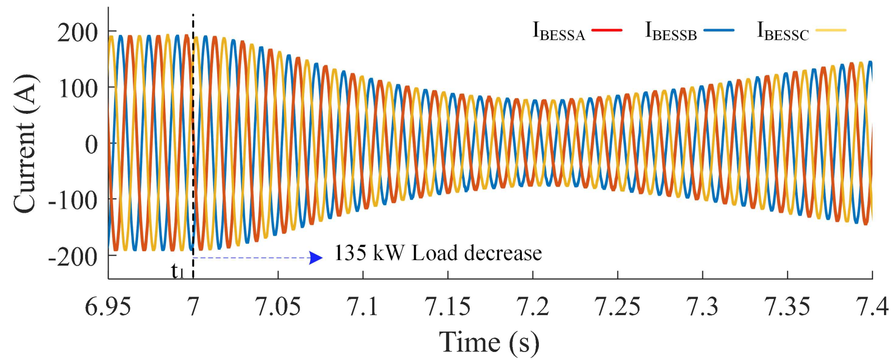

Figure 3. 24. Zoomed-in version of current dynamic of GFLI#6 at instant t= 7s: generation loss occurs, and the power-supply balance is established in transient period by contribution of GFLI.

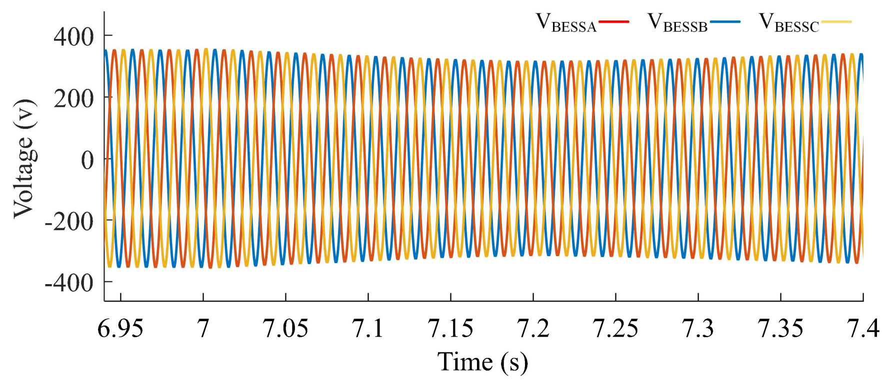

Figure 3. 25. Output voltage of GFLI at the point of interconnection: after 135 kw generation loss, the voltage keeps stable by fast frequency restoration.

command of AI-PRC. As shown, the maximum power contribution is around 20 kW to go along with the power rating restriction. The current and voltage dynamic of these inverters are illustrated in Figure 3. 16 and Figure 3. 17 respectively. As shown, the current increase based on the dynamic change of power reference, and the voltage is stable with an ignorable drop at the early time of disturbance. Figure 3. 18 and Figure 3. 19 demonstrate respectively the current and voltage of line 11 which is located at the MV cluster. As expected, the power flow level is elevated while the voltage level is kept at a nominal value. To assess the

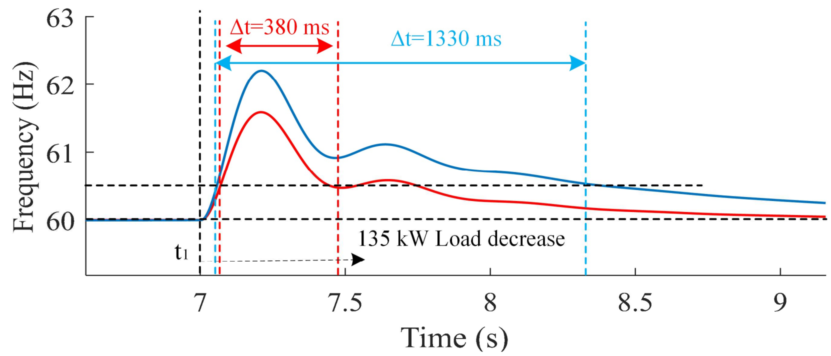

Figure 3. 26. Frequency dynamic comparison with and without deploying AI-PRC in GFLI#6 control loop: maximum frequency decreases around 1 Hz when AI-PRC is enabled, and the restoration time decreases about 1330 ms.

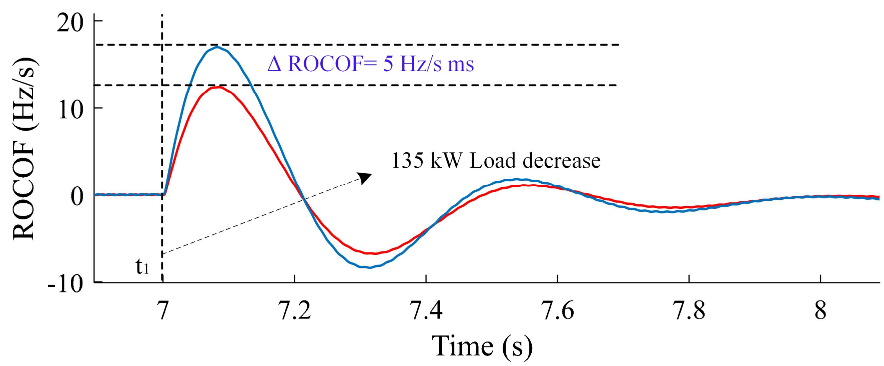

Figure 3. 27. Instantaneous ROCOF: generation loss occurs, peak values in ROCOF domain decreases by 5 Hz/s when AI-PRC is enabled for GFLI. ROCOF converges to zero in 1000 ms.

functionality of the proposed approach to fast frequency restoration while keeping the ROCOF in an acceptable range in a short time, Figure 3. 20 and Figure 3. 21 illustrate respectively the frequency excursion and ROCOF dynamic before and after this disturbance. As shown, the frequency is restored beyond 59.9 Hz around 76 ms while the frequency nadir differences with nominal value are kept in the band of 0.23 Hz. Should be remarked that this case study highlights the effective contribution of GFLIs in frequency restoration even by considering their power rating limitations. Moreover, the ROCOF is converged to zero around 700 ms, see Figure 3. 21.

3.7.3. Unplanned demand outage in a reconfigured grid with different inertia

To cover up all the grid potential disturbances and generalize the proposed approach, in this section, an unplanned outage occurs on the demand side. At instant t=7s, the 135-kW load is decreased. Moreover, some other effective elements in shaping the grid response dynamic are considered in this evaluation as well. The grid is reconfigured, the location of the supportive GFLI is changed and the total inertia of the grid is modified. Should be noted that, although the entire inertia of the grid is unknown parameter, however, by modifying the

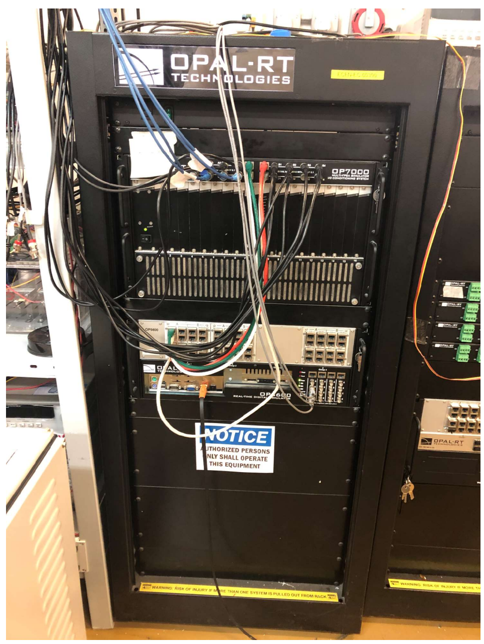

Figure 3. 28. OPAL-RT OP5600 platform: 14 bus PEDG is simulated and run in real-time for evaluating the performance of the proposed approach.

SG inertia constant, total grid inertia would be affected and running this use case can be an operational assessment of the trained neural network in the frequency trajectory prediction practice. As believed, the AI module ought to deliver a negative power reference to adjust the GFLI power reference in a way that power injection to the grid lessen. Though, the

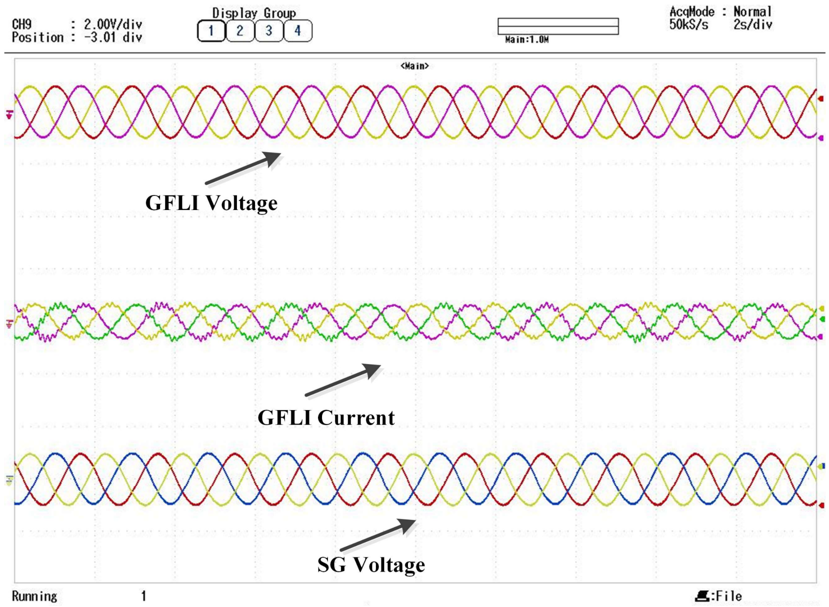

Figure 3. 29. Voltage and current of GFLI and synchronous machine voltage at steady state operation. Results have been captured by applying measurement gains.

inverter should sustain its local load that here is around 35 kW. In a steady state, the power injection was around 100 kW when the unplanned outage occurs. Figure 3. 22 shows the power dynamic of the inverter. As expected, the injecting power is decreased to the amount that no jeopardizations take places in the predefined constraints of inverter local load power. This Figure illustrates that the disturbance absolutely is restrained by 2.5s during the time that SG declines its output power to make up a new supply-demand balance operating point. Figure 3. 23 and Figure 3. 24 show the inverter current dynamic during the grid support. As obvious, the current gets the minimum acceptable value by 200 ms to dampen the disturbance and raises to the nominal value after about130 ms. Stable inverter output voltage at local POI is shown in Figure 3. 25 during the transient period. Frequency and ROCOF dynamics are demonstrated and assessed in Figure 3. 26 and Figure 3. 27 correspondingly. Figure 3. 26

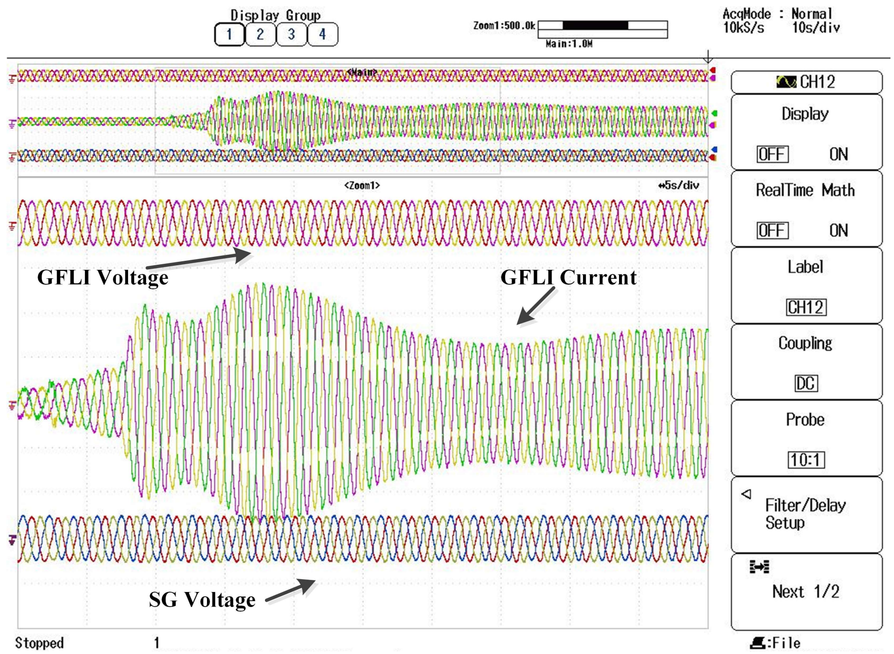

Figure 3. 30. Transient dynamic of voltage and current of GFLI and synchronous machine voltage when 200kW power mismatch occurs. Results have been captured by applying measurement gains.

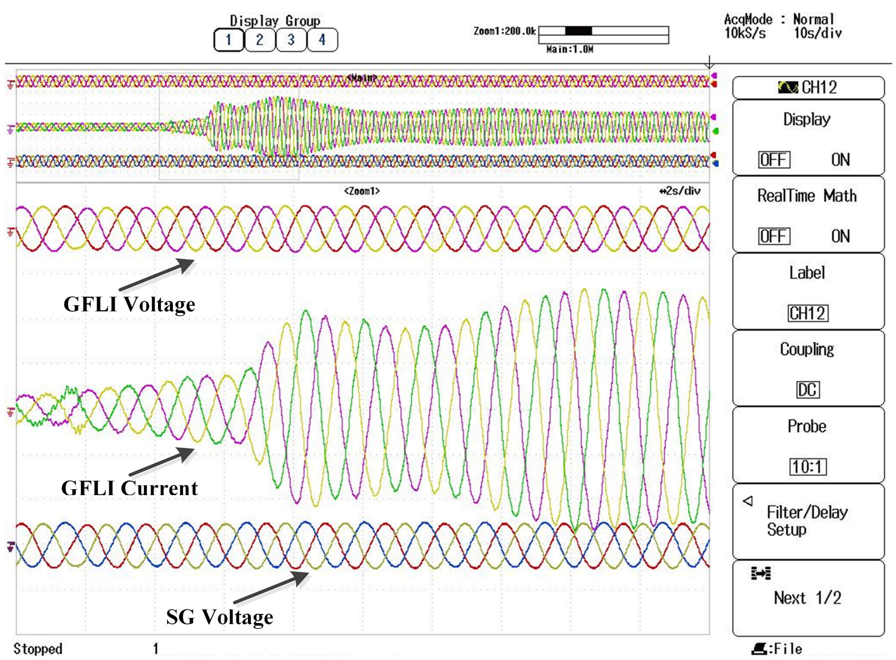

Figure 3. 31. Zoomed-in format of transient dynamic of voltage and current of GFLI and synchronous machine voltage when 200kW power mismatch occurs.

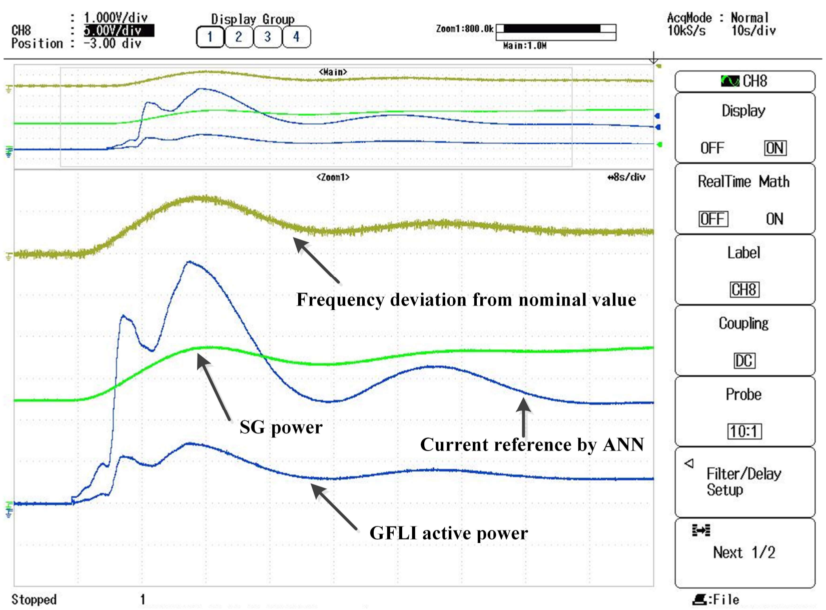

Figure 3. 32. AI-PRC outputs, frequency deviation and injected power by GFLI and synchronous machine for restoring the system frequency during power mismatch. Frequency excursion is damped by 640 ms.

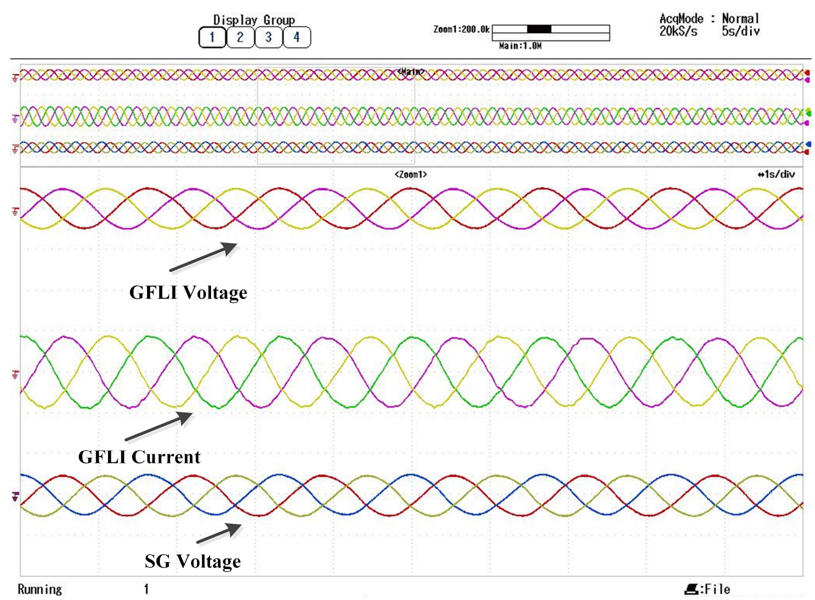

Figure 3. 33. Voltage and current of GFLI and synchronous machine voltage after handling system disturbance by GFLI contribution in transient, the grid continues its operation.

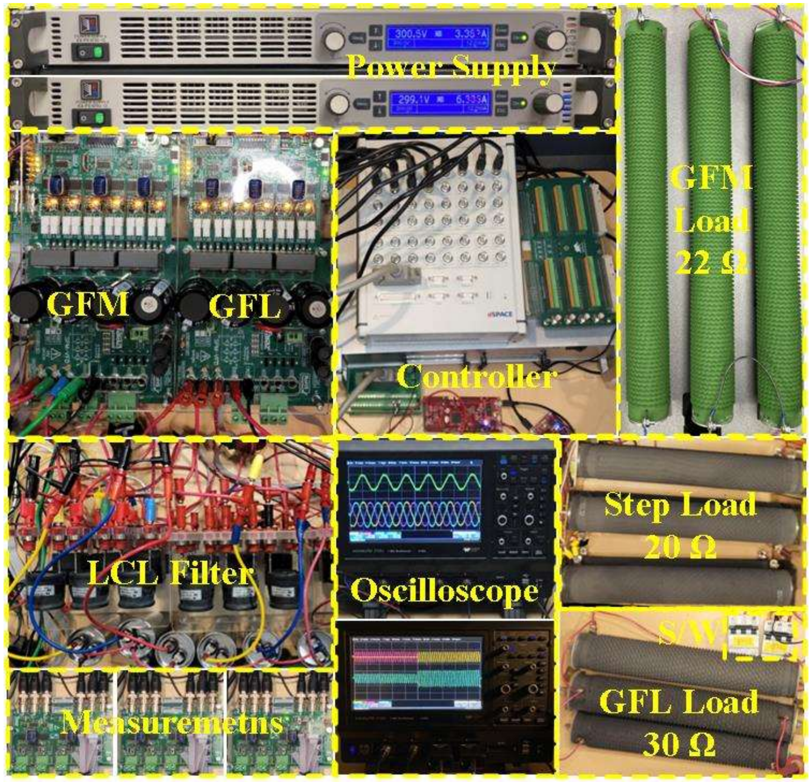

Figure 3. 34. Hardware setup for experimental validation of the proposed AI-PRC.

provides a detailed comparison of frequency dynamics with and without deploying the AI-PRC in GFLI control loops for the similar disturbance. As shown, frequency is controlled lower than 60.5 Hz in 380ms while without GFLI contribution this interval reaches 1330 ms. Moreover, the frequency peak is suppressed by 1 Hz more, by deploying the proposed approach. Regarding the ROCOF, a considerable 5 Hz/s improvement is achieved when the grid takes advantage of the GFLI equipped with the proposed AI module. See Figure 3. 27.

3.8. Realtime Simulation in OPAL-RT

In this section, the 14 bus PEDG is modeled and simulated in OPAL-RT OP5600 platform to validate the functionality of the proposed approach in real time. Figure 3. 28 shows the

Table 6. System Specifications

Parameter	Value & units
Dc link voltage V_{dc}	300V
Sampling time T_s	35µs
Inverter side inductance L_1	3.06mH
Grid side inductance L_2	1.364mH
Filter capacitor C_f	24.69µF
Capacitor ESR R_f	0.5Ω
Peak voltage V_g	150 V
Grid Frequency f_g	60Hz
GFMI rated power	5000 W
GFLI rated power	5000W
GFMI local load	30Ω
GFLI local load	22Ω
Step Load	20Ω

OPAL-RT that has been used for real time simulation in this work. Figure 3. 29 illustrates GFLI voltage and current as well as synchronous generator terminal voltage before applying the disturbance. As it is shown, voltage and currents are sinusoidal, and the grid variables are stable. It should be noted that the AI-PRC module is active in the control system of GFLI. To emulate a disturbance, DER 5 is disconnected from the rest of the grid. In this scenario, the PEDG experience 200kW power mismatch. As it is captured in Figure 3. 30, GFLI current increase and converge to another value in less than 325 ms and this is due to fast reaction of the implemented AI-PRC module to adjust the GFLI power set point based on grid's disturbances. The fast support of GFLI not only restores the frequency deviations to its nominal value but also keeps the grid voltage in the stable region. Figure 3. 31 shows the zoomed in format of Figure 3. 30 to clearly demonstrate the dynamic of GFLI which follow the AI-PRC output. Figure 3. 32 displays frequency dynamic deviation from its nominal value, the outputs of AI-PRC module, synchronous generator power dynamic, and GFLI powers dynamic in a single frame. When the power mismatch occurs, a notable deviation is seen in frequency. Here, the absolute value of frequency differences with its nominal value

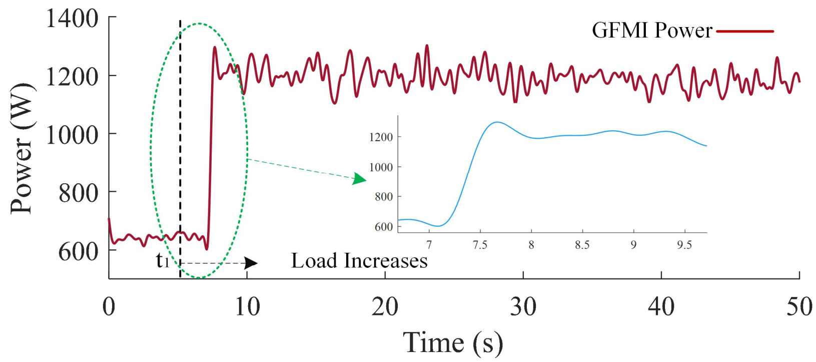

Figure 3. 35. GFMI power dynamic: Load increase in the grid while AI-PRC is disabled for GFLI.

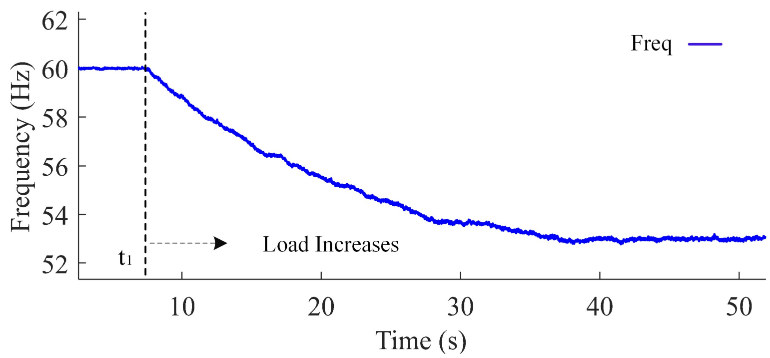

Figure 3. 36. Frequency dynamic: System loading increase while GFLI does not contribute to frequency restoration, also the restoration loop is disable in GFMI control loop. System frequency converges to other frequency point.

is shown. The AI-PRC module boosts up the current reference and the GFLI injects the requisite power to the grid. As seen, frequency excursion is damped by less than 640 ms. Due to the slow dynamic response of synchronous generator, GFLI continues injecting power till the synchronous generator catches up the mismatch power. Frequency reaches to its nominal value and the system keep on its normal operation steadily. Figure 3. 33 shows GFLI voltage, current and SG voltage after the disturbance is handled.

3.9. Experimental Results and Discussion

To assess the functionality of the proposed voltage and frequency restoration method by effective contribution of GFLIs, several use cases are experimentally tested and evaluated in a hardware setup depicted in Figure 3. 34. The understudy hardware emulates a realistic dynamic of a PEDG. Thus, voltage and frequency are built and controlled via a relatively low-inertia VSG-based GFMI. Also, a GFLI contributes to support the local loads with a constant power set point. Two power supplies provide the DC link voltage for both inverters' H-bridges. GFLI control loop is equipped with AI-PRC to interact dynamically with grid

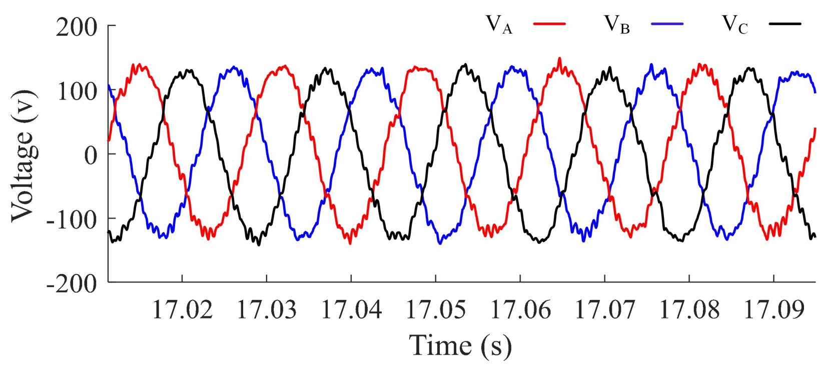

Figure 3. 37. Output voltage dynamic of GFMI: Voltage is stable after load disturbance.

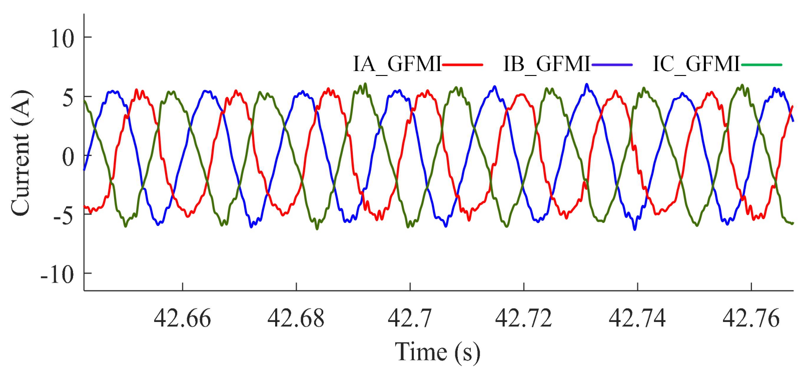

Figure 3. 38. Output current dynamic of GFMI: Current is stable after load disturbance.

during the potential disturbances in one of the provided case studies. Thorough technical specifications of the hardware components are listed in Table 6. Control mechanisms are implemented on a dSPACE control platform with turnaround time of 35 μs. In steady state, each inverter supplies their local loads. It is aimed to apply a step load compatible with grid nominal capacity at the POI and evaluate the system dynamics under different case studies.

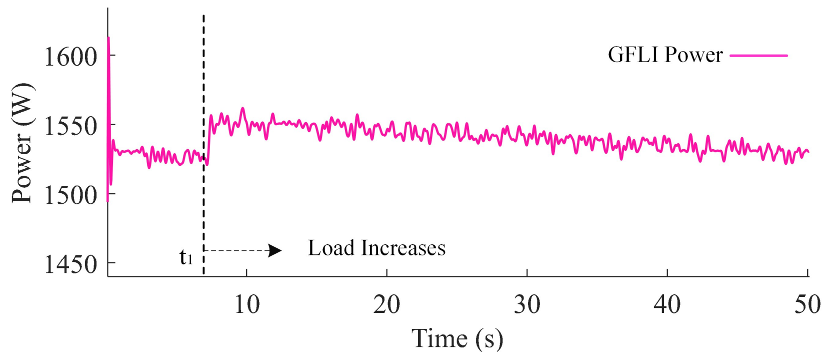

Figure 3. 39. GFLI output power dynamic: GFLI supply the local load at constant value before and after load disturbance, control system is not equipped with AI-PRC.

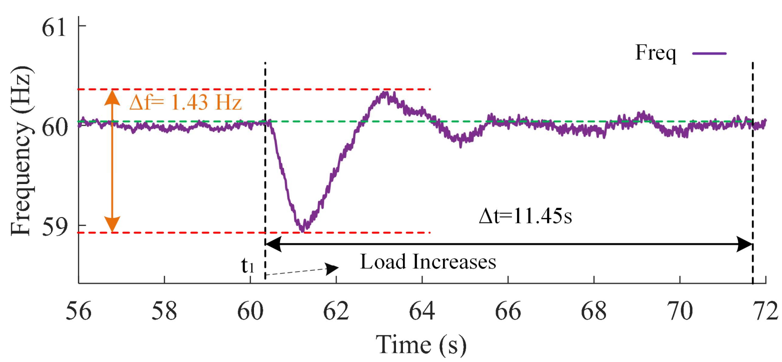

Figure 3. 40. Frequency dynamic: restoration loop is activated in GFMI power control loop. Frequency excursion is 1.43 Hz, and it is restored to nominal value with 11.45 s.

Due to the importance of control loop approach for supporting the low-inertia grids, three different case studies are considered by focusing on the practically used control approaches.

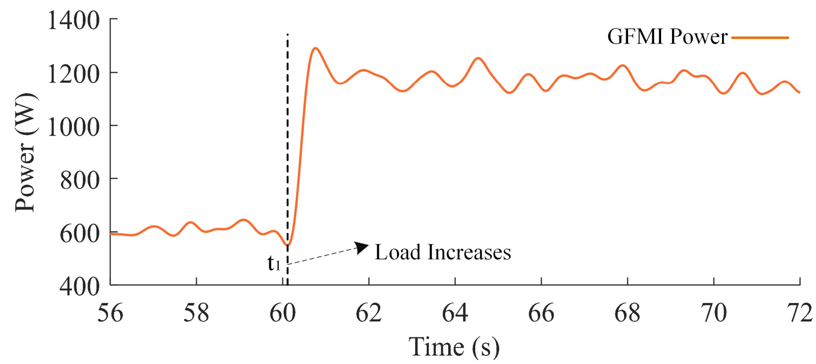

Figure 3. 41. GFMI power dynamic with restoration feature: Load increase in the grid while AI-PRC is disabled for GFLI.

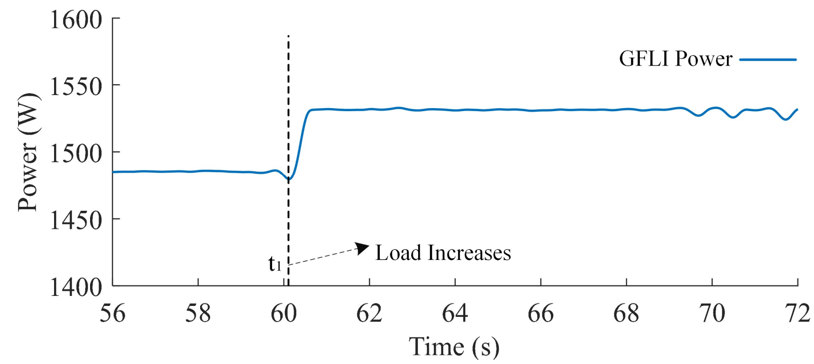

Figure 3. 42. GFLI power dynamic when AI-PRC: Load increase in the grid while AI-PRC is disabled for GFLI. Injecting power is constant before and after load disturbance.

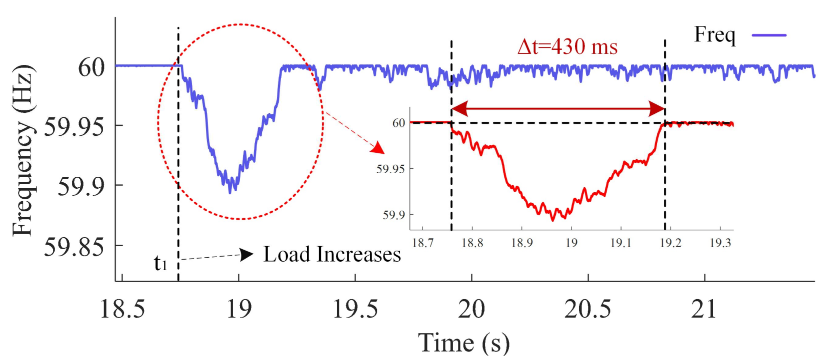

Figure 3. 43. Frequency dynamic: AI-PRC is enabled for GFLI, frequency excursion is 0.1 Hz, and it is restored to nominal value with 130 ms.

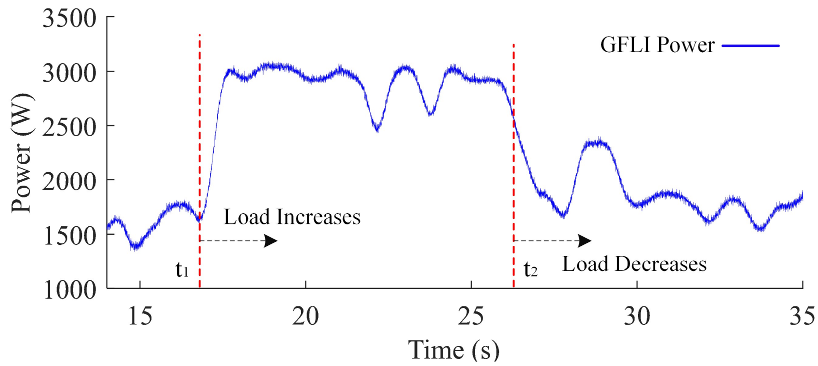

Figure 3. 44. Power injection by GFLI#6: load increases and the grid following contribute to frequency restoration.

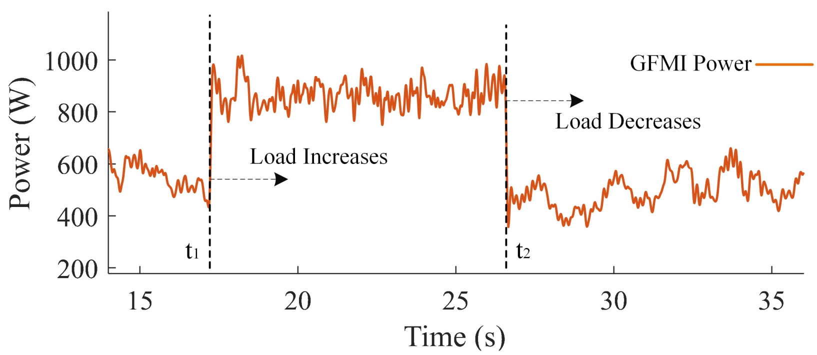

Figure 3. 45. Power injection by GFMI: load increases and the grid forming contributes to frequency restoration.

In the first case study, a step load occurs in the grid while the VSG-based GFMI controls the frequency excursions via implementing a linear governor. Here, the secondary layer of frequency restoration loop is deactivated. Figure 3. 35 shows the power dynamic of the GFMI. As shown, before stepping the load, GFMI is supporting a 600 W local load. After applying a step load around 1.5 kW, it is shown that a considerable frequency drop happens, see Figure 3. 36. This is due to the p-f droop-based control approach limitations that are tuned for certain range of load steps. Thus, if a sever disturbance occurs while the governor

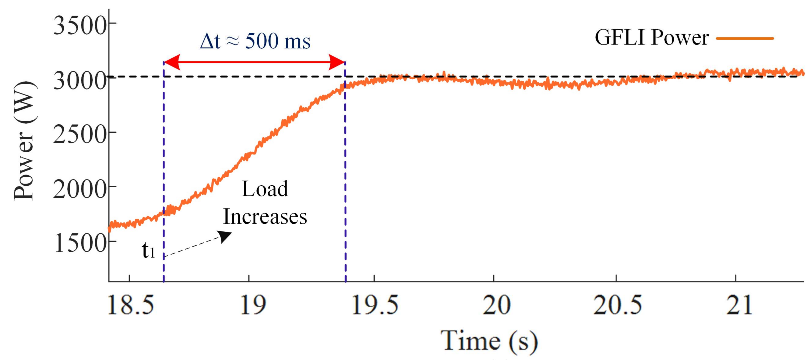

Figure 3. 46. Zoomed-in version of Fig. 39 around instant 17s.

is not equipped with restoration mechanism, the system would converge to another operation point. As shown, the frequency drops about 6 Hz and is fixed at another level. Should be mentioned that in this case study, the frequency protection relays has been locked to merely analyze the system dynamic. Moreover, it should be remarked that the filter structure that has been used in this hardware is *LCL*. Thus, the system loading is not purely resistive. Based on the power flow fundamentals, by decreasing the system frequency, the system inductance decreases. This will decrease the denominator of the power flow equation which results in an increase in the power flow amount. Additionally, VSG control loops follow the swing equations, thus if the frequency cannot be restored in a timely manner, the power difference is compensated by supporting the load in a different frequency operation point as can be understood from (3.1). Figure 3. 37 and Figure 3. 38 show the current and the voltage dynamic of the GFMI which are stable. Figure 3. 39 show the power dynamic of the GFLI. As expected, GFLI power injection should not vary before and after the disturbance.

In the second case study, the GFMI governor control loop is equipped with a well-tuned PI-based frequency restoration control mechanism. A step load around 600 W is applied on the grid. Figure 3. 40 illustrates the frequency dynamic. As shown, the system frequency is restored to the nominal value. However, the key point is the restoration time which is around 11.45 s in this low inertia grid, and this is due to the drawbacks of PI- based control approaches. Also, some high proportional and integral gains can enhance the restoration time, but those cannot be employed in a practical scenario. Indeed, if a sever load disturbance occurs, the frequency drop will push the protection relays to be triggered instantaneously. Figure 3. 41 and Figure 3. 42 show the GFMI and GFLI power dynamics respectively. As clear, the GFLI support the local load at constant power and GFMI supply the extra load.

In the third case study, a severe step load occurs in the grid while the GFLI is equipped with the AI-PRC module. Here, both GFMI and GFLI have effective contributions on the grid disturbances. Figure 3. 43 demonstrates system frequency dynamic. As shown, the frequency is restored to the nominal value of 60 Hz by 430 ms which is faster about 26 times compared to the PI-based control approach considering the severity of the disturbance. This shows the importance of dynamically contribution of GFLI in grid supporting. In fact, the system takes advantage from effective contribution of GFLIs in the transient periods that possibility of the blackout is high. Figure 3. 44 and Figure 3. 45 illustrate the power dynamic of GFLI and GFMI inverters before and after load disturbance. Moreover, to observe the fast power reference correction of GFLI that has been equipped with AI-PRC module, a zoomed-in version of Figure 3. 44 is shown in Figure 3. 46. As indicated, the system supports the extra load 1.5 kW with 500 ms.

3.10. Conclusion

An artificial intelligence-based power reference correction (AI-PRC) mechanism is proposed in this work to be deployed in GFLI's control loops. The proposed approach maximizes GFLI capabilities to have effective contributions to voltage and frequency restoration during grid disturbances. A two-layer feedforward artificial neural network (ANN) is learned by the Bayesian regularization algorithm (BRA) which facilitates the AI-PRC module to predict system frequency trajectory and provide the proper amount of power correction for GFLIs when the grid is confronted to any disturbances. Achieving this objective, PEDG's dominant dynamic rule to respond to any types of disturbances is found. Moreover, its validation is proved and generalized mathematically for a PEDG that comprises numerous GFLIs and GFMIs with a different types of control loops. For constructing the learning dataset, a nonlinear transient, and steady-state based-mathematical equation is solved for normal and sever disturbances. As the relation between the frequency and ROCOF with the required amount of power correction is found, the learning dataset is generated by sweeping all effective variables which shape the system's dynamics. Training the neural network by using BRA enhances the frequency trajectory prediction module even if the data size is limited, noisy or the inputs show high uncertainty. This fact independently is proved mathematically. Several use cases are simulated and analyzed in a realistic 14 bus PEDG by MATLAB/Simulink to evaluate the functionality of the proposed approach to enhance the grid resiliency. Moreover, a hardware setup that emulates PEDG dynamic is built, and several use cases are validated experimentally.

Chapter 4

4. Resiliency of Power Electronic Dominated Grids: Frequency Restoration Under Normal and Abnormal Disturbances

Parts of this chapter, including figures and text, are based on my following papers:

- M. Hosseinzadehtaher, A. Y. Fard and M. B. Shadmand, "Event-triggered Self-learning Control Scheme for Power Electronics Dominated Grid," 2021 IEEE Energy Conversion Congress and Exposition (ECCE), 2021, pp. 1103-1109.
- M. Hosseinzadehtaher, A. Y. Fard, M. B. Shadmand and P. Fajri, "Artificial Intelligence Inspired Model Predictive Control for Frequency Regulation in Power Electronics Dominated Grids," 2021 IEEE 12th International Symposium on Power Electronics for Distributed Generation Systems (PEDG), 2021, pp. 1-6.
- M. Hosseinzadehtaher, A. Khan, M. B. Shadmand and H. Abu-Rub, "Anomaly Detection in Distribution Power System based on a Condition Monitoring Vector and Ultra- Short Demand Forecasting," 2020 IEEE CyberPELS (CyberPELS), 2020, pp. 1-6.
- S. Harshbarger, M. Hosseinzadehtaher, B. Natarajan, E. Vasserman, M. Shadmand and G. Amariucai, "(A Little) Ignorance is Bliss: The Effect of Imperfect Model Information on Stealthy Attacks in Power Grids," 2020 IEEE Kansas Power and Energy Conference (KPEC), 2020, pp. 1-6.

4.1. Event-triggered Self-learning Control Scheme for Power Electronics Dominated Grid

The growing penetration of distributed energy resources (DERs) requires renovation of the conventional power grid into a new paradigm, so-called power electronics dominated grid (PEDG). Alongside the features introduced within this new concept, the PEDG is more prone to cyber-physical malicious activities because of the distributed communication infrastructure and accessibility of the resources. Some of these malicious activities e.g., stealthy attacks, are unobservable for the supervisory system until the control system diverges. Some of these attacks might result in loss of DER generation that could cause frequency deviations beyond permissible boundaries specified by the DERs grid integration standards. Thus, in this section, other applications of the previously proposed approach are provided.

An integrated data-driven and model-based predictive control (IDMPC) is implemented on power electronics interfaces of the distributed energy resources (DERs) at the grid-edge to enable the control of islanded grid-cluster frequency feature such as rate of change of frequency (ROCOF) and nadir frequency. The presented IDMPC scheme has fast dynamic response and is robust to system disturbances. The functionality of the proposed method for supporting the voltage and frequency of the grid is verified by some case studies.

Soon after, a review of the different cyber-attacks is provided in the literature review section, and their adverse impacts on the power system is discussed. As stealthy attacks are one of the most threatening events in power system, this type of attacks is discussed with more details in this chapter. To fulfill frequency restoration in the event of stealthy attacks, this section also proposes a novel shadow control scheme which leverages the advantages of artificial intelligence techniques for enhancing PEDG resiliency. A cohesive data-extracted methodology built-in a shadow control (CDMSC) scheme is developed with inherent features of the artificial neural networks (ANNs) to enhance the dynamic response of the system. When a stealthy attack occurs, the state variables easily become unstable while the observable and measurable global variables do not breach their standard ranges or at least violation occurs with some delay. Due to this unobservability and the intrinsic latency in common supervisory control techniques, there is a possibility that local DERs will be pushed islanded while the supply-demand balance is jeopardized before the supervisory layer of control take any effective action.

The proposed CDMSC approximates the grid's inertia by ANN module, accurately. Different practical frequency dynamics, ROCOF and inertia constant are considered in the training process to ensure all possible scenarios on a realistic power system. Moreover, several disturbances including, load disturbances and potential loss of generation are considered in this development. It should be remarked that oscillation pattern of frequency is dictated by the synchronous generators in the understudy system; thus, considered disturbances are used as inputs of swing equation and the required power is calculated based on the frequency excursion and ROCOF. This data is used as test data in training process. A feed-forward ANN with two layers is applied in key core of the shadow control scheme towards an event-triggered self-learning controller that is guiding supervisory controller. Bayesian algorithm is utilized in the training process and optimum numbers of hidden neurons are founded by several evaluation of training mechanism. During the normal operation of the PEDG, all DERs inject active power considering various criteria including, maximum available power, state of the charge, rate of power reserve, etc. If an unusual deviation on the frequency or its rate of change occurs, the artificial-intelligence-inspired shadow control of the grid cluster is activated to re-balance active power across the grid within a short timeframe while slow-response synchronous generators are trying to catch up. The ANN module of the proposed shadow control provides accurate feedbacks for the DER controller to support the grid frequency for any potential disturbances. The proposed shadow control framework is verified on a 14-bus PEDG system.

Also, in this chapter, a proactive intrusion detection system (IDS) as another safety layer is designed for smart distribution power systems. The considered attack scenario is manipulation of the advanced measuring infrastructures (AMIs) readings and/or smart inverters data. These manipulated data from the grid edge devices mislead the grid operator for making proper operational planning decisions. In a stealthy attack model, where the attacker compromises significant number of these smart devices, serious demand-supply unbalance can occur that may result in major blackouts. The proposed IDS is based on a condition monitoring vector (CMV) equipped with a learned ultra-short-term demand forecasting (USTDF) mechanism. This cybersecurity approach can verify smart devices readings. In the proposed method, the instantaneous difference of collected AMIs and other smart devices data with the ultra-short term forecasted demand is defined as the CMV. This vector probes a pre-defined error band for identifying the compromised smart devices. The learned USTDF mechanism is based on the distribution grid historical load profile and the temperature data for the goal area. An accurate multi-dimensional regression model is developed and learned for forecasting the load behavior in this area. Finally, the suspicious areas are flagged or become separated from the main grid by the network operator based on the proposed CMV outcomes and the output of decision-making module. The proposed IDS aims to enhance the cybersecurity of the smart devices at the grid-edge that plays major role in ensuring the resiliency of the grid. The theoretical analyses are verified by several case studies

4.2. Literature Review

The Renewable-based energy resources are becoming as the main suppliers in the new energy paradigm. This fact upgrades the traditional structure of the power system in a way that the generation and demand centers are situated in a closer proximity. Power electronics dominated grid (PEDG) is an inevitable consequence of this paradigm which can provide several advantages for the entire energy system. However, PEDG is susceptible to be confronted with some severe challenges which are mostly associated with the low level of system inertia [92].

Natural disasters, cyberattacks, and demand prediction uncertainty are perilous common occurrences in power system which can jeopardize the supply-demand balance easily. Contemplating the low inertia of the PEDG and its inherent structure, frequency and voltage regulation should be addressed properly to ensure system stability [92-94]. It should be remarked that if the employed frequency control scheme is not able to handle potential disturbances in a proper time frame, protection relays are triggered and consequently, load shedding or wide area blackout may happen [95, 96]. Additionally, based on the power system safety guidelines, the relays' settings are set and coordinated in a manner that are sensitive to the rate of change of frequency (ROCOF) [97]. Thus, the security of the energy supply steadiness in PEDG can easily be jeopardized if not properly controlled in a short time.

Numerous frequency regulation approaches have been studied in literature which can be categorized as: (i) energy supply control, and (ii) energy consumption control. Droop-based control approach is one of the leading methods which is used to enhance voltage and frequency regulation by focusing on the energy supply control of the grid. In fact, based on the *X/R* ratio of the system, power transfer behavior is formulated and used as the groundwork for this control scheme [98-104]. However, it should be noted that, droop gain tuning is highly correlated to the grid characteristic. In [105], a generalized droop control method is proposed which can regulate the PEDG voltage and frequency for a wide range of load disturbances. Nevertheless, this approach highly depends on the line parameters whereas the estimation of them is a challenging issue in PEDG. A new framework which is based on an adaptive neuro-fuzzy inference system is proposed in [105] to remove previous method dependency to the line parameters. Nonetheless, the training process is based on the limited number of grid configurations.

Some literatures have aimed to reduce the dependency of droop-based approaches on the grid topology. For example, in [106], a distributed-averaging proportional- integral technique is used to provide a proper frequency regulation in a microgrid. Although in this method, there is no requirement to have a prior knowledge about the grid topology. However, having nearest-neighbor communication is crucial for executing a proper control action. It is worthy to note that the idea of enhancing the frequency restoration by means of communication techniques has been surveyed with more details in [107-110]. Notwithstanding, having complicated and various communication infrastructure increase the system complexity and failure probability due to intentional or unintentional events which may results in grid instability [111-114].

In [115], a coordinated voltage and frequency methodology without needing any communication devices is proposed for filling the mentioned research gaps and enhancing dynamic performance of the system in response to large load disturbances. A distributed controller for the system components is used based on the different dynamic response to regulate voltage and frequency considering the IEEE standards as operation limits for islanded microgrid. Some adaptive roles are deployed for each device for regulating the frequency and voltage based on their response time in transient condition. However, deploying predefined adaptive roles makes the control technique complicated. Adding extra synchronous generators in the system is recommended by [116] for supporting the frequency regulation schemes. Although this approach increases the system inertia and thus enhances system stability during load disturbances, but it increases the system total cost as well as the power loss. Thus, it is essential to have a review on the control approaches which focus on the energy consumption side.

Some research articles have surveyed the effects of load and operating voltage variation on frequency restoration [117]. For instance, several centralized and decentralized load control techniques have been studied in [118] in this regard. In [119], a load control methodology is proposed that measures the frequency and ROCOF values and considers them as the inputs of a fuzzy control system. It should be mentioned that artificial intelligence

(AI) techniques have attracted more attentions in many research disciplines particularly when studying complex, multi-dimensional, and non-linear systems such as PEDG [120]. Some of these methods are so effective to be employed in real-time optimal control and providing remarkable results [121-124]; still, the challenge is the selection of a proper AI technique, as well as training and implementing them for the system in hand. A distributed automatic load frequency control methodology is developed in [125]. For solving optimal load control problem, the combination of power grid dynamic and proposed approach is interpreted as a partial prima-dual gradient algorithm. The control approach relies on local measurement and local communication. Nevertheless, energy consumption control methodologies require communication infrastructure and extra controllers for each single appliance which are known as the downsides of these approaches. Furthermore, the demand side management approaches are associated with a level of uncertainty which can easily jeopardize the system stability.

As mentioned, unlike the conventional power grid that large centralized power plants using non-renewable fuels (e.g., oil, coal, nuclear fuel, etc.) are the main providers, distributed energy resources (DERs) are expected to become the primary providers in the modernized power grid [126]. Although the concept of PEDG enables rising penetration of renewable resources across the grid, it introduces some challenges in privacy [127], stability [128], control [129], cyber-physical security [111, 113, 130], and planning [112]. These challenges need to be addressed to accelerate full implementation of this paradigm.

To ensure full control over the PEDG, the control hierarchy of the conventional power system, which is a three-layered control framework is adopted [131]. Power quality and stability of the grid are guaranteed by primary and secondary layers of the control hierarchy via high-bandwidth control techniques [132], while the tertiary layer confirms optimal operation of the entire system [94]. Satisfactory cooperation of the numerous agents i.e., smart inverters, sensors, smart meters, etc. across the PEDG requires adequate communications among these control layers that means a high traffic distributed communication infrastructure. The dispersed nature of communication infrastructure makes the entire PEDG more susceptible to cyberattacks. Various types of cyber events are studied in the literature including false data injection (FDI), denial of service (DoS) [133], man-in-the-middle malicious activities, stealthy attacks [114], and advanced persistent attacks. Each of these attack categories target different goals, differing from gaining illegal financial benefits to cascading failures of the grid, yielding to large-scale power outages. To prevent, detect, and mitigate these attacks, the PEDG must be equipped with intrusion detection systems (IDSs) [113, 134, 135]. Although various types of IDSs are proposed and implemented with proper performances, stealthy attacks on the state variables of the system are unobservable by the supervisory layers until their harmful intentions are attained on the system [136]. One of the main targets of the stealthy attacks on the power system is the frequency by deteriorating the active power balance across the grid that could cause vast outages [137].

Stealthy attacks on control systems have the potential to cause serious harm, as they are not readily detectable by any intrusion detection system. However, it is often the case that neither the controller nor the attacker can gather perfect information about the system model. It is shown in this work that while a small mismatch between model and reality can easily be managed by a robust controller, an attacker's imperfect knowledge of the system can thwart the stealth of the attack. This opens the door to a whole new class of defense mechanisms, which focus on maximizing the attacker's uncertainty about the system while maintaining the controller's uncertainty within the bounds of its robustness.

In this work, stealthy attacks are considered on the control signals of control systems. A stealthy attack is an attack on the control signal that drives the state of the system to be unstable, while the output of the system remains the same, and thus, the attack goes undetected. Stealthy attacks were introduced in [138], and subsequently applied to power systems in [139] – the latter also defines formal notions of undetectable and unidentifiable attacks. Much of the work on stealthy attacks in power systems is restricted to attacks on measurements. In this context, false data injection attacks are considered stealthy if they are within the span of the system's output matrix [140], [141], [142], [143], [144], and are undetectable by an anomaly detector based on the weighted least squares state estimation, or by a CUSUM-like system [145]. In [146], the authors analyzed the trade-off between the damage from an attack and the accuracy of the attacker's knowledge, in the context of a stealthy measurement attack where the attacker has imperfect knowledge of the system. The authors of [147] provide an extension of the weighted least squares state estimation anomaly detector by using multiple least trimmed squares state estimators. The purpose of this anomaly detector is to increase the anomaly detector's ability to detect an attack while remaining cost effective to implement. An online anomaly detector for attacks on power systems is proposed in [144]. This anomaly detector uses the topology processing, system parameters, and real-time load forecast information to predict the state of the system to compare with the state estimator. In [148], the authors emphasize the importance of securing the system at the network layer. This includes implementing a form of data authentication and using multipath routing of the date.

Countermeasures for the control-signal stealthy attack model in the general control system scenario are further developed in [149], [150], [151]. It was shown in [149] that perturbing the system matrices can reveal a stealthy attack. However, this model is unnecessarily limited by assuming that the attacker has full knowledge of the system. A stateful anomaly detector using a cumulative sum statistic is proposed in [150], meaning that the anomaly detector takes into consideration the state of the system, rather than the stateless anomaly detector which considers the observations. The authors analyze the effect of the control algorithm on the damage that can be done to the system and find that a nonlinear controller works best. In [152], the authors provide conditions for which an attacker is not able to mount a stealthy attack on a discrete time linear time-invariant system. The authors of [153] define the optimal attack strategy by analyzing the tradeoff between the increase in quadratic cost that an attack causes and the stealthiness of an attack.

Generally, in the power grid, the balance between demand and supply could be jeopardized due to major inaccuracies in generation/demand prediction algorithms, natural disasters, cyberattacks, etc. For maintaining a resilient and stable operation of the PEDG, demand and supply must stay balanced unceasingly [154]. In the conventional power system, considering the dynamics of the system frequency, which are mainly formed by the rotating inertia of synchronous machines [16], if a sudden loss of generation occurs, the rotating energy stored in the rotor is transformed into electrical power to meet the existing demand, which causes a transitory frequency drop. This frequency drop must be mitigated in a timely manner, otherwise the DERs will pushed to go islanded according to the grid integration standards e.g., IEEE 1547 [155]. Also, it is mandated by North American Reliability Corporation (NERC) that the first level of under-frequency load shedding (UFLS) relays should be triggered if the frequency drops down more than 0.7 Hz and the synchronous generator must be disconnected if the frequency goes beyond 61.8 Hz in a 60-Hz system.

Considering the distributed nature of the PEDG, frequency issue becomes more challenging due to the lower level of inertia in the PEDGs (< 2s) in comparison to traditional power grids (~ 10s) [156]. It must be taken into the account that in the islanded operation of the PEDG, not only the entire inertia level is low, but also there is no support from the upstream network. Thus, it is vital to equip the PEDG with robust, fast, and reliable frequency restoration control. If the frequency restoration control system is not able to cope with occurred disturbances within a short timeframe, protection relays will be triggered and a load shedding or a wide-area blackout might take place. Furthermore, based on the power system safety codes, the relays are set and coordinated in a manner that are sensitive to the rate of change of frequency (ROCOF), as well. It should be remarked that the entire system inertia controls the initial ROCOF when disturbances arise. Stealthy attacks on the state variables of the PEDG like inductor currents or capacitor voltages, attempt pushing some of the DERs across the grid to go islanded. Due to low inertia of the system, this would yield to substantial frequency deviations.

Numerous research articles have focused on frequency restoration from different perspectives [157]. Fundamentally, the frequency excursion problem in conventional power systems is regulated by leveraging two different control approaches. One is related to the synchronous generators' output control and the other focuses on the energy consumption control to restore frequency deviations, where the latter is recognized as load interruption [158]. Though, in the PEDG, mitigating substantial fluctuations on the frequency due to stealthy attacks needs a fast and precise approach to detect the required active power due to the generation loss, and compensate this amount in a timely manner, which is not achievable with the bulky-rotation-mass-based generation.

Smart grid is being equipped with lots of advanced measuring infrastructures (AMIs) and intelligent devices such as smart meters and inverters which are highly dependent on communication infrastructures. These newly added devices enhance the grid observability and controllability, but the power network is becoming more and more vulnerable to cyber-physical attacks. Thus, the network stability and energy availability could be jeopardized due to potential security breaches [159, 160]. Thus, it is crucial to equip the modernized power grid with proactive intrusion detection systems (IDS) to get full advantage of the smart devices at the edge [146, 161-166].

False data injection (FDI) is known as a common cyber threat in smart grid that can have severe effect on optimal operation and stability of the network [167]. Several studies in literature are proposing solutions for FDI detection and some new defense mechanisms in this regard [114, 168, 169]. In [170], a framework has been designed for detecting the FDI based attacks by using Kalman filter approach. To detect different attacks, the authors have used the x^2 detector, Euclidean detector and Kalman filter estimator. In [171], an attack model is studied which has negative impacts on the frequency of power system and the operation of electricity market. The developed anomaly detection is enhancing the cybersecurity of automatic generation control in power system.

Moreover, FDI attacks are investigated in [172], for a distribution system with unbalanced condition. A local state-based linear distribution system state estimation is proposed for this unbalanced system and then different construction of this type of attacks is investigated. Finally, the possibility of attacker's success is evaluated by numerical analysis.

In [163], the authors investigate the effect of hidden attacks which manipulates data injection on the AC state estimation. A method has been presented that can define the number of measurements. Nevertheless, this method depends on the system topology. The system will be more resilient to this type of attacks, if the numbers of the busses with no power injection are increased in the system. One limitation of this method is the restriction of the attack numbers which are applied on the system. In [173], the authors find a relation between the voltage stability of the system and the FDI attack by investigating the physical feature of the power system. A construction factor particle swarm optimization is implemented to categorize the level of vulnerability of the system nodes. In [174], the authors have studied the condition that several attack incidents are occurred on the power system simultaneously for manipulating the sate estimation. The attack has been modeled by series of linear programs. The authors have tried to make the condition more realistic by defining a constraint for their attacking vector. It is declared that the system can be secure if small subset of measurement can be kept safe to the attacks. In this regard, an algorithm has been proposed to select this subset of measurements. It worthy to mention that in a power system, selecting the aforementioned subset is known as a complex problem.

In [175], FDI attacks are detected by sparse optimization in a power system. In this method, the detection approach is modeled as the matrix separation problem. For recovering the states of power system and detecting the attacks, nuclear norm minimization and low rank matrix factorization approach are used. In [176], a centralized detector based on generalized likelihood ratio has been proposed for detecting the attack sequentially. This approach has acceptable robustness to various faked data. Also, a level-triggered sampling method is proposed for monitoring smart grid infrastructure. The aforementioned IDS have pros and cons. Some of them have developed models which may decrease the accuracy of the attack detection for high number of simultaneous attacks. Other drawbacks include computational burden and dependency on the power system topology. There are limited number of solutions reported in literature for real-time proactive IDS independent of the network topology for smart grid which is the aim of this chapter. Moreover, the proposed IDS can detect the simultaneous malicious attacks happening in different part of the network.

4.3. Proposed System Operational Concept for Evaluating IDMPC

Figure 4. 1 illustrates a cluster of PEDG which consists of synchronous generator, ESS interfaced with dual active bridge (DAB) converter, PV inverters, and aggregated load. PV inverters supply the local loads and are controlled in PQ mode. The system operates in islanded mode and is confronted with several disturbances. Thus, a frequency excursion is expected to occur with uncontrollable ROCOF without implementing an event-triggered frequency restoration and ROCOF minimization control scheme. A DAB converter interfaced with ESS is used to support the entire system during potential disturbances and due to the fast dynamic response of the DAB converter controller, frequency restoration is

enhanced. To provide accurate power reference for the DAB converter in response to frequency events, a two-layer feed-forward neural network is integrated in the control system. The major challenge is the training process for determination of the active power references to regulate frequency and ROCOF in the multi-dimensional and highly non-linear PEDG. To address this challenge, the root-causes of the frequency excursion are investigated for training process. It is worthy to note that the synchronous generator is the primary source for shaping the frequency profile of the islanded PEDG. In the next section, the proposed control scheme modules are formulated and discussed with more details.

4.4. Proposed Integrated Data-Driven and Model-Based Control Scheme Modules and Applied Training Mechanisms

System frequency is affected by any alterations in supply-demand balance based on the swing equation, which is given by,

$$T_m - T_e = 2H\,\Delta\dot{\omega} + D\,\Delta\omega \tag{4.1}$$

where T_m, T_e are turbine mechanical torque and electrical torque, respectively. D is defined as the damping coefficient. $\Delta\omega$ and $\Delta\dot{\omega}$ are known as deviations from synchronous speed and acceleration, respectively. Converting the torque variables to power, gives the swing equation in term of power by,

$$P_m - P_e = J\omega_m\left(\frac{d}{dt}\left(\frac{d}{dt}(\theta_m)\right)\right),\ \theta_m = \omega_s t + \delta_m \tag{4.2}$$

where P_m, P_e and ω_m are the mechanical power, electrical power, and angular velocity of the rotor, respectively. $J\omega_m$ is defined as the inertia constant of machine at synchronous speed of ω_s. Also, θ_m is defined as the angular position of the rotor with respect to the stationary axis and δ_m is the angular position with respect to the synchronously rotating reference frame. Rewriting (4.2) based on the kinetic energy of rotating mass gives,

$$\begin{gathered} P_m - P_e = \frac{d}{dt}(E_k),\ E_k = \frac{1}{2}J\left(\omega_m\right)^2 \\ P_m - P_e = J\omega_m \frac{d}{dt}(\omega_m),\ \Delta P = (4J\pi^2)f\frac{d}{dt}(f) \end{gathered} \tag{4.3}$$

where ΔP is the required power from external support for stabilizing the frequency excursions. f is the system frequency and f' is defined as the ROCOF. It should be remarked that, if ΔP has negative value, the whole system has extra power, and it should be absorbed by the energy storage systems. The proposed artificial neural network is trained by Bayesian regularization algorithm with thousands of epochs. For eliminating the grid topology influences and inertia effects on the proposed control method, different models of frequency deviation are defined and used as the inputs of swing equation which was detailed in previous chapter. Then, feasible solutions along with different inputs are registered in a database to be used as training data for ANN. Furthermore, different inertia constants are considered in swing equation. This fact makes the trained network a promising tool for providing robust and fast power command. Figure 4. 2 shows the training performance of ANN. It should be mentioned that the database has been divided randomly in a way that 70% of data is used for training process, 15% for validation, and 15% for testing process. As shown in the histogram of errors, most of the instances have negligible error values considering the required amount of power. In this work 40,000 sample data have been provided for input and target data which are sufficient for a network to be trained. Thus, the optimal active power reference for the ESS can be found in real-time which will be used as

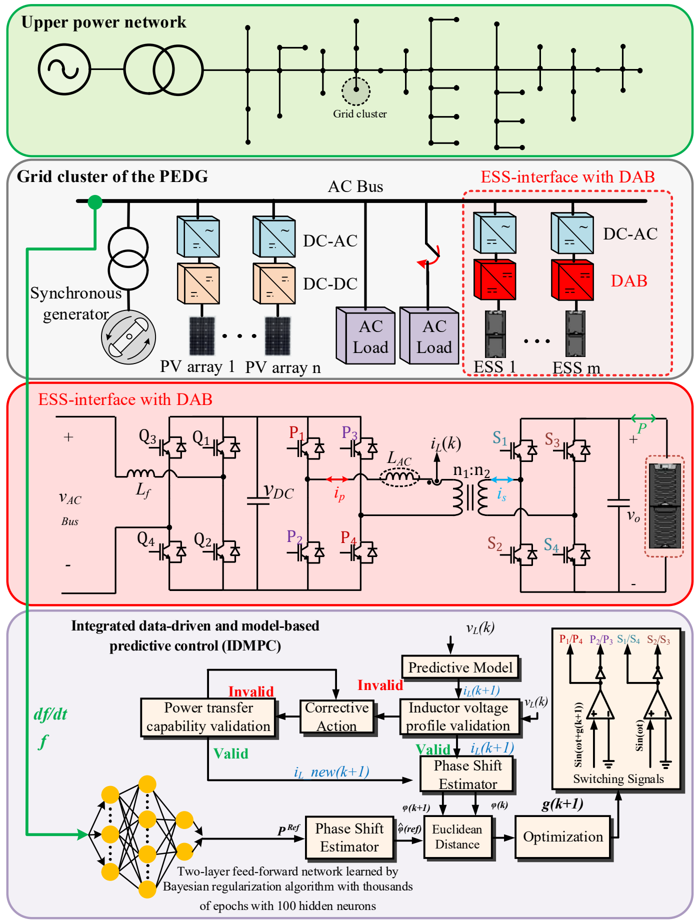

Figure 4. 1. PEDG schematic and the proposed integrated data-driven and model-based control (IDMPC) scheme.

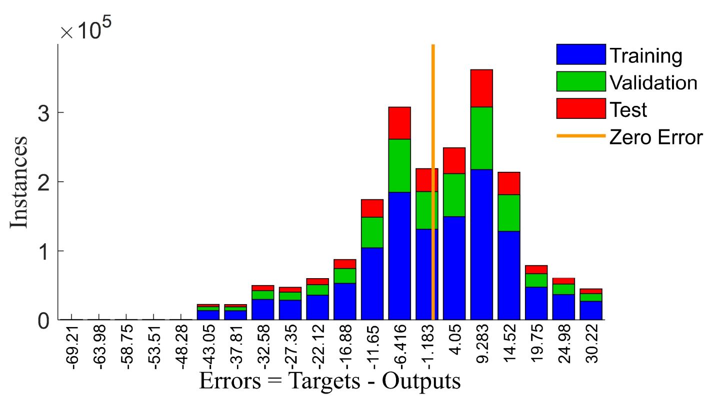

Figure 4. 2. Histogram of the differences between target values and output values after training the neural network.

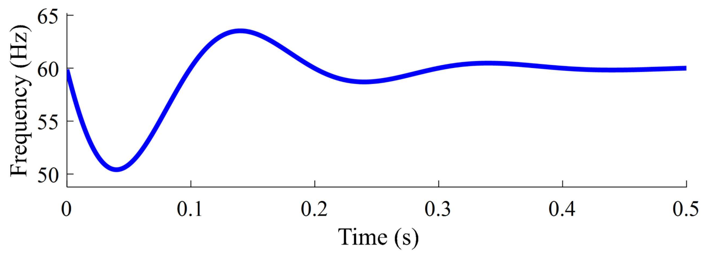

Figure 4. 3. A sample of frequency deviation profile when a large load disturbance occurs, and the system inertia is low for transient period.

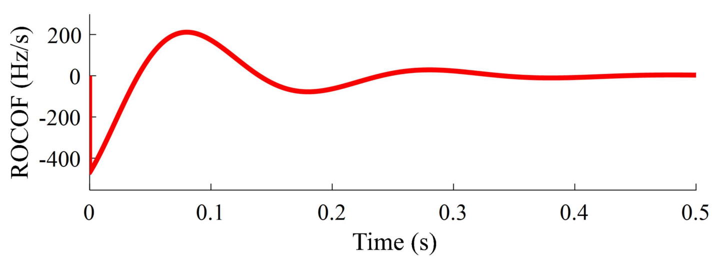

Figure 4. 4. A sample of ROCOF profile when a large load disturbance occurs, and the system inertia is low for transient period.

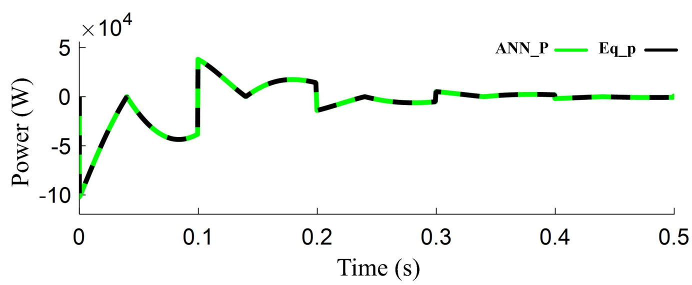

Figure 4. 5. A sample of power demand provided by equation and ANN output when a large load disturbance occurs based on frequency and ROCOF values.

an input to the model-based predictive control block of the proposed scheme (see Figure 4. 1). The predictive module starts its functionality by predicting the current in the AC-link inductor and is terminated by a precise approximation of the required phase shift for obtaining the optimal and the best possible switching signals. The output of the trained neural network implicitly provides the initial value of the phase shift when there is a load change in

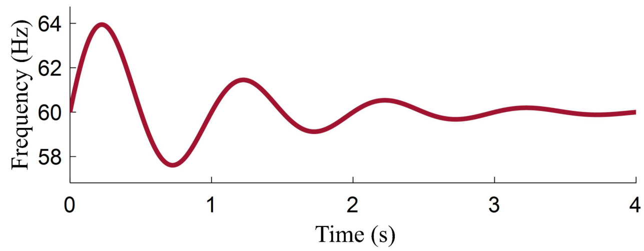

Figure 4. 6. A sample of frequency deviation profile when a large load disturbance occurs and the system inertia is high, frequency deviation is small, and the frequency oscillation is damped after 4 seconds.

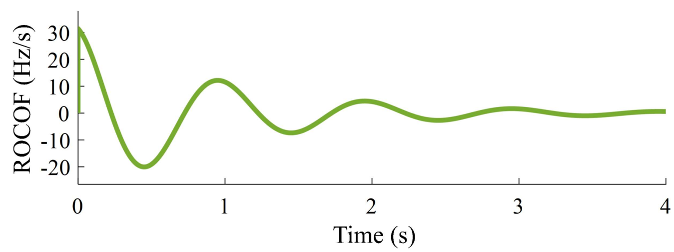

Figure 4. 7. A sample of ROCOF profile when a large load disturbance occurs and the system inertia is high, ROCOF has smaller values, and it reaches to zero. The frequency oscillation is damped after 4 seconds.

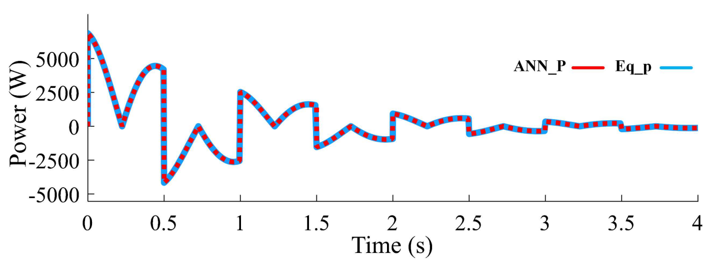

Figure 4. 8. A sample of frequency power demand provided by equation and ANN output when frequency oscillation is about 4 Hz, and the system inertia is high.

the system. The next step is the formulation and derivation of the predictive model of the DAB converter for injecting the determined optimal active power from ESS to the AC bus of the islanded PEDG. Two validation modules are presented for mitigating the potential error in the predicted AC-link inductor current of DAB converter. The control objective is to apply proper phase shift to the DAB converter for injecting the required active power to the system. The optimal switching states for DAB converter are determined by formulating a cost function. The cost function for determining the possible switching states is given by (4.4). Euclidean norm of the feasible phase shift is minimized with respect to the approximated phase shift reference which indirectly is determined by the trained neural network as explained earlier. The cost function is given by,

$$\begin{gathered}
\left|g\left(k+1\right)\right|=\sqrt{\left|\vec{m}_k\right|^2+\left|\vec{\hat{\varphi}}_{ref}\right|^2} \quad , \quad \left|\vec{m}_k\right|=\min\{\left|\vec{\varphi}_k\right|\left|\sin(\theta(k)\right|,\left|\vec{\varphi}_k\right|\cos(\theta(k))\} \\
\vec{\varphi}_k=\varphi(k)\vec{i}+\varphi\left(k+1\right)\vec{j}\,,\,\vec{\hat{\varphi}}_{ref}=\hat{\varphi}_{ref}\vec{k}\,,\;\theta(k)=\tan^{-1}\left(\frac{\varphi\left(k+1\right)}{\varphi\left(k\right)}\right) \\
\hat{i}=\frac{\varphi(k)}{\left|\varphi(k)\right|},\hat{j}=\frac{\varphi(k+1)}{\left|\varphi(k+1)\right|},\hat{k}=\frac{\hat{\varphi}_{ref}}{\left|\hat{\varphi}_{ref}\right|}
\end{gathered} \tag{4.4}$$

where $\varphi(k)$ is the shifted phase and $\varphi(k+1)$ is the predicted phase shift. Details of the function that provides a relation between inductor RMS value and the phase shift as well as the entire control approach were explained in previous chapter. In this section, the training process is discussed with more details. As mentioned, to have a comprehensive knowledge regarding the frequency behavior of a system, different disturbance scenarios are considered. It should be mentioned that the groundwork of this emulation is based on the feasible solutions of swing equation. In these solutions, two mathematical functions have effective roles. One is the sinusoidal term and the other is the exponential term which proved and discussed earlier in previous chapter.

Figure 4. 3. illustrates the emulated frequency excursion profile when a significant load disturbance occurs. In this scenario, the inherent grid inertia is low and frequency deviation is around 10 Hz. It is shown in Figure 4. 4 that the ROCOF alters from -400 to 200 (Hz/s). Analyzing the system damping behavior shows that the external supportive system has had

a fast dynamic response. Therefore, frequency oscillation has been damped after 0.5 s. The required active power that should be supplied by ESS is shown in Figure 4. 5. It should be noted that, this process provides a comprehensive database for training the ANN when the

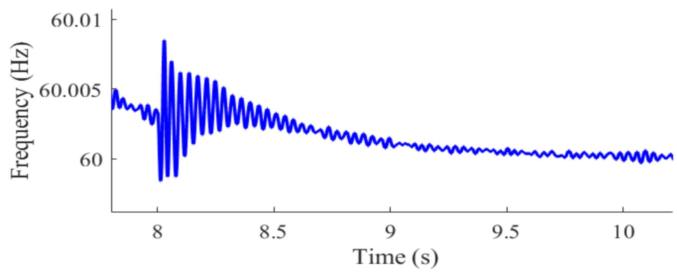

Figure 4. 9. Frequency profile, load is increased at t=8s and the IDMPC regulates frequency oscillation.

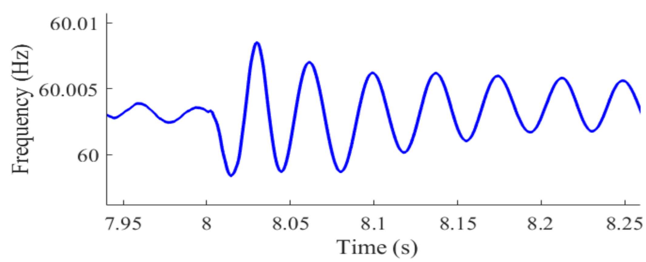

Figure 4. 10. Frequency profile zoomed around t=8s. load is increased at t=8s and the IDMPC regulates frequency oscillation.

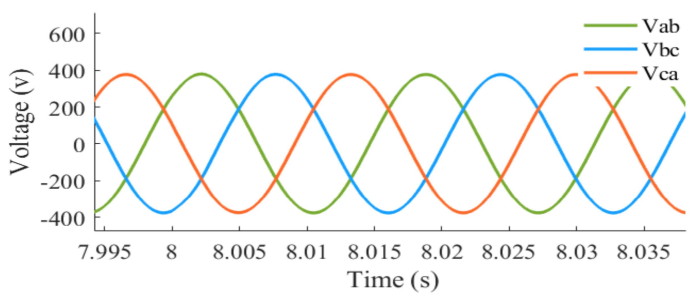

Figure 4. 11. Three phase AC Bus voltage profile. Load is increased at t=8s. The IDMPC handles voltage disturbance effectively.

system is confronted with a sever disturbance. Therefore, in a real energy system, some parts of these profiles might be chopped, and this is due to the fast triggering of the protection relays. Clearly, if the ESS interfaced with a bidirectional converter that is equipped with MPSC with fast dynamic response, quick damping process would be attainable during severe disturbances.

Another training scenario is related to the power system that is encountered with large disturbances while the inertia is relatively high. As depicted in Figure 4. 6, frequency deviation is about 4 Hz, and it is damped after 4s. Figure 4. 7 illustrates the ROCOF for this scenario. As it is expected, ROCOF varies between -20 to 30 (Hz/s). Figure 4. 8. demonstrates the required power for mitigating this type of disturbance. Due to the high inertia of the system, the power reference varies between -5 kW and 5 kW. It should be mentioned that. Based on the provided detailed proofs in previous chapter, for different value of natural and damped frequency, damping ratio, inertia constant, initial value of power angle and other effective variables, this kind of profiles can be constructed to be utilized in the learning database. Considering the training process and its unique learning algorithm, which was explained before, it is ensured that the ANN can detect wide range of load disturbances without having prior knowledge about the grid inertia and topology and provides proper reference for DAB converter to inject or absorb energy to the grid. As demonstrated in previous chapter, the AI-PRC can dynamically adjust their power references to be adopted with grid's real time disturbances. This feature of the proposed controller is known as one of the superiorities of this work in comparison to other frequency regulation methods.

The trained ANN is employed in a Simulink Model of the proposed cluster of PEDG by using the IDMPC approach. An increase in load (4kW) occurred at instant t=8s in all power feeders. Figure 4. 9 shows frequency profile in AC-bus. When the load disturbance occurs at instant t=8s, a drop in frequency is observed (see Figure 4. 9). The proposed IDMPC regulates both frequency and ROCOF smoothly. Figure 4. 10 has been zoomed around t=8s to show the frequency deviation and the effectiveness of the proposed IDMPC. Moreover, the effective consequence of this frequency restoration is visible in three phase voltages of AC-bus (see Figure 4. 11). As it is shown, load is increased at t=8s and the IDMPC handles voltage disturbances effectively and this is due to the fast frequency restoration.

4.5. General Discrete Time State Space Representation for Generating Stealthy Attacks

A general discrete time state space representation is used to define system by the following state and output equations,

$$x_{k+1} = Ax_k + Bu_k + v_k \tag{4.5}$$

$$y_k = Cx_k + w_k \tag{4.6}$$

Modified Linear Quadratic Gaussian (LQG) equations are shown below. *H*, *S*, and *T* are the solutions to the matrix Riccati difference equation which are defined using backwards recursion:

$$H_k = H_N + H_{k+1}A - H_{k+1}B(R + B^T S_{k+1}B)^{-1}B^T S_{k+1}A \tag{4.7}$$

$$S_k = A^T (S_{k+1} - S_{k+1}B(B^T S_{k+1}B + R)B^T S_{k+1})A + Q \tag{4.8}$$

$$T_k = T_N + A^T T_{k+1} - A^T S_{k+1}B(R + B^T S_{k+1}B)^{-1}B^T S_{k+1} \tag{4.9}$$

Here, N is the size of the finite horizon for the LQG. The initial conditions for these equations are $H_N = x_d^T Q$, $S_N = Q$, and $T_N = Qx_d$. Now, the rest of the equations used for the LQG control are defined as:

$$P_{k+1} = A(P_k - P_k C^T (CP_k C^T + W)^{-1} CP_k) A^T + V \tag{4.10}$$

$$K_k = (B^T S_{k+1} B + R)^{-1} B^T S_{k+1} A \tag{4.11}$$

$$L_k = P_k C^T (CP_k C^T + W)^{-1} \tag{4.12}$$

$$\hat{x}_{k+1} = A\hat{x}_k + Bu_k + L_{k+1}(y_{k+1} - C(A\hat{x}_k + Bu_k)) \tag{4.13}$$

$$u_k = -K_k \hat{x}_k + \frac{1}{2}(RB^T S_k B)^{-1}(B^T H_k^T B^T T_k) \tag{4.14}$$

These equations are defined using forward recursion. Equation (4.10) is the estimate covariance matrix P at the next time step. Equation (4.11) is the feedback gain at the current time step. Equation (4.12) is the Kalman gain at the current time step. Equation (4.13) is the state estimate at the next time step initialized to $\widehat{x_0} = E[x_0\, x_0^T]$. Finally, equation (4.14) is the control signal at the current time step.

The attack model that is used in this work has been described in [149]. It is a data injection attack that avoids triggering the anomaly detector by maintaining a normal output of the system (as if there were no attacker) while causing the states of the system to diverge. The attacker has access to the value of y_k and u_k at the current time step k, thus the attack a_k is executed by changing the control signal. Thus, a new state equation is given by,

$$x_{k+1} = Ax_k + B(u_k + a_k) + v_k \tag{4.15}$$

For the attack to be stealthy, a_k is defined by $a_k = Fz_k$,

where F is chosen such that $(A + BF)V^* \subseteq V^*$, meaning the attack is in the kernel of C, $z_{k+1} = (A+BF)z_k$, and V^* is the maximal output-nulling invariant subspace [149]. The idea of the maximal output-nulling invariant subspace is to design the attack such that replacing the control signal with the attack keeps the observations at zero. The initial condition for z is given by $z_0 \epsilon V^*$. The anomaly detector is triggered if the output statistics vary from the normal operation of the system by more than τ where τ is controlling the false positive to false negative tradeoff [149].

One can assume that the attacker has full knowledge of the system. However, this is not a realistic assumption, as small inconsistencies between the real system and the model are bound to exist even inside the controller. In the most general case, the attacker would have to learn the model as part of the attack. Though, the learning process is outside the scope of this work. Thus, the model uncertainty is simple represented by adding noise to the state matrices. For example, $A' = A + \Delta A$ where $\Delta A$is the attacker's uncertainty about the state matrix. It is shown that when the attacker does not have full knowledge of the system, a "stealthy" attack loses its stealth.

The proposed approach firstly is applied to a simple power system model with three inverters, in which an attacker can manipulate the PV inverters' active and reactive power set points (i.e., current reference and/or controller gains). The equivalent PV inverter model is illustrated in Figure 4. 12. The considered system includes loads at the point of PV generation.

It is assumed that the PV inverters' active and reactive power have been set to supply a major portion of the local loads. A sophisticated attacker can launch a stealthy attack by manipulating the PV inverter's reference currents in such a way that the demand-supply remains balanced in the system. This ensures that alarms will not be triggered, and the attack will remain undetected by the grid supervisor. Once the attacker has compromised a considerable number of PV sources, the inverters may trip due to violation of their stable operation regions. This can result in significant unbalance in demand-supply, unbalance in three-phase distribution feeder, transformer saturation and failure, and eventually a blackout. The continuous time state space representation of the PV inverter system can be found in Equations (4.16) and (4.17) as,

$$
\begin{bmatrix} \dot{i}^1_{1,p} \\ \dot{i}^1_{1,q} \\ \dot{i}^1_{2,p} \\ \dot{i}^1_{2,q} \\ \dot{v}_{c,p} \\ \dot{v}_{c,q} \\ \dot{x}_{1,p} \\ \dot{x}_{1,q} \\ \dot{x}_{2,p} \\ \dot{x}_{2,p} \end{bmatrix} =
\begin{bmatrix}
\frac{-R_1-R_3}{L_1} & \dot{\theta} & \frac{R_3}{L_1} & 0 & \frac{1}{L_1} & 0 & 0 & 0 & 0 & 0 \\
-\dot{\theta} & \frac{-R_1-R_3}{L_1} & 0 & \frac{R_3}{L_1} & 0 & \frac{1}{L_1} & 0 & 0 & 0 & 0 \\
\frac{-R_3-K_P}{L_2} & 0 & \frac{-R_1-R_3}{L_2} & \dot{\theta} & \frac{-1}{L_2} & 0 & \frac{K_R}{L_2} & 0 & 0 & 0 \\
0 & \frac{R_3-K_P}{L_2} & -\dot{\theta} & \frac{-R_1-R_3}{L_2} & 0 & \frac{-1}{L_2} & 0 & \frac{K_R}{L_2} & 0 & 0 \\
\frac{-1}{C} & 0 & \frac{1}{C} & 0 & 0 & \dot{\theta} & 0 & 0 & 0 & 0 \\
0 & \frac{-1}{C} & 0 & \frac{1}{C} & -\dot{\theta} & 0 & 0 & 0 & 0 & 0 \\
-1 & 0 & 0 & 0 & 0 & 0 & -0.6 & \dot{\theta} & -277.6 & 0 \\
0 & -1 & 0 & 0 & 0 & 0 & -\dot{\theta} & -0.6 & 0 & -277.6 \\
0 & 0 & 0 & 0 & 0 & 0 & 512 & 0 & 0 & \dot{\theta} \\
0 & 0 & 0 & 0 & 0 & 0 & 0 & 512 & -\dot{\theta} & 0
\end{bmatrix}
\begin{bmatrix} i^1_{1,p} \\ i^1_{1,q} \\ i^1_{2,p} \\ i^1_{2,q} \\ v_{c,p} \\ v_{c,q} \\ x_{1,p} \\ x_{1,q} \\ x_{2,p} \\ x_{2,p} \end{bmatrix} +
\begin{bmatrix}
\frac{-1}{L_1} & 0 & 0 & 0 \\
0 & \frac{-1}{L_1} & 0 & 0 \\
\frac{1}{L_2} & 0 & \frac{K_P}{L_2} & 0 \\
0 & \frac{1}{L_2} & 0 & \frac{K_P}{L_2} \\
0 & 0 & 0 & 0 \\
0 & 0 & 0 & 0 \\
0 & 0 & 0 & 0 \\
0 & 0 & 0 & 0 \\
0 & 0 & 0 & 0 \\
0 & 0 & 0 & 0
\end{bmatrix}
\begin{bmatrix} V_p \\ V_q \\ I^*_p \\ I^*_q \end{bmatrix}
\tag{4.16}
$$

$$
\begin{bmatrix} y_{eq_p} \\ y_{eq_q} \end{bmatrix} =
\begin{bmatrix}
1 & 0 & 0 & 0 & 0 & 0 & 0 & 0 & 0 & 0 \\
0 & 1 & 0 & 0 & 0 & 0 & 0 & 0 & 0 & 0
\end{bmatrix}
\begin{bmatrix} i^1_{1,p} \\ i^1_{1,q} \\ i^1_{2,p} \\ i^1_{2,q} \\ v_{c,p} \\ v_{c,q} \\ x_{1,p} \\ x_{1,q} \\ x_{2,p} \\ x_{2,p} \end{bmatrix}
\tag{4.17}
$$

In this model, $i^k_{j,p}$, $i^k_{j,q}$ are the in-phase components of the current injected in the grid by inverter number k in the dq frame. v_{cp} and v_{cq} are the filter capacitor voltages in the dq frame, $\dot{\theta}$ is the frequency inside the PV inverter, and K_P and K_R are the controller gains of the PR controller in the current control loop. The state space representation of the whole system, including three PV inverters, is given by,

$$A_{eq} = \begin{bmatrix} [A_1] & [0] & [0] \\ [0] & [A_2] & [0] \\ [0] & [0] & [A_3] \end{bmatrix},\ B_{eq} = \begin{bmatrix} [B_1] & [0] & [0] \\ [0] & [B_2] & [0] \\ [0] & [0] & [B_3] \end{bmatrix},\ C_{eq} = \big[[C] \quad [C] \quad [C]\big] \tag{4.18}$$

where, $[A_i]$, i=1, 2, 3, is the state matrix for each individual inverter. The representation of input and output matrices are stated similarly. It can be seen in C_{eq} that only the sum of the currents injected in the grid by all three inverters is observed. Here, $A_{eq}\epsilon\mathbb{R}^{30\times30}$, $B_{eq}\epsilon\mathbb{R}^{30\times30}$ and $C_{eq}\epsilon\mathbb{R}^{30\times30}$. The control input signal of the system is the set of all three PV inverter terminal voltages and all three PV inverter reference currents. This state space model is then transformed to discrete time with a sampling time of $1ps$. This sampling time was chosen to speed up the effect of the attack. The states of the system under attack can diverge much faster with a smaller sampling time.

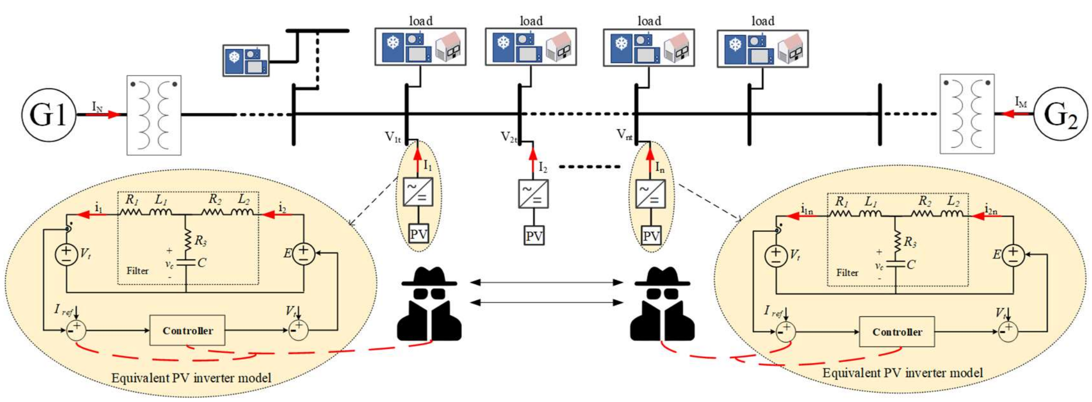

Figure 4. 12. Distribution power system with high penetration of PV inverters.

4.6. System Description for Evaluating the Proposed Cohesive Data-Extracted Methodology built-in a Shadow Control (CDMSC) Scheme

To study the proposed ANN-based shadow control, a realistic 14-bus power system is considered as depicted in Figure 4. 13. The 14-bus system has two voltage levels as medium voltage (MV) and low voltage (LV), where MV is at the 13.8 kV and LV is 220 V. The entire

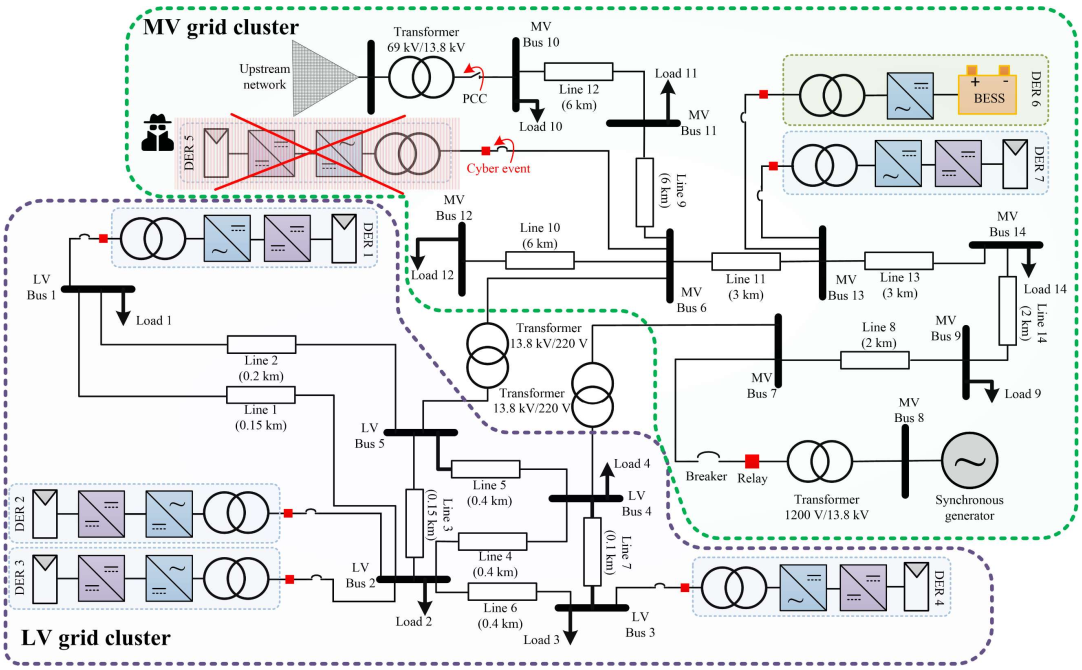

Figure 4. 13. The 14-bus PEDG under study.

system has the capability of connection/disconnection to/from the upstream network at 69 kV level via a substation connected to bus 10. In the islanded operation mode, an 800 kVA synchronous generator along with seven DERs feed the loads across the grid. The entire loading of the system is 500 kW, where 150 kW is provided by the synchronous machine and the rest is coming from the DERs. All the DERs are equipped with frequency relays and circuit-breakers to disconnect the DER in the occurrence of unpermitted frequency fluctuations. The MV and LV sections of the grid are interconnected through two 13.8 kV/200 V transformers, while the system has the capability of getting partitioned into two self-sufficient PEDG clusters with different voltage levels. In the considered attack model, the intruders using stealthy approaches push the DER 5 to disconnect from the grid. The rating of DER 5 is 270 kVA, as the main provider of the system. To maximize the attack impact, the attackers target the largest provider of the system. After disconnection of the

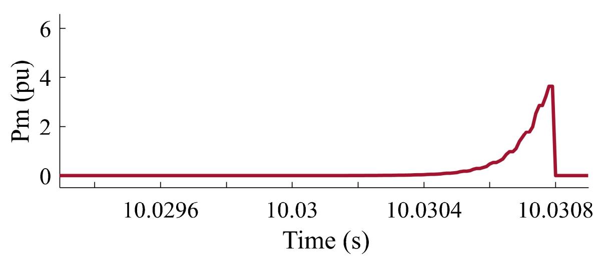

Figure 4. 14. The considered stealthy attack on PEDG access point: the attack is done on the governor controller and manipulate the regulated mechanical power fed to the turbine.

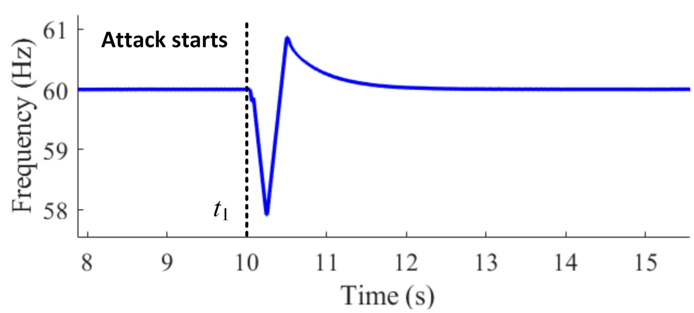

Figure 4. 15. System frequency dynamic: attack initiated at t1 = 10s and ends after 0.0308 s. System becomes unstable after 0.25 s due to the large frequency deviation.

DER, the frequency of the system drops suddenly due to significant mismatch between active power generation and consumption.

If the system only relies on the synchronous generator for compensating the active power, due to relatively low dynamic of synchronous generator, the frequency will drop below allowable boundaries and all the frequency relays would be triggered, which results in a backout across the grid. In the proposed approach, the shadow control of the cluster is activated due to the unexpected change in the system frequency. The ANN module of the shadow control accurately estimates the generation loss, and DER 6 which is a battery energy

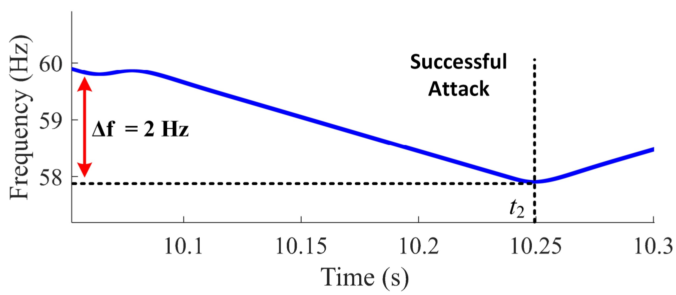

Figure 4. 16. System frequency dynamic: attack initiated at t1 = 10s and ended after 0.0308 s. System become unstable at t2 = 10.25 s, frequency deviation is more than 2 Hz, and the frequency protection relays are triggered.

storage system (BESS) provides the lost generation. Using the proposed approach, not only load shedding is not needed, but also the fast response of the inverter-based DER restores the grid frequency and keeps all the DERs connected.

4.6.1. Impacts of Stealthy Attack Without Resilient Self-Learning Control

Stealthy attacks are extremely menacing for the PEDG stability especially when the system inertia is comparatively low or mixed. The situation could be even more crucial if stealthy attacks occur in various grid access points. The main feature of the stealthy attacks is deceiving the supervisory layer such that the measured parameter alterations are unobservable while other system state variables are being diverged. This manipulation will result in failure of the entire system when the supervisory layer is not able to do any prevention nor detection strategies. A successful stealthy attack can be designed by formulating the approximated state-space model of a system even by having imperfect system information. In this work, stealthy attacks are implemented on several inverters of PEDG and the control input signals are manipulated by employing attack disturbance signals into the system controller.

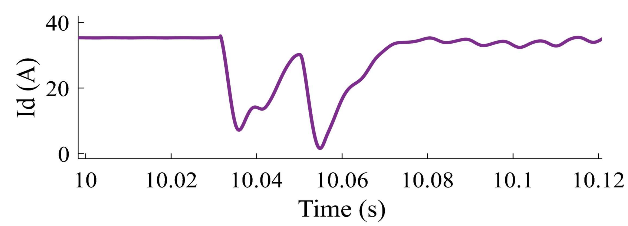

Figure 4. 17. d-component of the inverter current as the predefined state variable.

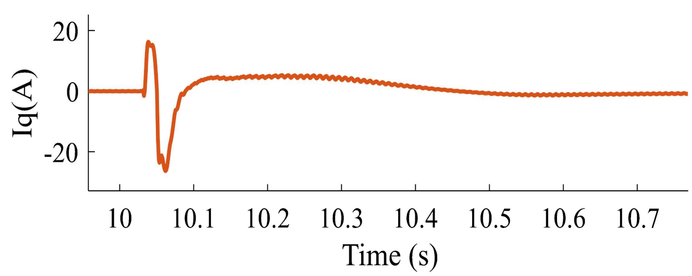

Figure 4. 18. q-component of the inverter current as the predefined state variable.

To have a better perspective on the effects of stealthy attacks on the understudy 14-bus PEDG, as a case study, a stealthy intrusion is applied on the governor of the synchronous generator. Figure 4. 14 depicts the attack signal model applied on the governor control. Similar attacks could happen on the DERs as well since the attacker could have access to the local controller of an inverter across of the PEDG. To show the effectiveness of attacks on the DERs, AC bus frequency dynamic is investigated from different aspects. Figure 4. 15 shows the frequency dynamic before and after the attack occurrence. System frequency is 60 Hz during the normal operation of the grid. At instant t_1 =10 s, the attack starts, and its duration is 0.0308 seconds. Considering the power system protection standards, frequency excursion of more than 2 Hz is defined as a risky violation for the system, thus the protection systems will be triggered, and the synchronous generator are separated from the system; consequently, this will increase the power-supply unbalance level and the entire energy system may experience

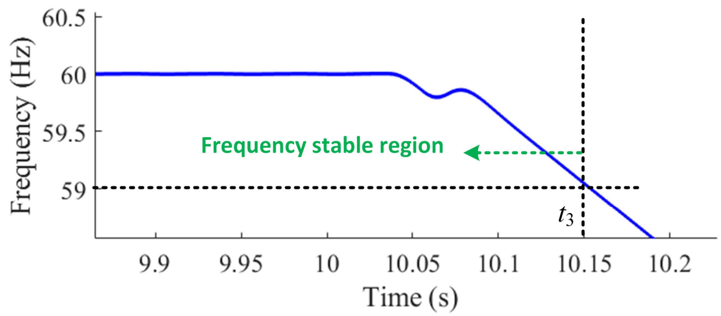

Figure 4. 19. System frequency dynamic: attack is done at t_1 = 10s and ended after 0.0308 s. System operates in stable region before t_3 = 10.15 s.

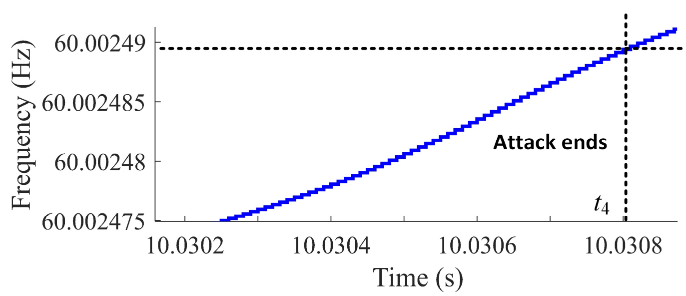

Figure 4. 20. Zoomed-in form of system frequency dynamic at the end of the attack duration: attack started at t_1 = 10s and ended at t_4 = 10.0308 s. system is stable when attack is ended, and the supervisory control layer cannot detect stealthy attack.

the blackout if disturbances are not mitigated in timely manner. To analyze frequency dynamic with more details, the zoomed-in version of Figure 4. 15 is illustrated to accurately demonstrate system dynamics during the attack. Figure 4. 16 shows that after 0.25 s, the system is not stable, and the relays have been activated. As expected in stealthy attacks, state

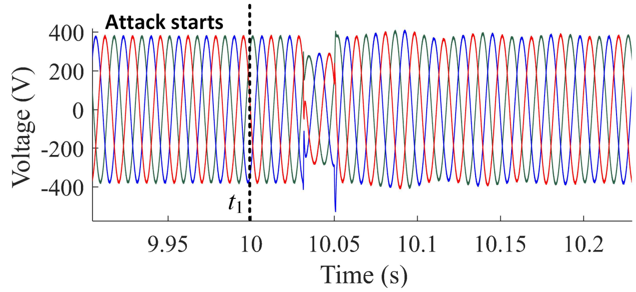

Figure 4. 21. AC bus voltage before and after the attack, voltage variation is in the acceptable standard range during the attack.

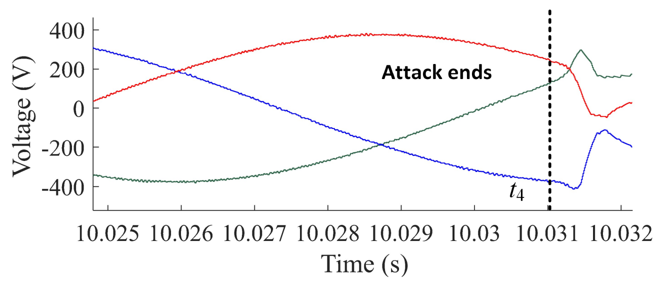

Figure 4. 22. System frequency dynamic: attack occurs at t1 = 10s and ends at t4 = 10.0308 s. System becomes unstable after 0.25 s due to the large frequency deviation.

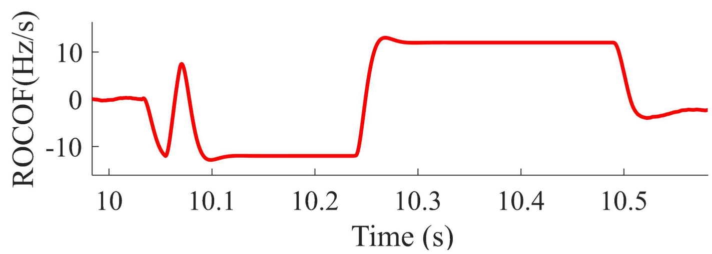

Figure 4. 23. Rate of change of frequency during stealthy attack

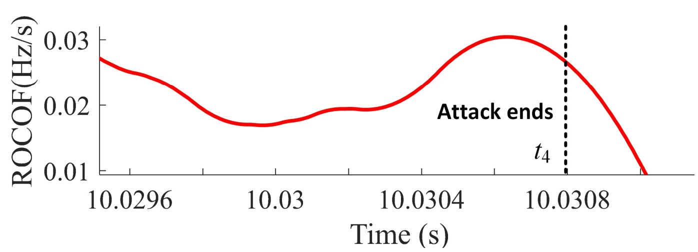

Figure 4. 24. Zoomed- in version of rate of change of frequency during stealthy attack. Attack ends at t_4 = 10.0308s, before t_4, ROCOF has standard pattern, so the relays will not be sensitive during the attack.

variables are diverged faster than the measured variables. These fast divergences trigger the local protection. Consequently, cascaded inverters tripping may occur which results in major blackout. This significant unbalance will result in huge frequency excursion and the supervisory layer is not able to take any protective action for restoring the system frequency. For describing this scenario, two state variables of the system which are *q* and *d* components of the inverter currents are shown in Figure 4. 17 and Figure 4. 18. As seen, the state variables have diverged faster than the observable variables to the supervisory controller which are the frequency and voltage of the AC bus. To shed light on this event, the frequency behavior of the system during attack interval are shown in Figure 4. 19 and Figure 4. 20. Figure 4. 19 states that before reaching to t_3 = 10.15 s, the supervisory controller cannot detect that any attacks on the grid while Fig. 5 and Fig. 6 illustrate that the state variables have violated the standard ranges after the attack ends at t_4 = 10.0308 s. Figure 4. 21 and Figure 4. 22attest that the AC bus voltage variations remain in a standard range while the state variables have been diverted. Moreover, ROCOF are seen in Figure 4. 23 and Figure 4. 24. These figures demonstrate that during the attack, ROCOF is negligible too; thus, the supervisory control will not observe the stealthy attacks while state variables are violating the standard ranges. This case study demonstrates the significance to have a self-learning control scheme for mitigating the impact of unobservable intrusions such as the stealth attack presented in this section. The proposed shadow controller brings an extra layer of intelligence to the supervisory layer for mitigating the unobservable stealthy attacks via a self-learning mechanism.

4.7. The Proposed ANN-based Shadow Control Framework

To mitigate the consequences of the stealthy attacks on the DERs of the PEDG, the system cannot rely on the high inertia synchronous generators, since by the time they catch up with the amount of the lost generation due to a cyber event, the frequency relays are triggered and the system has faced a large-scale blackout. The proposed solution in this work employs the fast controller of the BESS to cope with the active power lost. High-bandwidth control

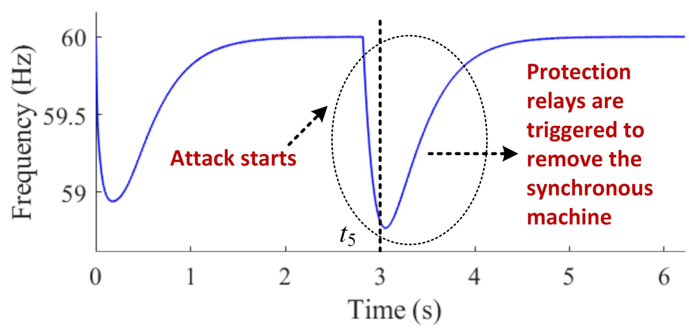

Figure 4. 25. AC bus frequency before and after the attack in absence of shadow control scheme, frequency variation is not in the acceptable standard range and the system collapses.

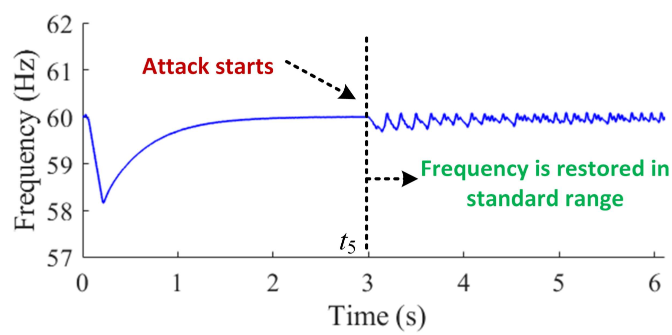

Figure 4. 26. AC bus frequency before and after the attack with employing the shadow control scheme, frequency variation is in the acceptable standard range and the system operates normally.

schemes e.g., model predictive control (MPC) can be utilized to implement primary control layer for DERs with fast dynamic response. The proposed shadow control framework

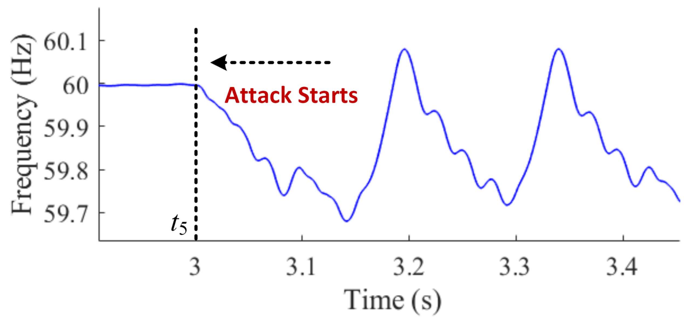

Figure 4. 27. Zoomed in version of AC bus frequency around t_5 = 3 s. Shadow controller is employed and the frequency variation is in the acceptable standard range.

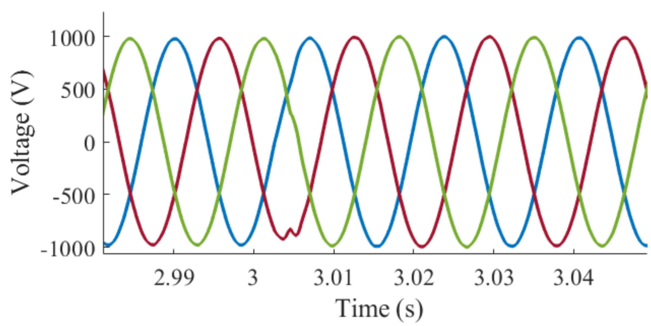

Figure 4. 28. AC bus voltage before and after the attack, voltage variation is in the acceptable standard range during the attack.

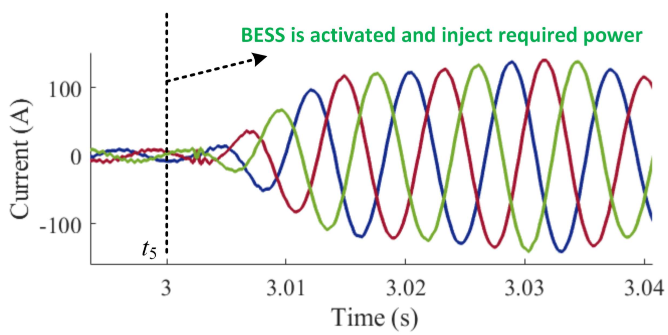

Figure 4. 29. Injected current by BESS to the grid after the attack, current is increased fast based on shadow controller command.

provides corrective active power for healing the system at very fast timescale; thus, the primary control layer of DER should have high bandwidth such as MPC. In this work, the previously developed MPC in chapter one, is utilized as the primary PQ controller for the

DERs. Since the supervisory layer of the system would not be able to observe the stealthy attacks, an ANN-based shadow control scheme is designed which only needs feedback from the cluster frequency and its ROCOF. The proposed cohesive data-driven-based scheme so-called CDMSC observes the frequency of the cluster and the rate it is being changed. Since the only input that the proposed shadow control scheme requires is the frequency, it would not be compromised. By proving the active power reference for the BESS of the cluster, the frequency can be restored in an ultra-fast timescale, thus mitigating the stealth attack impact.

4.7.1. Result and Discussion

In this section, the functionality of the proposed event-triggered ANN-based shadow control scheme is validated on the understudy 14-bus PEDG. The proposed shadow control scheme observes the global variables of the system and is activated when the supervisory layer does not take an effective action to support the system during disturbances. As explained, when a stealthy attack occurs, the inverters' state variables are diverged and manipulated PV inverters are removed from the grid by the protection system. The proposed shadow control supports the system frequency stability by injecting the required active power. Figure 4. 25 shows the system frequency during grid's normal operation when there is no shadow controller. At t_5 =3s, a stealthy attack is occurred, and a major part of grid generation is lost. As seen, frequency severely drops and violates the standard range. Although the synchronous machine tries to inject required amount of power but cannot support the grid in a timely manner due to its inherent slow dynamic response. In fact, the protection system removes the generator from the grid. To illustrate the effectiveness of the proposed shadow controller, the same stealthy attack scenario is repeated. Figure 4. 26 shows

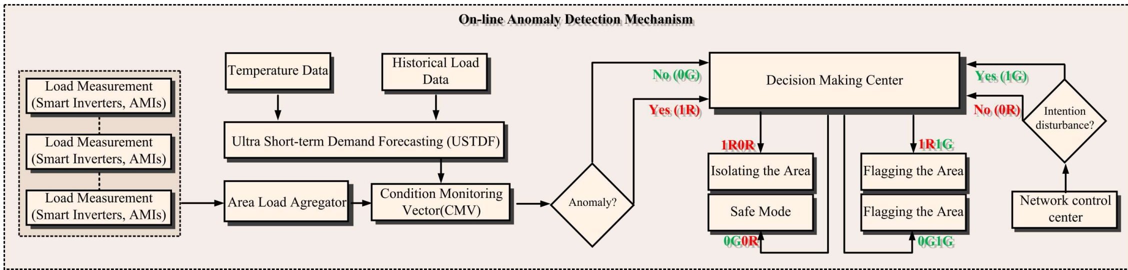

Figure 4. 30. The proposed on-line anomaly detection mechanism.

that sever frequency excursion is restored in a timely manner before the grid collapses. Figure 4. 27 shows the zoomed-in system frequency dynamics around t_5 = 3 s. This figure demonstrates that the frequency deviation is kept in the allowable range and the system operation continues without any challenges. Considering the harsh disturbances on the system, it is crucial to evaluate the voltage dynamics. Figure 4. 28 illustrate the AC bus voltage dynamic. As depicted, during the attack, voltage stability has been ensured due to the BESS's support guided by the shadow controller. The functionality of the shadow controller at the time of attack is illustrated in Figure 4. 29, where it illustrates the required injected current to the grid. As seen, the current is increased quickly while the grid codes are violated. Therefore, it is concluded that the proposed event-triggered technique can decline the ROCOF and nadir frequency in a proper time and the grid stability and resiliency is guaranteed during the potential disturbances.

4.8. Anomaly Detection in Distribution Power System based on a Condition Monitoring Vector and Ultra-Short Demand Forecasting

4.8.1. An Overview of the Proposed IDS for Distribution Power System

Figure 4. 30 illustrates an overview of the proposed IDS for distribution power system. The considered attack model is a manipulation of the AMIs readings and/or smart inverters data transmitted to the grid supervisory controller and operator which can result in supply-demand balance stability challenges. The cybersecurity analytics in this work is based on a condition monitoring vector (CMV) equipped with a learned ultra-short term demand forecasting (USTDF) mechanism to verify the smart devices readings and identify potential anomalies. Having an ultra-short demand forecasting feature, improves the forecasting accuracy, thus attack detection becomes easier. The suspicious grid clusters are flagged or isolated from the rest of the network for further analysis by the grid operator based on the proposed CMV outcomes. By isolating a grid cluster from the rest of the network, the stability of the entire grid system will not be jeopardized. In the proposed approach, the instantaneous difference of collected AMI and other smart devices data with the high accurate forecasted demand is defined as the error vector which is called CMV. This vector probes a predefined error band for cybersecurity analytics and identification of compromised smart devices. The learned USTDF mechanism is based on the distribution grid historical load profile and the temperature data. An accurate multi-dimensional regression model is developed and learned for forecasting the load behavior in this area. It is envisioned that the learned and forecasted demand could have a tolerance; similarly, the physical smart devices

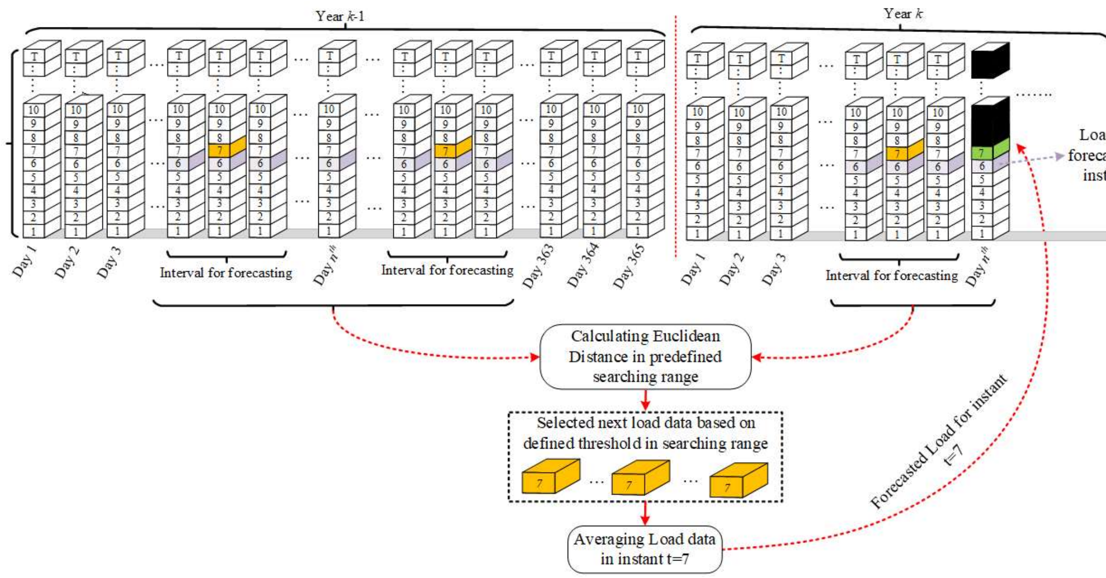

Figure 4. 31. The proposed ultra-short term demand forecasting approach for conditioning monitoring vector based cyber-security analytics.

readings have its inherent error in transmitted data to supervisory grid operator. Thus, considering these inevitable errors, a lower boundary error and an upper boundary error are defined to create an error band. In fact, the defined error band represents a bounded condition monitoring vector for anomaly detection in the area which has been equipped by this attack detection feature. If the CMV violates the pre-defined bands, the grid cluster or violating nodes will be flagged as "suspicious" cluster and the grid operator will not rely on the AMI readings, even the operator can isolate the suspicious grid to make the rest part of the system immune and stable. The network operator continues optimal control actions based on the USTDF and/or the nearby smart devices readings such as smart transformers, smart inverters, other healthy AMI, etc. Moreover, the verification of the attack incident is conducted by a decision-making module which evaluates the grid cluster level IDS outcomes with the upper layer grid operator. The objective of the decision-making module is to identify potential unexpected operational decisions versus cyber-attacks.

4.8.2. Ultra-Short Term Demand Forecasting Mechanism

The USTDF mechanism, Figure 4. 31, is based on the distribution grid historical load profile and the temperature data. An accurate multi-dimensional regression model is developed and learned for forecasting the load behavior in the grid cluster understudy. Building this model needs to have an accurate knowledge about the time series of the load. By analyzing the electric load data, it is observed that there is a repetitive behavior in this time series. This behavior is exclusive for each area of power system. As an example, Fig. 3 shows weekly behavior of electric load for a given grid cluster. Before making a robust regression model, load pattern was analyzed yearly, monthly, weekly and daily. For example, as it is shown in Figure 4. 32, different days in a week have a similar behavior approximately. In this work, for investigating the relation between independent and dependent value, high accurate models are developed. As an example, the model that shows the relation of the temperature with the energy consumption in the targeted grid areas was investigated. Then, the accuracy of this model was evaluated by the correlation coefficient, which is given by,

$$R=\frac{\sum_{i=1}^{n}\left(y_i-\sum_{i=1}^{n}y_i\right)\left(z_i-\sum_{i=1}^{n}z_i,\right)}{\sqrt{\sum_{i=1}^{n}\left(y_i-\sum_{i=1}^{n}y_i\right)^2\sum_{i=1}^{n}\left(z_i-\sum_{i=1}^{n}z_i,\right)^2}}\ ,\ z_i=f\left(x_i\right) \tag{4.19}$$

where, R is the correlation coefficient, x_i are independent variables, y_i are the real data and Z_i are the forecasted values which are estimated by the model. Also, it was observed that the temperature follows a repetitive pattern too. Intuitively, there is a relation between the temperature and the energy consumption; thus, there should be a mathematical relation between these variables. It should be noted that there is a considerable relation between past values and current values in most time series with repetitive pattern. Lag plots are known

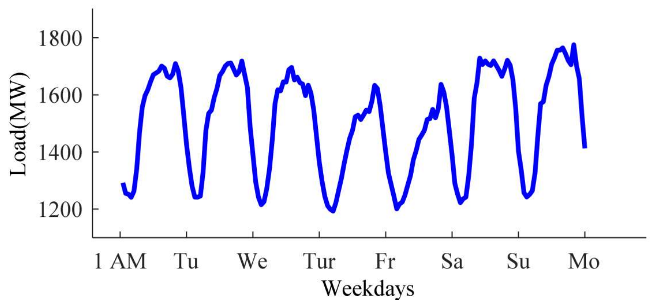

Figure 4. 32. Load pattern for one week: repetitive behavior of load is obvious.

as powerful and accurate tools for checking the randomness of a data set. In other word, a time series has no identifiable structure in its lag plot when it is included with random data. Therefore, if any FDI attack happens, these powerful tools can identify that the time series has been manipulated by attackers unless the operator is announced by the upper network controller. Investigating the load pattern via these mathematical tools, it is proved that this time series has a meaningful repetitive feature. Repeating pattern of load time series was analyzed by autocorrelation function too. To check a signal correlation with its previous values, autocorrelation function can be a proper approach. This function can identify hidden repeating pattern of signals that contain noises. This is given by,

$$r_k = \frac{\sum_{i=1}^{n-k}\left(y_i - \sum_{i=1}^{n} y_i\right)\left(y_{i+k} - \sum_{i=1}^{n} y_i,\right)}{\sum_{i=1}^{n}\left(y_i - \sum_{i=1}^{n} y_i\right)^2} \tag{4.20}$$

where, r_k shows the correlation between two independent variables of y_i and y_{i+k}. Autocorrelation coefficients for a sample load data were plotted in Fig. 4 and as it is shown, there is a high dependency between load values in current time with previous time. Also, daily repetitive behavior of the load was proved by this analysis. In order to find the samples which, have meaningful dependency with each other by autocorrelation coefficient, a confidence band should be considered. This band is defined by Bartlett's formula. In fact, this equation calculates a standard error for the autocorrelation function. This equation is given by,

$$SE_{ACF}=\sqrt{\frac{1}{n}\left(1+2\sum_{q=1}^{k-1}\left(\frac{\sum_{i=1}^{n-q}\left(y_i-\sum_{i=1}^{n}y_i\right)\left(y_{i+q}-\sum_{i=1}^{n}y_i\right)}{\sum_{i=1}^{n}\left(y_i-\sum_{i=1}^{n}y_i\right)^2}\right)^2\right)} \tag{4.21}$$

where, k is the lag number, n is the number of data samples and y_i is the ith sample in the time series. Coefficients that are stacked in the aforementioned band are not considered in this analysis. As it is shown in Figure 4. 33, the first sample had the value of 1. It's very reasonable that each part of a signal is exactly similar to itself. Second sample in this study

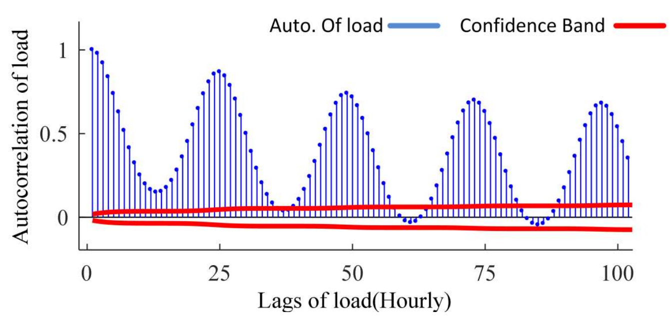

Figure 4. 33. Autocorrelation coefficients of load data with its confident band.

has the value that is almost one. This fact proves that there is a high correlation between current load data with previous hour load. 25th Sample is the next outstanding one that occurs 24 hours later exactly. This value reveals a high correlation of load in present time with consumption of 24 hours ago that is very logical. It should be noted that, these analyses were done for all variables that can have effect on the load value. Thus, the robust regression model is given by,

$$\Im_{t+\Delta t} = w_0 + w_1 \Im_t + w_2 \Im_s + w_3 T_t + w_4 D \tag{4.22}$$

where the weight factors (W_0 to W_4) are learned based on a deep learning method, $\Im_t$ is the load at time (t), $\Im_s$ is the load gradient between the present time (t) and the previous time $(t-\Delta t)$, T_t is the temperature, and D represents the days. The deep learning method repeats a mathematical process for finding the best weight factors which improve the accuracy of the model. The main principle for finding these weight factors is presented in the following. Given a general regression model as,

$$Z_i = a + bx_i + cy_i \tag{4.23}$$

where, z_i are independent variables which are estimated by x_i and y_i. The parameters a, b, and c are defined as the weight factors in this model. To find these coefficients, an error function E is defined as,

$$E = \sum_{i=1}^{n} \left(z_i - \left(a + bx_i + cy_i \right) \right)^2 \tag{4.24}$$

Then, three partial derivatives are calculated in term of all weight factors given by,

$$\begin{aligned} \frac{\partial E}{\partial a} &= 2\sum_{i=1}^{n} \left(z_i - \left(a + bx_i + cy_i \right) \right) = 0 \\ \frac{\partial E}{\partial b} &= 2\sum_{i=1}^{n} x_i \left(z_i - \left(a + bx_i + cy_i \right) \right) = 0 \\ \frac{\partial E}{\partial c} &= 2\sum_{i=1}^{n} y_i \left(z_i - \left(a + bx_i + cy_i \right) \right) = 0 \end{aligned} \tag{4.25}$$

For minimizing the error, all partial derivatives should be equal to zero. By solving (4.25), (4.26) can be determined as following,

$$
\begin{aligned}
\sum_{i=1}^{n} z_i &= a\sum_{i=1}^{n} 1 + b\sum_{i=1}^{n} x_i + c\sum_{i=1}^{n} y_i \\
\sum_{i=1}^{n} x_i z_i &= a\sum_{i=1}^{n} x_i + b\sum_{i=1}^{n} x_i^{2} + c\sum_{i=1}^{n} x_i y_i \\
\sum_{i=1}^{n} y_i z_i &= a\sum_{i=1}^{n} y_i + b\sum_{i=1}^{n} x_i y_i + c\sum_{i=1}^{n} y_i^{2}
\end{aligned} \tag{4.26}
$$

All weight factors can be determined by solving (4.26). The USTDF mechanism continues by mapping and extracting identical days based on Euclidean norm, which is given by,

$$
\begin{aligned}
&\|\Re\| = \sqrt{\Re_1^{'} + \Re_2^{'} + \Re_3^{'} + \Re_4^{'}} \\
&s.t. \\
&\Re_1^{'} = \mathrm{w}_1\left(\Im_t - \Im_t^P\right)^2, \Re_2^{'} = \mathrm{w}_2\left(\Delta\Im_s\right)^2 \\
&\Re_3^{'} = \mathrm{w}_3\left(\Delta T_t\right)^2, \Re_4^{'} = \mathrm{w}_4\left(\mathrm{w}_t - \mathrm{w}_P\right)^2 \\
&\Delta\Im_s = \Im_s - \Im_s^P, \quad \Im_s = \Im_t - \Im_{t-\Delta t}
\end{aligned} \tag{4.27}
$$

where $\Im_t^P$ and $\Im_s^P$ are the load and their respective gradient in previous days. This norm searches for identical days within a pre-defined searching range. The correlation among the day's load pattern (i.e., auto-correlation technique) is utilized to define the searching range for Euclidean norm engine. The $\|\Re\|$ is calculated based on a desired time interval for all pre-defined searching range. Once the $\|\Re\|$ is calculated in the defined time interval for all days in searching range, the days load data which have the $\|\Re\|$ value within a pre-defined threshold will be extracted. For example, in a case that the load data are susceptible to be manipulated by attackers, this time interval can be very short and the pre-defined threshold can be re-adjusted. The load at instant $(t+\Delta t)$ is forecasted by firstly mapping the t instant load with the loads in the built database and then averaging the load at $(t+\Delta t)^P$ in the database. This mechanism will update the historical load data and is repeated for the next time interval. The summary of this approach is illustrated in Figure 4. 31. Moreover, for evaluating the feasibility of the proposed approach, this mechanism was applied on a sample database

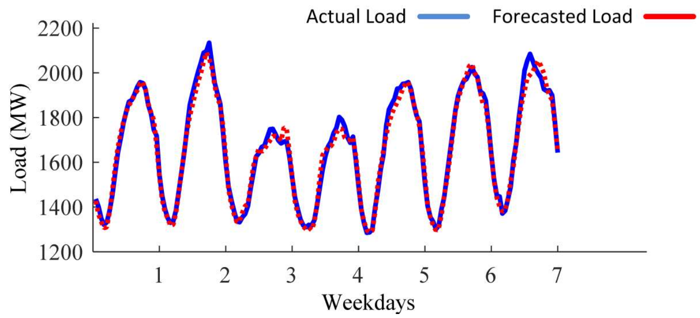

Figure 4. 34. Actual load and the forecasted load for one week.

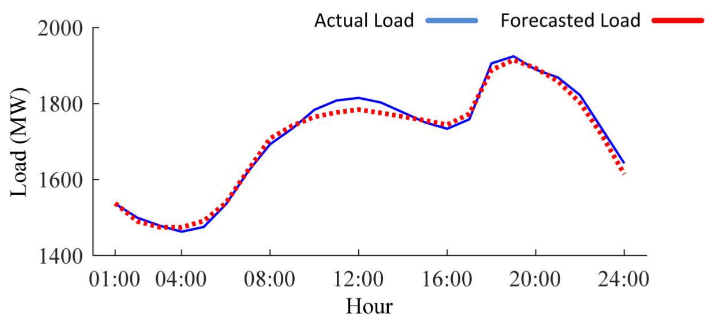

Figure 4. 35. Actual load and the forecasted load for 24 hours ahead.

which includes historical load data for a given geographical area. As it is shown in Figure 4. 34, the forecasting mechanism was performed for each day of one week. As the forecasted load plot is shown, forecasting error is negligible which demonstrates the accuracy of the proposed approach. Furthermore, Figure 4. 35 shows the performance of the proposed forecasting approach for a single day.

4.8.3. Intrusion Detection Based on Condition Monitoring Vector

The proposed IDS based on the forecasting approach of the previous section and a CMV is presented in this section. It is envisioned that the forecasted demand could have a limited tolerance, especially in the peak time of the energy consumption; similarly, the physical

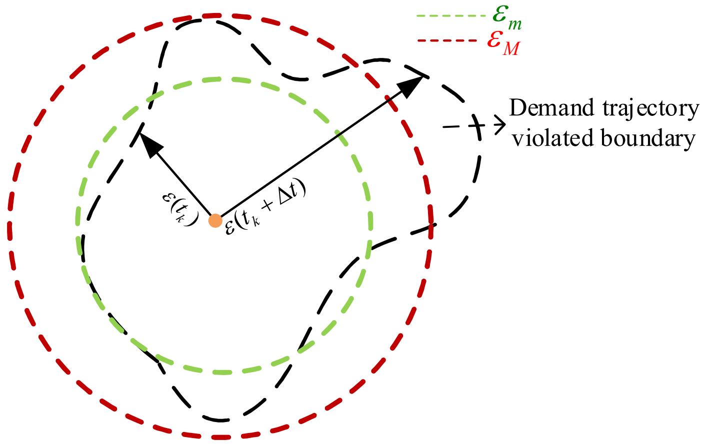

Figure 4. 36. The proposed condition monitoring vector mechanism.

smart devices readings have its inherent error in transmitted data to the supervisory grid operator. These two issues are known as the potential challenges of the proposed attack detection method. In other word, the attackers can manipulate the load data in a way that the grid operator does not understand that a stealthy attack is in progress. Therefore, if simultaneously, the attackers manipulate the load data in several parts of the network, there is a risk that suddenly a demand-supply unbalance condition occurs. The consequence of this attack is system frequency deviation from the nominal value which if not controlled properly, significant portion of the network may collapse. Thus, considering these inevitable errors, a lower boundary error (ε_m) and an upper boundary error (ε_M) are defined in this work, these two boundaries create an error band as following,

$$\varepsilon_m < \left\| \Im_m(t_k) - \Im_f(t_k) \right\| < \varepsilon_M \tag{4.28}$$

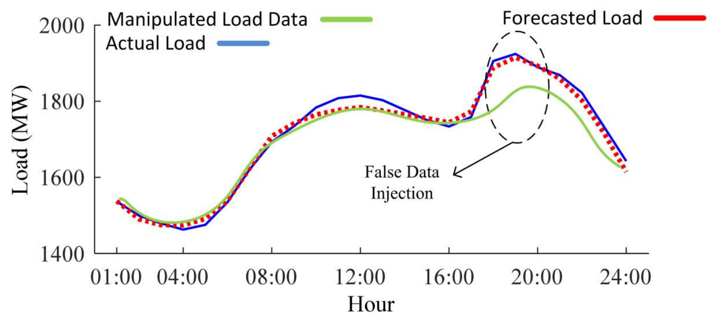

Figure 4. 37. An attack scenario by considering the real, forecasted and manipulated load data.

where $\Im_m(t_k)$ and $\Im_f(t_k)$ are measured load by AMIs and forecasted load at instant t_k by proposed USTDF mechanism respectively. In fact, (10) represents a bounded CMV for anomaly detection in a grid cluster, Figure 4. 36.

If the CMV violates the pre-defined upper bands (ε_M) or lower band (ε_m), the grid cluster will be flagged as "suspicious" cluster or be isolated from the entire system and the grid operator will not rely on the AMI readings. At this instant the proposed IDS triggers the decision-making module which is outlined in the next section of this work.

Based on the network condition, the operator may continue optimal control actions based on the USTDF and/or the nearby smart devices readings such as smart transformers, smart inverters, other healthy AMI, etc. Therefore, the proposed approach adds a layer of cyber-physical security to the power grid. For demonstration of the considered stealthy attack scenario and the proposed IDS, a cluster of a network has been investigated. As it is shown in Fig. 8, load profile has been forecasted by the proposed mechanism with high accuracy. It is observed that, there are small deviations between the actual load and the forecasted one. These deviations occur around 12 pm and 08 pm which are typically the peak hour of energy consumption. The attackers manipulate the grid-edge devices data of this cluster of the network. Manipulated load data are seen in green in Figure 4. 37. Attackers send fake data that are approximately similar to real data in most of the time and transmit to the operator. Thus, the network is operated normally. However, reaching around the second peak of the load profile, the attackers send load data that are much lower than the real data in the network. It should be noted that, this FDI is occurred before the real peak hour of the understudy network cluster. If the network operator cannot detect this anomaly in a proper time, the supply will be matched by the transmitted fake data. Considering several attacks are occurring on different clusters of the network simultaneously, most of the utilities decrease their supply logically based on the received new commands. This deviation between fake data and the real one is increased gradually by attackers. Exactly on the peak hour, a considerable mismatch between supply and demand occurs and the operator does not have enough time to do any effective corrective action for this unbalanced condition. Consequently, the power system frequency collapses and after that the system becomes unstable. If the control center of the network is equipped with the proposed IDS based on USTDF and a bounded CMV, this class of attacks can be detected in a timely manner and the grid operator can take proper decision to ensure energy services without interruption.

4.8.4. Decision Making Mechanism of the IDS

Based on the instantaneous condition of power system, there are possible situation where the network operators take operational corrective actions such as load shedding. These types of operational decision may mislead the proposed IDS. Thus, intentional disturbances should be identified to verify cyber threats detected. The proposed decision-making mechanism in the IDS in this work has four different inputs and outputs. Two of them are related to the outputs of the anomaly detection module and the other inputs come from the main network control center which has the authority to apply intentional changes on the system. In this work, these inputs are labeled by four characters which are color coded in Figure 4. 30. These labels are defined as 1R0R, 1R1G, 0G0R and 0G1G. When label 1R0R is received, it means that an anomaly has happened while the network control center has not triggered any corrective or precautionary actions on the system. This is the riskiest condition for the system because there is a high probability that a malicious attack is in progress on the system. In this case, the first defensive action is to isolate this cluster from the rest of the network.

In the case that an anomaly incident is detected, and the network control center take an intention corrective action such as load shedding, the cluster will be flagged to be diagnosed more accurately. If the operator confirms the system is safe, the flag will be removed. To operate the network safer, in the case that there is no anomaly signal from CMV, if the network control center transmits a code that states an intentional deviation has occurred in the network parameters, the system again is flagged to be checked and monitored with more details. For both mentioned cases, the labels are defined as 1R1G and 0G1G respectively. The only safe mode that the operator will not take any action is the time that the decision-making center receives the code 0G0R. This code guarantees that no anomaly occurred.

4.9. Conclusion

An integrated data-driven and model-based predictive control method was proposed for the frequency and voltage restoration of a cluster of PEDG in response to unexpected grid-events. A two-layer feed forward network was trained by considering wide range of frequency deviation and different dynamics of ROCOF profile. For providing training data, several frequencies dynamic models were solved by swing equation and the feasible outputs were used as training data. Finally, the trained ANN was employed to determine the optimal active power setpoints for the ESS for frequency restoration. The ESS was controlled via a DAB converter which utilized the determined optimal active power setpoint as a reference for a model-based predictive controller. The results show that the proposed IDMPC can restore the frequency and smooth the ROCOF profile in response to potential disturbances.

The security of control systems is crucial, as very simple cyber-attacks can affect the physical aspects of the system, and result in physical damage. This was shown in Sections (4.6.1) and (4.7.1) where the attacker was able to cause some of the systems' states to diverge. Also, it was discussed that the addition of a LQG controller does not affect the ability of an attacker to mount a stealthy attack. The initial state of the system also does not affect the ability of the system to reach a steady state. However, an attacker with imperfect knowledge about the system's model will not be successful in mounting a stealthy attack. Specifically, the attack either fails in causing some of the states to diverge, or it becomes easily detectable. Recall that the attack is effective only if it remains undiscovered, which varies with the level of uncertainty about the model parameters, and which in turn depends on the time allocated by the attacker to learning the model.

Thus, stealthy attacks should be considered as one strives to learn the most accurate model of a control system – a less than perfect model may be well within the control capabilities of the chosen controller, while providing immunity against stealthy attacks.

Vulnerabilities of the new energy paradigm, the PEDG, in the event of cyberattacks are among the most crucial challenges. Stealthy attacks, due to their unobservable natures by the supervisory layer, are among the most destructive cyber incidents. The stealthy attacks could deteriorate the balance between active power generation and consumption by pushing the DERs across the grid to go islanded. This will result in severe frequency drop. Although the existing synchronous generators will try to compensate loss of generation, due to their high inertia and slow response, the frequency relays might trigger and cascading failure occurs across the grid, yielding to large-scale blackouts. To overcome this challenge, an event-triggered ANN-based shadow control scheme was proposed in this chapter to ensure frequency restoration in the case of stealthy attacks. The proposed data-driven shadow control observes the frequency and its rate of change and behaves according to the real-time situation of the grid. In the case of loss of generation, the proposed shadow control is activated autonomously since it observes the frequency and ROCOF. Then, by accurately approximating the required active power, the BESS of located in the PEDG cluster compensates the active power. As mentioned, a two-layer feed-forward ANN is trained for the shadow controller. To test the proposed shadow control scheme, a real 14-bus PEDG with seven DERs is considered. The results without the proposed approach in the case of stealthy attacks illustrated divergence of the state variables yielding to unstable operation of the entire PEDG cluster. Results by employing the proposed ANN-based shadow control depicts significant improvements in the frequency restoration of the 14-bus system.

Finally, A proactive IDS for smart distribution power systems is presented in this chapter. The proposed IDS is based on an ultra-short-term demand forecasting mechanism, a condition monitoring vector, and a decision-making module. The demand forecasting approach is based on the historical data and the temperature. The mathematical analysis and the logic of this robust forecasting approach were explained. The condition monitoring vector is detecting the false data injection by leveraging the outcome of the demand forecasting. Upper and lower bands were defined in this mechanism based on the acceptable and inherent tolerance, both in forecasting and measurement processes. FDI detection loop was completed by designing a decision-making module. This module is responsible for verifying an attack incident by flagging or isolating the cluster of the network from the other part of the system.

Chapter 5

5. Conclusion

This dissertation concentrated on the resilient operation of active distribution networks via self-learning smart devices. Thus, in the first step, a comprehensive description of power electronic-dominated grids (PEDG) as an active distribution network was provided. All technical characteristics of PEDG as a new energy paradigm were analyzed and compared with the traditional power system. As the main objective of this dissertation, which is enhancing the resiliency of PEDG, this concept was detailed in the frame of PEDGs in the next step. PEDG resiliency concept as a sort of grid tolerance when encountered with a different type of disturbances was explained. Different aspects of this concept were demonstrated, and all drawbacks and consequences of a low-resilience grid were investigated. As PEDG suffers mainly from a lack of minimum required inertia, the study was narrowed on this topic and its corresponding challenges. Based on the resiliency concept, rapid and proper restoration of the power system is identified as a high-impact factor that can improve the grid's resiliency significantly. Thus, the study investigated the events that effortlessly jeopardize PEDG stability. Consequently, it was required to provide the stability concept, as a subset of resiliency with valid categories regarding this dissertation's objective. Normal and severe disturbances are common incidents in PEDG that can endanger system stability if not controlled properly and promptly. Thus, first, a general study regarding demand and supply stability was carried out. Later, different types of disturbances that can influence this type of stability were studied. Technical details that can clarify this idea were reviewed and analyzed as well. Due to the main feature of PEDGs, several grid-forming and grid-following inverters are employed to establish a demand-supply balance promptly. Hence, it was vital to assess the details of GFM and GFL inverters' interactions in the PEDG. In this regard, the study began by evaluating the main control concepts of these two inverter variants from basic to advanced control schemes. It was concluded that there is a high correlation between the dynamic response of these grid-supporting resources which enable system operators to replace their effective roles based on the grid's requirements. Thus, for enhancing PEDG resiliency, different approaches are proposed in this dissertation and each of them is applicable in a different layer of control while their core idea can be linked to each other. It is believed that by integrating all the proposed approaches in this dissertation, a puzzle is completed that illustrates a considerable enhancement in PEDG resiliency.

In chapter two, a primary control layer is proposed which enables a low-inertia power system (LIPS) to provide a fast response regarding grid disturbances. To achieve this objective, a model predictive self-healing control (MPSC) scheme is designed for a battery system interfaced dual active bridge (DAB) converter in a LIPS that experiences severe disturbances. A novel self-healing control loop is proposed that utilizes the feasible range of power transfer in conjunction with the AC-link inductor's voltage profile. The proposed method can validate and autonomously correct the predicted current and phase shift in the DAB converter interfaced with a battery system. The devised control scheme on the DAB converter prevents voltage and frequency collapse in a hybrid AC/DC LIPS, particularly during severe load disturbances that occur periodically which can be a threatening phenomenon for a hybrid AC/DC LIPS. Also, system stability was studied based on

Lyapunov stability analysis. The theoretical concepts were validated by several case studies implemented on a hardware-in-the-loop (HIL) testbed of a small scaled-microgrid. The case studies demonstrated voltage and frequency regulation of the understudy system with fast dynamic response during severe disturbances. Moreover, the proposed MPSC performance was compared with proportional-integral (PI) based control to highlight the priority of the proposed control approach. Based on the importance of PEDG resiliency and the high possibility of instability in this low inertia system, it was decided to design and develop an additional intelligent control layer to realize a self-learning control scheme with ultra-fast frequency restoration in the PEDG. Thus, the research moved on toward maximizing the GFLI's capabilities in rapid restoration of the grid during normal and severe disturbances.

In Chapter three, a frequency restoration method is proposed to enhance PEDG resiliency by maximum utilization of GFLIs capability. An artificial intelligence-based power reference correction (AI-PRC) module is designed and developed for GFLIs to autonomously heal their predefined power setpoints during potential disturbances. A detailed mathematical proof is presented to demonstrate that the grid forming (GFM) and GFL inverters' control rules intrinsically follow the underlying dynamic of the swing-based machines to extend the stability boundary of low inertia PEDGs. Considering this fact, comprehensive transient and steady state-based mathematical models that can deal with all grid's characteristic alterations are used in this chapter. The concept of this dynamic model is exploited to construct a thorough learning database that includes all grid physical features such as feasible alterations in PEDG configurations, demand and supply side disturbances, a wide range of inertia constants, grid's natural and damping frequency as well as the optimal injecting/absorbing power to/from the grid. The proposed approach incorporates all PEDG's effective variables for shaping the dynamic response during potential disturbances. Later, a neural network is trained by deploying the Bayesian regularization algorithm (BRA). In the training process, the constructed mathematically based learning data is employed, and the entire AI-PRC module is implemented in the control loop of GFLIs to adjust their pre-defined power references in real time based on the grid's disturbances. Thus, the main contribution of this work is to address the shortcomings of frequency restoration of state-of-the-art VSG-based or droop-based GFLIs and GFMIs via re-defining GFLI role at grid-edge equipped with the proposed AI-PRC. Several use cases were simulated and analyzed in a realistic 14-bus PEDG by MATLAB/Simulink and OPAL-RT simulator to evaluate the functionality of the proposed approach for enhancing grid resiliency. Moreover, several experimental assessments were conducted to support the simulation outcomes and provide practical validation of the proposed frequency restoration mechanism. In the final step along with the objective of this work, the application of the proposed approaches was evaluated on the cybersecurity challenges of PEDG. Should be remarked that PEDG'S resiliency will be enhanced significantly if cybersecurity breaches are damped promptly. Thus, in the next chapter, the proposed approach was leveraged to realize an event-triggered control scheme and provide a proper and safe reaction to potential security breaches. Moreover, the negative consequences of stealthy cyber-attacks on control signals were damped by the proposed approach. To add another safety layer for PEDG to achieve maximum resiliency, a proactive intrusion detection system (IDS) is designed for smart distribution power systems as well.

Thus, in chapter four, an integrated data-driven and model-based predictive control (IDMPC) is implemented on power electronics interfaces of the distributed energy resources (DERs) at the grid-edge to enable the control of islanded grid-cluster frequency feature such as rate of change of frequency (ROCOF) and nadir frequency. The presented IDMPC scheme has a fast dynamic response and is robust to system disturbances. The functionality of the proposed method for supporting the voltage and frequency of the grid is verified by some case studies. Also, to fulfill frequency restoration in the event of stealthy attacks, a novel shadow control scheme is designed which leverages the advantages of artificial intelligence techniques for enhancing PEDG resiliency. A cohesive data-extracted methodology built-in a shadow control (CDMSC) scheme is developed with inherent features of the artificial neural networks (ANNs) to enhance the dynamic response of the system. The proposed CDMSC approximates the grid's inertia by ANN module, accurately. Different practical frequency dynamics, ROCOF, and inertia constant are considered in the training process to ensure all possible scenarios on a realistic power system. Moreover, several disturbances including, load disturbances and potential loss of generation are considered in this development. It should be remarked that the considered disturbances are used as inputs of the swing equation and the required power is calculated based on the frequency excursion and ROCOF. This data is used as test data in the training process. A feed-forward ANN with two layers is applied in the key core of the shadow control scheme towards an event-triggered self-learning controller that is guiding the supervisory controller. A Bayesian algorithm is utilized in the training process and optimum numbers of hidden neurons are founded by several evaluations of the training mechanism. The proposed shadow control framework was verified on a 14-bus PEDG system. Moreover, a proactive intrusion detection system (IDS) as another safety layer is designed for smart distribution power systems. The considered attack scenario is manipulation of the advanced measuring infrastructures (AMIs) readings and/or smart inverters data. The proposed IDS is based on a condition monitoring vector (CMV) equipped with a learned ultra-short-term demand forecasting (USTDF) mechanism. This cybersecurity approach can verify smart device readings. In the proposed method, the instantaneous difference between collected AMIs and other smart device data with the ultra-short term forecasted demand is defined as the CMV. This vector probes a pre-defined error band for identifying the compromised smart devices. The learned USTDF mechanism is based on the distribution grid historical load profile and the temperature data for the goal area. An accurate multi-dimensional regression model is developed and learned for forecasting the load behavior in this area. Finally, the suspicious areas are flagged or become separated from the main grid by the network operator based on the proposed CMV outcomes and the output of the decision-making module. The proposed IDS aims to enhance the cybersecurity of the smart devices at the grid edge that plays a major role in ensuring the resiliency of the grid. Finally, the theoretical analyses were verified by several case studies.

5.1. Future Works

The conducted research described in this dissertation can be continued to encompass the subsequent future works:

I. Developing a further AI-based technique that generally follows the major thought of the proposed AI-PRC in this dissertation to directly address the voltage control of

PEDG. This notion should take into consideration the locations of DERs that are equipped with AI-based techniques as the nodal voltage is not a global variable.

II. Coupling the conducted research in this dissertation with the AI-based technique can regulate nodal voltages, will enhance grid resiliency in a more inclusive manner. Some advanced techniques are needed to realize how active and reactive power variations in PEDG can influence the grid voltage and frequency.

6. Appendix

6.1. Permission from the IEEE website (RightsLink) regarding Thesis/Dissertation reuse

This appendix presents the copyright permissions for the articles, whose contents were utilized in my dissertation. The list of the articles includes several journal, conference, and workshop publications: IEEE Transaction on Energy Conversion, 2020, IEEE Energy Conversion Congress and Exposition (ECCE, 2021), IEEE Industrial Electronics Magazine, 2020, IEEE Power Electronics Magazine, 2021, IEEE 12th International Symposium on Power Electronics for Distributed Generation Systems (PEDG, 2021), IEEE International Conference on Smart Grid and Renewable Energy (SGRE 2019), IEEE International Conference on Smart Grid and Renewable Energy (SGRE 2022), IEEE CyberPELS, 2020, IEEE Kansas Power and Energy Conference (KPEC, 2020), IEEE Transactions on Industrial Electronics, 2022.

The copyright permissions for reusing the published materials are presented in the Appendix.

Appendix (Continued)

CCC RightsLink

Home | Help | Email Support | Sign in | Create Account

On the Stability of the Power Electronics-Dominated Grid: A New Energy Paradigm

IEEE Requesting permission to reuse content from an IEEE publication

Author: Ahmad Khan

Publication: IEEE Industrial Electronics Magazine

Publisher: IEEE

Date: December 2020

Thesis / Dissertation Reuse

The IEEE does not require individuals working on a thesis to obtain a formal reuse license, however, you may print out this statement to be used as a permission grant:

Requirements to be followed when using any portion (e.g., figure, graph, table, or textual material) of an IEEE copyrighted paper in a thesis:

1) In the case of textual material (e.g., using short quotes or referring to the work within these papers) users must give full credit to the original source (author, paper, publication) followed by the IEEE copyright line © 2011 IEEE.
2) In the case of illustrations or tabular material, we require that the copyright line © [Year of original publication] IEEE appear prominently with each reprinted figure and/or table.
3) If a substantial portion of the original paper is to be used, and if you are not the senior author, also obtain the senior author's approval.

Requirements to be followed when using an entire IEEE copyrighted paper in a thesis:

1) The following IEEE copyright/ credit notice should be placed prominently in the references: © [year of original publication] IEEE. Reprinted, with permission, from [author names, paper title, IEEE publication title, and month/year of publication]
2) Only the accepted version of an IEEE copyrighted paper can be used when posting the paper or your thesis on-line.
3) In placing the thesis on the author's university website, please display the following message in a prominent place on the website: In reference to IEEE copyrighted material which is used with permission in this thesis, the IEEE does not endorse any of [university/educational entity's name goes here]'s products or services. Internal or personal use of this material is permitted. If interested in reprinting/republishing IEEE copyrighted material for advertising or promotional purposes or for creating new collective works for resale or redistribution, please go to http://www.ieee.org/publications_standards/publications/rights/rights_link.html to learn how to obtain a License from RightsLink.

If applicable, University Microfilms and/or ProQuest Library, or the Archives of Canada may supply single copies of the dissertation.

BACK CLOSE WINDOW

Appendix (Continued)

RightsLink

Home | Help | Email Support | Sign in | Create Account

Towards Intelligent Power Electronics-Dominated Grid via Machine Learning Techniques

Requesting permission to reuse content from an IEEE publication

Author: Omar H. Abu-Rub

Publication: IEEE Power Electronics Magazine

Publisher: IEEE

Date: March 2021

Thesis / Dissertation Reuse

The IEEE does not require individuals working on a thesis to obtain a formal reuse license, however, you may print out this statement to be used as a permission grant:

Requirements to be followed when using any portion (e.g., figure, graph, table, or textual material) of an IEEE copyrighted paper in a thesis:

1) In the case of textual material (e.g., using short quotes or referring to the work within these papers) users must give full credit to the original source (author, paper, publication) followed by the IEEE copyright line © 2011 IEEE.
2) In the case of illustrations or tabular material, we require that the copyright line © [Year of original publication] IEEE appear prominently with each reprinted figure and/or table.
3) If a substantial portion of the original paper is to be used, and if you are not the senior author, also obtain the senior author's approval.

Requirements to be followed when using an entire IEEE copyrighted paper in a thesis:

1) The following IEEE copyright/ credit notice should be placed prominently in the references: © [year of original publication] IEEE. Reprinted, with permission, from [author names, paper title, IEEE publication title, and month/year of publication]
2) Only the accepted version of an IEEE copyrighted paper can be used when posting the paper or your thesis on-line.
3) In placing the thesis on the author's university website, please display the following message in a prominent place on the website: In reference to IEEE copyrighted material which is used with permission in this thesis, the IEEE does not endorse any of [university/educational entity's name goes here]'s products or services. Internal or personal use of this material is permitted. If interested in reprinting/republishing IEEE copyrighted material for advertising or promotional purposes or for creating new collective works for resale or redistribution, please go to http://www.ieee.org/publications_standards/publications/rights/rights_link.html to learn how to obtain a License from RightsLink.

If applicable, University Microfilms and/or ProQuest Library, or the Archives of Canada may supply single copies of the dissertation.

BACK CLOSE WINDOW

Appendix (Continued)

CCC RightsLink

Home | Help | Email Support | Sign in | Create Account

IEEE Requesting permission to reuse content from an IEEE publication

Anomaly Detection in Distribution Power System based on a Condition Monitoring Vector and Ultra- Short Demand Forecasting

Conference Proceedings: 2020 IEEE CyberPELS (CyberPELS)

Author: Mohsen Hosseinzadehtaher

Publisher: IEEE

Date: 13 October 2020

Thesis / Dissertation Reuse

The IEEE does not require individuals working on a thesis to obtain a formal reuse license, however, you may print out this statement to be used as a permission grant:

Requirements to be followed when using any portion (e.g., figure, graph, table, or textual material) of an IEEE copyrighted paper in a thesis:

1) In the case of textual material (e.g., using short quotes or referring to the work within these papers) users must give full credit to the original source (author, paper, publication) followed by the IEEE copyright line © 2011 IEEE.
2) In the case of illustrations or tabular material, we require that the copyright line © [Year of original publication] IEEE appear prominently with each reprinted figure and/or table.
3) If a substantial portion of the original paper is to be used, and if you are not the senior author, also obtain the senior author's approval.

Requirements to be followed when using an entire IEEE copyrighted paper in a thesis:

1) The following IEEE copyright/ credit notice should be placed prominently in the references: © [year of original publication] IEEE. Reprinted, with permission, from [author names, paper title, IEEE publication title, and month/year of publication]
2) Only the accepted version of an IEEE copyrighted paper can be used when posting the paper or your thesis on-line.
3) In placing the thesis on the author's university website, please display the following message in a prominent place on the website: In reference to IEEE copyrighted material which is used with permission in this thesis, the IEEE does not endorse any of [university/educational entity's name goes here]'s products or services. Internal or personal use of this material is permitted. If interested in reprinting/republishing IEEE copyrighted material for advertising or promotional purposes or for creating new collective works for resale or redistribution, please go to http://www.ieee.org/publications_standards/publications/rights/rights_link.html to learn how to obtain a License from RightsLink.

If applicable, University Microfilms and/or ProQuest Library, or the Archives of Canada may supply single copies of the dissertation.

BACK CLOSE WINDOW

Appendix (Continued)

Home | Help | Email Support | Sign in | Create Account

RightsLink

(A Little) Ignorance is Bliss: The Effect of Imperfect Model Information on Stealthy Attacks in Power Grids

Conference Proceedings: 2020 IEEE Kansas Power and Energy Conference (KPEC)
Author: Stephanie Harshbarger
Publisher: IEEE
Date: July 2020

IEEE Requesting permission to reuse content from an IEEE publication

Thesis / Dissertation Reuse

The IEEE does not require individuals working on a thesis to obtain a formal reuse license, however, you may print out this statement to be used as a permission grant:

Requirements to be followed when using any portion (e.g., figure, graph, table, or textual material) of an IEEE copyrighted paper in a thesis:

1) In the case of textual material (e.g., using short quotes or referring to the work within these papers) users must give full credit to the original source (author, paper, publication) followed by the IEEE copyright line © 2011 IEEE.
2) In the case of illustrations or tabular material, we require that the copyright line © [Year of original publication] IEEE appear prominently with each reprinted figure and/or table.
3) If a substantial portion of the original paper is to be used, and if you are not the senior author, also obtain the senior author's approval.

Requirements to be followed when using an entire IEEE copyrighted paper in a thesis:

1) The following IEEE copyright/ credit notice should be placed prominently in the references: © [year of original publication] IEEE. Reprinted, with permission, from [author names, paper title, IEEE publication title, and month/year of publication]
2) Only the accepted version of an IEEE copyrighted paper can be used when posting the paper or your thesis on-line.
3) In placing the thesis on the author's university website, please display the following message in a prominent place on the website: In reference to IEEE copyrighted material which is used with permission in this thesis, the IEEE does not endorse any of [university/educational entity's name goes here]'s products or services. Internal or personal use of this material is permitted. If interested in reprinting/republishing IEEE copyrighted material for advertising or promotional purposes or for creating new collective works for resale or redistribution, please go to http://www.ieee.org/publications_standards/publications/rights/rights_link.html to learn how to obtain a License from RightsLink.

If applicable, University Microfilms and/or ProQuest Library, or the Archives of Canada may supply single copies of the dissertation.

BACK　　CLOSE WINDOW

Appendix (Continued)

RightsLink

Home | Help | Email Support | Sign in | Create Account

IEEE Requesting permission to reuse content from an IEEE publication

Model Predictive Self-healing Control Scheme for Dual Active Bridge Converter

Conference Proceedings:
2019 2nd International Conference on Smart Grid and Renewable Energy (SGRE)

Author: Mohsen Hosseinzadehtaher

Publisher: IEEE

Date: November 2019

Thesis / Dissertation Reuse

The IEEE does not require individuals working on a thesis to obtain a formal reuse license, however, you may print out this statement to be used as a permission grant:

Requirements to be followed when using any portion (e.g., figure, graph, table, or textual material) of an IEEE copyrighted paper in a thesis:

1) In the case of textual material (e.g., using short quotes or referring to the work within these papers) users must give full credit to the original source (author, paper, publication) followed by the IEEE copyright line © 2011 IEEE.
2) In the case of illustrations or tabular material, we require that the copyright line © [Year of original publication] IEEE appear prominently with each reprinted figure and/or table.
3) If a substantial portion of the original paper is to be used, and if you are not the senior author, also obtain the senior author's approval.

Requirements to be followed when using an entire IEEE copyrighted paper in a thesis:

1) The following IEEE copyright/ credit notice should be placed prominently in the references: © [year of original publication] IEEE. Reprinted, with permission, from [author names, paper title, IEEE publication title, and month/year of publication]
2) Only the accepted version of an IEEE copyrighted paper can be used when posting the paper or your thesis on-line.
3) In placing the thesis on the author's university website, please display the following message in a prominent place on the website: In reference to IEEE copyrighted material which is used with permission in this thesis, the IEEE does not endorse any of [university/educational entity's name goes here]'s products or services. Internal or personal use of this material is permitted. If interested in reprinting/republishing IEEE copyrighted material for advertising or promotional purposes or for creating new collective works for resale or redistribution, please go to http://www.ieee.org/publications_standards/publications/rights/rights_link.html to learn how to obtain a License from RightsLink.

If applicable, University Microfilms and/or ProQuest Library, or the Archives of Canada may supply single copies of the dissertation.

BACK CLOSE WINDOW

Appendix (Continued)

RightsLink

Home | Help | Email Support | Sign in | Create Account

IEEE
Requesting permission to reuse content from an IEEE publication

Event-triggered Self-learning Control Scheme For Power Electronics Dominated Grid

Conference Proceedings: 2021 IEEE Energy Conversion Congress and Exposition (ECCE)
Author: Mohsen Hosseinzadehtaher
Publisher: IEEE
Date: 10 October 2021

Thesis / Dissertation Reuse

The IEEE does not require individuals working on a thesis to obtain a formal reuse license, however, you may print out this statement to be used as a permission grant:

Requirements to be followed when using any portion (e.g., figure, graph, table, or textual material) of an IEEE copyrighted paper in a thesis:

1) In the case of textual material (e.g., using short quotes or referring to the work within these papers) users must give full credit to the original source (author, paper, publication) followed by the IEEE copyright line © 2011 IEEE.
2) In the case of illustrations or tabular material, we require that the copyright line © [Year of original publication] IEEE appear prominently with each reprinted figure and/or table.
3) If a substantial portion of the original paper is to be used, and if you are not the senior author, also obtain the senior author's approval.

Requirements to be followed when using an entire IEEE copyrighted paper in a thesis:

1) The following IEEE copyright/ credit notice should be placed prominently in the references: © [year of original publication] IEEE. Reprinted, with permission, from [author names, paper title, IEEE publication title, and month/year of publication]
2) Only the accepted version of an IEEE copyrighted paper can be used when posting the paper or your thesis on-line.
3) In placing the thesis on the author's university website, please display the following message in a prominent place on the website: In reference to IEEE copyrighted material which is used with permission in this thesis, the IEEE does not endorse any of [university/educational entity's name goes here]'s products or services. Internal or personal use of this material is permitted. If interested in reprinting/republishing IEEE copyrighted material for advertising or promotional purposes or for creating new collective works for resale or redistribution, please go to http://www.ieee.org/publications_standards/publications/rights/rights_link.html to learn how to obtain a License from RightsLink.

If applicable, University Microfilms and/or ProQuest Library, or the Archives of Canada may supply single copies of the dissertation.

BACK | CLOSE WINDOW

Appendix (Continued)

CCC RightsLink

Home | Help | Email Support | Sign in | Create Account

Artificial Intelligence Inspired Model Predictive Control for Frequency Regulation in Power Electronics Dominated Grids

IEEE Requesting permission to reuse content from an IEEE publication

Conference Proceedings:
2021 IEEE 12th International Symposium on Power Electronics for Distributed Generation Systems (PEDG)

Author: Mohsen Hosseinzadehtaher

Publisher: IEEE

Date: 28 June 2021

Thesis / Dissertation Reuse

The IEEE does not require individuals working on a thesis to obtain a formal reuse license, however, you may print out this statement to be used as a permission grant:

Requirements to be followed when using any portion (e.g., figure, graph, table, or textual material) of an IEEE copyrighted paper in a thesis:

1) In the case of textual material (e.g., using short quotes or referring to the work within these papers) users must give full credit to the original source (author, paper, publication) followed by the IEEE copyright line © 2011 IEEE.
2) In the case of illustrations or tabular material, we require that the copyright line © [Year of original publication] IEEE appear prominently with each reprinted figure and/or table.
3) If a substantial portion of the original paper is to be used, and if you are not the senior author, also obtain the senior author's approval.

Requirements to be followed when using an entire IEEE copyrighted paper in a thesis:

1) The following IEEE copyright/ credit notice should be placed prominently in the references: © [year of original publication] IEEE. Reprinted, with permission, from [author names, paper title, IEEE publication title, and month/year of publication]
2) Only the accepted version of an IEEE copyrighted paper can be used when posting the paper or your thesis on-line.
3) In placing the thesis on the author's university website, please display the following message in a prominent place on the website: In reference to IEEE copyrighted material which is used with permission in this thesis, the IEEE does not endorse any of [university/educational entity's name goes here]'s products or services. Internal or personal use of this material is permitted. If interested in reprinting/republishing IEEE copyrighted material for advertising or promotional purposes or for creating new collective works for resale or redistribution, please go to http://www.ieee.org/publications_standards/publications/rights/rights_link.html to learn how to obtain a License from RightsLink.

If applicable, University Microfilms and/or ProQuest Library, or the Archives of Canada may supply single copies of the dissertation.

BACK | CLOSE WINDOW

7. References

[1] B. K. Bose, "Global Energy Scenario and Impact of Power Electronics in 21st Century," *IEEE Transactions on Industrial Electronics,* vol. 60, no. 7, pp. 2638-2651, 2013, doi: 10.1109/TIE.2012.2203771.

[2] F. Blaabjerg and K. Ma, "Future on Power Electronics for Wind Turbine Systems," *IEEE Journal of Emerging and Selected Topics in Power Electronics,* vol. 1, no. 3, pp. 139-152, 2013, doi: 10.1109/JESTPE.2013.2275978.

[3] O. Ellabban, H. Abu-Rub, and F. Blaabjerg, "Renewable energy resources: Current status, future prospects and their enabling technology," *Renewable and Sustainable Energy Reviews,* vol. 39, pp. 748-764, 2014/11/01/ 2014, doi: https://doi.org/10.1016/j.rser.2014.07.113.

[4] "Global Wind Report 2018," Global Wind Energy Council, Belgium, 2019.

[5] "Global market outlook for solar power 2019-2023," Solar Power Europe, Belgium, 2019.

[6] "New Energy Outlook 2019," BloombergNEF, USA, 2019.

[7] Q. Peng, Q. Jiang, Y. Yang, T. Liu, H. Wang, and F. Blaabjerg, "On the Stability of Power Electronics-Dominated Systems: Challenges and Potential Solutions," *IEEE Transactions on Industry Applications,* vol. 55, no. 6, pp. 7657-7670, 2019.

[8] F. Blaabjerg, Y. Yang, D. Yang, and X. Wang, "Distributed Power-Generation Systems and Protection," *Proceedings of the IEEE,* vol. 105, no. 7, pp. 1311-1331, 2017, doi: 10.1109/JPROC.2017.2696878.

[9] A. Khan, M. Hosseinzadehtaher, M. B. Shadmand, S. Bayhan, and H. Abu-Rub, "On the Stability of the Power Electronics-Dominated Grid: A New Energy Paradigm," *IEEE Industrial Electronics Magazine,* vol. 14, no. 4, pp. 65-78, 2020, doi: 10.1109/MIE.2020.3002523.

[10] A. Mohammed, S. S. Refaat, S. Bayhan, and H. Abu-Rub, "AC Microgrid Control and Management Strategies: Evaluation and Review," *IEEE Power Electronics Magazine,* vol. 6, no. 2, pp. 18-31, 2019.

[11] S. D. silva, M. Shadmand, S. Bayhan, and H. Abu-Rub, "Towards Grid of Microgrids: Seamless Transition between Grid-Connected and Islanded Modes of Operation," *IEEE Open Journal of the Industrial Electronics Society,* vol. 1, pp. 66-81, 2020, doi: 10.1109/OJIES.2020.2988618.

References (Continued)

[12] X. Wang and F. Blaabjerg, "Harmonic Stability in Power Electronic-Based Power Systems: Concept, Modeling, and Analysis," *IEEE Transactions on Smart Grid,* vol. 10, no. 3, pp. 2858-2870, 2019.

[13] J. Sun, G. Wang, X. Du, and H. Wang, "A Theory for Harmonics Created by Resonance in Converter-Grid Systems," *IEEE Transactions on Power Electronics,* vol. 34, no. 4, pp. 3025-3029, 2019.

[14] *IEEE Guide for Design, Operation, and Integration of Distributed Resource Island Systems with Electric Power Systems, IEEE Std. 1547.4*, IEEE, 2011.

[15] T. S. Tran, D. T. Nguyen, and G. Fujita, "The Analysis of Technical Trend in Islanding Operation, Harmonic Distortion, Stabilizing Frequency, and Voltage of Islanded Entities," *Resources,* vol. 8, no. 1, p. 14, 2019.

[16] J. Liu, Y. Miura, and T. Ise, "Comparison of Dynamic Characteristics Between Virtual Synchronous Generator and Droop Control in Inverter-Based Distributed Generators," *IEEE Transactions on Power Electronics,* vol. 31, no. 5, pp. 3600-3611, 2016.

[17] Q. Zhong and G. Weiss, "Synchronverters: Inverters That Mimic Synchronous Generators," *IEEE Transactions on Industrial Electronics,* vol. 58, no. 4, pp. 1259-1267, 2011.

[18] Q. Zhong, "Virtual Synchronous Machines: A unified interface for grid integration," *IEEE Power Electronics Magazine,* vol. 3, no. 4, pp. 18-27, 2016.

[19] S. Sahoo, T. Dragičević, and F. Blaabjerg, "Cyber Security in Control of Grid-Tied Power Electronic Converters–Challenges and Vulnerabilities," *IEEE Journal of Emerging and Selected Topics in Power Electronics,* pp. 1-1, 2019.

[20] F. Pasqualetti, F. Dörfler, and F. Bullo, "Attack Detection and Identification in Cyber-Physical Systems," *IEEE Transactions on Automatic Control,* vol. 58, no. 11, pp. 2715-2729, 2013.

[21] Y. Mo *et al.*, "Cyber–Physical Security of a Smart Grid Infrastructure," *Proceedings of the IEEE,* vol. 100, no. 1, pp. 195-209, 2012.

[22] A. B. Smith. U.S. Billion-dollar Weather and Climate Disasters, 1980 - present (NCEI Accession 0209268). [indicate subset used]. NOAA National Centers for Environmental Information [Online] Available: https://doi.org/10.25921/stkw-7w73

References (Continued)

[23] S. D'Silva, M. Hosseinzadehtaher, M. B. Shadmand, S. Bayhan, H. Abu-Rub, and T. Huang, "Coordinated Power Reserve Control of PV Sources For Frequency Restoration in Power Electronics Dominated Grid," in *2022 3rd International Conference on Smart Grid and Renewable Energy (SGRE)*, 20-22 March 2022 2022, pp. 1-7, doi: 10.1109/SGRE53517.2022.9774085.

[24] A. Khan, S. D. silva, A. Y. Fard, M. B. Shadmand, and H. Abu-Rub, "On Stability of PV Clusters With Distributed Power Reserve Capability," *IEEE Transactions on Industrial Electronics,* vol. 68, no. 5, pp. 3928-3938, 2021, doi: 10.1109/TIE.2020.2987291.

[25] Q. Zhong and Z. Lyu, "Droop-Controlled Rectifiers That Continuously Take Part in Grid Regulation," *IEEE Transactions on Industrial Electronics,* vol. 66, no. 8, pp. 6516-6526, 2019.

[26] R. S. Balog, M. Metry, and M. Shadmand, "The load as a controllable energy asset in dc microgrids," in *Energy Engineering*, *DC Distribution Systems and Microgrids*: Institution of Engineering and Technology, 2018, pp. 153-187.

[27] G. Delille, B. Francois, and G. Malarange, "Dynamic Frequency Control Support by Energy Storage to Reduce the Impact of Wind and Solar Generation on Isolated Power System's Inertia," *IEEE Transactions on Sustainable Energy,* vol. 3, no. 4, pp. 931-939, 2012.

[28] N. Pogaku, M. Prodanovic, and T. C. Green, "Modeling, Analysis and Testing of Autonomous Operation of an Inverter-Based Microgrid," *IEEE Transactions on Power Electronics,* vol. 22, no. 2, pp. 613-625, 2007, doi: 10.1109/TPEL.2006.890003.

[29] A. Khan, M. Easley, M. Hosseinzadehtaher, M. B. Shadmand, H. Abu-Rub, and P. Fajri, "PLL-less Active and Reactive Power Controller for Grid-Following Inverter," in *2020 IEEE Energy Conversion Congress and Exposition (ECCE)*, 11-15 Oct. 2020 2020, pp. 4322-4328, doi: 10.1109/ECCE44975.2020.9236408.

[30] A. Khan, M. Hosseinzadehtaher, and M. B. Shadmand, "Single Stage PLL-less Decoupled Active and Reactive Power Control for Weak Grid Interactive Inverters," *IFAC-PapersOnLine,* vol. 53, no. 2, pp. 12390-12395, 2020/01/01/ 2020, doi: https://doi.org/10.1016/j.ifacol.2020.12.1267.

[31] M. F. Umar, M. Hosseinzadehtaher, and M. B. Shadmand, "Enabling Aggregation of Heterogenous Grid-Forming Inverters via Enclaved Homogenization," *IEEE Access,* vol. 10, pp. 94765-94777, 2022, doi: 10.1109/ACCESS.2022.3204340.

References (Continued)

[32] A. Y. Fard, M. Hosseinzadehtaher, M. B. Shadmand, and S. K. Mazumder, "Cyberattack Resilient Control for Power Electronics Dominated Grid with Minimal Communication," in *2021 IEEE 12th International Symposium on Power Electronics for Distributed Generation Systems (PEDG)*, 28 June-1 July 2021 2021, pp. 1-6, doi: 10.1109/PEDG51384.2021.9494218.

[33] W. W. Weaver, R. D. Robinett, D. G. Wilson, and R. C. Matthews, "Metastability of Pulse Power Loads Using the Hamiltonian Surface Shaping Method," *IEEE Transactions on Energy Conversion,* vol. 32, no. 2, pp. 820-828, 2017, doi: 10.1109/TEC.2017.2652980.

[34] D. A. M. Al-Falahi, T. Tarasiuk, G. S. Jayasinghe, Z. Jin, H. Enshaei, and M. J. Guerrero, "AC Ship Microgrids: Control and Power Management Optimization," *Energies,* vol. 11, no. 6, 2018, doi: 10.3390/en11061458.

[35] T. Van Vu, D. Gonsoulin, F. Diaz, C. S. Edrington, and T. El-Mezyani, "Predictive control for energy management in ship power systems under high-power ramp rate loads," *IEEE Transactions on Energy Conversion,* vol. 32, no. 2, pp. 788-797, 2017.

[36] T. Tarasiuk and M. Gorniak, "Load sharing in ship microgrids under nonsinusoidal conditions—Case Study," *IEEE Transactions on Energy Conversion,* vol. 32, no. 2, pp. 810-819, 2017.

[37] G. S. Jayasinghe, L. Meegahapola, N. Fernando, Z. Jin, and M. J. Guerrero, "Review of Ship Microgrids: System Architectures, Storage Technologies and Power Quality Aspects," *Inventions,* vol. 2, no. 1, 2017, doi: 10.3390/inventions2010004.

[38] A. Boveri, F. Silvestro, M. Molinas, and E. Skjong, "Optimal sizing of energy storage systems for shipboard applications," *IEEE Transactions on Energy Conversion,* vol. 34, no. 2, pp. 801-811, 2018.

[39] S. G. Jayasinghe, D. M. Vilathgamuwa, and U. K. Madawala, "Direct integration of battery energy storage systems in distributed power generation," *IEEE Transactions on Energy Conversion,* vol. 26, no. 2, pp. 677-685, 2011.

[40] Q. Xiao, L. Chen, H. Jia, P. W. Wheeler, and T. Dragičević, "Model Predictive Control for Dual Active Bridge in Naval DC Microgrids Supplying Pulsed Power Loads Featuring Fast Transition and Online Transformer Current Minimization," *IEEE Transactions on Industrial Electronics,* vol. 67, no. 6, pp. 5197-5203, 2020, doi: 10.1109/TIE.2019.2934070.

References (Continued)

[41] A. Zare, S. D'Silva, M. F. Umar, and M. B. Shadmand, "Smart Battery Cells for Maximum Utilization in Power Electronics Dominated Grids," in *2022 3rd International Conference on Smart Grid and Renewable Energy (SGRE)*, 20-22 March 2022 2022, pp. 1-6, doi: 10.1109/SGRE53517.2022.9774203.

[42] J. Hu, P. Joebges, G. C. Pasupuleti, N. R. Averous, and R. W. De Doncker, "A Maximum-Output-Power-Point-Tracking-Controlled Dual-Active Bridge Converter for Photovoltaic Energy Integration Into MVDC Grids," *IEEE Transactions on Energy Conversion,* vol. 34, no. 1, pp. 170-180, 2018.

[43] F. Xue, R. Yu, and A. Q. Huang, "A 98.3% Efficient GaN Isolated Bidirectional DC–DC Converter for DC Microgrid Energy Storage System Applications," *IEEE Transactions on Industrial Electronics,* vol. 64, no. 11, pp. 9094-9103, 2017, doi: 10.1109/TIE.2017.2686307.

[44] T. Zhao, G. Wang, S. Bhattacharya, and A. Q. Huang, "Voltage and Power Balance Control for a Cascaded H-Bridge Converter-Based Solid-State Transformer," *IEEE Transactions on Power Electronics,* vol. 28, no. 4, pp. 1523-1532, 2013, doi: 10.1109/TPEL.2012.2216549.

[45] W. L. Malan, D. M. Vilathgamuwa, and G. R. Walker, "Modeling and Control of a Resonant Dual Active Bridge With a Tuned CLLC Network," *IEEE Transactions on Power Electronics,* vol. 31, no. 10, pp. 7297-7310, 2016, doi: 10.1109/TPEL.2015.2507787.

[46] Z. Shan and J. Jatskevich, "Digital and analog implementations of nonlinear-feedforward controller for a dual-active-bridge converter," in *2015 IEEE Energy Conversion Congress and Exposition (ECCE)*, 20-24 Sept. 2015 2015, pp. 4337-4342, doi: 10.1109/ECCE.2015.7310273.

[47] X. Li and Y. Li, "An Optimized Phase-Shift Modulation For Fast Transient Response in a Dual-Active-Bridge Converter," *IEEE Transactions on Power Electronics,* vol. 29, no. 6, pp. 2661-2665, 2014, doi: 10.1109/TPEL.2013.2294714.

[48] G. G. Oggier, M. Ordonez, J. M. Galvez, and F. Luchino, "Fast Transient Boundary Control and Steady-State Operation of the Dual Active Bridge Converter Using the Natural Switching Surface," *IEEE Transactions on Power Electronics,* vol. 29, no. 2, pp. 946-957, 2014, doi: 10.1109/TPEL.2013.2256150.

[49] D. Segaran, D. G. Holmes, and B. P. McGrath, "Enhanced Load Step Response for a Bidirectional DC–DC Converter," *IEEE Transactions on Power Electronics,* vol. 28, no. 1, pp. 371-379, 2013, doi: 10.1109/TPEL.2012.2200505.

References (Continued)

[50] Z. Li, Y. Xia, C. Su, J. Deng, J. Fu, and W. He, "Missile Guidance Law Based on Robust Model Predictive Control Using Neural-Network Optimization," *IEEE Transactions on Neural Networks and Learning Systems,* vol. 26, no. 8, pp. 1803-1809, 2015, doi: 10.1109/TNNLS.2014.2345734.

[51] M. Easley, A. Y. Fard, F. Fateh, M. B. Shadmand, and H. Abu-Rub, "Auto-tuned Model Parameters in Predictive Control of Power Electronics Converters," in *2019 IEEE Energy Conversion Congress and Exposition (ECCE)*, 29 Sept.-3 Oct. 2019 2019, pp. 3703-3709, doi: 10.1109/ECCE.2019.8912881.

[52] W. Alhosaini, Y. Wu, and Y. Zhao, "An Enhanced Model Predictive Control Using Virtual Space Vectors for Grid-Connected Three-Level Neutral-Point Clamped Inverters," *IEEE Transactions on Energy Conversion,* vol. 34, no. 4, pp. 1963-1972, 2019, doi: 10.1109/TEC.2019.2923370.

[53] S. Vazquez, J. Rodriguez, M. Rivera, L. G. Franquelo, and M. Norambuena, "Model Predictive Control for Power Converters and Drives: Advances and Trends," *IEEE Transactions on Industrial Electronics,* vol. 64, no. 2, pp. 935-947, 2017, doi: 10.1109/TIE.2016.2625238.

[54] S. Vazquez *et al.*, "Model Predictive Control: A Review of Its Applications in Power Electronics," *IEEE Industrial Electronics Magazine,* vol. 8, no. 1, pp. 16-31, 2014, doi: 10.1109/MIE.2013.2290138.

[55] Y. Zhang and H. Yang, "Model-Predictive Flux Control of Induction Motor Drives With Switching Instant Optimization," *IEEE Transactions on Energy Conversion,* vol. 30, no. 3, pp. 1113-1122, 2015, doi: 10.1109/TEC.2015.2423692.

[56] J. Rodriguez *et al.*, "State of the Art of Finite Control Set Model Predictive Control in Power Electronics," *IEEE Transactions on Industrial Informatics,* vol. 9, no. 2, pp. 1003-1016, 2013, doi: 10.1109/TII.2012.2221469.

[57] S. Dutta, S. Hazra, and S. Bhattacharya, "A Digital Predictive Current-Mode Controller for a Single-Phase High-Frequency Transformer-Isolated Dual-Active Bridge DC-to-DC Converter," *IEEE Transactions on Industrial Electronics,* vol. 63, no. 9, pp. 5943-5952, 2016, doi: 10.1109/TIE.2016.2551201.

[58] L. Chen *et al.*, "Moving Discretized Control Set Model-Predictive Control for Dual-Active Bridge With the Triple-Phase Shift," *IEEE Transactions on Power Electronics,* vol. 35, no. 8, pp. 8624-8637, 2020, doi: 10.1109/TPEL.2019.2962838.

References (Continued)

[59] M. Hosseinzadehtaher, A. Khan, M. Easley, M. B. Shadmand, and P. Fajri, "Self-Healing Predictive Control of Battery System in Naval Power System With Pulsed Power Loads," *IEEE Transactions on Energy Conversion,* vol. 36, no. 2, pp. 1056-1069, 2021, doi: 10.1109/TEC.2020.3014294.

[60] "Report on the Investigation of the Catastrophic Failure of a Capacitor in the AFT Harmonic Filter Room on Board RMS Queen Mary 2 while Approaching Barcelona on 23 September 2010. Report No 28/2011. Available online: http://www.maib.gov.uk/publications/investigation_reports/2011/qm2.cfm."

[61] Rules for Classification Ships, Part 4 Systems and components*, Chapter 8 Electrical installations. Det Norske Veritas GL Edition: Høvik, Norway, 2011. Available online: https://rules.dnvgl.com/docs/pdf/DNV/rulesship/2011-01/ts408.pdf*.

[62] J. Wolfe and M. J. Roa, "Advanced Methods for Tabulation of Electrical Loads During Special Modes of Marine Vessel Operation," *IEEE Transactions on Industry Applications,* vol. 53, no. 1, pp. 667-674, 2017, doi: 10.1109/TIA.2016.2602343.

[63] T. J. McCoy, "Trends in ship electric propulsion," in *IEEE Power Engineering Society Summer Meeting*, 21-25 July 2002 2002, vol. 1, pp. 343-346 vol.1, doi: 10.1109/PESS.2002.1043247.

[64] J. S. Chalfant and C. Chryssostomidis, "Analysis of various all-electric-ship electrical distribution system topologies," in *2011 IEEE Electric Ship Technologies Symposium*, 10-13 April 2011 2011, pp. 72-77, doi: 10.1109/ESTS.2011.5770844.

[65] American Bureau of Shipping. International Naval Ships, Guide for Building and Classing, Part 4 Vessel Systems and Machinery, American Bureau of Shipping*; International Association of Classification Societies, Requirements Concerning Electrical and Electronic Installations; IACS Req.: Houston, TX, USA, 2016.*

[66] G. Sulligoi *et al.*, "Naval smart grid: Integrated Power System for all electric naval vessels with control and reliability characteristics," in *2014 AEIT Annual Conference - From Research to Industry: The Need for a More Effective Technology Transfer (AEIT)*, 18-19 Sept. 2014 2014, pp. 1-6, doi: 10.1109/AEIT.2014.7002060.

[67] E. Skjong, E. Rødskar, M. Molinas, T. A. Johansen, and J. Cunningham, "The Marine Vessel's Electrical Power System: From its Birth to Present Day," *Proceedings of the IEEE,* vol. 103, no. 12, pp. 2410-2424, 2015, doi: 10.1109/JPROC.2015.2496722.

[68] H. Hegner and B. Desai, "Integrated fight through power," in *IEEE Power Engineering Society Summer Meeting*, 21-25 July 2002 2002, vol. 1, pp. 336-339 vol.1, doi: 10.1109/PESS.2002.1043245.

References (Continued)

[69] M. W. Rose and R. M. Cuzner, "Fault isolation and reconfiguration in a three-zone system," in *2015 IEEE Electric Ship Technologies Symposium (ESTS)*, 21-24 June 2015 2015, pp. 409-414, doi: 10.1109/ESTS.2015.7157927.

[70] S. Bose, B. Natarajan, C. Scoglio, S. Das, and N. N. Schulz, "Analysis of robustness for shipboard power system with non-radial power flow," in *2011 IEEE Electric Ship Technologies Symposium*, 10-13 April 2011 2011, pp. 181-186, doi: 10.1109/ESTS.2011.5770863.

[71] J. G. Ciezki and R. W. Ashton, "Selection and stability issues associated with a navy shipboard DC zonal electric distribution system," *IEEE Transactions on Power Delivery,* vol. 15, no. 2, pp. 665-669, 2000, doi: 10.1109/61.853002.

[72] U. Markovic, O. Stanojev, P. Aristidou, E. Vrettos, D. Callaway, and G. Hug, "Understanding Small-Signal Stability of Low-Inertia Systems," *IEEE Transactions on Power Systems,* vol. 36, no. 5, pp. 3997-4017, 2021, doi: 10.1109/TPWRS.2021.3061434.

[73] L. Meegahapola, P. Mancarella, D. Flynn, and R. Moreno, "Power system stability in the transition to a low carbon grid: A techno-economic perspective on challenges and opportunities," *WIREs Energy and Environment,* vol. 10, no. 5, p. e399, 2021, doi: https://doi.org/10.1002/wene.399.

[74] G. Yuan, "Grid-Forming Technologies Enabling a Decarbonized Power System [Technology Leaders]," *IEEE Electrification Magazine,* vol. 10, no. 1, pp. 7-9, 2022, doi: 10.1109/MELE.2021.3139204.

[75] Y. Lin *et al.*, "Research Roadmap on Grid-Forming Inverters," United States, 2020-11-11 2020. [Online]. Available: https://www.osti.gov/biblio/1721727

[76] J. Hernandez-Alvidrez, R. Darbali-Zamora, J. D. Flicker, M. Shirazi, J. VanderMeer, and W. Thomson, "Using Energy Storage-Based Grid Forming Inverters for Operational Reserve in Hybrid Diesel Microgrids," *Energies*, vol. 15, no. 7, doi: 10.3390/en15072456.

[77] R. Rosso, X. Wang, M. Liserre, X. Lu, and S. Engelken, "Grid-forming converters: an overview of control approaches and future trends," in *2020 IEEE Energy Conversion Congress and Exposition (ECCE)*, 11-15 Oct. 2020 2020, pp. 4292-4299, doi: 10.1109/ECCE44975.2020.9236211.

[78] E. A. A. Coelho, P. C. Cortizo, and P. F. D. Garcia, "Small-signal stability for parallel-connected inverters in stand-alone AC supply systems," *IEEE Transactions on Industry Applications,* vol. 38, no. 2, pp. 533-542, 2002, doi: 10.1109/28.993176.

References (Continued)

[79] B. K. Poolla, D. Groß, and F. Dörfler, "Placement and Implementation of Grid-Forming and Grid-Following Virtual Inertia and Fast Frequency Response," *IEEE Transactions on Power Systems,* vol. 34, no. 4, pp. 3035-3046, 2019, doi: 10.1109/TPWRS.2019.2892290.

[80] Q. C. Zhong and G. Weiss, "Synchronverters: Inverters That Mimic Synchronous Generators," *IEEE Transactions on Industrial Electronics,* vol. 58, no. 4, pp. 1259-1267, 2011, doi: 10.1109/TIE.2010.2048839.

[81] V. Karapanos, P. Kotsampopoulos, and N. Hatziargyriou, "Performance of the linear and binary algorithm of virtual synchronous generators for the emulation of rotational inertia," *Electric Power Systems Research,* vol. 123, pp. 119-127, 2015/06/01/ 2015, doi: https://doi.org/10.1016/j.epsr.2015.02.004.

[82] Á. Ortega and F. Milano, "Combined Frequency and RoCoF Control of Converter-Interfaced Energy Storage Systems," *IFAC-PapersOnLine,* vol. 52, no. 4, pp. 240-245, 2019/01/01/ 2019, doi: https://doi.org/10.1016/j.ifacol.2019.08.198.

[83] D. Sun, H. Liu, S. Gao, L. Wu, P. Song, and X. Wang, "Comparison of Different Virtual Inertia Control Methods for Inverter-based Generators," *Journal of Modern Power Systems and Clean Energy,* vol. 8, no. 4, pp. 768-777, 2020, doi: 10.35833/MPCE.2019.000330.

[84] U. Tamrakar, D. Shrestha, M. Maharjan, B. P. Bhattarai, T. M. Hansen, and R. Tonkoski, "Virtual Inertia: Current Trends and Future Directions," *Applied Sciences*, vol. 7, no. 7*,* doi: 10.3390/app7070654.

[85] I. Serban and C. P. Ion, "Microgrid control based on a grid-forming inverter operating as virtual synchronous generator with enhanced dynamic response capability," *International Journal of Electrical Power & Energy Systems,* vol. 89, pp. 94-105, 2017/07/01/ 2017, doi: https://doi.org/10.1016/j.ijepes.2017.01.009.

[86] X. Meng, J. Liu, and Z. Liu, "A Generalized Droop Control for Grid-Supporting Inverter Based on Comparison Between Traditional Droop Control and Virtual Synchronous Generator Control," *IEEE Transactions on Power Electronics,* vol. 34, no. 6, pp. 5416-5438, 2019, doi: 10.1109/TPEL.2018.2868722.

[87] P. Babahajyani, F. Habibi, and H. Bevrani, "An On-Line PSO-Based Fuzzy Logic Tuning Approach: Microgrid Frequency Control Case Study," in *Handbook of Research on Novel Soft Computing Intelligent Algorithms: Theory and Practical Applications*, P. M. Vasant Ed. Hershey, PA, USA: IGI Global, 2014, pp. 589-616.

References (Continued)

[88] S. Syan and G. R. Biswal, "Frequency control of an isolated hydro power plant using artificial intelligence," in *2015 IEEE Workshop on Computational Intelligence: Theories, Applications and Future Directions (WCI)*, 14-17 Dec. 2015 2015, pp. 1-5, doi: 10.1109/WCI.2015.7495537.

[89] Z. Yan and Y. Xu, "A Multi-Agent Deep Reinforcement Learning Method for Cooperative Load Frequency Control of a Multi-Area Power System," *IEEE Transactions on Power Systems,* vol. 35, no. 6, pp. 4599-4608, 2020, doi: 10.1109/TPWRS.2020.2999890.

[90] Y. Liang, X. Zhao, and L. Sun, "A Multi-Agent Reinforcement Learning Approach for Wind Farm Frequency Control," *IEEE Transactions on Industrial Informatics,* pp. 1-10, 2022, doi: 10.1109/TII.2022.3182328.

[91] S. Rozada, D. Apostolopoulou, and E. Alonso, "Load Frequency Control: A Deep Multi-Agent Reinforcement Learning Approach," in *2020 IEEE Power & Energy Society General Meeting (PESGM)*, 2-6 Aug. 2020 2020, pp. 1-5, doi: 10.1109/PESGM41954.2020.9281614.

[92] A. Khan, M. Hosseinzadehtaher, M. B. Shadmand, S. Bayhan, and H. Abu-Rub, "On the Stability of the Power Electronics-Dominated Grid: A New Energy Paradigm," *IEEE Industrial Electronics Magazine,* vol. 14, no. 4, 2020.

[93] Q. Peng, Q. Jiang, Y. Yang, T. Liu, H. Wang, and F. Blaabjerg, "On the Stability of Power Electronics-Dominated Systems: Challenges and Potential Solutions," *IEEE Transactions on Industry Applications,* vol. 55, no. 6, 2019.

[94] A. Y. Fard and M. B. Shadmand, "Multitimescale Three-Tiered Voltage Control Framework for Dispersed Smart Inverters at the Grid Edge," *IEEE Transactions on Industry Applications,* vol. 57, no. 1, pp. 824-834, 2021, doi: 10.1109/TIA.2020.3037287.

[95] G. Andersson *et al.*, "Causes of the 2003 major grid blackouts in North America and Europe, and recommended means to improve system dynamic performance," *IEEE Transactions on Power Systems,* vol. 20, no. 4, 2005.

[96] Y. Wang, C. Chen, J. Wang, and R. Baldick, "Research on Resilience of Power Systems Under Natural Disasters—A Review," *IEEE Transactions on Power Systems,* vol. 31, no. 2, 2016.

[97] J. C. M. Vieira, W. Freitas, X. Wilsun, and A. Morelato, "Efficient coordination of ROCOF and frequency relays for distributed generation protection by using the application region," *IEEE Transactions on Power Delivery,* vol. 21, no. 4, 2006.

References (Continued)

[98] E. Barklund, N. Pogaku, M. Prodanovic, C. Hernandez-Aramburo, and T. C. Green, "Energy Management in Autonomous Microgrid Using Stability-Constrained Droop Control of Inverters," *IEEE Transactions on Power Electronics,* vol. 23, no. 5, 2008.

[99] M. B. Delghavi and A. Yazdani, "An Adaptive Feedforward Compensation for Stability Enhancement in Droop-Controlled Inverter-Based Microgrids," *IEEE Transactions on Power Delivery,* vol. 26, no. 3, 2011.

[100] M. B. Delghavi and A. Yazdani, "A Unified Control Strategy for Electronically Interfaced Distributed Energy Resources," *IEEE Transactions on Power Delivery,* vol. 27, no. 2, 2012.

[101] G. Diaz, C. Gonzalez-Moran, J. Gomez-Aleixandre, and A. Diez, "Scheduling of Droop Coefficients for Frequency and Voltage Regulation in Isolated Microgrids," *IEEE Transactions on Power Systems,* vol. 25, no. 1, 2010.

[102] J. M. Guerrero, J. C. Vasquez, J. Matas, L. G. d. Vicuna, and M. Castilla, "Hierarchical Control of Droop-Controlled AC and DC Microgrids—A General Approach Toward Standardization," *IEEE Transactions on Industrial Electronics,* vol. 58, no. 1, 2011.

[103] J. A. P. Lopes, C. L. Moreira, and A. G. Madureira, "Defining control strategies for MicroGrids islanded operation," *IEEE Transactions on Power Systems,* vol. 21, no. 2, 2006.

[104] T. L. Vandoorn, B. Renders, L. Degroote, B. Meersman, and L. Vandevelde, "Active Load Control in Islanded Microgrids Based on the Grid Voltage," *IEEE Transactions on Smart Grid,* vol. 2, no. 1, 2011.

[105] H. Bevrani and S. Shokoohi, "An Intelligent Droop Control for Simultaneous Voltage and Frequency Regulation in Islanded Microgrids," *IEEE Transactions on Smart Grid,* vol. 4, no. 3, 2013, doi: 10.1109/TSG.2013.2258947.

[106] J. W. Simpson-Porco, Q. Shafiee, F. Dörfler, J. C. Vasquez, J. M. Guerrero, and F. Bullo, "Secondary Frequency and Voltage Control of Islanded Microgrids via Distributed Averaging," *IEEE Transactions on Industrial Electronics,* vol. 62, no. 11, 2015.

[107] A. Micallef, M. Apap, C. Spiteri-Staines, J. M. Guerrero, and J. C. Vasquez, "Reactive Power Sharing and Voltage Harmonic Distortion Compensation of Droop Controlled Single Phase Islanded Microgrids," *IEEE Transactions on Smart Grid,* vol. 5, no. 3, 2014.

References (Continued)

[108] Q. Shafiee, J. M. Guerrero, and J. C. Vasquez, "Distributed Secondary Control for Islanded Microgrids—A Novel Approach," *IEEE Transactions on Power Electronics,* vol. 29, no. 2, 2014.

[109] M. Savaghebi, A. Jalilian, J. C. Vasquez, and J. M. Guerrero, "Secondary Control for Voltage Quality Enhancement in Microgrids," *IEEE Transactions on Smart Grid,* vol. 3, no. 4, 2012.

[110] H. S. V. S. K. Nunna and S. Doolla, "Multiagent-Based Distributed-Energy-Resource Management for Intelligent Microgrids," *IEEE Transactions on Industrial Electronics,* vol. 60, no. 4, 2013.

[111] A. Y. Fard, M. B. Shadmand, and S. K. Mazumder, "Holistic Multi-timescale Attack Resilient Control Framework for Power Electronics Dominated Grid," in *2020 Resilience Week (RWS)*, 19-23 Oct. 2020 2020, pp. 167-173, doi: 10.1109/RWS50334.2020.9241270.

[112] M. Hosseinzadehtaher, A. Khan, M. B. Shadmand, and H. Abu-Rub, "Anomaly Detection in Distribution Power System based on a Condition Monitoring Vector and Ultra- Short Demand Forecasting," in *2020 IEEE CyberPELS (CyberPELS)*, 13-13 Oct. 2020 2020, pp. 1-6, doi: 10.1109/CyberPELS49534.2020.9311534.

[113] A. Khan, M. Hosseinzadehtaher, M. B. Shadmand, D. Saleem, and H. Abu-Rub, "Intrusion Detection for Cybersecurity of Power Electronics Dominated Grids: Inverters PQ Set-Points Manipulation," in *2020 IEEE CyberPELS (CyberPELS)*, 13-13 Oct. 2020 2020, pp. 1-8, doi: 10.1109/CyberPELS49534.2020.9311538.

[114] S. Harshbarger, M. Hosseinzadehtaher, B. Natarajan, E. Vasserman, M. Shadmand, and G. Amariucai, "(A Little) Ignorance is Bliss: The Effect of Imperfect Model Information on Stealthy Attacks in Power Grids," in *2020 IEEE Kansas Power and Energy Conference (KPEC)*, 13-14 July 2020 2020, pp. 1-6.

[115] H. M. Ibrahim, M. S. E. Moursi, and P. Huang, "Adaptive Roles of Islanded Microgrid Components for Voltage and Frequency Transient Responses Enhancement," *IEEE Transactions on Industrial Informatics,* vol. 11, no. 6, 2015.

[116] J. Bomer, K. Burges, C. Nabe, and M. Poller, "All island TSO facilitation of renewables study—Final report for work package 3," EirGrid, Dublin Ireland, Tech. Rep. Jun. 2010.

[117] F. C. Schweppe, R. D. Tabors, J. L. Kirtley, H. R. Outhred, F. H. Pickel, and A. J. Cox, "Homeostatic Utility Control," *IEEE Transactions on Power Apparatus and Systems,* vol. PAS-99, no. 3, 1980.

References (Continued)

[118] A. Molina-García, F. Bouffard, and D. S. Kirschen, "Decentralized Demand-Side Contribution to Primary Frequency Control," *IEEE Transactions on Power Systems,* vol. 26, no. 1, 2011.

[119] P. C. Taylor, "Distributed intelligent load control of autonomous renewable energy systems," University of Manchester, 2001.

[120] O. H. Abu-Rub, A. Y. Fard, M. F. Umar, M. Hosseinzadehtaher, and M. B. Shadmands, "Towards Intelligent Power Electronics-Dominated Grid via Machine Learning Techniques," *IEEE Power Electronics Magazine,* vol. 8, no. 1, pp. 28-38, 2021, doi: 10.1109/MPEL.2020.3047506.

[121] N. E. Nilsson, "Application of computer artificial intelligence techniques to analyzing the status of typical utility electrical power plant systems," *IEEE Transactions on Energy Conversion,* vol. 4, no. 1, 1989.

[122] Y. Xu and J. V. Milanović, "Artificial-Intelligence-Based Methodology for Load Disaggregation at Bulk Supply Point," *IEEE Transactions on Power Systems,* vol. 30, no. 2, 2015.

[123] Y. Wu, C. Lee, C. Chen, K. Hsu, and H. Tseng, "Optimization of the Wind Turbine Layout and Transmission System Planning for a Large-Scale Offshore WindFarm by AI Technology," *IEEE Transactions on Industry Applications,* vol. 50, no. 3, 2014.

[124] E. Serban, C. Pondiche, and M. Ordonez, "Islanding Detection Search Sequence for Distributed Power Generators Under AC Grid Faults," *IEEE Transactions on Power Electronics,* vol. 30, no. 6, 2015.

[125] X. Chen, C. Zhao, and N. Li, "Distributed Automatic Load-Frequency Control with Optimality in Power Systems," in *2018 IEEE Conference on Control Technology and Applications (CCTA)*, 21-24 Aug. 2018 2018.

[126] B. Kroposki *et al.*, "Achieving a 100% Renewable Grid: Operating Electric Power Systems with Extremely High Levels of Variable Renewable Energy," *IEEE Power and Energy Magazine,* vol. 15, no. 2, pp. 61-73, 2017, doi: 10.1109/MPE.2016.2637122.

[127] P. McDaniel and S. McLaughlin, "Security and Privacy Challenges in the Smart Grid," *IEEE Security & Privacy,* vol. 7, no. 3, pp. 75-77, 2009, doi: 10.1109/MSP.2009.76.

References (Continued)

[128] A. Khan, S. D. silva, A. Y. Fard, M. B. Shadmand, and H. A. Abu-Rub, "On Stability of PV Clusters with Distributed Power Reserve Capability," *IEEE Transactions on Industrial Electronics,* pp. 1-1, 2020, doi: 10.1109/TIE.2020.2987291.

[129] S. D'silva, A. Khan, M. F. Umar, M. B. Shadmand, and H. Abu-Rub, "On Stability of Hybrid Power Ramp Rate Control for High Photovoltaic Penetrated Grid," in *2020 IEEE Energy Conversion Congress and Exposition (ECCE)*, 11-15 Oct. 2020 2020, pp. 2806-2813, doi: 10.1109/ECCE44975.2020.9235460.

[130] A. Y. Fard, M. Hosseinzadehtaher, M. B. Shadmand, and S. K. Mazumder, "Cyberattack Resilient Control for Power Electronics Dominated Grid with Minimal Communication," presented at the The IEEE 12th International Symposium on Power Electronics for Distributed Generation Systems (PEDG 2021), Chicago, IL, USA, 2021.

[131] A. Bidram and A. Davoudi, "Hierarchical Structure of Microgrids Control System," *IEEE Transactions on Smart Grid,* vol. 3, no. 4, pp. 1963-1976, 2012, doi: 10.1109/TSG.2012.2197425.

[132] M. Hosseinzadehtaher, A. Khan, M. Easley, M. B. Shadmand, and P. Fajri, "Self-healing Predictive Control of Battery System in Naval Power System with Pulsed Power Loads," *IEEE Transactions on Energy Conversion,* pp. 1-1, 2020, doi: 10.1109/TEC.2020.3014294.

[133] A. Hansen, J. Staggs, and S. Shenoi, "Security analysis of an advanced metering infrastructure," *International Journal of Critical Infrastructure Protection,* vol. 18, pp. 3-19, 2017.

[134] J. Valenzuela, J. Wang, and N. Bissinger, "Real-time intrusion detection in power system operations," *IEEE Transactions on Power Systems,* vol. 28, no. 2, pp. 1052-1062, 2013, doi: 10.1109/TPWRS.2012.2224144.

[135] Z. Zhang, M. Easley, M. Hosseinzadehtaher, G. Amariucai, M. B. Shadmand, and H. Abu-Rub, "An Observer Based Intrusion Detection Framework for Smart Inverters at the Grid-Edge," in *2020 IEEE Energy Conversion Congress and Exposition (ECCE)*, 11-15 Oct. 2020 2020, pp. 1957-1962, doi: 10.1109/ECCE44975.2020.9235863.

[136] P. Cheng, Z. Yang, J. Chen, Y. Qi, and L. Shi, "An Event-Based Stealthy Attack on Remote State Estimation," *IEEE Transactions on Automatic Control,* vol. 65, no. 10, pp. 4348-4355, 2020, doi: 10.1109/TAC.2019.2956021.

References (Continued)

[137] X. He, X. Liu, and P. Li, "Coordinated False Data Injection Attacks in AGC System and Its Countermeasure," *IEEE Access,* vol. 8, pp. 194640-194651, 2020, doi: 10.1109/ACCESS.2020.3033566.

[138] R. S. Smith, "A decoupled feedback structure for covertly appropriating networked control systems," *IFAC Proceedings Volumes,* vol. 44, no. 1, pp. 90-95, 2011.

[139] F. Pasqualetti, F. Dörfler, and F. Bullo, "Cyber-physical attacks in power networks: Models, fundamental limitations and monitor design," in *2011 50th IEEE Conference on Decision and Control and European Control Conference*, 2011: IEEE, pp. 2195-2201.

[140] G. Dán and H. Sandberg, "Stealth attacks and protection schemes for state estimators in power systems," in *2010 first IEEE international conference on smart grid communications*, 2010: IEEE, pp. 214-219.

[141] M. Esmalifalak, L. Liu, N. Nguyen, R. Zheng, and Z. Han, "Detecting stealthy false data injection using machine learning in smart grid," *IEEE Systems Journal,* vol. 11, no. 3, pp. 1644-1652, 2014.

[142] M. Esmalifalak, H. Nguyen, R. Zheng, and Z. Han, "Stealth false data injection using independent component analysis in smart grid," in *2011 IEEE international conference on smart grid communications (SmartGridComm)*, 2011: IEEE, pp. 244-248.

[143] M. A. Rahman, E. Al-Shaer, and M. A. Rahman, "A formal model for verifying stealthy attacks on state estimation in power grids," in *2013 IEEE International Conference on Smart Grid Communications (SmartGridComm)*, 2013: IEEE, pp. 414-419.

[144] A. Ashok, M. Govindarasu, and V. Ajjarapu, "Online detection of stealthy false data injection attacks in power system state estimation," *IEEE Transactions on Smart Grid,* vol. 9, no. 3, pp. 1636-1646, 2016.

[145] M. N. Kurt, Y. Yılmaz, and X. Wang, "Real-time detection of hybrid and stealthy cyber-attacks in smart grid," *IEEE Transactions on Information Forensics and Security,* vol. 14, no. 2, pp. 498-513, 2018.

[146] A. Teixeira, S. Amin, H. Sandberg, K. H. Johansson, and S. S. Sastry, "Cyber security analysis of state estimators in electric power systems," in *49th IEEE conference on decision and control (CDC)*, 2010, pp. 5991-5998.

References (Continued)

[147] Y. Chakhchoukh and H. Ishii, "Enhancing robustness to cyber-attacks in power systems through multiple least trimmed squares state estimations," *IEEE Transactions on Power Systems,* vol. 31, no. 6, pp. 4395-4405, 2016.

[148] O. Vuković, K. C. Sou, G. Dán, and H. Sandberg, "Network-layer protection schemes against stealth attacks on state estimators in power systems," in *2011 IEEE International Conference on Smart Grid Communications (SmartGridComm)*, 2011: IEEE, pp. 184-189.

[149] A. Teixeira, I. Shames, H. Sandberg, and K. H. Johansson, "Revealing stealthy attacks in control systems," in *2012 50th Annual Allerton Conference on Communication, Control, and Computing (Allerton)*, 2012: IEEE, pp. 1806-1813.

[150] D. I. Urbina *et al.*, "Limiting the impact of stealthy attacks on industrial control systems," in *Proceedings of the 2016 ACM SIGSAC Conference on Computer and Communications Security*, 2016, pp. 1092-1105.

[151] W. Aoudi, M. Iturbe, and M. Almgren, "Truth will out: Departure-based process-level detection of stealthy attacks on control systems," in *Proceedings of the 2018 ACM SIGSAC Conference on Computer and Communications Security*, 2018, pp. 817-831.

[152] S. D. Bopardikar and A. Speranzon, "On analysis and design of stealth-resilient control systems," in *2013 6th International Symposium on Resilient Control Systems (ISRCS)*, 2013: IEEE, pp. 48-53.

[153] R. Zhang and P. Venkitasubramaniam, "Stealthy control signal attacks in linear quadratic Gaussian control systems: Detectability reward tradeoff," *IEEE Transactions on Information Forensics and Security,* vol. 12, no. 7, pp. 1555-1570, 2017.

[154] M. Braun *et al.*, "The Future of Power System Restoration: Using Distributed Energy Resources as a Force to Get Back Online," *IEEE Power and Energy Magazine,* vol. 16, no. 6, pp. 30-41, 2018, doi: 10.1109/MPE.2018.2864227.

[155] "IEEE Standard for Interconnection and Interoperability of Distributed Energy Resources with Associated Electric Power Systems Interfaces," *IEEE Std 1547-2018 (Revision of IEEE Std 1547-2003),* pp. 1-138, 2018, doi: 10.1109/IEEESTD.2018.8332112.

[156] H. Gu, R. Yan, and T. K. Saha, "Minimum Synchronous Inertia Requirement of Renewable Power Systems," *IEEE Transactions on Power Systems,* vol. 33, no. 2, pp. 1533-1543, 2018, doi: 10.1109/TPWRS.2017.2720621.

References (Continued)

[157] S. Xu, Y. Xue, and L. Chang, "Review of Power System Support Functions for Inverter-Based Distributed Energy Resources- Standards, Control Algorithms, and Trends," *IEEE Open Journal of Power Electronics,* vol. 2, pp. 88-105, 2021, doi: 10.1109/OJPEL.2021.3056627.

[158] H. Huang and F. Li, "Sensitivity Analysis of Load-Damping Characteristic in Power System Frequency Regulation," *IEEE Transactions on Power Systems,* vol. 28, no. 2, pp. 1324-1335, 2013, doi: 10.1109/TPWRS.2012.2209901.

[159] J. Qi, I. Dobson, and S. Mei, "Towards Estimating the Statistics of Simulated Cascades of Outages With Branching Processes," *IEEE Transactions on Power Systems,* vol. 28, no. 3, pp. 3410-3419, 2013, doi: 10.1109/TPWRS.2013.2243479.

[160] J. Qi, S. Mei, and F. Liu, "Blackout Model Considering Slow Process," *IEEE Transactions on Power Systems,* vol. 28, no. 3, pp. 3274-3282, 2013, doi: 10.1109/TPWRS.2012.2230196.

[161] T. Baumeister, "Literature review on smart grid cyber security," *Collaborative Software Development Laboratory at the University of Hawaii,* 2010.

[162] G. N. Sorebo and M. C. Echols, *Smart grid security: an end-to-end view of security in the new electrical grid*. CRC Press, 2011.

[163] G. Hug and J. A. Giampapa, "Vulnerability assessment of AC state estimation with respect to false data injection cyber-attacks," *IEEE Transactions on smart grid,* vol. 3, no. 3, pp. 1362-1370, 2012.

[164] S. Sridhar, A. Hahn, and M. Govindarasu, "Cyber–physical system security for the electric power grid," *Proceedings of the IEEE,* vol. 100, no. 1, pp. 210-224, 2011.

[165] O. Kosut, L. Jia, R. J. Thomas, and L. Tong, "Malicious data attacks on the smart grid," *IEEE Transactions on Smart Grid,* vol. 2, no. 4, pp. 645-658, 2011.

[166] A. J. Wood, B. F. Wollenberg, and G. B. Sheblé, *Power generation, operation, and control*. John Wiley & Sons, 2013.

[167] G. Liang, J. Zhao, F. Luo, S. R. Weller, and Z. Y. Dong, "A review of false data injection attacks against modern power systems," *IEEE Transactions on Smart Grid,* vol. 8, no. 4, pp. 1630-1638, 2016.

[168] Z. Zhang, M. Easley, M. Hosseinzadehtaher, G. Amariucai, M. Shadmand, and H. Abu-Rub, "An Observer Based Intrusion Detection Framework for Smart Inverters

at the Grid-Edge," in *Energy Conversion Congress and Exposition 2020 (ECCE 2020)*, Detroit, MI, USA, 2020.

[169] A. Y. Fard, M. Easley, G. T. Amariucai, M. B. Shadmand, and H. Abu-Rub, "Cybersecurity Analytics using Smart Inverters in Power Distribution System: Proactive Intrusion Detection and Corrective Control Framework," in *2019 IEEE International Symposium on Technologies for Homeland Security (HST)*, 5-6 Nov. 2019 2019, pp. 1-6, doi: 10.1109/HST47167.2019.9032978.

[170] K. Manandhar, X. Cao, F. Hu, and Y. Liu, "Detection of faults and attacks including false data injection attack in smart grid using Kalman filter," *IEEE transactions on control of network systems,* vol. 1, no. 4, pp. 370-379, 2014.

[171] S. Sridhar and M. Govindarasu, "Model-based attack detection and mitigation for automatic generation control," *IEEE Transactions on Smart Grid,* vol. 5, no. 2, pp. 580-591, 2014.

[172] P. Zhuang, R. Deng, and H. Liang, "False data injection attacks against state estimation in multiphase and unbalanced smart distribution systems," *IEEE Transactions on Smart Grid,* vol. 10, no. 6, pp. 6000-6013, 2019.

[173] A. Anwar, A. N. Mahmood, and Z. Tari, "Identification of vulnerable node clusters against false data injection attack in an AMI based Smart Grid," *Information Systems,* vol. 53, pp. 201-212, 2015/10/01/ 2015, doi: https://doi.org/10.1016/j.is.2014.12.001.

[174] T. T. Kim and H. V. Poor, "Strategic protection against data injection attacks on power grids," *IEEE Transactions on Smart Grid,* vol. 2, no. 2, pp. 326-333, 2011.

[175] L. Liu, M. Esmalifalak, Q. Ding, V. A. Emesih, and Z. Han, "Detecting false data injection attacks on power grid by sparse optimization," *IEEE Transactions on Smart Grid,* vol. 5, no. 2, pp. 612-621, 2014.

[176] S. Li, Y. Yılmaz, and X. Wang, "Quickest detection of false data injection attack in wide-area smart grids," *IEEE Transactions on Smart Grid,* vol. 6, no. 6, pp. 2725-2735, 2015.

VITA

NAME:	Mohsen Hosseinzadehtaher
EDUCATION:	M.Sc. Electrical Engineering, Amirkabir University of Technology, Tehran, Iran, 2014.
	Ph.D. Electrical and Computer Engineering, University of Illinois at Chicago, Chicago, IL, USA, 2022.
PROFESSIONAL EXPERIENCE:	Seniore engineer, Quanta Technology, Lombard, IL, USA, Dec 2022.
	R&D engineer, Quanta Technology, Lombard, IL, USA, Sep 2021 –Aug 2022.
	General Chair and Founder of IEEE Kansas Power & Energy Conference (KPEC 2020), Manhattan, KS, USA, 2020.
	Vice-Chair of IEEE joint IAS-PELS-PES branch chapter at Kansas State University, Manhattan, KS, USA, 2018-2020.
	Session Chair of the 2021 IEEE 12th International Symposium on Power Electronics for Distributed Generation Systems, Chicago, IL, USA, 2021.
HONOURS AND AWARDS:	Best Paper Award from the 2019 IEEE Conference on Smart Grid and Renewable Energy.
	IEEE 2019 IAS Myron Zucker Student Faculty Grant, for the project "Compact, Reliable, and Robust GaN-based Active Rectifiers for More Electric Aircraft".
	IEEE 2019 IAS Outstanding Branch Chapter Award, Kansas State University IAS branch chapter.
	IEEE ECCE 2021 Attendance Grant Award.
	IEEE ECCE 2019 Travel Award.
	IEEE IAS Annual Meeting 2019 Travel Grant Award.
	IEEE eGrid 2018 Full Support Award.
MEMBERSHIP	IEEE

VITA (Continued)

	IEEE IAS
	IEEE PES
	IEEE IES
	IEEE PELS
REVIEWER:	IEEE Transactions on Smart Grid
	IEEE Transactions on Industrial Electronics
	IEEE Transactions on Industry Application
	IET Renewable Power Generation
	IEEE Applied Power Electronics Conference & Exposition
	IEEE Energy Conversion Congress & Expo
	IET Power Electronics
	International Federation of Automatic Control's Conference
	Dynamic Systems and Control Conference
JOURNALS:	M. Hosseinzadehtaher, A. Zare, A. Khan, M. F. Umar, S. D'silva, and M. B. Shadmand, "Towards More Resilient Low Inertia Power Electronic Dominated-Grid: Grid-Following Inverters' Maximum Capability Utilization ", IEEE Transactions on Industrial Electronics, Submitted.
	M. Hosseinzadehtaher, A. Khan, M. Easley, M. B. Shadmand, P. Fajri "Self-healing Predictive Control of Battery System in Naval Power System with Pulsed Power Loads", IEEE Transactions on Energy Conversion, 2020, Manuscript ID is TEC-00311-2020.
	A. Khan, M. Hosseinzadehtaher, M. B. Shadmand, S. Bayhan, H. Abu-Rub. "On Stability of Power Electronics Dominated Grid" IEEE Industrial Electronics Magazine, 2020, Manuscript ID: F-0015-IEM-02-2020.

VITA (Continued)

M. F. Umar, M. Hosseinzadehtaher and M. B. Shadmand, "Enabling Aggregation of Heterogenous Grid-Forming Inverters via Enclaved Homogenization," in IEEE Access, vol. 10, pp. 94765-94777.

Kumar, Ritesh, Mohsen Hosseinzadehtaher, Nathan Hein, Mohammad Shadmand, S. V. Jagadish, and Behzad Ghanbarian. "Challenges and advances in measuring sap flow in agriculture and agroforestry: A review with focus on nuclear magnetic resonance." Frontiers in Plant Science: 4118.

Omar H. Abu-Rub, Amin Y. Fard, Muhammad Farooq Umar, M. Hosseinzadehtaher, M. B. Shadmand, "Towards Intelligent Power Electronics-dominated Grid via Machine Learning Techniques," IEEE Power Electronics Magazine, published in February 2021's issue., Electronic ISSN: 2329-9215.

CONFERENCE: M. Hosseinzadehtaher, Amin Y. Fard, Mohammad B. Shadmand, Poria Fajri "Artificial Intelligence Inspired Model Predictive Control for Frequency Regulation in Power Electronics Dominated Grids", 2021 IEEE 12th International Symposium on Power Electronics for Distributed Generation Systems (PEDG 2021), USA, 2021.

M. Hosseinzadehtaher, D. Tiwari, N. Kouchakipour, A. Momeni, M. Lelic and Z. Wu, "Grid Resilience Assessment during Extreme Fast Charging of Electric Vehicles via Developed Power Hardware-in-the-Loop," 2022 IEEE Transportation Electrification Conference & Expo (ITEC), 2022, pp. 929-934.

M. Hosseinzadehtaher, Amin Y. Fard, Mohammad B. Shadmand "Event-triggered Self-learning Control Scheme For Power Electronics Dominated Grid", IEEE Energy Conversion Congress & Expo (IEEE ECCE) 2021, Vancouver, Canada, 2021.

VITA (Continued)

M. Hosseinzadehtaher, A. Khan, M. B. Shadmand, H. Abu-Rub “Anomaly Detection in Distribution Power System based on a Condition Monitoring Vector and Ultra- Short Demand Forecasting”, IEEE CyberPELS 2020, Miami, FL, USA, 2020.

M. Hosseinzadehtaher, A. Khan, M. W. Baker and M. B. Shadmand, "Model Predictive Self-healing Control Scheme for Dual Active Bridge Converter," 2019 2nd International Conference on Smart Grid and Renewable Energy (SGRE), 2019, pp. 1-6. “Best paper award.”

M. Hosseinzadehtaher, M. Greidanus, H. Althuwaini, K. Sullivan, M. B. Shadmand and S. K. Mazumder, "Differential Power Processing-based Constant Power Generation towards Grid-friendly Photovoltaic System," 2022 3rd International Conference on Smart Grid and Renewable Energy (SGRE), 2022, pp. 1-6.

S. D’Silva, M. Hosseinzadehtaher, M. B. Shadmand, S. Bayhan, H. Abu-Rub and T. Huang, "Coordinated Power Reserve Control of PV Sources For Frequency Restoration in Power Electronics Dominated Grid," 2022 3rd International Conference on Smart Grid and Renewable Energy (SGRE), 2022.

M. F. Umar, M. Hosseinzadehtaher and M. B. Shadmand, "Homogeneity Realization for Cluster of Heterogeneous Grid-forming Inverters," 2021 6th IEEE Workshop on the Electronic Grid (eGRID), 2021.

M. F. Umar, M. Hosseinzadehtaher and M. B. Shadmand, "Enforcing Coherency in the Cluster of Grid-forming Inverters in Power Electronics-Dominated Grid," 2021 IEEE 22nd Workshop on Control and Modelling of Power Electronics (COMPEL), 2021.

A. Khan, M. Hosseinzadehtaher, M. B. Shadmand, Danish Saleem, H. Abu-Rub “Intrusion Detection for Cybersecurity of Power Electronics Dominated Grids: Inverters PQ Set-Points Manipulation”, IEEE CyberPELS 2020, Miami, FL, USA, 2020.

VITA (Continued)

A. Khan, M. Hosseinzadehtaher, Mohammad B. Shadmand, Sudip K. Mazumder “Cybersecurity Analytics for Virtual Power Plants," 2021 IEEE 12th International Symposium on Power Electronics for Distributed Generation Systems (PEDG 2021), USA, 2021

Amin Y. Fard, M. Hosseinzadehtaher, Mohammad B. Shadmand, Sudip K. Mazumder “Cyberattack Mitigation via Grid Clustering and Distributed Control of Smart Inverters with Minimal Communication," 2021 IEEE 12th International Symposium on Power Electronics for Distributed Generation Systems (PEDG 2021), USA, 2021.

Stephanie Harshbarger, M. Hosseinzadehtaher, Bala Natarajan, Eugene Vasserman, M. B. Shadmand, George Amariucai “(A Little) Ignorance is Bliss: The Effect of Imperfect Model Information on Stealthy Attacks in Power Grids”, IEEE Kansas Power and Energy Conference (KPEC), Manhattan, KS, USA, 2020.

A. Khan, M. Hosseinzadehtaher, M. Easley, M. B. Shadmand and H. Abu-Rub “Single Stage PLL-less Direct PQ Control with Active Power Decoupling Capability for Grid-Tied Inverters”, 2020 IEEE Energy Conversion Congress and Exposition (ECCE), Detroit, Michigan, USA, 2020.

A. Khan, M. Easley, M. Hosseinzadehtaher, M. B. Shadmand and H. Abu-Rub “Single Stage PLL-less Decoupled Active and Reactive Power Control for Grid Interactive Inverters”, 2020 IEEE Energy Conversion Congress and Exposition (ECCE), Detroit, Michigan, USA, 2020.

Z. Zhang, M. Easley, M. Hosseinzadehtaher, George Amariucai, M. B. Shadmand, H. Abu-Rub “An Observer Based Intrusion Detection Framework for Smart Inverters at the Grid-Edge”, 2020 IEEE Energy Conversion Congress and Exposition (ECCE), Detroit, Michigan, USA, 2020.

A. Khan, M. Hosseinzadehtaher, M. B. Shadmand, “Single Stage PLL-less Decoupled Active and Reactive Power Control for Single Phase Weak Grid-Connected Inverters”, 21st IFAC World Congress, 2020 (IFAC 2020), Berlin, Germany, 2020.

VITA (Continued)

A. Khan, M. Hosseinzadehtaher, A. Y. Fard and M. B. Shadmand, "Active Power Decoupling Control for Rectifiers with Variable Frequency Supply for More Electric Aircraft," 2021 IEEE Industry Applications Society Annual Meeting (IAS), 2021, pp. 1-8, doi: 10.1109/IAS48185.2021.9677409.

A. Khan, M. Hosseinzadehtaher, M. B. Shadmand and S. K. Mazumder, "Cybersecurity Analytics for Virtual Power Plants," 2021 IEEE 12th International Symposium on Power Electronics for Distributed Generation Systems (PEDG), 2021, pp. 1-5, doi: 10.1109/PEDG51384.2021.9494255.

Z. Zhang, A. W. Oluwafemi, M. Hosseinzadehtaher and M. B. Shadmand "Current Observer Based Predictive Decoupled Power Control Grid-Interactive Inverter", 2020 IEEE Texas Power and Energy Conference (TPEC), College Station, TX, USA, 2020, pp. 1-6.

M. Easley, M. Hosseinzadehtaher, A. Y. Fard, M. B. Shadmand and H. Abu-Rub, "Computationally-efficient Hierarchical Optimal Controller for Grid-tied Cascaded Multilevel Inverters," 2019 IEEE Energy Conversion Congress and Exposition (ECCE), Baltimore, MD, USA, 2019, pp. 219-224.